Laboratori d'Enginyeria Marítima
UNIVERSITAT POLITÈCNICA DE CATALUNYA

Hydrodynamic response of a shallow and microtidal estuary: Alfacs Bay. From high to low frequency processes.

Tesi presentada per Pablo Cerralbo Peñarroya per optar al grau de doctor/a per la Universitat Politècnica de Catalunya. La tesi doctoral ha estat realitzada al Departament d'Enginyeria Hidràulica, Marítima i Ambiental, dins el Programa de Doctorat Interuniversitari en Ciències del Mar (UPC/UB/CSIC).

Barcelona, 2015

PhD Student:

Pablo Cerralbo Peñarroya

PhD Director:

Manel Grifoll i Colls

PhD Director:

Manuel Espino

Als meus pares, Rosa i Pepe,
i a la Judit, pel camí fet i el que tot just comença

One never notices what has been done;
one can only see what remains to be
done.

Marie Curie

Agraïments /Acknowledgments

Vull agrair d'una forma molt especial al màxim responsable de que jo comencés, i acabés, aquesta etapa, el meu director de la tesi, en Manel Grifoll. És evident que sense l'ajuda i la quantitat ingent de temps que m'has dedicat, això no hagués estat possible, així que moltes gràcies per tot: discussions, idees, correccions (algunes d'elles recurrents),... De fet, gran part de la possible rellevància científica d'aquesta investigació es deu a la teva ajuda. Tenim pendent una mariscada.

A en Manolo Espino (el co-director d'aquest treball), moltes gracies per oferir-me la possibilitat de fer aquesta tesi, les hores dedicades i la capacitat de poder guiar-me en molts instants cap on anar. De la mateixa forma, vull donar les gracies a l'altre gran responsable de que pogués començar la carrera científica al LIM, en Vicenç Gracia. Del mateix departament, zona campus nord, agrair a tots per l'ajuda i el companyerisme quan he estat de visita per la zona "alta" (Eva, Mercè, Cari, Marc, ...). Voldria agrair de forma especial al personal d'administració: Alba, Emilia, Carme, Marisol i Genoveva. En tot moment heu fet que qualsevol de les gestions fos la cosa més senzilla possible (i sempre amb un somriure a la cara), i això tot i que soc un negat i pregunto les coses 30 cops...

Evidentment, agrair a tots els companys (i amics) del sector Barceloneta. És aquí on més hores he passat els últims 4 anys i mig. Gràcies al Juan, Irene, Fede i Jaime pels somriures de bon matí, l'ajuda amb temes de programació (bàsica eh..) i entendre el mon del LINUX i els "paths". A l'Elena per les hores compartides al despatx cara a cara, les penes i les alegries explicades i els viatges a congressos per Europa (impressionant el primer Eurogoos). Gràcies a l'Arnel, Borja i Prashant per les estones passades i els dinars (amb les corresponents galetes i dolços de sobretaula). Per no deixar-me ningú (n'han passat uns quants per aquell despatxos), gràcies a tots: Ester, Inma, Marta, Augusto, Ricardo i Jonathan.

A nivel científico, quería agradecer de forma especial a Arnoldo. Creo que para mí fuiste un input de frescor e ideas muy importante en un momento en el que no terminábamos de saber hacia dónde ir. Ha sido una gran experiencia y una forma diferente de hacer ciencia. Espero que en el futuro podamos trabajar juntos.

Una gran part de la feina s'ha centrat en la descripció a partir de mesures a la badia dels Alfacs, i sincerament han estat uns dels millor moments relacionats amb la tesi (junt amb algun moment de màxima revelació científica...). Aquí, agrair de forma especial al Joan, en Jordi i en Quim. Crec sincerament que el departament té molta sort de tenir un equip de tècnics oceanogràfics (i meteorològics) com el que té. Sou molt bons. Haurem de repetir algun arrosset amb galeres.

Volia també esmentar en aquest punt a en Jaume Piera, amb qui he coincidit en campanyes i reunions varies. L'interès i les ganes de dur a terme nous i variats projectes, així com el gran esperit científic que demostra dia a dia son molt encoratjadors.

Als amics, a tots: als ambientòlegs, menorquins, els que venien amb el pack “Soy” i ja son també dels meus, i als de tota la vida. Gràcies per les calçotades, sopars, dinars, birres i gintònics, viatges, etc.... Ho he de resumir així de ràpid perquè sinó em sortiria una altra tesi, ja ho sabeu.

Moltes gràcies a la segona família que he tingut aquests anys, en Josep i la Manoli (i en Jordi i la Montse clar!). Gràcies per acollir-me i tractar-me com si fos un dels vostres (mentre no sigui carnaval clar.. ;P).

Als meus, als de casa. Rosa i Pepe (mare i pare). Gràcies per TOT, qualsevol cosa que digui quedarà curta. Poc més puc dir, i més després de l'últim ensurt que hem tingut. Això si, prou excursions al Montgrí, i més viatges per Paris i dinars d'estrelles...

I finalment, a la Judit. Les raons? Ja les saps. Per ser qui ets i deixar-me compartir tot això amb tu. Ara tot just arribem al final d'un camí i en comencem un de nou. Que fem? Som-hi? Ja veurem on ens durà.....

Summary

Using both observations and modelling tools, it is investigated the main hydrodynamic response mechanisms of a microtidal and shallow bay in the Mediterranean Sea: Alfacs Bay.

Main objectives are considered using different time-scales approximations: from high frequency processes (corresponding periods of 1 to 3h), through tidal and daily wind influence, to low frequency and average response (days and weeks).

Results revealed a clear circulation dominated by seiches on high frequency scales, demonstrating the effects on water column stratification. Moreover, spatial wind variability becomes a relevant mechanism influencing the hydrodynamic response under energetic wind events. The response at low frequency scales is determined by the combined effects of winds and gravitational circulation mainly due to the freshwater inputs.

Both Bay's geometry -shape and shallow depths- and stratification are found to be much relevant in all the hydrodynamics mechanisms analysed. The results allow the better understanding of main hydrodynamics patterns of an area with strong anthropogenic pressure and notably social and economic role in the region, and being applicable to similar domains. As such, these bodies of water are exposed to several environmental and management problems and need to be considered for pollution protection issues.

Key words: *Alfacs Bay, hydrodynamics, seiches, winds, mixing, low-frequency processes, numerical models, ROMS.*

Resum

A partir de l'ús combinat d'observacions i eines de modelat numèric s'han investigat els principals mecanismes de resposta hidrodinàmica en una badia micromareal i poc profunda de la mar Mediterrània: la badia dels Alfacs.

Els principals objectius van des de l'anàlisi de processos físics d'alta freqüència (períodes associats de 1 a 3h), passant per l'anàlisi de les marees i els vents, fins l'anàlisi del comportament hidrodinàmic de baixa freqüència.

Els resultats mostren un clar domini de les seiches en les corrents d'alta freqüència, demostrant la influencia d'aquest fenomen sobre l'estratificació en la columna d'aigua. La variabilitat espacial dels vents esdevé un mecanisme rellevant alhora de considerar la resposta de la badia als esdeveniments més energètics. Finalment, la resposta en baixa freqüència es veu fortament condicionada per la interacció entre els vents i la circulació gravitacional induïda per les aportacions d'aigua dolça.

Tant la geometria de la badia (forma i escassa profunditat) com l'estratificació tenen una importància cabdal en els mecanismes hidrodinàmics descrits. Els resultats obtinguts permeten conèixer millor la hidrodinàmica en una zona de forta pressió antropogènica i amb una rellevància social i econòmica important , sent les conclusions extrapolables a dominis similars. Així mateix, aquest tipus d'entorn es troba contínuament exposat a impactes ambientals i problemes de gestió, i el correcte coneixement de les seves característiques resulta indispensable per a les corresponents polítiques de protecció i conservació.

Paraules clau: *Badia dels Alfacs, hidrodinàmica, seiches, vents, processos de barreja, processos de baixa freqüència, model numèric, ROMS*

Publications

Peer Reviewed International Journals

Cerralbo, P., Grifoll, M., Valle-Levinson, A., Espino, M., 2014. Tidal transformation and resonance in a short, microtidal Mediterranean estuary (Alfacs Bay in Ebre delta). Estuar. Coast. Shelf Sci. 145, 57–68. doi:10.1016/j.ecss.2014.04.020

Cerralbo, P., Grifoll, M., Moré, J., Bravo, M., Afif, A.S., Espino, M., 2015. Wind variability in a coastal area (Alfacs Bay , Ebro River delta). Adv. Sci. Res. 12, 11–21. doi:10.5194/asr-12-11-2015

Cerralbo, P., Grifoll, M., Espino, M., 2015. Hydrodynamic response in a microtidal and shallow bay under energetic wind and seiche episodes. J. Mar. Syst. 149, 1–13. doi:10.1016/j.jmarsys.2015.04.003

Conference contributions

Cerralbo, P., Grifoll, M., Cateura, J., Puigdefàbregas, J., Sospedra, J., Espino, M., 2012. Respuesta hidrodinámica a un evento de brisa marina en la bahía dels Alfacs (Delta del Ebre). EOF 2012 - II Encuentro Oceanografía Física Española: Conocer los Mares para el Beneficio de la Sociedad. Poster. Madrid, Spain.

Cerralbo, P., Grifoll, M., Valle-Levinson, A., Espino, M., 2013. Tidal propagation in a Mediterranean microtidal bay (Alfacs). CIESM-The Mediterranean science comission (40th edition). Oral and poster presentation. Marseille, France.

Cerralbo, P., Grifoll, M., Espino, M. 2014. Hydrodynamic characterization of a microtidal estuary during summer in the NW Mediterranean Sea. EGU 2014 - European Geosciences Union General Assembly 2014. Oral Presentation

Cerralbo, P., Grifoll, M., Espino, M. 2014. Spatial wind heterogeneity in coastal areas and its effects on water circulation (The Alfacs Bay case, Ebre Delta). 14th EMS Annual Meeting & 10th European Conference on Applied Climatology (ECAC). Oral and Poster presentation.

Cerralbo, P., Grifoll, M., Espino, M. 2015. Procesos de mezcla asociados a ondas de resonancia en geometrías semi-encerradas (el caso de la bahía dels Alfacs, Delta del Ebro). XIII Jornadas Españolas de Ingeniería de Costas y Puertos. Avilés. Oral Presentation.

Publications under preparation

Cerralbo, P., Grifoll, M., Espino, M. Modelling circulation patterns induced by spatial wind variability in small-size microtidal coastal embayment.

Cerralbo, P., Grifoll, M., Espino, M. Low Frequency response in a shallow microtidal bay.

Table of Contents

List of Figures

List of Tables

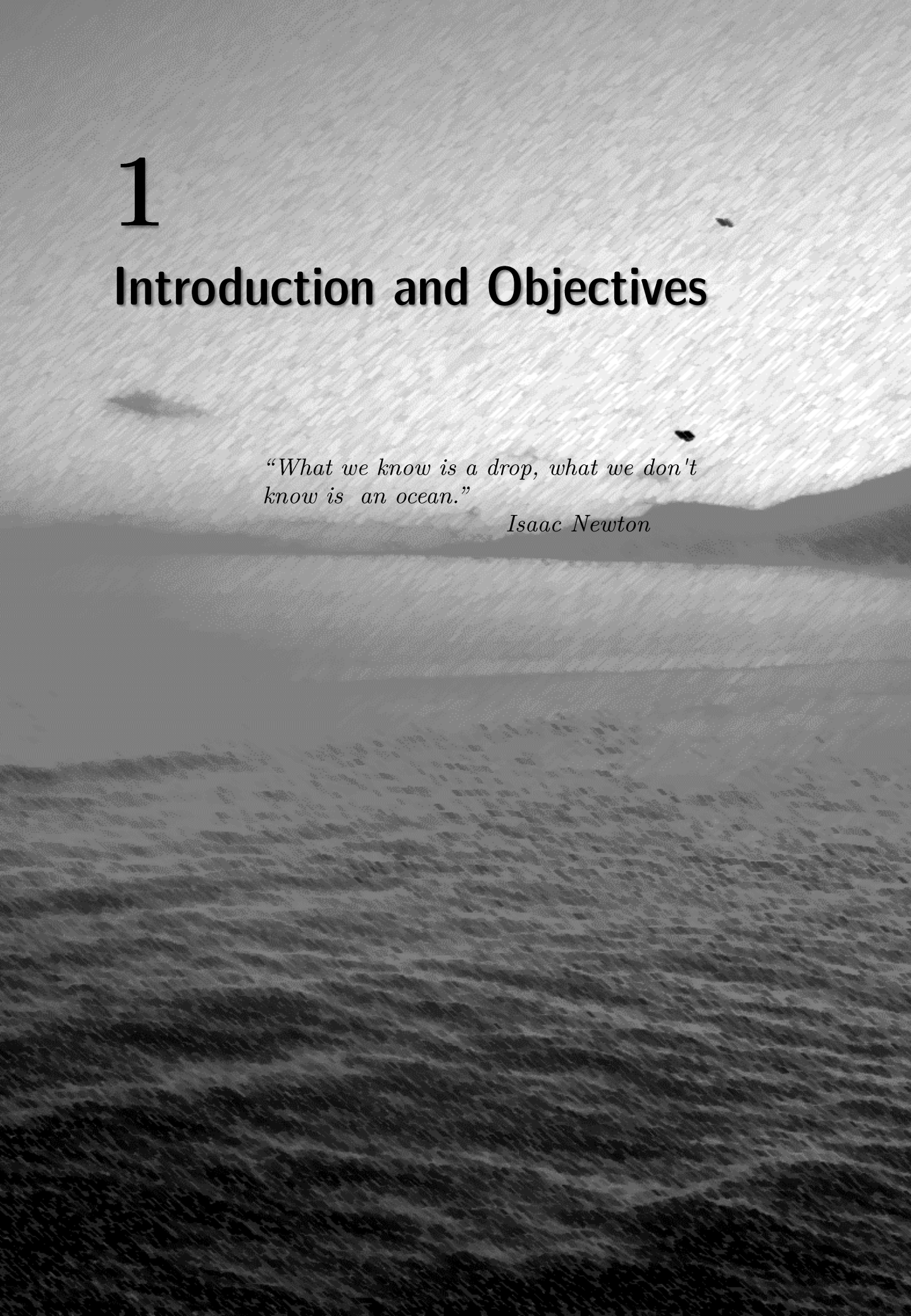

1

Introduction and Objectives

"What we know is a drop, what we don't know is an ocean."

Isaac Newton

1. Coastal Areas and Estuaries

Coastal seas are one of the most important areas of the world oceans from a human perspective. We use these areas for food supplies via fishing, as a source of nonrenewable (i.e sand and gravel extraction) and renewable resources (i.e. aquaculture); for power and transportation, as well as for waste disposal and for recreation. Moreover, half of the world's population now lives within 60 km of the coast, and as populations grow (a growth that will be predominantly in coastal areas), uses of the coastal zone will increasingly come into conflict (Jickells, 1998; Halpern et al. 2008).

One of the most characteristic features of coastal areas are the estuaries. Nowadays, the most widely and accepted definition of an estuary was proposed by Cameron and Pritchard (1963): "a semi-enclosed and coastal body of water with free communication to the ocean and within which ocean water is diluted by freshwater derived from land".

Conceptually, the freshwater entering into a semi-enclosed basin establishes longitudinal density gradients that result in long-term surface outflow and net inflow underneath (estuarine or gravitational circulation). Though there is only a density difference of about 2% between fresh and sea water, it is sufficient to induce horizontal pressure gradients which affect the flow. So, in classical estuaries, freshwater input is the main driver of the long-term (order of months) circulation through the addition of buoyancy (Valle-Levinson, 2010). Occasionally, temperature can be a dominant factor when surface heating provides sufficient density differences to maintain gravitational circulation (i.e. Cheng at. 2010).

To compare different kind of estuaries a scheme of classification is required. Many different schemes are possible, depending on which criteria are used. The most common and well-known classifications are based on:

a) *Water balance*: This classification is based on the main direction of surface and water layers, which depends on the density balance between inner bay/estuary and open sea, and could be defined as a positive or invers estuarine circulation. Positive estuary is when surface water layers move towards the open sea. On the other hand, inverse circulation is established when highest densities are found inside, thus surface flow from the open sea to the inner bay is promoted (i.e. when evaporation exceeds precipitation).

b) *Geomorphology* (Pritchard 1952): It consists in a topographic classification defining three main types of estuaries: coastal plain, fjord, and bar-built. Coastal plain

estuaries were formed by the flooding of river valleys following a rise in sea level over geological time. Fjords are river valleys deepened by glaciers during the last ice age. Finally, bar-built estuaries are drowned river valleys with a high sedimentation rate. They mostly are very shallow, with depths of a few meters.

c) *Vertical structure of salinity* (Pritchard, 1952; Cameron and Pritchard, 1963): The degree of mixing between the two water layers (fresh versus saltier) within the estuary defines the salinity structure and plays an important role in the characteristics of internal water exchange and circulation. Options are: salt-wedge, strongly stratified, weakly stratified and well-mixed. Salt-wedge estuary shows lighter freshwater floating on top of the denser saltwater. The vertical salinity distribution (and thus density) has a very sharp jump at the depth of the interface between the two layers. Weakly stratified (partially mixed) occurs when the tidal range is sufficiently large to produce turbulent mixing between the two layers in the estuary, then the salinity gradient is less steep than in the highly stratified estuary but due to the salt balance there still has to exist a two-layer flow. Well-mixed means that the vertical salinity differences become negligible, stablishing a longitudinal salinity gradient from head to mouth of the estuary.

Most of the estuarine regions cannot be classified in a fixed way, because these kind of environments are continually evolving and changing in function of river flow (or freshwater inputs), marine processes and weather patterns. In fact, same estuary may include areas with completely different behavior (i.e. mixed on the mouth and stratified on the head). Moreover, all these physical forcing and the corresponding hydrodynamic response involves a wide range of characteristic time scales: from few seconds (capillary and wind-waves due to wind), hours (seiches, winds and tides), days (diurnal tides, storms …) to months (gravitational circulation) and even years (sea level rise) (summarized in Fig 1.1b). With an introductory purpose, the main forcings involved in the heat, salinity and momentum balance of a semi-enclosed water body are schematized in Fig 1.1a. Each estuary responds differently, with particular balance of magnitudes and time-scales. For instance, wind driven circulation presents significant differences in shallow estuaries (e.g. Noble, 1996) in comparison to deep ones (e.g. Rockwell Geyer et al. 2000). Moreover, the water current modulation of the bathymetry and the coastal constrain introduces non-linearity and transition features in the hydrodynamics which are restricted by the estuary length (e.g. Luettich et al. 2002). On the other hand, the role that plays the hydrographic structure in the water current (stratification) also alters the water current response, as described in Whitney and Codiga (2011), showing how the wind flow response under strong stratification shows differentiate behavior in comparison to well-

mixed estuary. At the same time, the salinity balance downstream induced by freshwater inputs leads to horizontal baroclinic pressure acting at a relative large time scales in comparison to wind-induced and tidal circulation. In that sense, the relevance of each mechanism obviously would depend of the specific location.

All these complex estuarine variability is summarized by Ketchum (1952): "The paradox thus lies in the recognized fact that estuaries are similar enough to constitute an integrated field of investigation, but at the same time estuaries are so different in details that generalizations are dangerous".

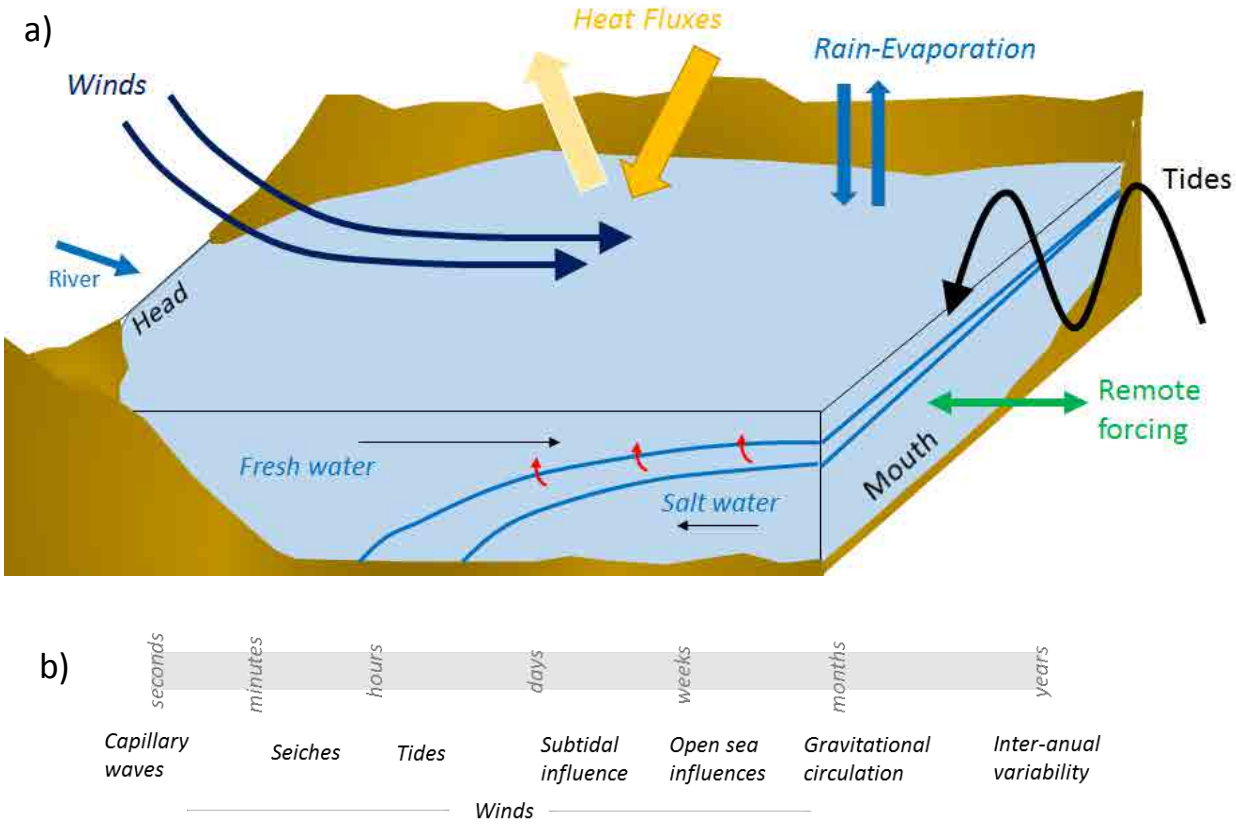

Figure 1.1. a) Conceptual scheme of the estuarine circulation in a salt-wedge estuary. Main forcing are shown: tides, winds, freshwater and heat fluxes. As fresh water is less dense than saltwater, it moves above the seawater. A sharp boundary is created between the water masses, with fresh water on top and a wedge of saltwater on the bottom. Some mixing does occur at the boundary between the two water masses. b) A diagram of the main processes and their corresponding time-scales is shown.

Additionally, different economic, touristic and social actors interact in estuarine environments. Considering the multiple factors that have an impact over estuarine regions, it is essential an exhaustive study in each particular case in order to define the spatial and temporal variability and to understand its general behavior in an accurate way.

The study area of this thesis is Alfacs Bay. This area is part of the Ebro Delta (NW Mediterranean Sea), which extends around 25 kilometers offshore and forms two semi-enclosed bays (Alfacs to the south and Fangar to the north) on the lateral margins (Fig 1.2). The superficial hydrology of the Delta is an artificial system strongly conditioned by the rice cultivation (Canicio and Ibañez, 1996). Both bays receive direct freshwater input (loaded with nutrients) from the drainage channels of rice fields in the surrounding area 9 to 10 months per year. Therefore, these bays are considered as an estuarine environments due to the interaction of freshwater from the rice fields and the saltier water from the Mediterranean Sea. Moreover, this region stands out by a well-known and recognized ecologic and economical relevance, being most of the economy of the area depending on the natural and touristic resources of the Delta (rice fields, aquiculture, tourism, fisheries …) (Slootweg et al. 2008).

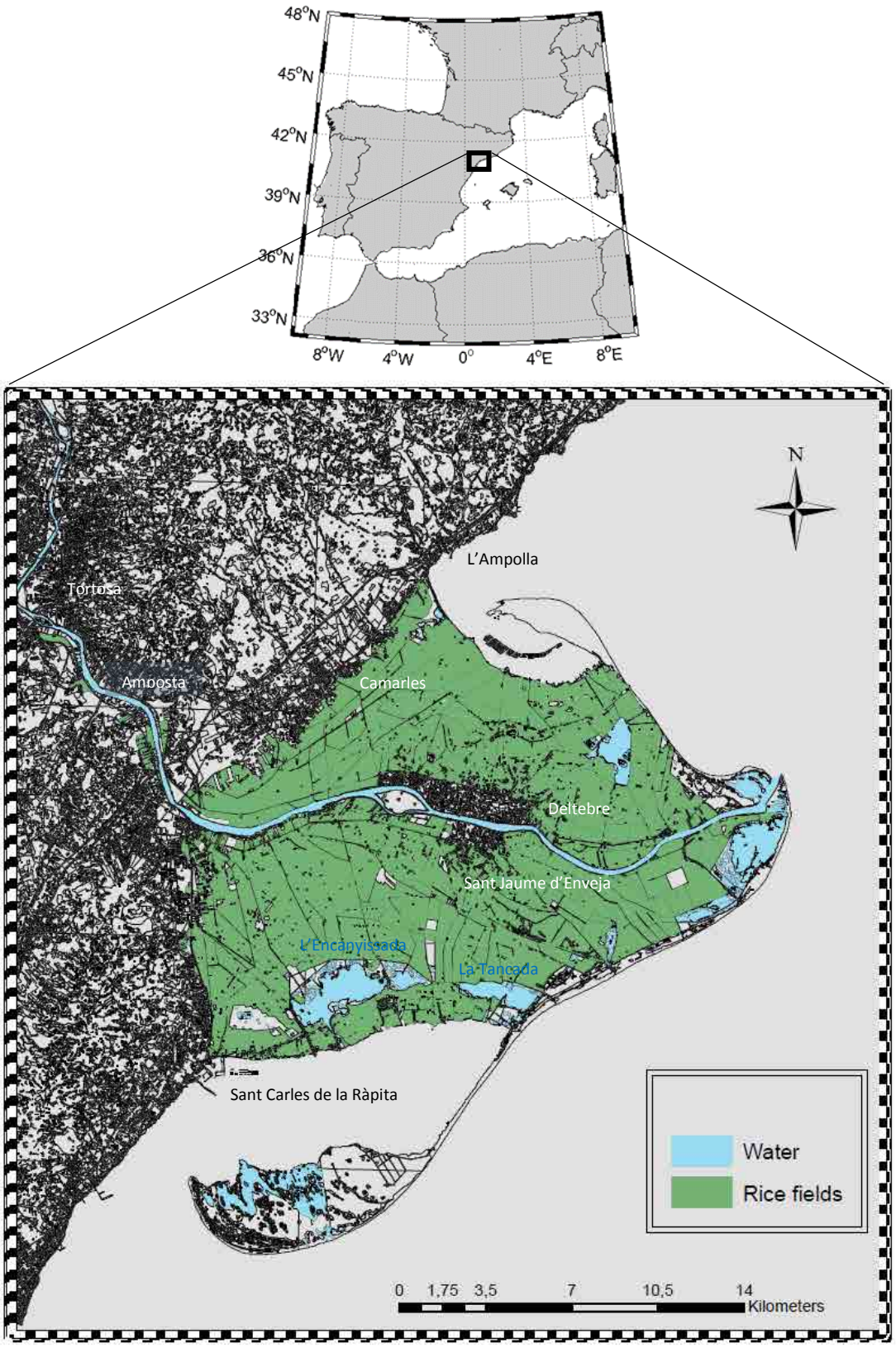

Figure 1.2. Land uses map of the Ebro Delta for the year 2009. Only main water inland bodies (in blue) and rice fields are shown in color. The raw data comes from CREAF (*Centre de Recerca Ecològica I Aplicacions Forestals*), Generalitat de Catalunya.

2. Study area

In order to explain some of the main peculiarities and characteristics of the area of study, it is important to take into consideration the river and the area where it is located, the Ebro Delta. Then, description of the main geographic, economic and physical characteristics of Alfacs Bay, and a review of the state of the art on the hydrodynamics are summarized.

2.1 The Ebro River and the Delta

The Ebro River is the second large river in the Iberian Peninsula (after Duero), draining a basin of approximately 85.530 km^2, and finally debouching into the Mediterranean Sea at Tortosa. The river regime is defined with yearly average flow of 425 $m^3 \cdot s^{-1}$ (Batalla et al. 2004), although varies largely with seasons, with maximum flows in February-April (662 $m^3 \cdot s^{-1}$) and minimum in August (135 $m^3 \cdot s^{-1}$) (Mestres et al. 2003). The river flow is highly regulated with 187 reservoirs with total capacity equivalent to ~60% of the annual runoff. These dams have supposed a reduction of more than 99% in sediment transport, a virtual suppression of peaks (Ibañez et al. 1996) and a reduction of the seasonal differences, as shown in Fig 1.3 (Curcó, 2006) .

The Ebro Delta, located on the Spanish western Mediterranean coast (Fig 1.2), occupies 320 km^2 and is the second largest wetland area in the western Mediterranean (after the French Camargue). It dates from the end of the last ice age when eustatic changes lead to its growth, with the deltaic progradation only occurring during episodes of relative stability between sea level variations (Maldonado, 1972). Canicio and Ibañez demonstrate that the origin of the Ebro Delta is as old as other Holocene Deltas, and suggested that the tip of the Delta 6000 BP was not farther landward than the present fluvial island of Gracia (Canicio and Ibañez, 1999). As a consequence of the drastic decrease in river sediment discharge in the last century (i.e. Mequinença, Mediano and Ribarroja dams build during 1968 and 1969, with capacities of ~1000, 500 and 136 hm^3 respectively), the action of marine processes dominates the present evolution of the delta coast, becoming a wave-dominated coast (Guillén and Palanques, 1997). The main factors controlling the re-shaping of the Delta are waves (short-time scales) and mean water level variations (long-term) (Jiménez et al. 1997). In that sense, Alvarado-Aguilar et al. (2012) defined the Delta as highly sensitive to changes in sea level, proposing that between 45-61% of the areas will be affected considering low and high IPCC (Intergovernmental Panel on Climate Change) scenarios. Moreover, the existing subsidence (vertical sinking from compaction) rates will lead to flooding of 26% of the Delta by 2100.

They propose the adaptation to sea level rise as a plausible option to mitigate these effects. Other authors (Ibañez et al. 1997) proposed diverting freshwater and sediment from the river to the wetlands, in order to achieve accretion rates as high as relative sea level rises rates (i.e. by-passing sediments from Mequinença and Ribarroja dams).

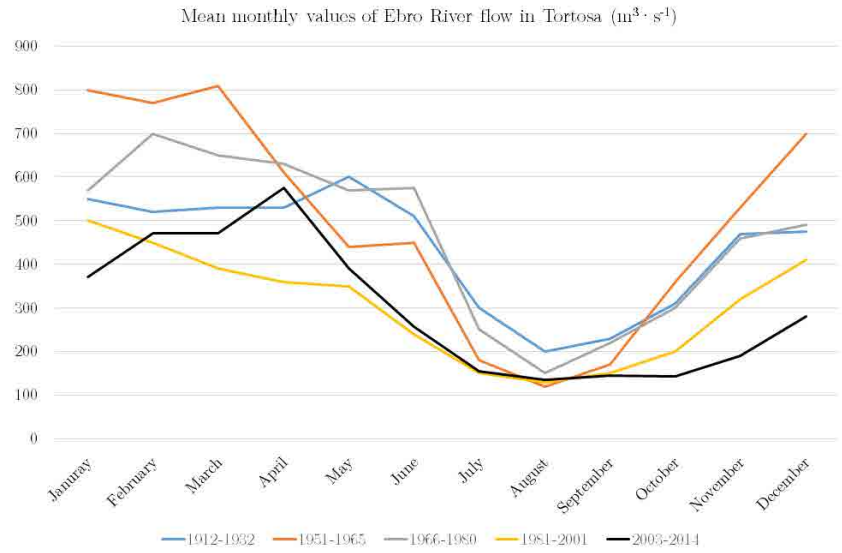

Figure 1.3. Historical evolution of the river discharge since 1912 and its monthly distribution in different periods. Data between 1912 and 2001 adapted from Curcó 2006. Data between 2003 and 2014 from "*Confederación Hidrográfica del Ebro*" (http://www.saihebro.com).

From the socio-economic point of view, the total population of the Delta is 55.928 (Idescat, data from 2011) and are distributed in 7 villages: Amposta, Sant Carles de la Rapita, Deltebre, l'Aldea, Camarles, Sant Jaume d'Enveja and l'Ampolla. The main economic activities are agriculture, fisheries, aquiculture and tourism. According to Slootweg et al. (2008), agriculture represents 50% of the total economy of the region (estimated in 120 million euros), followed by tourism (25%), fisheries and aquiculture. Agriculture activities focus in rice cultivation, which occupies around 60-65% of the deltaic plain. In Fig 1.2 the extension of the rice fields in the Ebro Delta is shown. Rice production (≈120.000 tonnes $\cdot$ yr^{-1}) in the Delta accounts for 98% of total production in Catalonia and is the 3rd most important of Europe (Slootweg et al. 2008). On the other hand, the only relevant industry in the area is the extraction of sea salt ("Trinitat saltworks") with approximately 70.000 tons per year. Sea fishing, centered on the ports of L'Ampolla, Deltebre and Sant Carles de la Ràpita (locations in Fig 1.3); represents around 10% of the total catch for Catalonia. On the other hand, inland fishing is carried out in the inner lagoons of L'Encanyissada, La Tancada,

El Canal Vell and Les Olles, still following the traditional draw system, and being one of the main sites for glass eel capture along the Mediterranean coast of the Iberian Peninsula (Lopez and Gisbert, 2009). Nowadays, the importance of aquiculture is increasing, focused on the cultivation of mussels (*Mytilus galloprovincialis*) and oysters (*Crassostrea gigas*) on both bays (Alfacs and Fangar), with a total amount of 3000 tones $\cdot$ year^{-1} (Slootweg et al. 2008). Mussels are cultured in suspension on a total of 166 fixed rafts, with 90 farms in Alfacs and 76 in Fangar (Galimany et al. 2011). The growth and mortality of mussels cultured in both bays (mostly in Alfacs) are affected by the high seawater temperatures reached during July and August, stopping the growth and increasing mortalities of adults and juveniles. Moreover, episodes of toxic algal blooms or toxic shellfish in the nearby harvesting areas may impossibility their commercialization (Ramón et al. 2005).

From the ecological point of view, this environment is located at the interface between terrestrial and coastal areas, being the second most important west Mediterranean wetland (second in the Iberian Peninsula after Doñana). The low elevation of the Ebro Delta -with about 50 % of the surface under 0.5 m above mean sea level (Alvarado-Aguilar et al. 2012)- and abundance of water and nutrients have created an ideal habitat for wetland ecosystems, with high primary productivity and assisting in functions such as nutrient removal and sediment retention (Ibáñez et al. 2010). The natural park has been a Ramsar site (Convention on Wetlands of International Importance, www.ramsar.org) since 1993 and it forms part of the European Union`s Natura 2000 Network. Rice fields (flooded several months a year), together with the lagoons, have contributed to the biodiversity of the Delta, in particular to the presence of many species of aquatic birds. Of the 600 species of birds described in Europe, 350 have been sighted here (Council of Europe, 2005). In addition, deltaic systems also serve as critical habitat for many species of wildlife and fisheries (Prat and Ibáñez 1995). Due to these high natural values, about 7.800 ha of the deltaic surface has been protected under the designation of Natural Park (http://parcsnaturals.gencat.cat/es/delta-ebre), including a wide typology of locations as freshwater, brackish and saline lagoons, salt marshes and coastal sandy areas.

On the other hand, several authors have investigated the oceanographic processes on the adjacent shelf, observing that the mesoscale and regional circulation also plays an important role on the circulation in front of Ebro Delta. In general terms, the waters of the northwestern region of the Mediterranean Sea follow the continental shelf break in a flow that appears to be linked to a permanent shelf/slope density front (Font, 1990; Millot, 1999). The Ebro Delta is located on a transition area between a narrow stretch of continental shelf (approximately 10 km wide) in the north, and a broader region (about 50 km wide) in the

south (Fig 1.4 shows the isobaths in front of the Delta at 100m interval). Salat (1995) shows how the shelf/slope current is deflected in front of Ebro Delta, where the slope orientation changes at the beginning of the wide continental shelf. Then, the circulation over the wide shelf (south lee) is anti-cyclonic, generating a clockwise eddy in the lee side of deltaic forms (Fernández-Nóvoa et al. 2015). This circulation is dominated by local winds (Font, 1990) and inertial oscillations (Salat et al. 1992), acting as a trap for the Ebro River discharges (Salat, 1995). The interaction of the river plume with general circulation shows a southward displacement of the plume even in the absence of wind (more than 70% of the plume is located south of the river mouth under any wind condition) (Fernández-Nóvoa et al. 2015).

2.2 Alfacs Bay

2.2.1. Location and main dimensions

As mentioned above, Alfacs Bay is located in the Ebro Delta. This area is highly influenced by the water coming from the rice fields that are in the surroundings. On the right margin of the Delta there are a two completely isolated systems: one for the irrigation (300 km of channels), and another for the drainage (600 km) of the rice fields. These drainage channels debouch into and outside the bay (to the open sea). In that sense, Alfacs Bay receive direct freshwater input from the drainage channels of rice fields in the surrounding area 9 to 10 months per year. The flow of water is mainly powered by gravity, although on some occasions (mostly during September when the rice cut and typical storms of the area coincides) the use of pumps is necessary. The mean drainage flow is considered to be equal to 0.7 $l \cdot ha^{-1} \cdot m^{-2}$ (http://www.comunitatregants.org/). Although various authors have suggested that the total amount of water from drainage channels that receive Alfacs Bay is still not clear. Canicio and Ibañez (1996) studied the hydrology of the system and defined an approximately 10 $m^3 \cdot s^{-1}$ of freshwater fluxes through the drainage system to the bay during the wet season (+ 2 $m^3 \cdot s^{-1}$ from l'Encanyissada coastal lagoon). During dry season, the total amount of freshwater discharge is almost impossible to take into account because it is only related to Ullals (underground water overflowing in natural wells with $1m^3 \cdot s^{-1}$). Moreover, some authors have also pointed out the presence of non-described freshwater inputs through the subsoil (Camp and Delgado, 1987) which could influence the winter hydrography of the bay. Nowadays, and since 1999 with the application of the agro-environmental measures from the European Union (Regulation CEE 1257/1999), the freshwater inputs to the bay could be divided in three periods during the year: rice fields flooded (April-September), ecological measures addressed

to favour aquatic fauna (September-January) and dry rice fields (February-April) (Serra et al. 2007).

The main dimensions of the bay could be summarized as approximately 16 km long and ≈4 km wide, with an average depth of about 4 m and maximum of 6.5 m, in the middle of the bay. The mouth is about 2.5 km wide, with central channel of 6.5m and shallow shoals of around 1-2m on both sides (Fig 1.4).

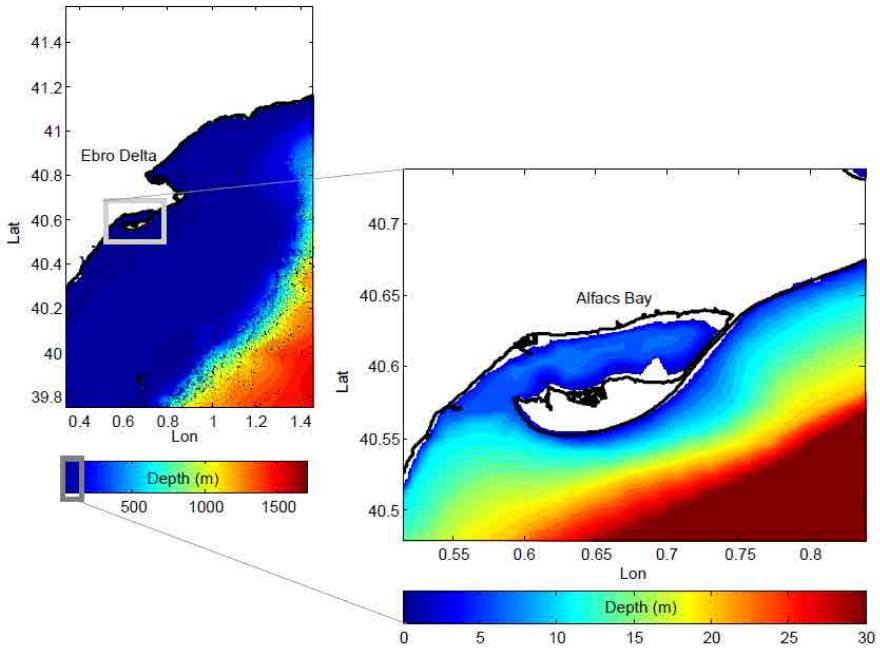

Figure 1.4. Bathymetry for the Ebro's Delta shelf (on the left) and the Alfacs Bay (right image). Image a shows the transition area between a narrow stretch of continental shelf (approximately 10 km wide) in the north, and a broader region (about 50 km wide) in the south. The colorbars means for different scales.

The sea bed is made of muddy (with largest percentages in the middle of the bay) and silty sediments are present close to the freshwater outflows (Palacin et al. 1991).

Alfacs Bay can be geomorphologically classified (Pritchard 1952) as a bar-built estuary formed by the sediment of the Ebro River in conjunction with near shore dynamics. The bay is surrounded by rice fields on the north, and sand beach closing it on the eastern side. Monstià Serra, with maximum altitudes around 700m, closes the bay on the north-west side.

2.2.2 Climatology

As mentioned above, estuarine behavior is highly influenced by environmental conditions, and there are several climatological aspects that may have an impact over Alfacs bay hydrodynamics. These are:

- Winds: The synoptic winds on the Catalan coast are affected by orographic constraints, such as the blocking winds of the Pyrenees that promote tramuntana (N) and mistral (NW) winds over some areas, and the wind channeling due to river valleys (Sánchez-Arcilla et al. 2008). Winds in the bay have been characterized as having a northwestern and southwestern predominance (Fig 1.5), with the strongest ones coming from the NW (channelized by the Ebro River valley) (Camp, 1994; de Pedro, 2007; Llebot et al., 2013). Furthermore, some authors have reported a high spatial heterogeneity of the wind fields inside the bay (Camp, 1994) which could influence the hydrographic and hydrodynamic response.

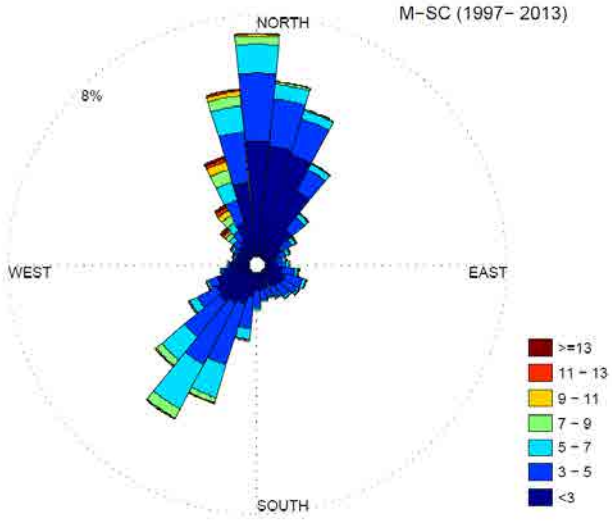

Figure 1.5. Wind rose from 1997 to 2013 showing the average hourly winds in M-SC. All data comes from "*Xarxa d'Instruments Oceanogràfics i Meteorològics*".

- Rainfall: The mean precipitation measured in Tortosa between 1961 and 1986 (26 years) was 565 mm $\cdot$ year^{-1} (Sainz-Elipe et al. 2010). During that period, the driest months (<40mm $\cdot$ month^{-1}) are January-February and July-August. On the other hand, the maximum rainfalls were observed during May and September-October. Mean annual evaporation in the region is about 1000 mm $\cdot$ year^{-1} (*Instituto Geográfico Nacional*, www.ign.es). Therefore, evaporation clearly exceeds precipitation rates.

- **Temperature:** The temperature climatology (Fig 1.6a and 1.6b) shows highest temperatures measured at Sant Carles de la Rapita during July and August (weekly mean of 25ºC) and lowest during winter (weekly means of 10ºC). However, the intra-daily temperature variability is much higher, showing for example oscillations of more than 8ºC during summer (and eventually higher during spring period).

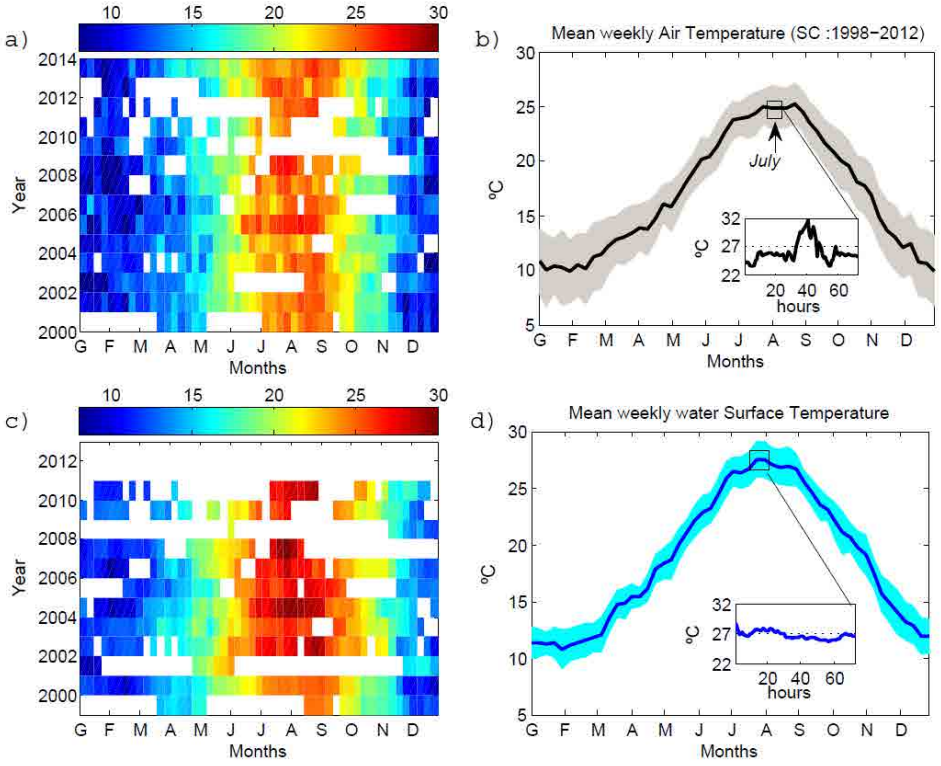

Figure 1.6. Seasonal distribution of weekly mean (from hourly data) air temperature (a) and surface water temperature (c) measured in Sant Carles de la Rapita during the period between 1998 and 2012. Images b and d shows the mean value (thick lines) and the shaded area represents the corresponding deviation from mean values (standard deviation). Small inner panels inside b and d shows the hourly air and surface water temperature during 17-19 th July 2005.

2.2.3 Hydrography and Hydrodynamics

Temperature water observations at the inner harbor of Sant Carles de la Rapita during the period 1998-2010 are summarized in Fig 1.6c and 1.6d. Maximum weekly mean values reaches values around 28ºC. During winter, minimum temperatures are around 10-12ºC. Similar results were observed on the inner bay during period 1990-2004 (Llebot et al. 2011), revealing that the deep layer was warmer than the shallow layer during the fall and winter months and

colder during spring and summer. The general hydrography of the Alfacs Bay has been investigated in the past defining it as a salt-wedge estuary (Camp and Delgado, 1987; Camp, 1994), with a persistent structure throughout most of the year with a salty layer in the bottom and a freshwater layer on top due to freshwater inputs (observations in inner bay and close to the northern margin). Bottom salinity ranged between 31 and 36 psu in the shallow layers with the higher salinities during the closed channel period (Llebot et al. 2011). This stratification prevails, although a well-mixed water column has been observed during some windy events (Camp and Delgado 1987). Residence time was estimated in Camp (1994) using a mass balance and mean flows from the observations through the variations on the typical hydrographical structures. They conclude that residence times oscillates between 10 to 14 days respectively during open-channel season. The reduction of freshwater flux during the closed channel season reduces the exchange of water with the Mediterranean, increasing the residence time of freshwater instead of raising salinity. Berdalet et al. (2014) using numerical model found similar residence time (although defining it as the time for which at least 50% of the particles remain in the bay), and strongly determined by the estuarine circulation induced by freshwater inputs (residence time was around 4-5 times more during closed channels season). On larger time-scales, Solé et al. (2009), using Huang's empirical mode decomposition analysis on meteorological and hydrographic time series, found that the drainage channels were the main agents that control the observed stratification at seasonal scales.

The analysis of currents was firstly presented in Camp (1994), with a current meter in front of the bay mouth (close to harbor dock) showing that the mean direction of the flow was along the axis of the bay. Moreover, he observed a periodicity of 3h in the currents. DePedro (2007) through current observations (current meter at 4.5m on the bay mouth) and meteorological data found small correlation between winds and currents and define the density gradients as the main circulation forcing. Recently, Llebot (2010) and Llebot et al. (2013) used numerical modeling to analyze the hydrodynamics during characteristic wind events and revealed the relative importance of winds and gravitational circulation using scaling factors such as the Wedderburn number. Observations on a central point of the bay (first time that currents are measured at the entire water column in Alfacs Bay) also revealed punctual reversals on the estuarine circulation due to sea breezes.

The role of rotational effects in a barotropic ocean is determined through the Rossby Radius of Deformation (R_r) as $R_r = (\sqrt{g \cdot h})/f$, being h the water depth, g the gravity (=9.81 m $\cdot$ s^{-2}) and f the Coriolis parameter (equal to 10^{-4} s^{-1} at latitudes of 45º). For depths of 4m, in Alfacs Bay the R_r is around 100km, much bigger than the bay dimensions. However, considering the

observed stratification Llebot et al. (2013) obtained the Internal Rossby Radius of Deformation $R_{ri} = (\sqrt{(\Delta\rho/\rho) \cdot g \cdot h_1})/f$, being $\Delta\rho$ the density gradient, ρ is the density of water and h_1 the depth of the surface water layer. They found Internal Rossby radius of deformation of 1-4 km, thus indicating the relevance of Coriolis in the circulation influenced by buoyancy effects in Alfacs Bay.

The most accurate information on tides in the bay comes from the annual reports of the *Xarxa d'Instruments Oceanogràfics i Meteorològics* (known by the acronym XIOM and described in detail in Bolaños et al. 2009). Analyses of yearly sea-level time series in Sant Carles de la Ràpita harbor since 1998 show that the main harmonics, in order of importance, are K_1, M_2, O_1, P_1, S_2 and N_2. They define the form factor taking into account the main diurnal and semidiurnal tidal harmonics as follows:

$$F = \frac{K_1 + O_1}{M_2 + S_2} \tag{1}$$

Bolaños et al. (2009) found F values of around 1.3. Therefore, the tidal regime in Alfacs Bay can be described as a mixed tide with semidiurnal dominance. Using residual analysis (difference between observations and tidal harmonics), they also found oscillations of around 3 h in some instances. These oscillations were also observed by Camp (1994) in observations of currents in the bay mouth using spectral analysis techniques (and defining them as "seiches"). Despite all these studies, tidal and other bay-scale wave propagation behavior in Alfacs Bay have not been analyzed in detail.

The interaction between tides and freshwater fluxes was analyzed in Llebot (2010) through the dimensionless Estuarine Richardson number. This balance determines whether the bay is well-mixed o remains stratified. In this case the freshwater inputs are considered as a source of buoyancy ($\Delta\rho \cdot g \cdot Q$), where $\Delta\rho$ is the density gradient and Q the freshwater inflow. The destabilizing component (mixing) is given by ρ (density of water), W (estuary width) and U_t (the root mean square velocity due to tide generated currents).

$$Ri_E = \frac{\Delta\rho \cdot g \cdot Q}{\rho \cdot W \cdot U_t^3} \tag{2}$$

When Ri_E is very large the estuary will be strongly stratified, and when Ri_E is small the estuary will be well mixed and the stratification presence can be neglected. Fischer et al. (1979) proposed the transition range between 0.08 (lower values indicates well mixed estuary) and 0.8 (higher values indicates stratification). Considering only tides as a mixing mechanism, Llebot (2010) found that for Alfacs Bay the Ri_E was always much higher than 0.8, thus indicating strongly stratified system.

The importance of the bay in terms of biological and ecological perspectives is demonstrated due the amount of studies on the nutrients and biogeochemical cycles (Delgado, 1989; Palacin et al. 1991; Palacín et al. 1992), the presence of sea-grass *Cymodocea nodosa* (Perez et al. 1994), fishes, and analysis of aquaculture of molluscs and their productivity (Galimany et al. 2011). On the other hand, several authors have described the presence of HABs (Harmful Algal Blooms). For example, a recurrent annual bloom of *Gyrodinium corsicum* (Delgado, 1998) are accompanied by the death of fish in aquaculture ponds (*Sparus aurata*), raft cultures of mussels (*Mytilus galloprovincialis*) and wild fauna of the bay (Garcés et al. 1999). Other examples of HABs are described in Delgado et al. (1990) and Vila et al. (2001). These HABs (or dinoflagellates blooms) and, generally speaking phytoplankton distribution, are suggested to be related with physical parameters as salinity (Benito et al. 2015), stratification and residence times (Garcés et al. 1999; Llebot et al. 2011). For example, Llebot et al. (2011) studied how the temporal patterns of a 13-year series of chlorophyll-a and phytoplankton were related to the variability of hydrographic variables (i.e. water, temperature, salinity and stratification).

3. Motivation

Considering the relevant economic, social and ecologic role of the region, as well as the importance and direct relationship that some of the activities have with the waters of the Alfacs Bay, the main aim of this thesis is to focus on understanding and describing some of the fundamental hydrodynamic processes that occur in Alfacs Bay and the associated physical mechanisms. For that purpose, several observations and field measurements of different hydrodynamic variables (e.g. currents, sea level and winds) have been analyzed in detail. Furthermore, the application of numerical modeling allows to cover some of the gaps in the field measurements and extend the results at a general description.

The particularity of this emplacement is given by its microtidal behavior, the shallow water depths and the constant and low freshwater inputs. The introduction highlighted some of the previous investigations in Alfacs Bay, specifically considering the oceanographic field and the link between ecology and physical parameters (Camp and Delgado, 1987; Camp, 1994; de Pedro, 2007; Solé et al. 2009; Llebot, 2010; Galimany et al. 2011; Llebot et al. 2013; Artigas et al. 2014). Despite the relative extensive bibliography, several questions remain unclear.

Due to the low tidal amplitude of Mediterranean Sea, usually, the tides are not studied in detail as in other places with higher tidal amplitudes. However, the detailed knowledge of sea level variations and the corresponding behavior is important due to its influence on processes as induced tidal currents, mixing, coastal flooding and sea level rise (e.g. Alvarado-Aguilar et al. 2012).

On the other hand, the three thesis previously cited (among other research papers and technical reports) found periodicities inside the bay (co-oscillating waves). Camp (1994) suggested to investigate this phenomena in detail in order to assess their relative importance on processes as flow interchanges through the bay mouth and the cross-isopycnal mixing. As far as I know no previous research has worked on this topic.

Furthermore, the spatial wind heterogeneity over the Alfacs Bay was also described in Camp (1994), although without observational data to support it, and only based on personal experience and communications from the inhabitants of the area. In this case, both observations and numerical model allow the beginning of investigation of this topic in Alfacs bay.

Besides, whilst seasonal temperature and salinity evolution and their relation with environmental factors have been treated by previous investigations (e.g. Solé et al. 2009), the

hydrodynamic response at low frequency scales inside the bay has been not investigated yet. Additionally, the deployment of the different kinds of instrumentation allowed to confirm and investigate several processes and their corresponding mechanisms that still remained opened.

Following the scheme presented in Fig 1.1, the thesis develop a systematic description of the main hydrodynamics considering processes that affect at different time and length scales.

4. Objectives and outline of the thesis

The aim of this thesis is:

1. To investigate the tidal propagation inside the bay and the periodicities (seiches).
2. To investigate the hydrodynamic/ hydrographic response to the most energetic events (high frequency processes)
    a. Response to winds.
    b. Response to seiches.
3. To characterize the wind spatial variability and its influence on the hydrodynamic patterns.
4. To define the hydrodynamic response at low-frequency time-scales.

The structure of the thesis is as follows: chapter 2 is oriented to introduce the different field campaigns from which all the data is obtained, as well as the implementation and validation of the hydrodynamic numerical model utilized. Tidal transformation and resonance processes are described in chapter 3. The corresponding current response to tides, seiches and winds, as well as their effects on water column stratification are investigated in chapter 4. Wind spatial variability through observations, and the corresponding effects on hydrodynamic response is examined using numerical models in chapter 5. Then, the some of the low frequency scale processes are also detailed in chapter 6.

All the results presented in the chapters 3 to 6 have been obtained by the author and by other members of the research group, in the framework of the MESTRAL project. These chapters are structured as scientific papers, which can result in some reiteration but allows them being read as independent pieces.

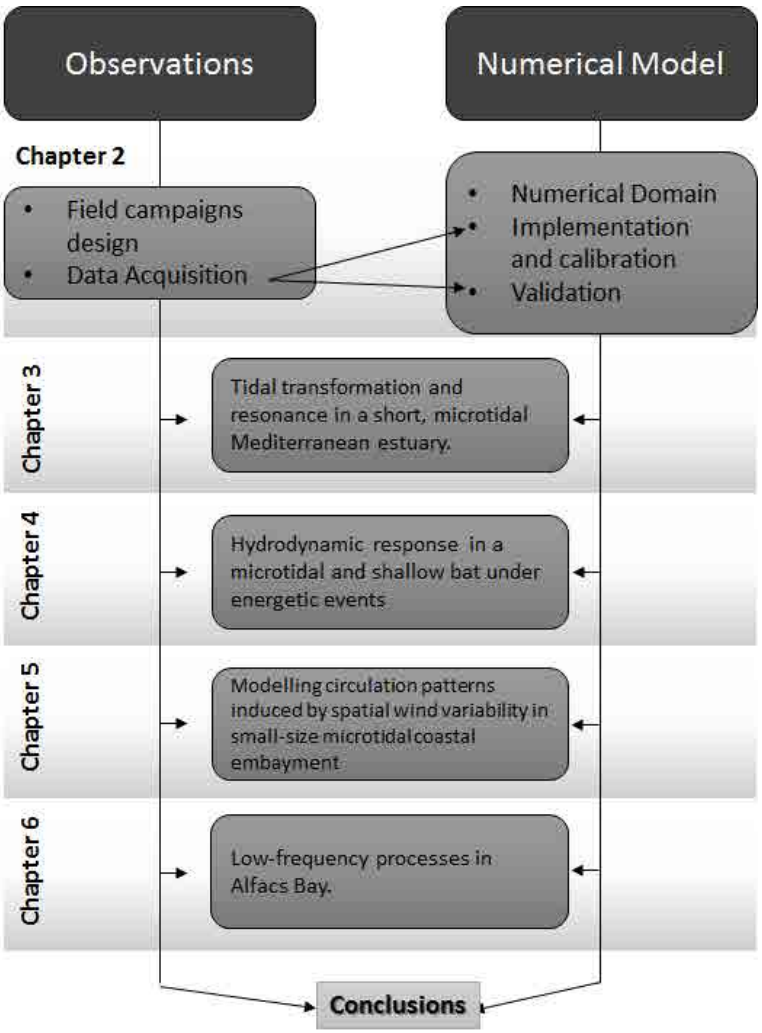

Figure 1.7. Thesis Outline Diagram.

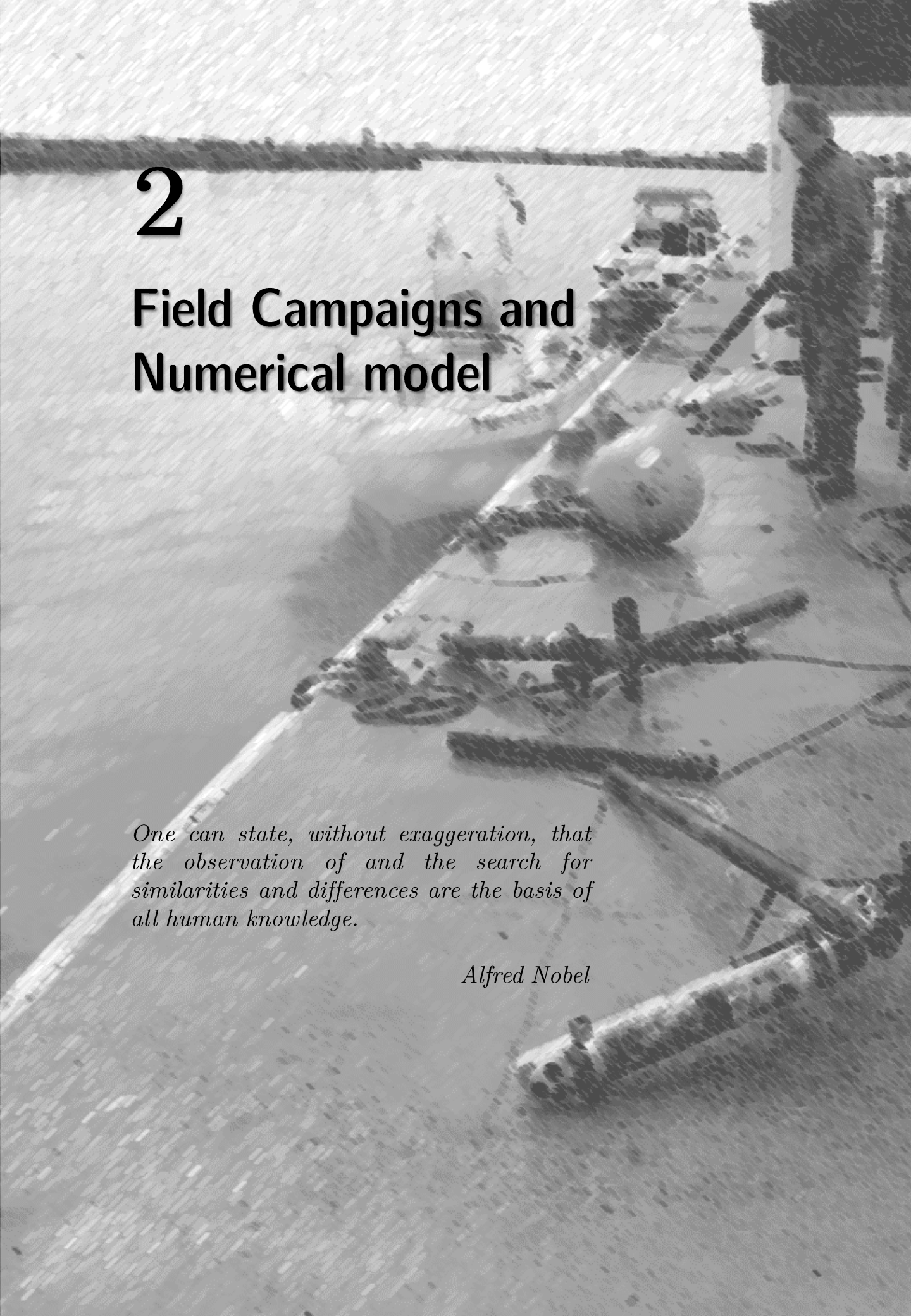

2

Field Campaigns and Numerical model

One can state, without exaggeration, that the observation of and the search for similarities and differences are the basis of all human knowledge.

Alfred Nobel

1. Field Campaigns

1.1. MESTRAL Project

The bulk of observations done through several field campaigns in Alfacs Bay during 2012-2014 and presented in this thesis have been funded by national Spanish project. This project is called MESTRAL, which stands for "Modelling and advanced observational tEchnologies to link tranSport processes, opTically-active constituents, and wateR light-field vAriability in a coastaL ecosystem". It was a collaborative project between different organizations: being the most representative the Spanish National Research Council (*Consejo Superior de Investigaciones Científicas*, CSIC) and Maritime Engineering Laboratory (*Laboratori de Ingenieria Marítima*, LIM) from Polytechnic University of Catalonia (UPC).

One of the main goals of this project was to characterize in detail the circulation patterns in Alfacs Bay, a very important ecological system not only from the scientific point of view -many research projects have been developed there- but also for its economical uses (tourism, fisheries and commercial activities). To this end, it was proposed to record a large set of observational data from different sources (current-meters, classical CTD profiles and also through autonomous vehicles, etc.) that would be used to compare with the data obtained from remote sensing image analysis and numerical models. All the field campaigns and some of the measurement systems used by LIM research group are described in this chapter. The different field campaigns are summarized in a diagram in Fig 2.1.

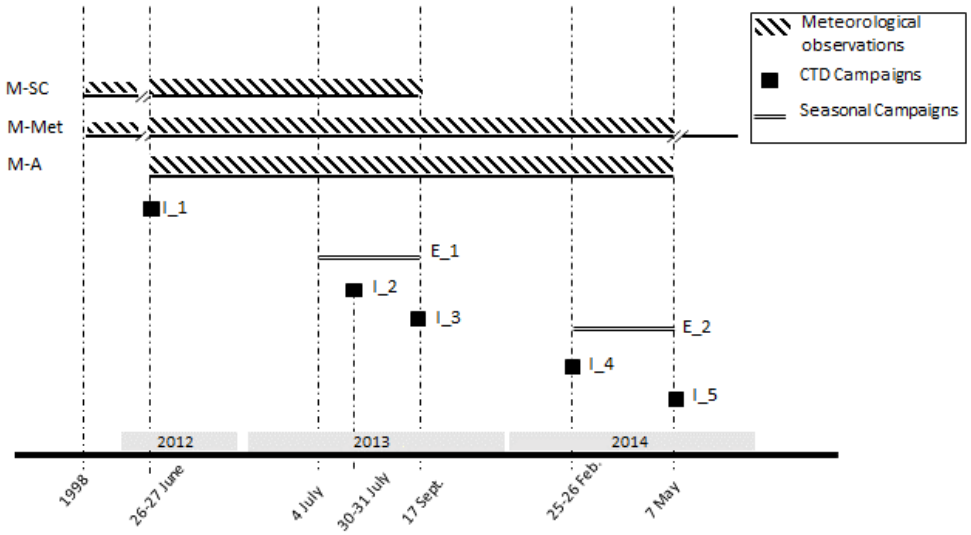

Figure 2.1. Schematic summary of the different oceanographic campaigns as well as the deployment periods for the meteorological stations. M-SC: Sant Carles de la Ràpita; M-Met: Meteocat station (IRTA); M-A: Alcanar station, I: CTD campaigns (1 or 2 days); E: Seasonal campaigns.

Even the most analyzed and discussed part of the observations are described in the following chapters, in this section the different field campaigns performed, the instrumentation deployed and their main technical setting and characteristics are detailed.

1.2. CTD Campaigns

From June 2012 to May 2014 five short time-length (1 or 2 days) oceanographic campaigns were done in Alfacs bay. The variables recorded were temperature and salinity (and derived density).

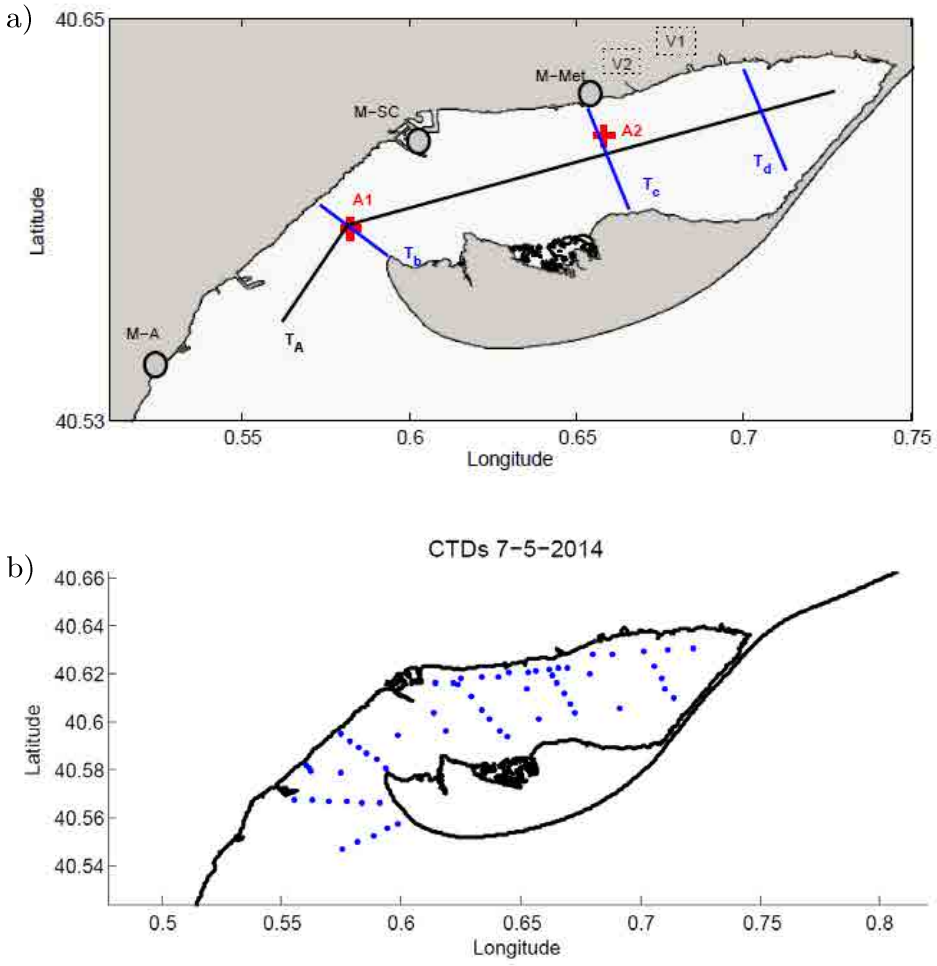

Figure 2.2. a) Location of the main measurement points. Gray circles shows the location of the three meteorological stations: M-A (Alcanar), M-SC (Sant Carles de la Ràpita), M-Met (IRTA, Servei Meteorologic de Catalunya). Red crosses shows mooring locations A1 and A2. Black line for the longitudinal transect (T_A) and blue lines for the cross-shore transects (T_b, T_c and T_d). Dashed squares shows the V1 and V2 locations. b) Blue dots shows the location for all the CTD profiles performed during I-5 campaign (7^{th} May 2014).

For temperature and salinity we used two Conductivity, Temperature and Density profilers (CTD hereafter) Sea-Bird Electronics (SBE 19plus). Generally, and when it was possible, both

CTDs were used in different boats in order to survey the designed transects as quickly as possible, avoiding the effects of diurnal heat fluxes variability on temperature measures. The campaign periods are summarized in Fig 2.1 and table 2.1. During each campaign a set of longitudinal and transversal CTD transects were designed (In Fig 2.2 some of these transects are shown). The total CTD profiles obtained through the different campaigns were around 220. As example. Fig 2.2b shows the location of all CTD profiles performed at 7th May 2014 (I-5).

The first CTD measurement during each of the field campaigns was done simultaneously with both profilers in the Sant Carles de la Rapita harbour, with the objective to ensure the similarity of the observations. Results shown good agreement. Generally both sensors worked properly, except one day that a problem with pressure sensor invalidates the data processing. The raw data was post-processed with the software provided by Sea bird Electronics (http://www.seabird.com/), filtering and averaging the observations each 25 cm. Moreover, sensor data recorded on descent and ascent were compared to ensure reliability of the measurements. The utilization of these CTDs along the different campaigns allowed us to characterize the hydrographic structure under spring-summer and winter conditions (which represents open and closed freshwater drainage channels conditions). A set of figures (Fig 2.3 to 2.5) shows the salinity and temperature distribution along the transects defined in Fig 2.2a during different seasons. A picture of the CTD profilers is shown in Fig 2.6.

During summer 2012 and 2013 (Fig. 2.3) the salinity and temperature were contributing positively to the water column stratification. Salinity and temperature stratification were observable along all the bay (along and across the bay), with a clear sea water intrusion on the deeper layers and freshwater surface layer flowing towards the bay mouth. These profiles corresponds to typical summer conditions (see Camp and Delgado, 1987; Camp, 1994; Artigas et al., 2014). On both T_c and T_d transects the lateral variability of freshwater surface layer was evident, with the freshest water close to the northern margin, where the drainage channels are located. On the bay mouth, a tilt on the isopycnals were observed, probably related to the combined influence of freshwater input location and sea breezes regime (diurnal winds from the south), pulling freshwater to the northern shoals and promoting upwelling of salty deep water layer on the southern margin.

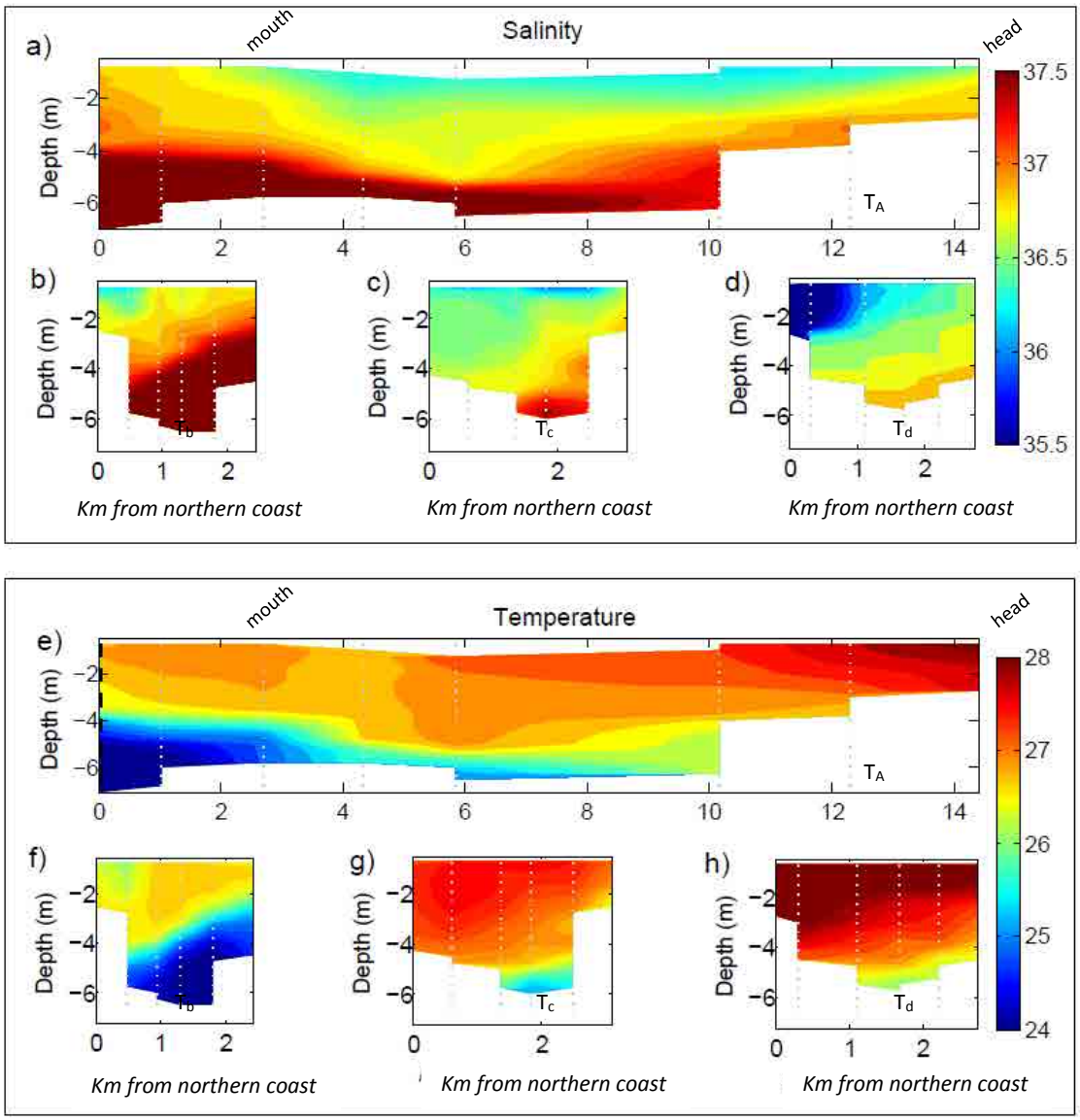

Figure 2.3. Transects (shown in Fig 2.2) T_a T_b, T_c and T_d for both salinity (upper panel) and temperature (lower panel) during July 2013. Dotted vertical lines indicates the location of each CTD profile. Contour interval is 0.2 for all the images. Temperature is in ºC and salinity in psu.

In comparison, February 2014 (Fig 2.4) shows completely different picture. The inner bay was well-mixed, with no stratification in salinity. Small thermal differences between surface and bottom layers were detected. Even the drainage channels were closed (rice fields were completely dried), the salinity on the bay was lower than the observed outside the bay. This agrees with previous studies (Artigas et al., 2014; Camp and Delgado, 1987), who observed similar patterns during closed channels and related it to unknown freshwater sources. However, and due to the lack of more CTD on the following days, it is not possible to confirm if this situation reflects a stable or transient state of the bay. On the other hand, an estuarine front

is found on the bay mouth, where inner bay freshwater interacts with the open-sea saltier and warmer water.

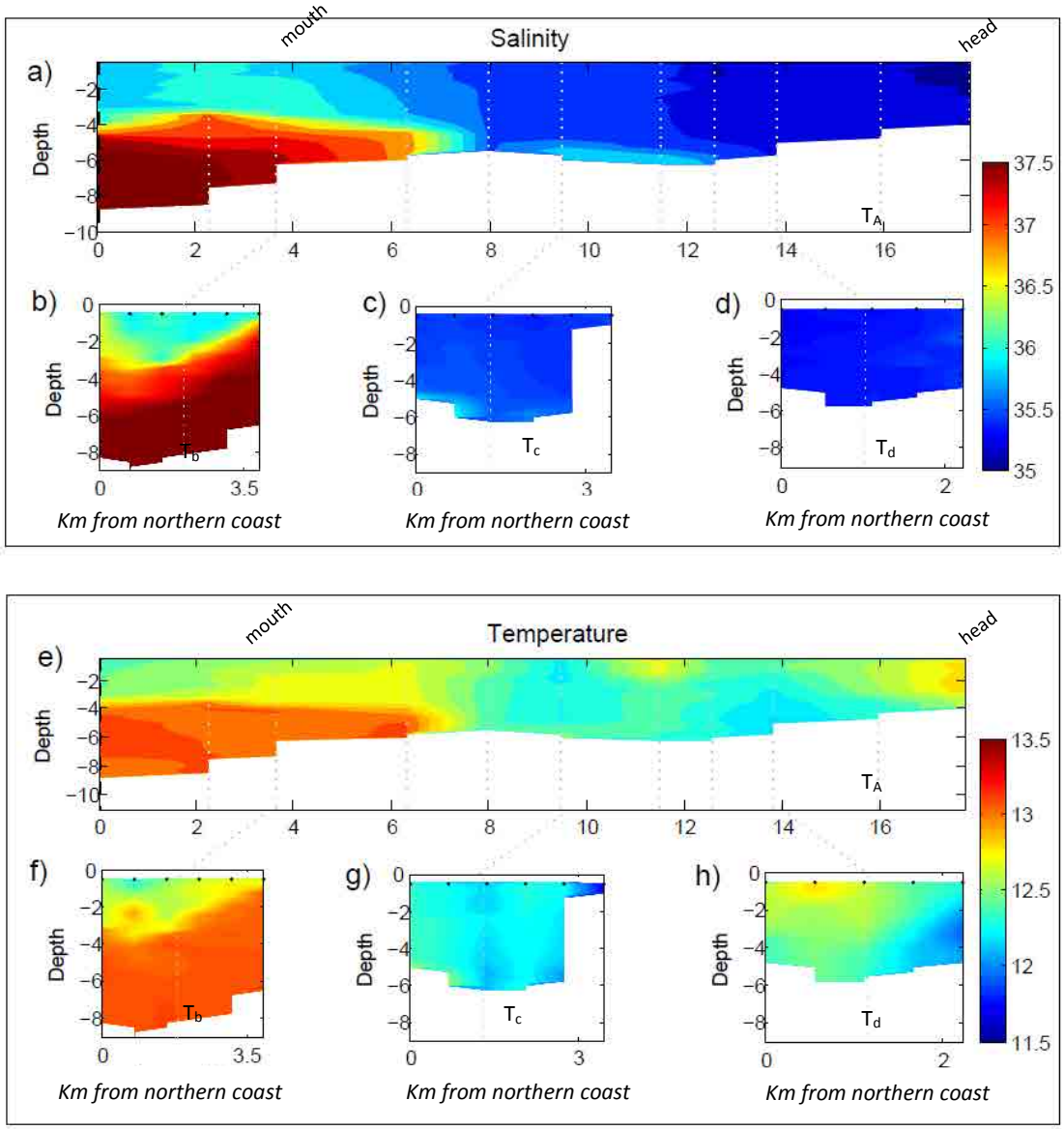

Figure 2.4. Transects (shown in Fig 2.2) T_a T_b, T_c and T_d for both salinity (upper panel) and temperature (lower panel) during February 2014. Dotted vertical lines indicates the location of each CTD profile. Contour interval is 0.2 for all the images. Temperature is in ºC and salinity in PSU.

A few months later, during May 2014 a typical period of drainage channels opened is observed (Fig 2.5), with maximum inputs of freshwater sources and lower rates of evaporation, thus promoting the minimum salinities on the bay. However, during this period, the intrusion of salty water from the open sea is evident as it was during summer, stablishing a well-defined stratified system in almost all the bay.

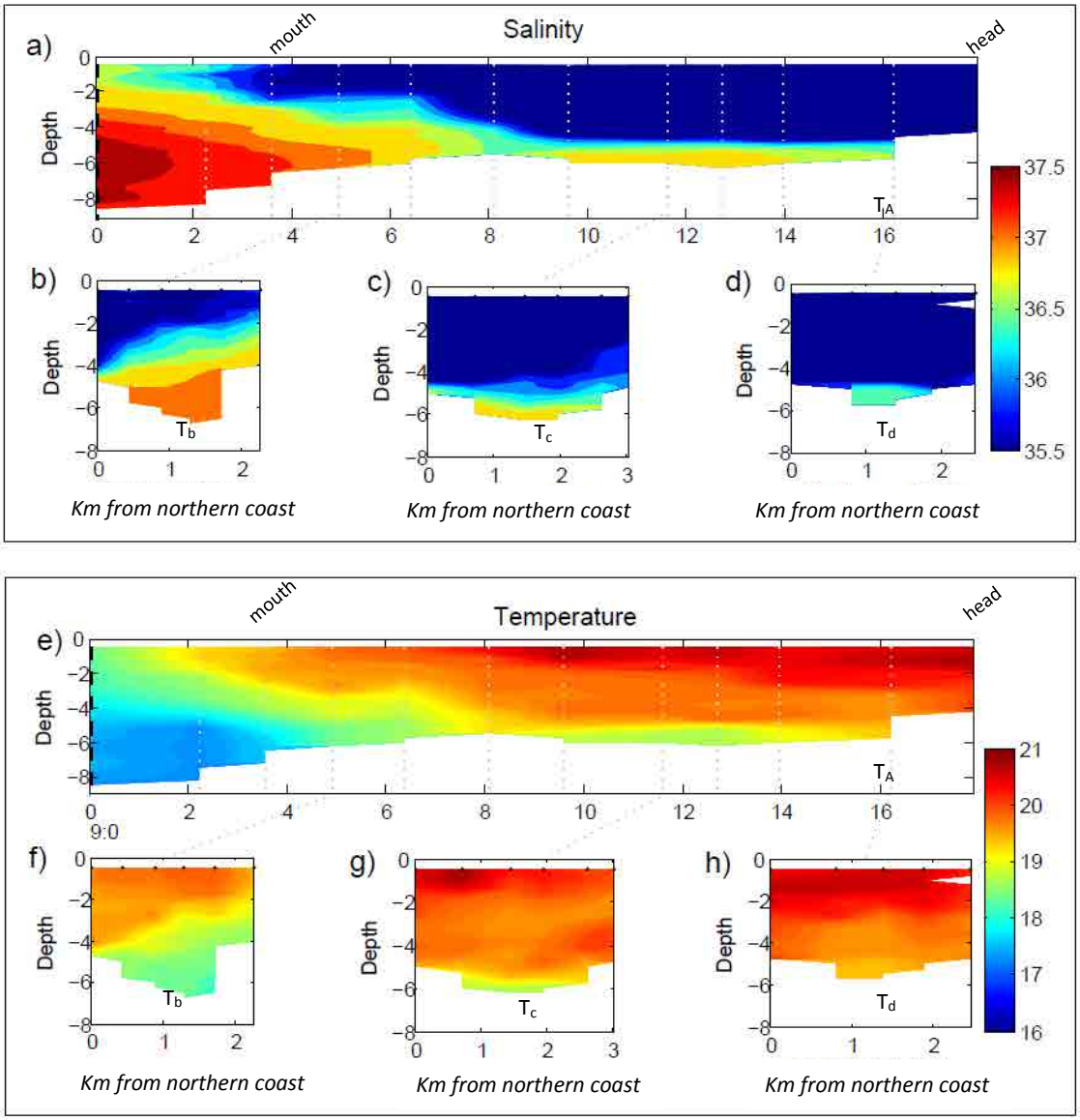

Figure 2.5. Transects (shown in Fig 2.2) T_a T_b, T_c and T_d for both salinity (upper panel) and temperature (lower panel) during February 2014. Dotted vertical lines indicates the location of each CTD profile. Contour interval is 0.2 for all the images. Temperature is in ºC and salinity in PSU.

Summarizing, the water density distribution along the bay and its vertical structure is variable, with higher influence of the freshwater inputs in the inner bay, and the open sea salt water intrusion in the bay mouth. The observed salinity differences between surface and bottom layers oscillates between 1 and 5 psu, with the highest differences during spring and beginning of winter. On the other hand, temperature shows maximum differences between surface and bottom layers during summer (5ºC). On winter, minimum temperatures are observed at the surface layers. Using the thermodynamic equation of state for sea water -EOS 80, Millero and Poisson (1981) - the contribution of salinity and temperature gradients to density are assessed. In this case, a variation of 1 psu (with temperature at 25ºC) implies density variation of ≈0.7

kg · m-3. On the other hand, fixing salinity at 37 psu and varying temperature to 26ºC (variation of -1ºC) the density variation is ≈0.3 kg · m-3. Therefore, the contribution of salinity to density variation is 2 or 2.5 times the temperature influence. This implies that the major contribution to density variation in Alfacs Bay is related to salinity differences (as observed by Llebot, 2010). However, during spring and summer, the contribution of temperature influences the density structure with same magnitude than salinity (i.e. in areas with lower freshwater influence).

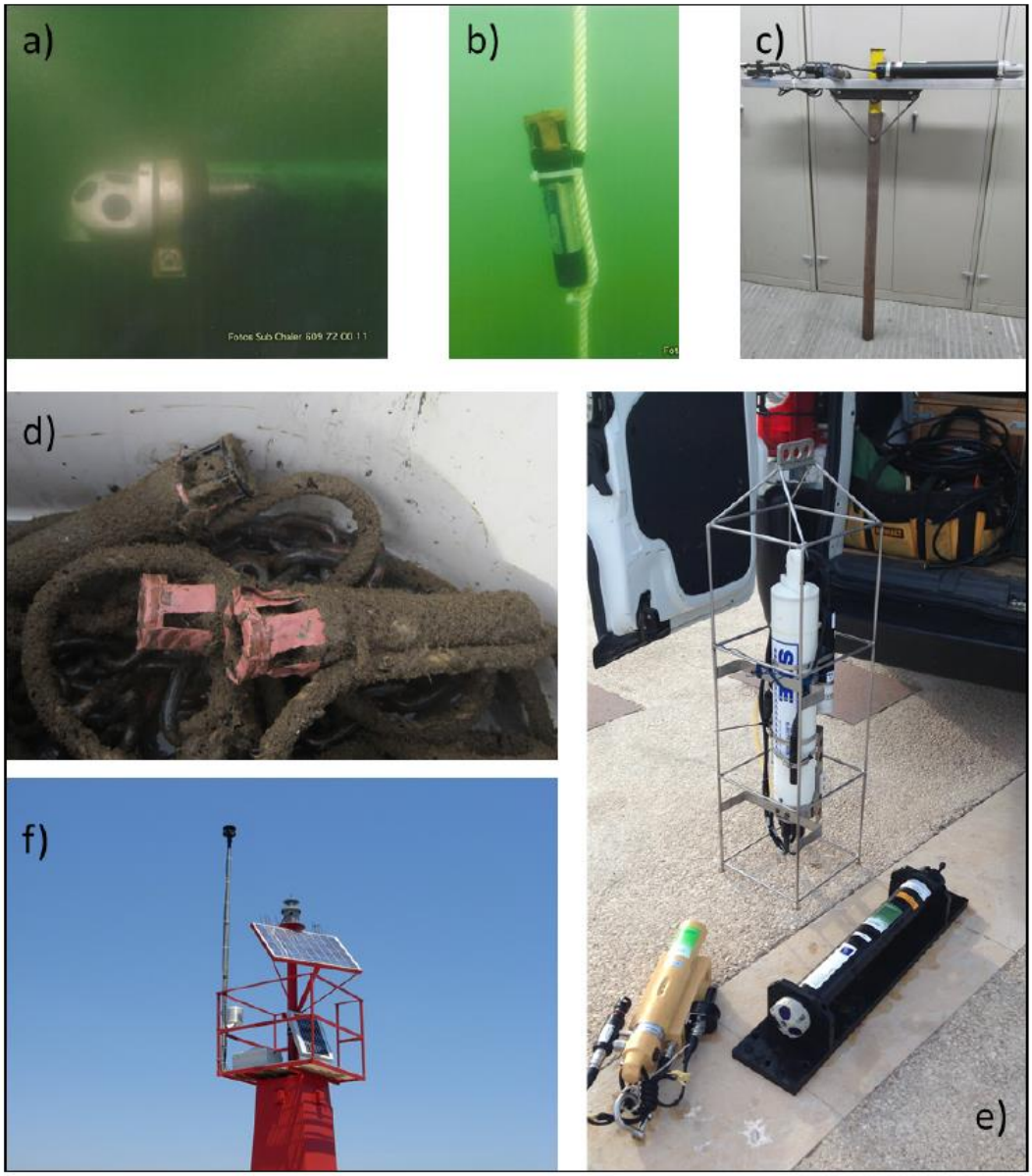

Figure 2.6. Pictures of different observational equipment: a) Aquadopp on the bay mouth during the mooring day. Picture done by "*Sub Chaler*"; b) CT on the A2 mooring system; c) aquadopp system before the mooring; d) 3 CT sensors on May 2014, with all the biofouling covering them; e) CTD profilers and ADCP used during daily campaigns; f) Meteorological station deployed in Alcanar (M-A).

1.3. Seasonal Campaigns

Long-term sea-level data from the XIOM network tidal gauge -Xarxa d'Intruments Meteorològics de Catalunya, Bolaños et al. (2009)- mounted in Sant Carles de la Ràpita harbor (Fig 2.2, M-SC) were used to obtain the main tidal harmonics and to carry out the analysis of residual sea-level (observed sea level without astronomic tides). Main results are summarized in chapter 3. Data were available from 1998 to the present, but different instruments were used over this period: an Aanderaa WLR 7 water-level recorder with pressure corrections from a meteorological station (1998-2007); an Aanderaa WLTS 3791 water-level recorder with autocompensation (2007-2010); and a Vegapuls 62 radar (2010-summer 2013). Due to the variety of instrumentation deployed, the annual means were detrended. Tidal analysis was carried out with the post-processed data using T_TIDE software (Pawlowicz et al., 2002) to obtain tidal constituents. Additionally, a fast Fourier transform (FFT) was applied to the residual sea-level in order to analyze the relevance of non-astronomical signal within the bay. In this case, in order to obtain statistical significance, the mean and standard deviation were obtained for 1024 data groups (10-min records, around 287 data sets).

Table 2.1. Oceanographic instrumentation used and working periods (locations in Fig 2.2). All data has 10-minute sampling interval.

Variables measured (and location)	ID	Type	Deploy	Instrumental Recovery	Period Length
Sea level (Sant Carles de la Ràpita)	M-SC	Anderra (WLR7)	1998	2007	9 years
		Anderaa (WLTS)	2007	2010	3 years
		Vegaplus 62 Radar	2010	2013	3 years
ADCP+sea level (mouth).	A1	Nortek (Aquadopp)	4/7/13	17/9/13	75 days
ADCP+sea level (bay)	A2	Nortek (Aquadopp)	4/7/13	17/9/13	75 days
Sea level (drainage channel 1)	V-1	Vegaplus 62 Radar	4/7/13	30/7/13	27 days
Sea level (drainage channel 2)	V-2	Vegaplus 62 Radar	30/7/13	17/9/13	48 days

Moreover, a limited-time field campaign was carried out in summer 2013 to investigate the tidal propagation within Alfacs Bay. Two 2 MHz Nortek Aquapros equipped with pressure sensors (nominal resolution 1 mm for sea-level variations) were deployed from 4 July 2013 to 17 September 2013 in the bay mouth and in the middle of the bay (Fig 2.2, "A1" and "A2" for mouth and inner bay, respectively). Both instruments were configured to record 10-min averages from 10 measurements per min for both eastward and northward velocities and for

bottom pressure. Sea level was obtained taking into account both bottom pressure systems and the atmospheric pressure recorded at Sant Carles de la Ràpita (Fig 2.2, "M-SC"). Moreover, a Vegaplus 62 radar was deployed at location 1 (Fig 2.2, "V-1") from 7 to 30 July 2013 and then moved to location 2 (Fig 2.2, "V-2") from 30 July to 17 September 2013. Data from these sensors were used to validate the numerical model through spectral analysis, and then to study the evolution of tidal amplitudes and phases along the bay and in the shallow drainage channels next to the bay. All instruments used and periods measured are summarized in Table 2.1. Main results are presented and discussed in chapter 3.

For current measurements, the bulk of the observational data corresponds to two extensive (around 2 months) field campaigns from July to mid-September 2013 and February to May 2014 (summer and spring campaigns, Table 2.1). The data set consists of two Acoustic Doppler Current Profilers (A1 and A2 in Fig 2.2) configured to record 10-min average data from 10 registers per min and with vertical cells of about 25cm, and also equipped with pressure and temperature sensors. The accuracy of the measures is 1% of measured value $\pm 0.5 \mathrm{cm} \cdot \mathrm{s}^{-1}$ (http://www.nortek-as.com/). Both ADCPs were mounted on the seabed at 6.5m depth. The blanking distance was around 0.4m. In both places we have considered for the analysis the measurements recorded from the first cell on the bottom layer until approximately 0.5-1m below the surface (20 cells of 25cm). Main results are presented and discussed on following chapters.

Moreover, three temperature and salinity sensors (CTs) were deployed on A2 at 0.7, 1.7 and 3m, and at 0.5, 2, and 4m depth for the summer and spring extensive field studies respectively. These sensors were recording minutely data. Only temperature data from these sensors is discussed in following chapters, because salinity data was too short, less than 15 days, due to biofouling effects. However, this salinity data has been used to compare it with numerical model results (validation). Schematic diagram for both A1 and A2 moorings is shown in Fig 2.7.

Finally, atmospheric data (wind, atmospheric pressure, solar radiation and humidity) were obtained from three fixed land stations: Alcanar (M-A), Sant Carles (M-SC) from XIOM network, and Alfacs-Meteocat (M-Met) which belongs to the automatic weather stations network of the Meteorological Service of Catalunya (www.meteo.cat). The geographical location are shown in Fig 2.2. Both M-A and M-SC are at 10 m above the ground, while M-Met measures at 2m. In order to compare wind intensities from all stations, we have adapted the measurements at 2m to the standard height of 10m. The method adapted in Herrera et al. (2005) from Oke (1987) is used to compute the velocities at 10m (w_{10}) from the observed values (w_h), as $w_{10} = w_h \frac{log\left(\frac{10}{z_s}\right)}{log\left(\frac{h}{z_s}\right)}$, where h represents the measurement height (2m). Following Agterberg

and Wieringa (1989) we have considered a typical roughness (z_s) for plains with low vegetation (rice fields) of ≈0.03m. The roughness variability in function of the wind direction is not considered.

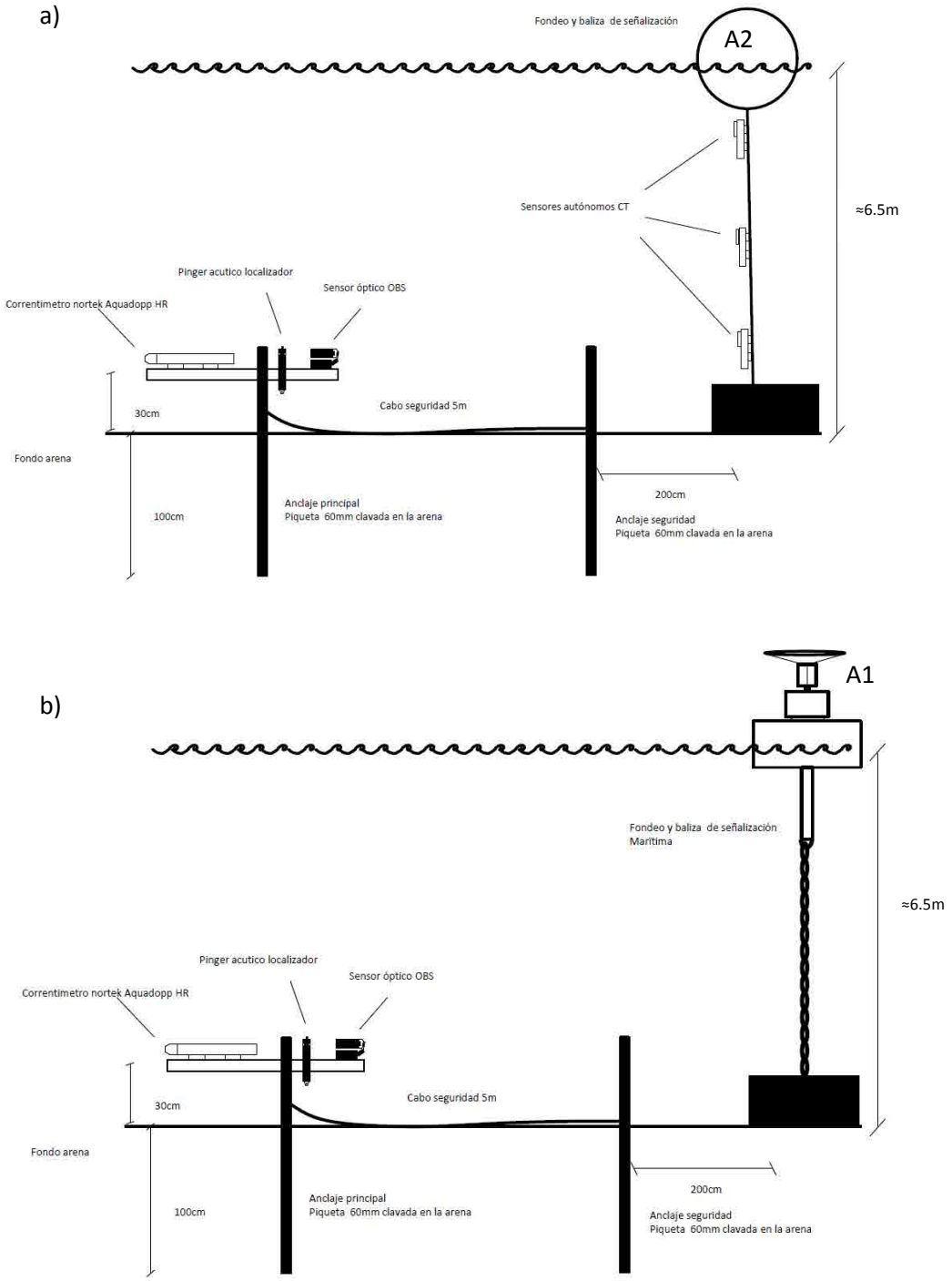

Figure 2.7. Mooring systems in both A1 (bottom image) and A2 (upper image). Source: Joan Puigdefàbregas, Jordi Catura and Quim Sospedra (Laboratori d'Enginyeria Marítima)

2. Numerical Models

2.1 ROMS (Regional Ocean Modelling Systems)

2.1.1 Description

The three-dimensional hydrodynamic model used in this thesis is the Regional Ocean Modeling System (ROMS). The present form of ROMS is an evolution of the S-Coordinate Rutgers University Model (SCRUM) described by Song and Haidvogel (1994). ROMS is a free-surface, hydrostatic, primitive equation ocean model that uses stretched, terrain-following coordinates in the vertical and orthogonal curvilinear coordinates in the horizontal. Numerical aspects are described in detail in Shchepetkin and McWilliams (2005) and a complete description of the model, documentation and code are available at the ROMS website: http://myroms.org. Considerable examples of ROMS applications in regional and coastal processes are found in the current scientific literature -e.g. Warner et al. (2005); Ferrer et al. (2009); Lee and Valle-Levinson (2012)-. At smaller scales and higher resolutions, there are several examples of the application of this model in small coastal estuaries and lagoons and for a wide range of objectives: resonance analysis (Zhong et al., 2008), tidal dynamics (Ganju et al., 2012), design of operational systems (Cerralbo et al., 2012; Costa et al., 2012) and harbor management (Grifoll et al., 2011, 2010).

According to the specific investigation objectives, in this thesis different model implementations have been used. For instance, several schematic idealizations of Alfacs Bay were defined in order to understand different processes dismissing the bathymetric effects, lateral roughness or keeping the boundaries away from the domain. Each of this specific applications are introduced in the corresponding chapter.

2.1.2 Analytical application (tidal and seiche propagation)

In chapter 3, where the tidal propagation and seiche characteristics are investigated, only the barotropic motion is analyzed; the model implementation consists of a regular grid of 153 x 106 points with a spatial resolution of about 150 m (in both x and y) and 6 sigma levels in the vertical. The bottom boundary layer is parameterized with a logarithmic profile using a characteristic bottom roughness height of 0.002 m. Vertical eddy viscosity and diffusivity are computed using the 2.5 Mellor-Yamada turbulence parameterization -described in Warner et al. (2005)-. The main configuration values for the model are summarized in Table 2.2. More

details on boundary conditions and the different numerical tests for this application are described on chapter 3.

2.1.3. Realistic application

For realistic simulations a high resolution grid domain is used with dx≈100m resolution and 12 vertical levels. Main dimensions and configuration parameters are summarized in Table 2.2. The objectives of this implementation were related with different topics investigated in this thesis. In particular: 1) perform a realistic simulation for both field campaigns and validate the model results with the observations; 2) reproduce a stable stratification and analyze the effects of the seiches over the water column stratification (chapter 4), 3) investigate the wind variability in the hydrodynamics (chapter 5) and 4) determine the 2D averaged circulation (chapter 6).

Table 2.2. Configuration values used for the numerical simulations on Chapter 3-4-5-6.

Parameter	Analytical	Realistic
L (number of I-direction rho points)	153	186
M (number of J-direction rho points)	106	101
N (number of vertical levels)	6	12
H min	1m	1m
H max	10m	10m
Bottom roughness	0.002 m	0.002 m
Vtransform	2	2
Vstretching	4	4
θ_s	3	3
θ_B	1	1
Dx	150 m	100 m
Freshwater inputs	No	Yes (≈10 $m^3 \cdot s^{-1}$)
Buffer area	Yes	No
Chapter reference:	3	4-5-6

The limits of the numerical domain as well as the horizontal mesh grid and an example of vertical discretization are shown in Fig 2.8. In this configuration, the freshwater inputs are considered. Following technical documentation from the "Comunitat de Regants del Marge Dret" a set of 8 freshwater inputs have been included, corresponding to the main drainage discharge points. Each drainage channel have associated a theoretical rice field area (with an evacuation flow of 0.7 $l \cdot ha^{-1} \cdot s^{-1}$). Moreover, in order to consider the freshwater corresponding to Ullals (1.5 $m^3 \cdot s^{-1}$ from Curcó, 2006), a flow of 0.75 $m^3 \cdot s^{-1}$ have been added to the two drainage points with higher flows (R4 and R7). Moreover, a flow of 2 $m^3 \cdot s^{-1}$ (Canicio and Ibañez, 1996) from the coastal lagoon l'Encanyissada is also contemplated. Summarizing, during

open channels season (April-December) a total amount of 9.5 $m^3 \cdot s^{-1}$ of freshwater is considered (all the inputs are summarized in Table 2.3). This values are similar to the ones used in previous studies (10 $m^3 \cdot s^{-1}$ in Llebot, 2010). During winter season, a minimum flow is considered (1 $m^3 \cdot s^{-1}$). This value is arbitrary due to the lack of reliable data for that period. The salinities in the freshwater inputs are set to 5 psu for the entire simulation. Temperatures are defined from the climatic 8 years temperature data of l'Encanyissada lagoon (data provided by "*Parc natural del Delta de l'Ebre*") as shown in Fig 2.9.

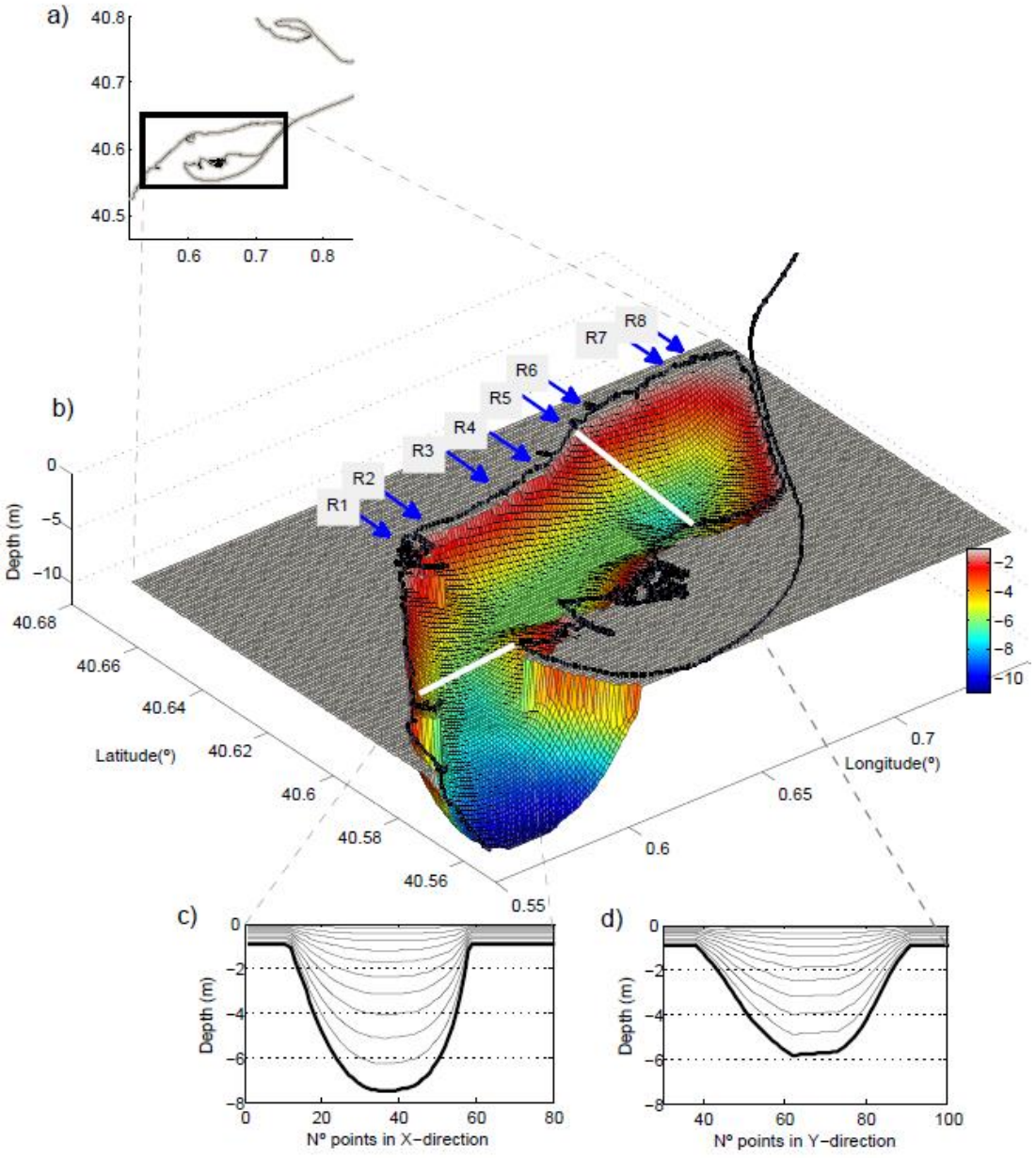

Figure 2.8. Numerical mesh model. Image a) shows the limits of the numerical domain used for all the numerical simulations in Alfacs Bay. Image b) shows the horizontal discretization and the smoothed bathymetry used. On the northern shore the different freshwater inputs are shown. More information for the freshwater flows on Table 2.2. White thick lines shows the location of the two sections shown in images c) and d). These sections shows and example of the vertical discretization used (12 vertical levels).

Table 2.3. Freshwater drainage channels considered in numerical simulations. Locations shown in Fig 2.1.

Code	Name	Flow (summer) $m^3 \cdot s^{-1}$	Flow winter $m^3 \cdot s^{-1}$
R1	Puig I Jardí	0.327	0.03
R2	Molinet	0.19	0.02
R3	Maquineta	0.27	0.03
R4	Campredo	2.27+0.75	0.21
R5	Cinta	0.17	0.02
R6	Fortaleza	0.12	0.01
R7	Sequia Alta	2.5+0.75	0.23
R8	Madalenes	0.16	0.02
E1	Encanyissada	2	0.4
TOTAL		10	1

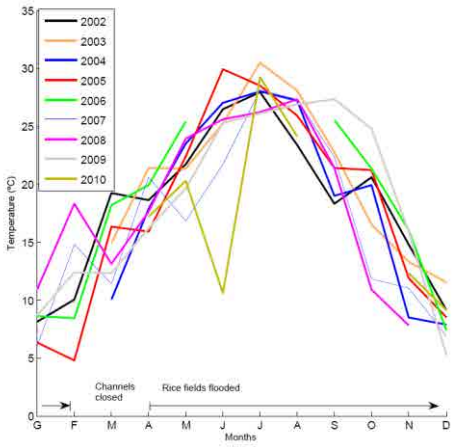

Figure 2.9. Monthly mean water temperature values registered at the Encanyissada coastal lagoon during the period 2002-2010. Data from "*Parc Natural del Delta de l'Ebre*".

The bottom boundary layer was parameterized with a logarithmic profile using a characteristic bottom roughness height of 0.002 m. The turbulence closure scheme for the vertical mixing is Generic Length Scale (GLS), described in Warner et al. (2005) and tuned to behalf as MY2.5 (k-kl). The main configuration values for the model are summarized in Table 2.2. A two year simulation (2012-2013) was performed in order to obtain realistic 3-dimensional temperature and salinity fields. The sea-level and water currents at the boundaries were imposed from hourly sea level data obtained on Sant Carles de la Rapita accommodating the perpendicular water velocities at the open boundary axis consistent with the Chapman and Flather OBC algorithms. Temperature and salinity were interpolated from MyOcean products at 6h data (Tonani et al., 2009). Atmospheric forcing and heat fluxes were obtained from M-A and M-Met stations.

The temperature and salinity fields modelled in the long-term simulations were used as initial and boundary conditions for two simulations coinciding with summer (3 months and named SS, Summer Simulation) and winter (one month, named WS, Winter Simulation) field campaigns described on observations section of this chapter. For SS and WS open boundary is forced with depth-averaged velocities and sea level measured at A1 (10' data). On SS freshwater inputs at set equal to 10 $m^3 \cdot s^{-1}$, whilst in WS they are 1 $m^3 \cdot s^{-1}$. For both periods, the validation of the model has been done over the sea level, velocities in A1 and A2, as well as temperature and salinity data on A2.

2.1.4. Model Validation

The models performance of the analytical implementation (2.1.2) is evaluated by comparing sea level spectral amplitudes between observations and numerical simulations. Main results are summarized and discussed on chapter 3 where the numerical results shows a good agreement with the observations in terms of spectral distribution.

For the realistic application (2.1.3) the hydrodynamic model is validated using observational data of SS and WS periods. Basic statistics (correlation factor and bias), skill score -Skill assessment index SK (Wilmott, 1981)- and Cost function, χ (Holt et al., 2005) between observations and modelling results are used to validate the numerical model (see summary for all the results in Table 2.4).

Correlation factor quantifies the strength of a linear relationship between two variables, and are defined as standardized covariance. Values close to one indicates strong linear correlation (positive or negative correlation depending on the sign), while 0 indicates no linear relationship.

$$r(o,m) = \frac{\sum_{i=1}^{n}(m_i - \bar{m}) \cdot (o_i - \bar{o})}{n \cdot \sigma_o \cdot \sigma_m} \tag{1}$$

In all formulas o represents observational data, m modelling results and n for the total amount of observational data used, and the over bar (—) denotes all data length averaged values

The skill score described in Wilmott (1981) and Warner (2005) is defined as:

$$SK1 = 1 - \frac{\sum_{i=1}^{n}(m_i - o_i)^2}{\sum_{i=1}^{n}(|m_i - \bar{o}| + |o_i - \bar{o}|)^2} \tag{2}$$

In this case values close to one indicates good agreement and equal to 0 indicates complete disagreement.

The cost function (χ) is described in Holt et al. (2005) as:

$$\chi^2 = \frac{1}{N\sigma_o^2}\sum_{i=1}^{n}(m_i - o_i)^2 \tag{3}$$

Being σ^2 the variance of observations (squared of standard deviation). The cost function (χ) is defined as a measure of the ratio of model error to the observed variance. For χ, an acceptable predictive skill of the model is related with values lower than 1 (RMS error smaller than the standard deviation from observations), and well modelled variable threshold situated on 0.4 (Holt et al. 2005).

Correlation for sea level during SS simulation period is 0.89 and 0.85 for A1 and A2 respectively. SK1 shows values higher than 0.9 and χ close to 0 for both locations. Similar values are obtained for winter period (WS). In consequence, the agreement for sea level is considered almost optimum.

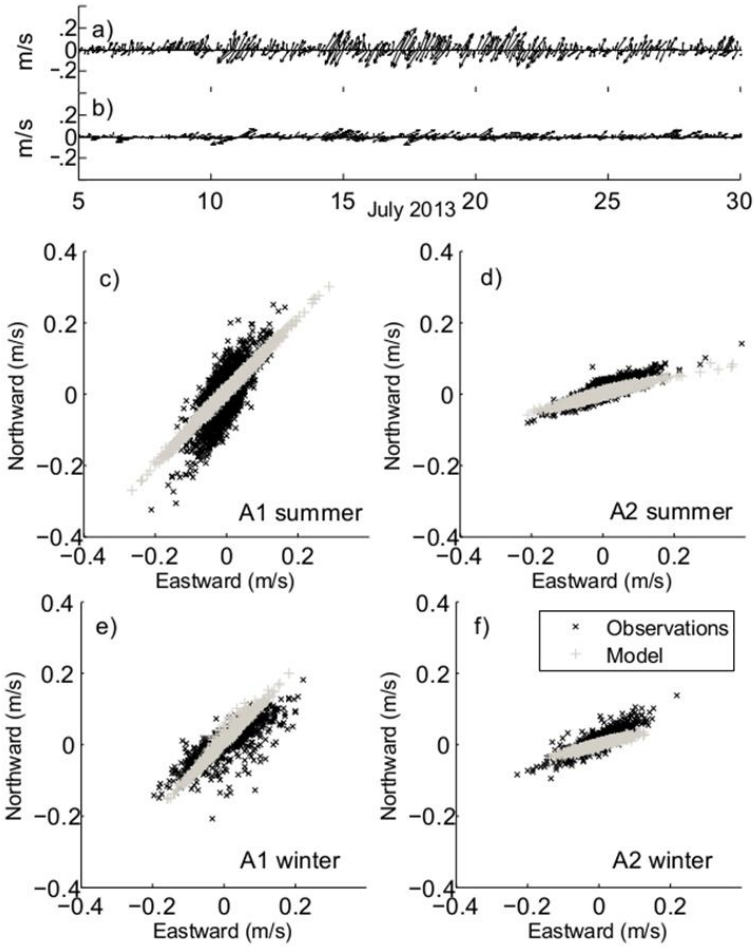

Figure 2.10. Observational and modelled currents in A1 and A2. a) and b) shows the observed depth-averaged velocities in A1 and A2 respectively during July 2013. Images c) and d) presents the scatter plot on A1 and A2 between eastward and northward depth-averaged velocities for both observational and modelled data during summer 2013. Same for winter campaign in images e) and f).

During summer (SS), depth averaged velocities for north component shows correlations of 0.73 (A1) and 0.77 (A2), and values of SK1 and χ indicates also good agreement (Table 2.4). East-West component shows higher agreement at A2 for all skill scores, while at A1 better agreement is observed on north component. The larger correlation in meridional or zonal direction in both places is related to the prevalent alongshore direction due to the bathymetry influence on water circulation (Fig 2.10c and 2.10d). Due to the prevalence of barotropic seiche motion, the axis with major variability corresponds to alongshore directions in both places (Fig 2.10a and Fig 2.10b). The scatter plot between depth-averaged velocities observed and modelled showed a significant level of agreement in both components (Fig 2.10c, 2.10d, 2.10e and 2.10f). During winter, the skill scores shows better performance of the model in comparison to summer period. The correlation for depth-averaged velocities are between 0.8 and 0.9 (with the exception northward component in A2). However, this period has only one month of data.

Table 2.4. Skill assessment between observed and simulated water currents, sea level, temperature and salinity (summer 2013 and winter 2014).

		Bias		r		*X*		*SK1*	
		Summer	Winter	Summer	Winter	Summer	Winter	Summer	Winter
Sea Lev (cm)	A1	0.04	0.48	0.91	0.91	0.06	0.06	0.93	0.94
	A2	-0.58	0.44	0.84	0.89	0.08	0.06	0.91	0.94
East (cm/s)	A1	-	-	0.73	0.9	0.25	0.06	0.79	.93
	A2	-	-	0.77	0.81	0.14	0.1	0.86	0.88
North (cm/s)	A1	-	-	0.84	0.86	0.08	0.11	0.91	0.92
	A2	-	-	0.62	0.63	0.36	0.3	0.71	0.57
Temp A2 (C^o)	.5m	0.8	-1.8	0.95	0.91	.5	0.86	.79	0.71
	3m	0.9	-1.9	0.83	0.91	.6	0.93	.77	0.68
	6m	2.1	-1.7	-0.29	0.92	1.1	1.3	-0.56	0.67
Salt (PSU)*	.5m	1.73	0.53	-0.2	-0.2	18	19.7	0	-0.007
	3m	0.63	0.41	0.38	-0.1	1.6	31	0.12	-0.004

*Only 15 days of data

The velocity components are rotated in order to describe the maximum variability in one axis, which is called hereafter alongshore due to its alignment with the central axis of the bay. Main axis is obtained on winter at 36^o and 26^o anticlockwise for A1 and A2 respectively, and during summer at 59^o and 24^o for A1 and A2 respectively. The alongshore velocities measured in both A1 and A2 considering vertical variability are graphically compared in Fig 2.11 with modeling results for both locations and seasons using Taylor diagram (Taylor, 2001). In this diagram,

the comparison between observations and model are shown in terms of correlation, the centered root mean squared difference (CRMSD) and the standard deviations. In order to compare in the same figure different vertical layers against observations, the standard deviations and CRMSD are normalized over the standard deviation of the corresponding observations (Grifoll et al., 2013).

The normalized standard deviation used in Taylor Diagram:

$$\mathrm{STD}_{\mathrm{m-o}} = \frac{\left(\sqrt{\frac{\sum_{i=1}^{n}(m_i - \bar{m})}{n}}\right)}{\sigma_o} \tag{4}$$

And normalized root mean square error:

$$\mathrm{CRMSE}(m,o) = \frac{\sqrt{\frac{\sum_{i=1}^{n}[(o_i - \bar{o}) - (m_i - \bar{m})]^2}{n}}}{\sigma_o} \tag{5}$$

The model skill improves as the points get closer to the observation reference point. The proximity of A1 to imposed open boundary conditions induces better agreement than A2, where the role of bay dynamics (stratification or non-linearity induced by bottom friction) is complex and modifies de water response. On the other hand, during winter (WS) all the skill scores indicates better modelling performance than summer probably due to the discrepancies on the modelled stratification (higher during summer period).

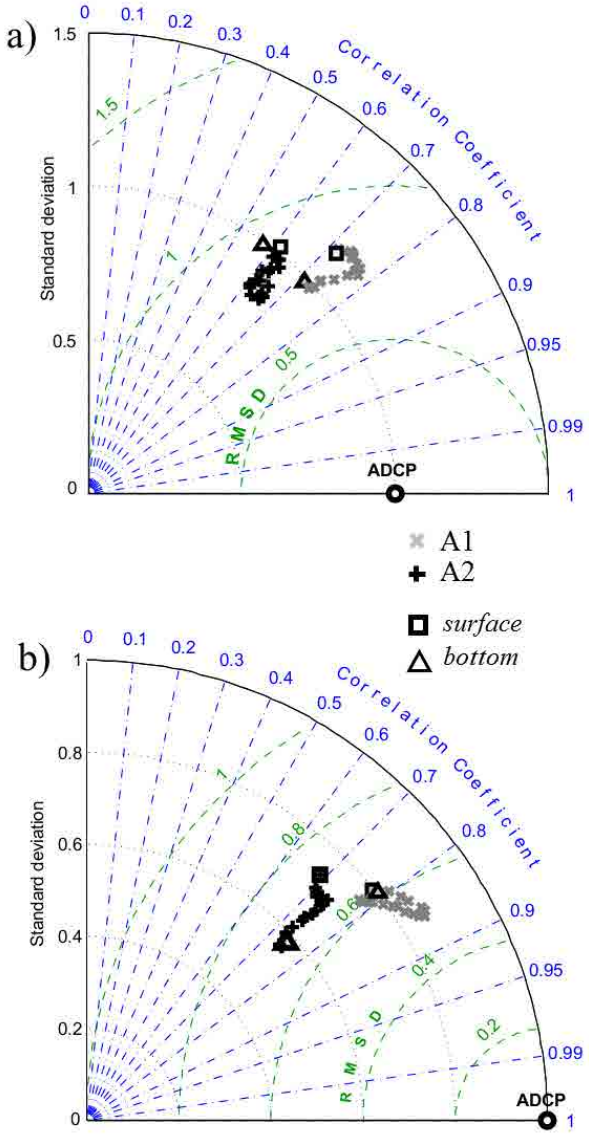

Figure 2.11. Taylor diagram illustrating the match of modelled along-shore velocities in A1 (grey) and A2 (black) to its corresponding observational data. Summer 2013 on (a), and winter 2014 in image (b). Both model and observational data are averaged in vertical layers of 25cm.

Modelled temperature is compared with CTs and temperature sensor from ADCP revealing high correlation and good skill assessment factors for inner bay (A2) surface sensors. At 3m depth, the correlation is still good but lower than surface. However, during summer, on bottom layers the correlation is close to 0 indicating low agreement with observational data, whilst during winter the modelled bottom layer temperature follows the observational data. The discrepancies between model and observed values in surface layers during summer may be related to differences in the atmospheric heat fluxes and the mixing processes modelled in the water column. The mean differences observed from surface to bottom almost differs in more than 2ºC for the entire summer (Fig 2.12), while model reveals differences about 0.5ºC. The bias shows how the model overestimate the temperature during summer and underestimate it during winter. However, the period and magnitude of the diurnal oscillations are well reproduced by the model. Maximum RMSE is around 1.3 ºC and similar to previous modelling works at the Alfacs Bay (Llebot et al., 2013).

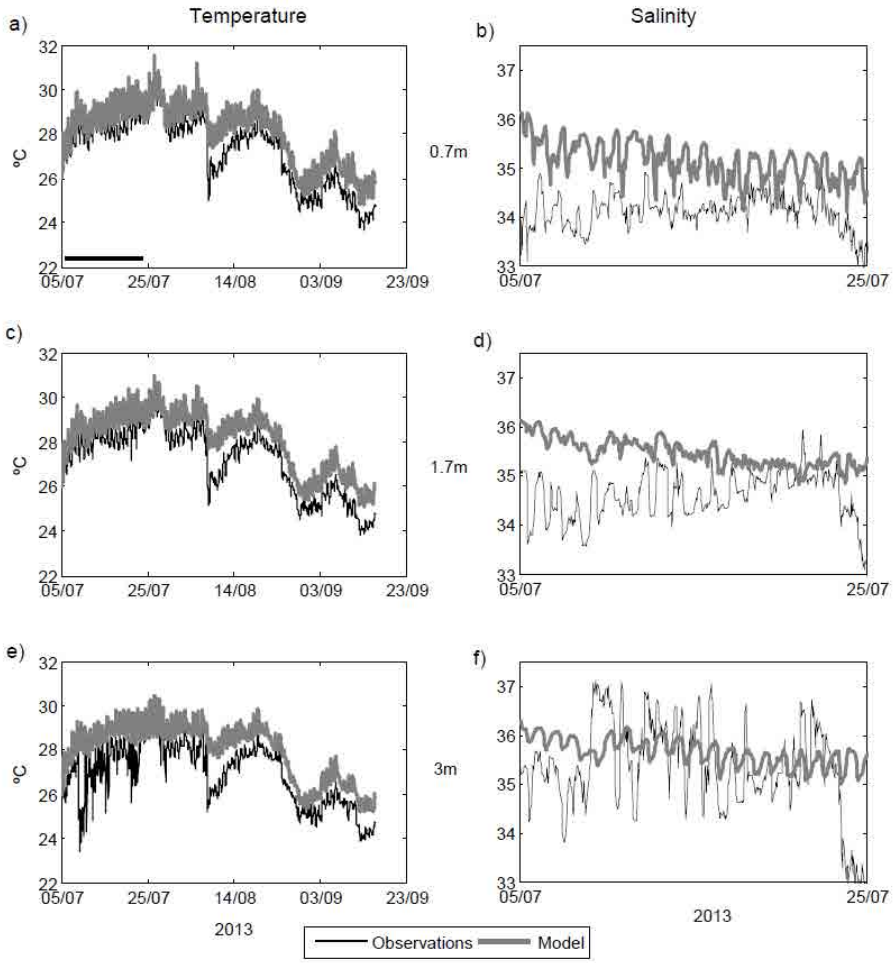

Figure 2.12. a, c and e) Temperature observations and modelled results in A2 at different depths (0.7; 1.7 and 3m) during summer 2014. b, d and f) Salinity observations and modelled results in A2 at different depths (0.7; 1.7 and 3m) between 5th and 25th July.

Finally, salinity data was only available for the beginning of the summer campaign (around 15 days) due to biofouling. Moreover, on winter, sensor at 4m did not work properly during the whole campaign. During summer, the differences between 3m and surface were around 1.5 psu in A2, while in the model these differences were around 0.3-0.4 psu. Correlation is quite poor, but only 15 days of data are used to validate the results (Fig 2.12). The discrepancies of the numerical results and the observations seems to indicate the presence of other sources of freshwater fluxes not considered (i.e. groundwater fluxes or an increase of continental run-off no monitored) and a possible overestimation of the mixing. During winter, the salinity bias on both 0.5m and 2m layers were lower, but still showing higher values in the model than in observed data. This agrees with previous studies that observed how during winter, even the drainage channels are closed (no water in rice fields), the bay still received freshwater inputs (lower salinity than open sea) (Camp and Delgado, 1987). In general, the model reproduces the stratification of the bay, even with lower density gradients between surface and bottom layers than observed.

2.2 Atmospheric Models

2.2.1. Description

Two different atmospheric models results are used to validate the numerical outputs and assess the spatial heterogeneity in the bay. Numerical outputs are provided by Meteocat, which uses the Weather Research and Forecasting (WRF) (Skamarock et al., 2008). Two different configurations depending on grid resolution have been analyzed: 9 and 3km (named hereafter WRF9 and WRF3). The main model parameters are summarized in Table 2.5. The model implementation differs in both spatial and temporal resolution. More configuration details are available at http://www.meteo.cat.

Table 2.5. Summary of the main characteristics of the three different model configurations used in this thesis.

Model	Domain	Nominal Resolution	Lead Time	Outputs
WRF9	Iberian Peninsula	9 km	72 h	3 h
WRF3	NE Spain	3 km	48 h	1h
CALMET	SW Catalonia	0.4 km	48 h	1h

These configurations correspond to the available products of the Meteocat meteorological operational forecast system. On the other hand, an additional simulation has been considered to derive atmospheric data at a very high resolution (400 m). In particular, the WRF-ARW outputs at 3km are downscaled by a diagnostic meteorological model called CALMET. CALMET, a component of the CALPUFF Modeling System designed for the simulation of atmospheric pollution dispersion (Scire et al., 1999), is a diagnostic three-dimensional meteorological model which includes parameterized treatments of slope flows, kinematic terrain effects and terrain blocking effects, among others. These particular aspects help to better represent regional flows with an efficient computational cost. For all the verification processes the daily first 24 h of prediction from the operational system are used.

2.2.2. Model Verification

In this section, the results of verification studies to assess the performance of wind velocity and direction prediction from the models against the observation are presented. The verification of both WRFs (WRF3 and WRF9) and CALMET is shown in Fig 2.13 for summer 2013 (Fig

2.13a) and winter 2014 (Fig 2.13b). We chose that period in order to coincide the meteorological observations and model results with oceanographic data. Verification of all the models and resolutions is done against hourly-averaged observations. The wind module velocities measured in both M-A and M-SC are graphically compared to modelling results for both systems (model data is interpolated through bi-lineal interpolation to corresponding points) using a Taylor diagram (Taylor, 2001). In summer 2013, better correlation (around 0.6) is observed in M-SC, while in M-A the values decrease to ≈0.5. The standard deviation shows that the model presents lower-amplitude variations than the observed values. In spring 2014 only measurements from M-A were available.

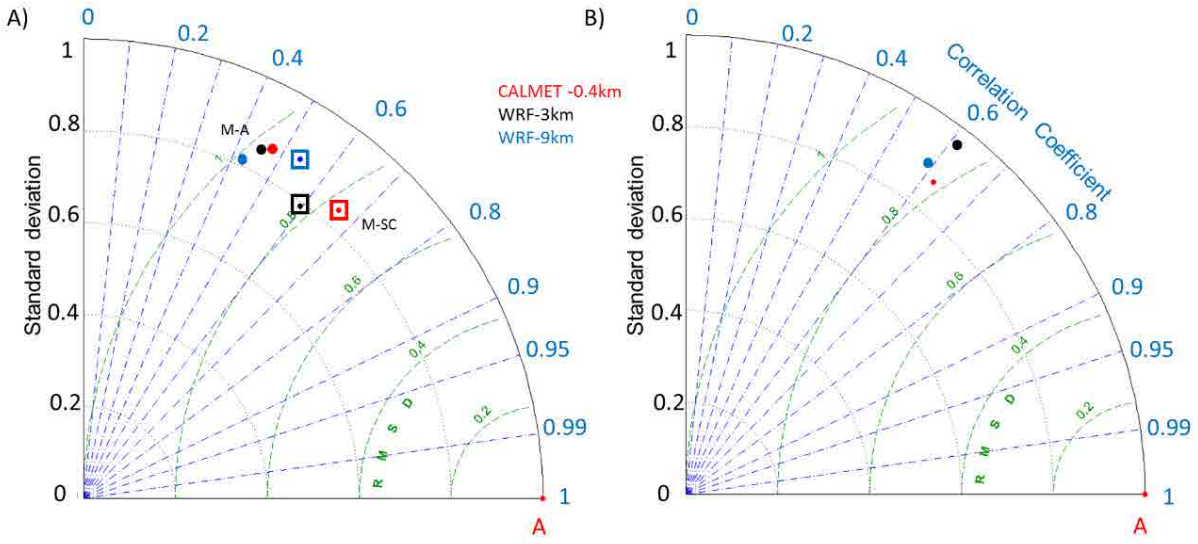

Figure 2.13. Taylor diagram comparing observation and modelled winds: (A) summer 2013 and (B) winter 2014 for both M-A (colored dot) and M-SC (colored square filled with dot) model configurations (red for CALMET, black WRF3 and blue for WRF9) compared with corresponding meteorological station. Both modelled standard deviations and RMSD are normalized over observational standard deviation.

In this period, the correlations are larger for all meteorological models, and the standard deviations are more similar to the observations. Differences through different models are only observable in M-SC location data, revealing the highest correlations and lower errors in higher-resolution models (best results corresponding to CALMET). In M-A, the models do not show noticeable differences. The wind module velocities measured in both M-A and M-SC are compared in Fig. 2.14a and b, respectively, for summer 2013 with modelling results using a Weibull distribution. Weibull distribution is a two-parameter function commonly used to fit the wind speed frequency distribution. In both stations, the best fit between the model and

observational Weibull distributions is observed for CALMET. In M-A, CALMET and the observational distribution show almost equally shaped coefficient; even observational data present stronger winds. WRF3 also has similar shape, with even more energy distributed at medium wind intensities (= 3m $\cdot$ s^{-1}). WRF9 seems to overestimate the mean winds.

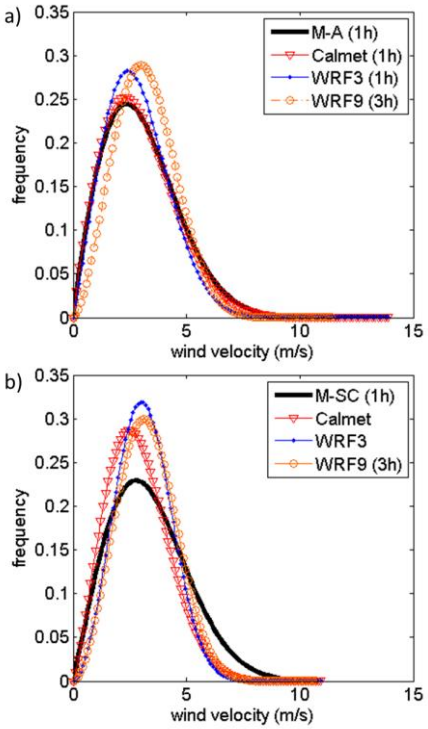

Figure 2.14. Weibull distributions for summer 2013 in M-A (a) and M-SC (b). Black line for observational data (hourly) and colored lines for each model configurations (red for CALMET, blue for WRF3 and orange for WRF9).

In M-SC, winds from CALMET are the most similar to observations, even overestimating the frequency of mean winds, and then not reproducing the maximum intensities (6– 10 m $\cdot$ s^{-1}). On the other hand, WRF3 and WRF9 overestimate both mean wind intensities and corresponding frequencies. In the winter season, observations show higher wind intensities, and both CALMET and WRF3 present Weibull shapes (not shown) similar to observations. Some characteristic events representing the most usual winds in the area have also been analyzed in order to investigate the behavior of each model under different conditions (summarized in Table 2.6).

A period of 3 days of characteristic wind conditions is considered to compare observations and numerical outputs. Results show that winds from CALMET and WRF3 have higher correlations (except in north-west 2) than WRF9. The worst results are observed during northwesterly winds in summer 2013. This is due to the topography effect being the observed wind in M-A not well reproduced by any models. Slightly better results are obtained in M-SC, especially by CALMET (but still with poor correlation). This event was characterized by its shortness (less than 6–8 h) and unsteadiness.

On the other hand, in the winter period, another NW wind event (lasting for more than 1 day) was reproduced with noticeable agreement in M-A. In this case, the simulation WRF9 seems to reproduce well the winds in M-A, but no data for M-SC are available to compare. Southern winds – southeast and diurnal regime of sea breeze – are better reproduced by the finest models, being the highest improvement between WRF3 and WRF9. Considering the daily duration of the sea breeze – between 6 and 8 h – all the models would be able to reproduce it (Table 2.6). However, the temporal variability of such processes only is reproduced by 1-h temporal resolution models.

Table 2.6. Correlation among the three different atmospheric models and observational data for three days long events during summer'13 and winter'14. No correlation for winter 2014 periods (M-SC was dismantled on September 2013).

	Day	M-A			M-SC		
		WRF9	WRF3	CALMET	WRF9	WRF3	CALMET
North West	8/8/2013	.02	.01	.12	.21	.40	.46
North West 2	4/4/2014	.80	.72	.75	-	-	-
South East	13/8/2013	.43	.64	.64	.58	.71	.75
Sea Breezes	6/7/2013	.64	.67	.74	.64	.66	.76
North East	28/3/2014	.75	.86	.83	-	-	-

3

Tidal transformation and resonance in a short, microtidal Mediterranean estuary (Alfacs Bay in Ebre delta)

The most exciting phrase to hear in science, the one that heralds new discoveries, is not 'Eureka!' but 'That's funny...'

Isaac Asimov

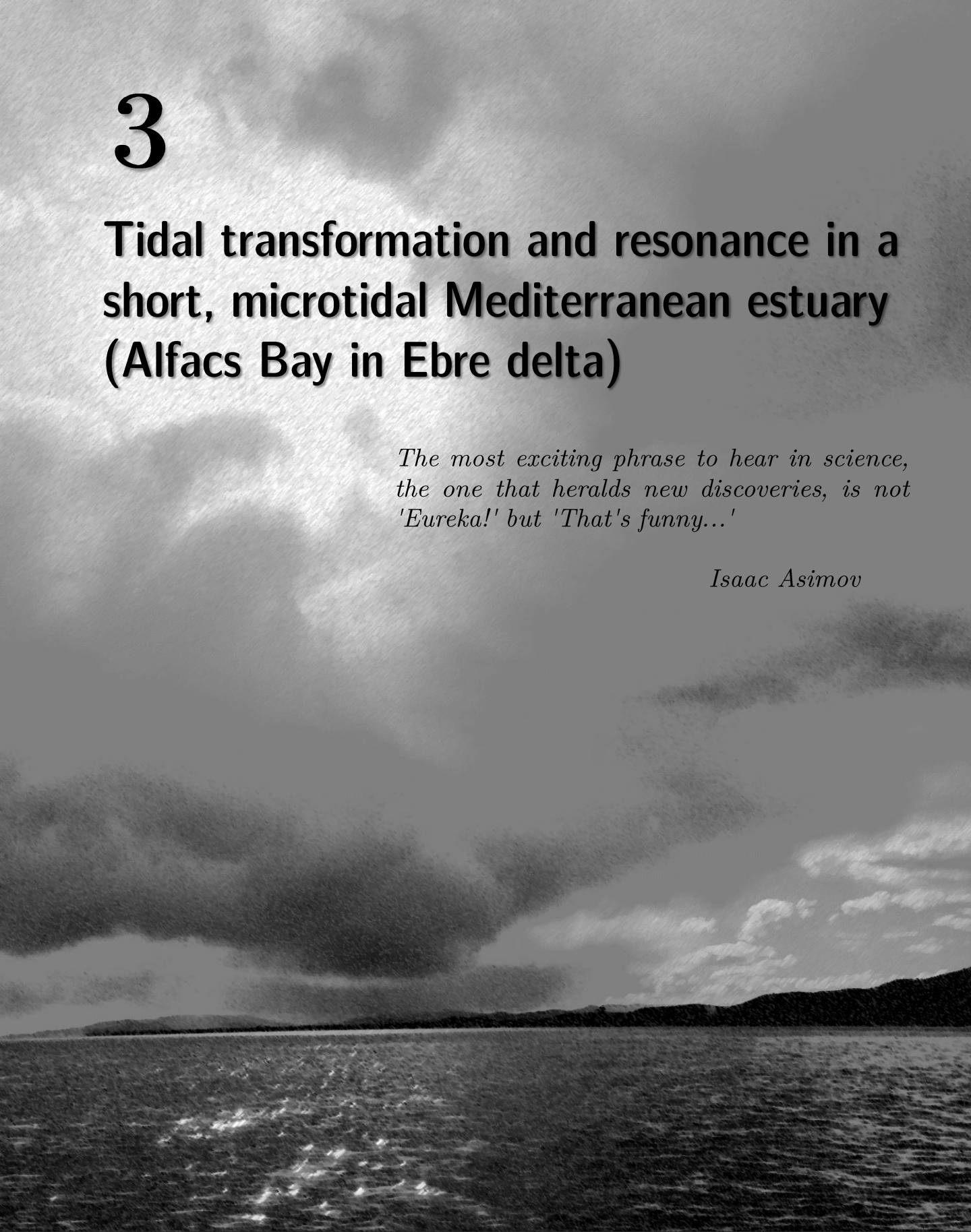

Cerralbo, P., Grifoll, M., Valle-Levinson, A., & Espino, M. (2014). Tidal transformation and resonance in a short, microtidal Mediterranean estuary (Alfacs Bay in Ebre delta). *Estuarine, Coastal and Shelf Science*, *145*, 57–68. doi:10.1016/j.ecss.2014.04.020

Abstract

Tidal and subtidal waves are analyzed with sea-level data and numerical modeling in a short and microtidal embayment, Alfacs Bay (NW Mediterranean Sea). Data analysis exhibits tidal wave amplification and seiching (characteristic period of 3.5 h) along the bay. Numerical results show an eight-fold increase in quarter-wave resonant wave amplitudes from the mouth to the head of the bay. This amplification follows the classical description of a standing wave. Moreover, resonant wave velocities measured and computed at the bay mouth (node location) are about one order of magnitude higher than tidal currents. Analysis of astronomic tidal propagation in the bay reveals similar behavior for diurnal and semidiurnal constituents. Tidal waves amplify along the bay by 3% for diurnal and 10% for semidiurnal constituents. Numerical simulations conducted with different domains indicate that geometric effects dominate over frictional influences in causing the wave behavior. This behavior is consistent with the existence of a quasi-steady standing wave within the bay.

1. Introduction

Tides are one of the main mechanisms that drive circulation in estuaries and coastal embayments, and they have been the object of observational studies, theoretical solutions and numerical modeling. In addition to describing the tidal waves themselves, studies have explored the generation of overtides and resonance. Various perspectives and examples can be found in Speer et al. (1991) and Mirfenderesk & Tomlinson (2009), who analyzed the appearance of overtides as a result of bottom friction and continuity constraints. Zhong et al. (2008) and Bowers & Lennon (1990) studied resonance periods of large estuaries and their implications on the circulation. Winant (2007) and Waterhouse et al. (2011) used analytical models to explain the main physics of tidal propagation in semi-enclosed coastal zones. Friedrichs (2010) showed different scenarios (i.e. long/short, deep/shallow estuaries) and identified the main physical mechanisms and governing balances that describe variations in tidal amplitude, phase and velocity along the estuary in each case. He also presented a review that showed that tidal amplitude, phase speed and the relative phase between tidal velocity and elevation in most estuaries are largely controlled by the competition between bottom friction and channel convergence. One of his main conclusions was that, in short estuaries, characterizing long waves as standing or progressive solely on the basis of the phase relationship between velocity and elevation could potentially lead to confusion. This was also pointed out in Friedrichs & Aubrey (1994). Woo & Yoon (2011) used three-dimensional hydrodynamic models in order to ascertain the main physical factors that influence channel-dependent tidal propagation and stated that the main factors that change tidal amplitudes are bottom friction, river discharge and the existence of tidal flats. Ranasinghe & Pattiaratchi (2000) studied tidal propagation in three narrow microtidal inlets connected to wide, shallow estuarine basins and showed tidal attenuation as the signal propagated into the estuary. The aforementioned studies examine a wide range of tidal characteristics (i.e. diurnal, semidiurnal, macrotidal, mesotidal and microtidal) and different environments, such as long/short and deep/shallow. As a consequence, the results also cover a wide range of possibilities: tidal signal amplification (defined as a hypersynchronous estuary) in Woo & Yoon (2011), tidal damping in Ranasinge & Pattiaratchi (2000), a progressive wave in the Delaware Estuary (USA) in Friedrichs & Aubrey (1994), and a mix of progressive and standing wave in the same estuary in Bowers & Lennon (1990).

Long-period (> infragravity waves) standing oscillations in estuaries or harbors are known as seiches (harbor or coastal seiches), and can produce damaging surges (Montserrat et al. 1991), as well as enhanced horizontal water currents (Rabinovich, 2009). In long estuaries, several authors have pointed the possibility of similar periods on bay (estuary) resonance and tides

(Garret, 1972). On the other hand, smaller embayments and harbors have seiche periods much shorter than tides (Vilibic & Mihanovic, 2005). Moreover, in microtidal environments the amplitude of these oscillations could easily be the same as the tidal amplitude (and wind surge), or even exceed it (Rabinovich & Montserrat, 1996). Furthermore, there are cases in which the tidal propagation dynamics remains unclear (i.e. short, shallow and microtidal embayments).

The purpose of this chapter is to gain knowledge on tidal propagation in short, microtidal coastal embayments. A small bay in the Mediterranean Sea is chosen for this investigation (Alfacs Bay). Although Alfacs Bay has been studied extensively in the past, tidal wave propagation and transformation caused by the shoreline influence has not received much attention. The study combines observations with the application of a numerical model in realistic and simplified scenarios. We begin by describing the tidal characteristics of the bay and the tidal propagation from mouth to head using sea-level observations. We then describe the tidal propagation using a numerical model in order to distinguish between frictional and geometric effects, including bay-orientation change and coastline constraints.

Analysis of yearly sea-level time series in Sant Carles de la Ràpita harbor since 1998 -tide gauge location marked by "SC" in Fig 2.1 (chapter 2)- show that the main harmonics, in order of importance, are K_1, M_2, O_1, P_1, S_2 and N2. They define the form factor taking into account the main diurnal and semidiurnal tidal harmonics as follows:

$$F = \frac{K_1 + O_1}{M_2 + S_2} \tag{1}$$

Bolaños et al. (2009) found F values of around 1.3. Therefore, the tidal regime in Alfacs Bay can be described as a mixed tide with semidiurnal dominance. Using residual analysis (difference between observations and tidal harmonics), they also found oscillations of around 3 h in some instances. Instrumentation details are resumed in Chapter 2.

2. Numerical Model and Geometric Domain

2.1. Model configuration

The three-dimensional hydrodynamic model used is the Regional Ocean Modelling System (ROMS). General configuration and validation details are summarized in chapter 2. In this chapter, the analytical implementation is used. Main model configuration parameters are summarized in Table 3.1. In order to provide suitable boundary information for the numerical domain, a buffer area was implemented. This area consisted of a channel (around 20 km long) perpendicular to the mouth with a constant depth of 10 m. This buffer area avoids spurious dynamics near the mouth and allows suitable transfer of the boundary information to the inner domain. Tidal forcing is introduced as a surface elevation on the open boundary decomposed into the four major tidal constituents (K1, O1, S2 and M2) as (2), obtained in a 15-year tidal analysis, and as a simple wave equation with an amplitude of 0.01 m and periods ranging from 1 h to 24 h for the resonance test:

$$sea\ level(t) = \sum_{i=0}^{n} a_i\, cos(w_i t + \theta_i) \qquad (2)$$

In (2), a is the tidal amplitude, w is the wave frequency and θ is the phase of each i tidal harmonic used. Sea level was imposed at the open boundary using the Chapman condition. Barotropic velocity was imposed using the Flather condition, following the recommendations of Carter & Merrifield (2007). Radiation conditions were established at the end of the channel. Baroclinic forcing, river discharge and heat fluxes were not included in the simulations, as the purpose here is to study barotropic tides in the bay.

Table 3.1. Configuration values used for the numerical simulations.
* For experiment GRID0.

Parameter	Numerical Value
L (number of I-direction rho points)	153
M (number of J-direction rho points)	106 (180*)
N (number of vertical levels)	6
Hmax	10m (channel)
Hmin	1m
Baroclinic time step	120 s
Barotropic time step	40 s
Horizontal harmonic mixing coef.	5 m^2/s
Bottom roughness	0.002 m
Dx	150 m

Different domains were used in order to conduct numerical experiments (presented in Fig 3.1). The first one (GRID0, Fig 3.1a) was the simplest schematization of the bay and was a straight channel 16.5km long, 4.5km wide and 4.5m deep. The second grid (GRID1, Fig 3.1b) was a channel that changed orientation and had a constant depth of 4.5 m. The objective for these two scenarios was to observe tidal propagation in the estuary when there were no major coastline irregularities, with and without bay orientation change. The third configuration (GRID2, Fig 3.1c) included coastline convergence, approximating the real morphology but still with flat bottom. The fourth configuration (GRID3, Fig 3.1d) considered the real bathymetry and coastline. The depth of GRID0, GRID1 and GRID2 domains was chosen in order to preserve the total volume of the four configurations (variations smaller than 0.5% of the total volume). Thirty days of simulation were performed in order to analyze the amplitudes and phases with harmonic analysis, excluding 10 days of spin-up. For resonance tests, spectral analysis was carried out for 30 semidiurnal cycles using amplitudes of one point at the mouth and one point at the head of the bay.

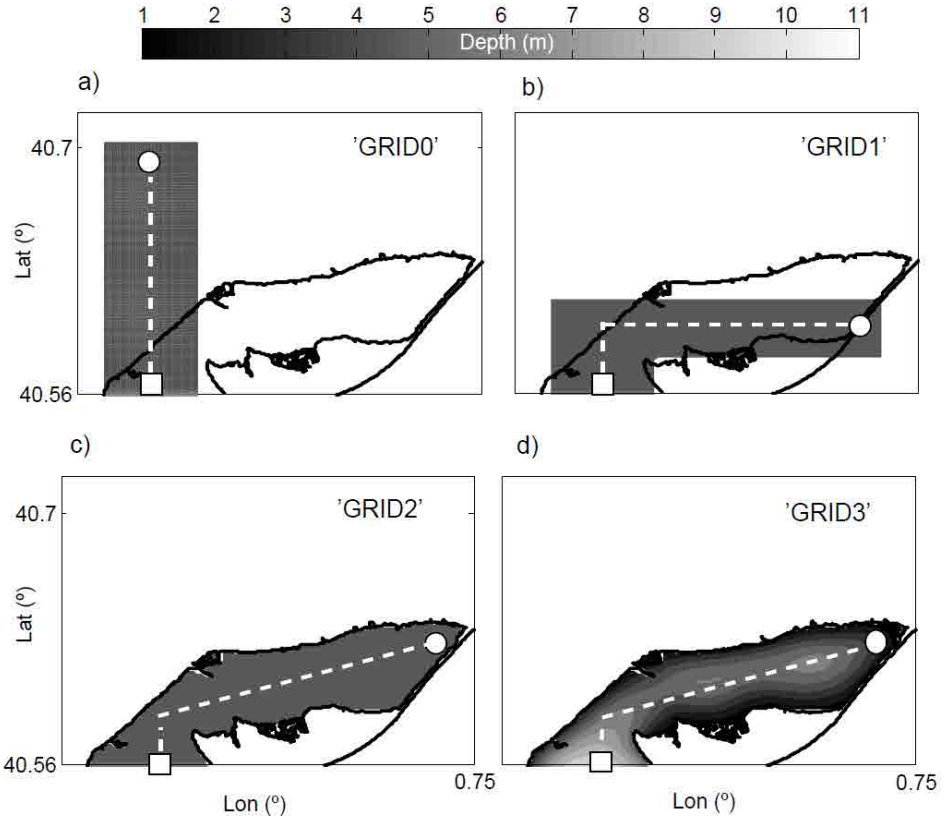

Figure 3.1. Different grids used in numerical simulations: a to d: GRID0, GRID1, GRID2 and GRID3. In each one of them, white dotted line represents transect used for the amplitude and phase analysis. White square and circle indicates the reference point on the mouth and head respectively. Colorbar represents the bathymetry (in meters).

2.2 Test Cases

***Experiment 1*:** Tidal propagation: GRID0, GRID1, GRID2 and GRID3 domains were used with sea level imposed as a boundary condition (compound wave with the main harmonics). The results of the GRID3 test were used to analyze tidal propagation in the system. The effects of bay orientation change, coastline convergence and bottom friction on tidal propagation were determined with the GRID0, GRID1 and GRID2 results.

***Experiment 2*:** Resonance test: For this experiment, only GRID3 was used. The objective was to investigate the resonance period of the bay by representing its wave propagation, amplitude and phase variation, as well as the velocities associated with the resonant wave. For this purpose, several analytical cosine functions were prescribed at the open boundary with periods ranging from 1 h to 24 h (Δt=1 h) (Zhong et al. 2008). Amplitudes of 0.01 m were imposed at the boundary. The model started from rest and ran 30 cycles after 48 h of spin-up. The wave amplitudes at the mouth and the head of the bay were obtained through spectral analysis, as well as at both locations of bottom-pressure measurements ("A1" and "A2").

Experiment 3: Bottom friction sensitivity: Bottom friction parameterization can be changed in the numerical simulations to determine its relative importance. A sensitivity test was carried out for the bottom roughness (Zob) through log-profile parameterization (Warner et al., 2008). The values of Zob used were 0.004 m for a high-friction test (GRID3-HF), in which the values used in GRID3 were doubled, and 0.001 m in the low-friction test (GRID3-LF), in which the values used in GRID3 were halved. These values agree with other numerical applications (Guo & Levinson, 2007; Warner et al. 2008). All test cases and their main characteristics are summarized in Table 3.2.

Table 3.2. Summary of the numerical experiments designed.

Experiment	Name test	Characteristics
1-Tidal propagation	GRID0	Geometric shape + flat bottom
	GRID1	Geometric shape + axis-turn + flat bottom
	GRID2	Coastline + flat bottom
	GRID3	Coastline + bathymetry
2-Ressonance test	From 1h to 24h. (time interval 1 hour)	Realistic geometry, sea level forced by sinusoidal periods from 1 to 24h
3-Friction	GRID3-HF	Variation of friction : High friction (Zob=0.004m)
	GRID3-LF	Variation of friction : Low friction (Zob=0.001m)

3. Results

3.1 Tidal Analysis

The main constituents described by the 15-year harmonic analysis of sea level in Sant Carles de la Ràpita harbor (Fig 2.1 in chapter 2, "SC") are shown in Table 3.3. Three new tidal harmonics not present in the XIOM network's yearly analysis appear: solar annual (Sa), solar semiannual (Ssa) and S1. The amplitudes of these harmonics are quite noticeable, with Sa being the main tidal amplitude and Ssa having values close to those of K_1 and M_2. However, owing to their long periods and corresponding wavelengths they are not relevant to the tidal currents. Shallow tidal harmonics (i.e. M_3, MN_4, M_4, MS_4) are also revealed in the analysis but have relatively small amplitudes. Fig 3.2a illustrates the decomposition in astronomical tide and residual for September 2011. The black thick line represents the hourly astronomical tide and the black thin line represents the residual for the same period.

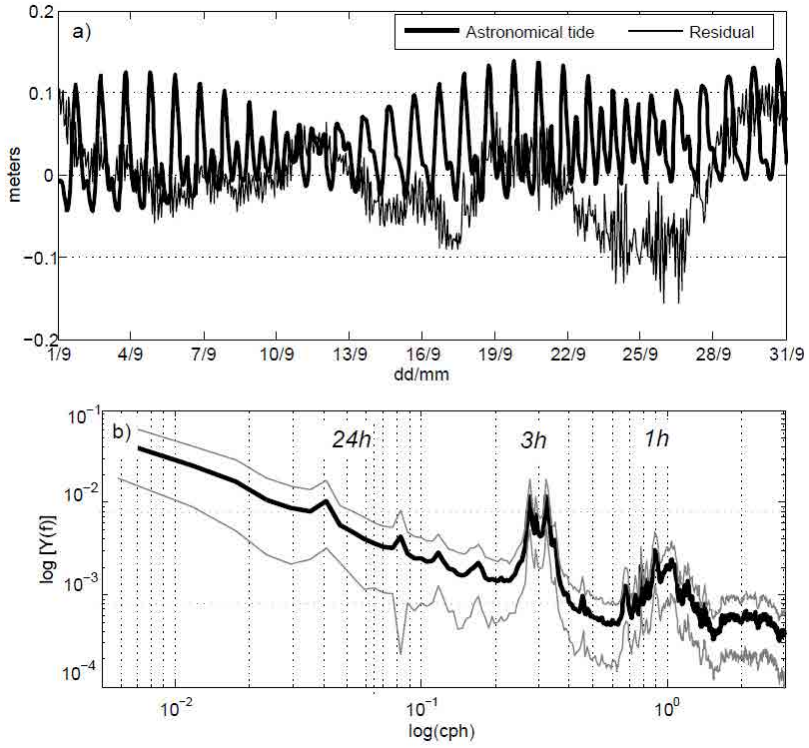

Figure 3.2. Tidal analysis in the Alfacs Bay. a) Black thick line for September 2011 sea level normalized over yearly mean from 1998 to 2012 in Sant Carles de la Ràpita (SC in Fig 3.1). Black thin line for corresponding residual. b) Power spectra of the 1998-2011 sea level residual. Black dotted line shows standard deviation for each frequency. Values in the plot show the corresponding period in hour.

Fig 3.2b presents the power spectrum of the 15-year 10 min residuals. This analysis reveals spectral peaks at different periods of interest: around 3-h, diurnal and semidiurnal components, and a broad band peak centered on 1-h. Over a 30-day period, from 14 July to 14 August 2013, sea-level variations were recorded by each instrument deployed in the field campaign; these

variations are shown in Fig 3.3 (plots *a* to *d* correspond to A1, A2, V-1 and V-2 points summarized in Table 2.1). Only from 22 to 26 July the astronomical signal is identifiable in A1 and A2 (Fig 3.3a and Fig 3.3b). The rest of the time, sea-level shows high variability without a clear signal of the astronomical band. In Fig 3.3c the sea level variation for V-1 presents lower amplitude in comparison to the mentioned stations, whereas in V-2 (Fig 3.3d) the sea level variation shows similar values and ranges to A2 (Fig 3.3b). Light grey boxes mark events during which marked 3-h oscillations were observed, while the dark grey box identifies events with noticeable 1-h oscillations (note sea level amplitude of about 70 cm). The depth-averaged alongshore component for the same period recorded at A1 and A2 is presented in Fig 3.3e and 3.3f, respectively. These panels show relevant variability, without an astronomical signal observed at both sites. Averaged currents at A1 are larger than those observed at A2 (6.8 $cm \cdot s^{-1}$ in mouth and 4.7 $cm \cdot s^{-1}$ in inner bay). On the rotated axis, the standard deviations in the alongshore direction are between 4 and 6 times larger than crosshore current standard deviation. Main fluctuations in the alongshore component are associated with seiching oscillations (light and dark grey boxes in Fig 3.3). During the marked periods, alongshore velocities are intensified at the 1-h seiche period (velocities up to 50 $cm \cdot s^{-1}$ during 4 August).

Table 3.3. Tidal components for 15-year harmonic analysis of sea level in Sant Carles de la Ràpita (SC in Fig 2.1). Asterisk mark the tides that the sum represents more than 95% of total tidal amplitude. Double asterisk identifies tides used in numerical tests.

Tidal component	Period (1/frequency) in h	Amplitude in m	Phase in º
Annual			
Sa	365.17 days	0.059	250.34
Ssa	182.58 days	0.032	82.11
Diurnal			
O_1**	25.82	0.021*	111.18
P_1	24.06	0.012*	147.32
S_1	24.00	0.012*	242.40
K_1**	23.93	0.033*	161.69
Semidiurnal			
N_2	12.66	0.007*	204.46
M_2**	12.42	0.033*	214.65
S_2**	12.00	0.009*	232.29
K_2	11.97	0.003	223.58
M_3	8.28	0.002	168.12
MN_4	6.27	0.002	323.70
M_4	6.21	0.006	4.27
MS_4	6.10	0.004	69.11

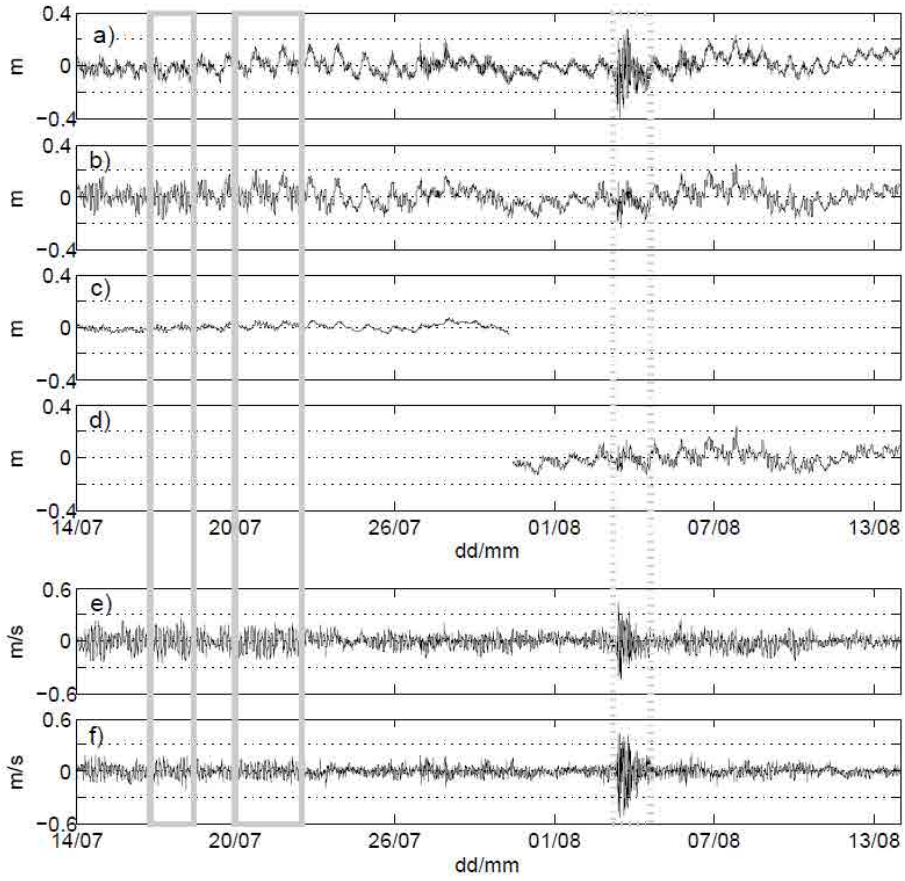

Figure 3.3. Sea level records from July 14th to August 14th 2013 on A1 (a), A2 (b), V-1 (c) and V-2 (d). Depth-averaged alongshore velocities from A1 and A2 are presented on plots e and f respectively. Continuous and dashed grey boxes marks periods with three and one hour's sea level oscillations respectively.

Spectral analysis of each sea-level time series shown in Fig 3.3 is presented in Fig 3.4. Frequencies corresponding to diurnal and semidiurnal tides are represented with similar intensities in A1, A2 and V-2. The 3-h period (frequencies of close to 0.3 cph) is most pronounced at A2 and V-2. Moreover, frequencies of around 1 (equal to a 1-h period) are only relevant at A1. Frequencies close to 6-h period (between semidiurnal and 3-h) show also noticeable intensities corresponding to MN_4, M_4, MS_4 (described on the inter-annual sea level analysis). Furthermore, peaks around 2 and 2.5-h period are shown in Fig 3.4. These peaks are reported for the first time in this system and present similar intensities in A1, A2 and V-2 (Fig 3.4a, Fig 3.4b and Fig 3.4d). All peaks at V-1 (Fig 3.4c) have lower amplitudes than at the other sites.

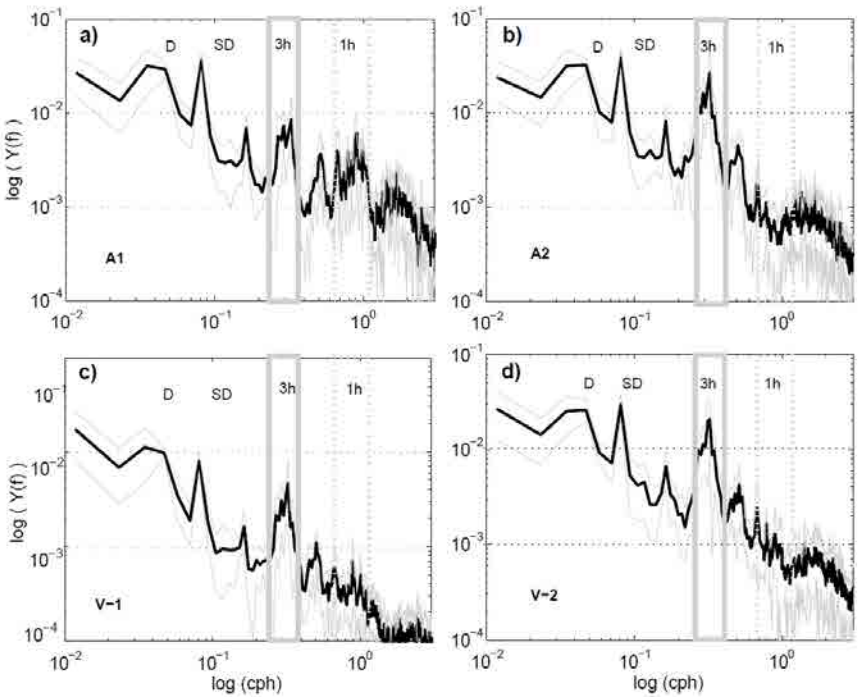

Figure 3.4 Power spectra of sea level records at A1 (a), A2 (b), V-1 (c) and V-2 (d). Grey thin line for standard deviation. D and SD shows diurnal and semidiurnal frequencies respectively. Light grey boxes show most noticeable frequencies detected on 3h, and dashed grey for 1h frequencies. Plots *a* and *b* (A1 and A2, respectively) account for almost 70 days of analysis, while *c* (V-1) and *d* (V-2) account for 25 and 45 days, respectively.

Grey diamonds in Fig 3.5a show the observed ratio between the A2 and A1 spectra for each of the most relevant frequencies identified in Fig 3.3 (i.e. 1-h, 2-2.5-h, 3-h, 6-h, 12-h and 24-h). Periods of 1-h revealed ratios around five times lower in the inner bay than in the bay mouth, while all other frequencies showed higher values (around three times for 3-h, and close to 3% for 24 h) in the inner bay. There is also a ~35% amplification of the 2.5h signal from A1 to A2.

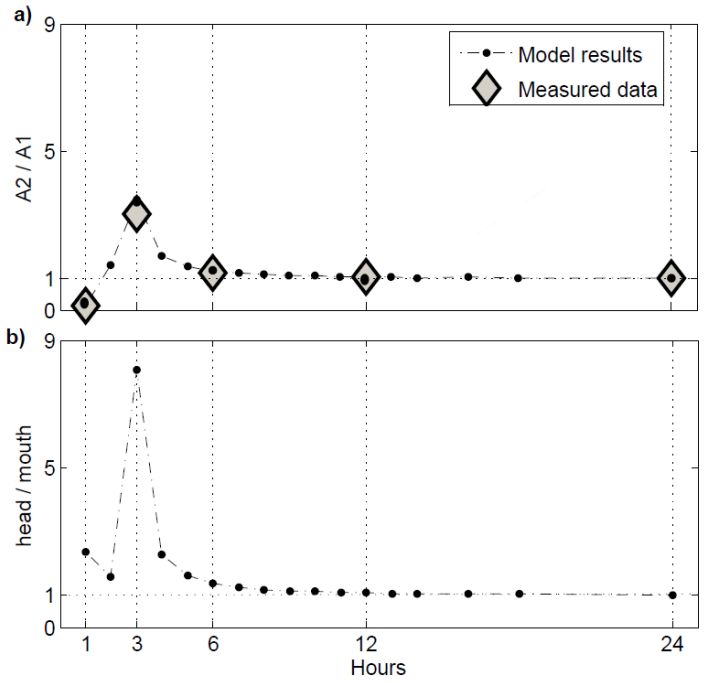

Figure 3.5. Observational and modeled spectrum comparison results. a) Relative amplitude values from A2 to A1 for both observational data (grey diamonds) and modeling results (black circles). b) Relative amplitudes values at the head in relation to the mouth for resonance tests (location in Fig 3.1d).

3.2 Numerical Results

The models performance is evaluated by comparing sea level spectral amplitudes between observations and numerical simulations (Fig 3.5). Black dots in Fig 3.5a show the relative magnitude of sea level between A2 and A1 obtained by spectral analysis of each numerical simulation. The numerical results show agreement with the observations in terms of spectral distribution. The amplitude relation for numerical tests from the inner point of the bay to the mouth (points described in Fig 3.1 as "reference" and "head") is presented in Fig 3.5b. In this case, the clearest differences with respect to Fig 3.5a were in the 1-h and 3-h periods. For the 1-h test case in Fig 3.5b, amplitudes were close to twice as high at the head as at the mouth. For the 3-h period, however, the amplitude at the head was approximately eight times as high as at the mouth. For periods larger than 4-h, the relative amplitude values tended to decrease in a gentle gradient but were always greater than 1.

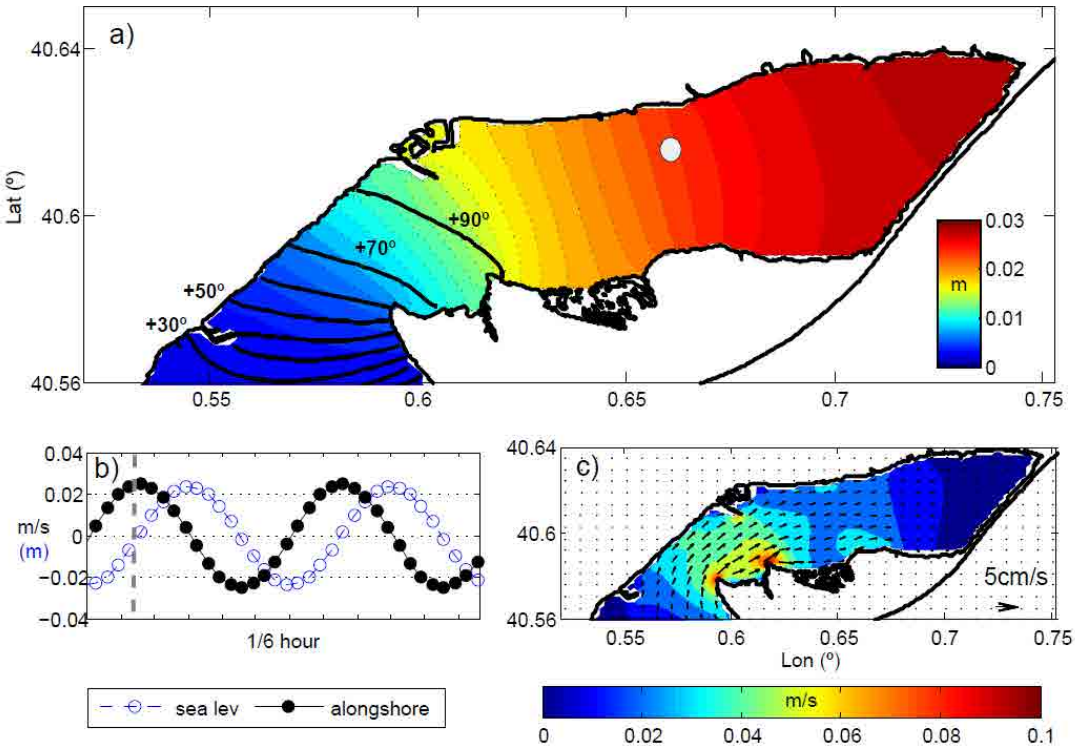

Figure 3.6. Numerical results for 3h wave period. a) Co-range and co-phase diagram. Dashed lines for absolute seiche amplitude, and continuous lines for phase values. b) Sea level (empty circles) and alongshore depth-averaged velocities (black filled circles) modelling results in A2 location. c) Model results for depth-averaged speeds in $m \cdot s^{-1}$ corresponding to the instant marked with dashed line in plot 6b.

Amplitudes and phases are shown throughout the bay for a 3-h wave in Fig 3.6a. The phases ranged from 0º to 90º at the mouth (along a 5 km stretch) and then remained almost constant

throughout the rest of the bay (with variations of less than 10º over a stretch of more than 10 km). The 3-h amplitudes demonstrated a progressive amplification of the signal along the bay, with values ranging from 0.004 m at the mouth to nearly 0.03 m at the head. The 3-h sea-level and depth-averaged alongshore velocity are shown for one location (black point in Fig 3.6a) in Fig 3.7b. A clear advance of around 40 min was observed between alongshore velocities and sea level. The vertical dotted line defines the instant plotted in Fig 3.6c, which corresponds to the maximum flood depth-averaged velocities. The lowest 3-h velocities (close to still waters) were found near the head (for ebb, the velocity ranges were almost the same), while the highest velocities (almost 8 cm · s^{-1}) occurred near the mouth.

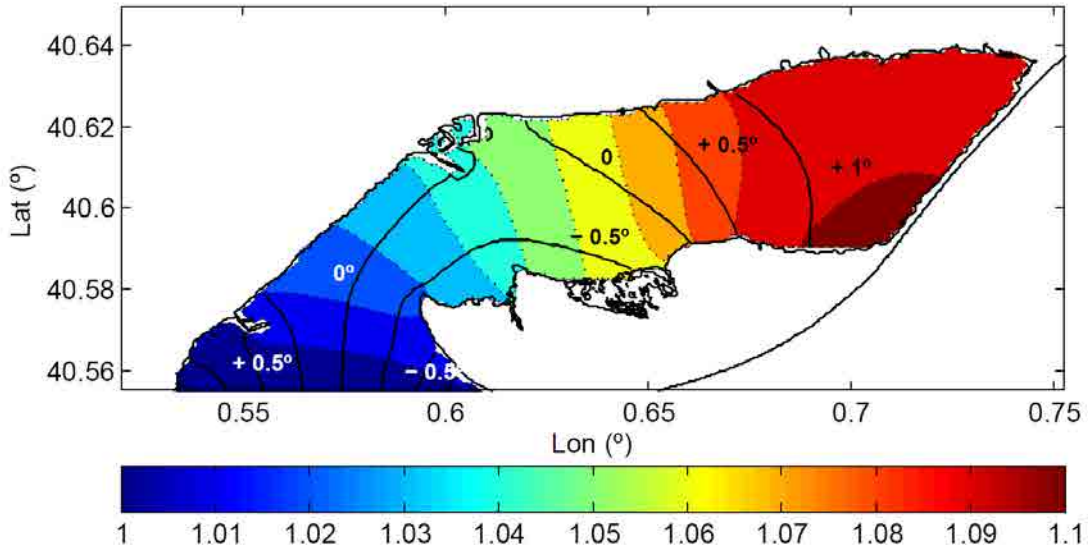

Figure 3.7 Co-tidal chart (M_2) from numerical results in the GRID3 test case. Relative amplitude variations (dotted line and color scale) and phase lag in degrees (black line) to the bay mouth reference point defined on Fig 3.1d.

The numerical results for tidal propagation in the GRID3 configuration for the M_2 component are presented in Fig 3.7. The amplitudes are plotted with reference to the amplitude at the bay mouth (Fig 3.1c) following (3); while the phase (black line) is plotted as a phase lag from any point in the bay to the mouth (Fig 3.1c) as (4).

$$Amplitude\_variation_{(i,j)} = \frac{A_{(i,j)}}{A_{(x_{ref},y_{ref})}} \tag{3}$$

$$Phase\_lag_{(i,j)} = P_{(i,j)} - P_{(x_{ref},y_{ref})} \tag{4}$$

In (3) and (4), i and j represent the matrix index in the x and y directions, respectively; A and P are the amplitude and phase, respectively; and x_{ref} and y_{ref} are the coordinates for a location chosen as reference. The bay exhibited an amplitude increase, with the highest values found near the head, while the phase lag between the mouth and the head was less than 2º. The tidal amplitude differences between the mouth and the head were close to 10% for the M_2 constituent. Similar patterns were obtained for the rest of the harmonics, with values ranging from 3% for diurnal tides to 11% for S_2 tides (Table 3.4).

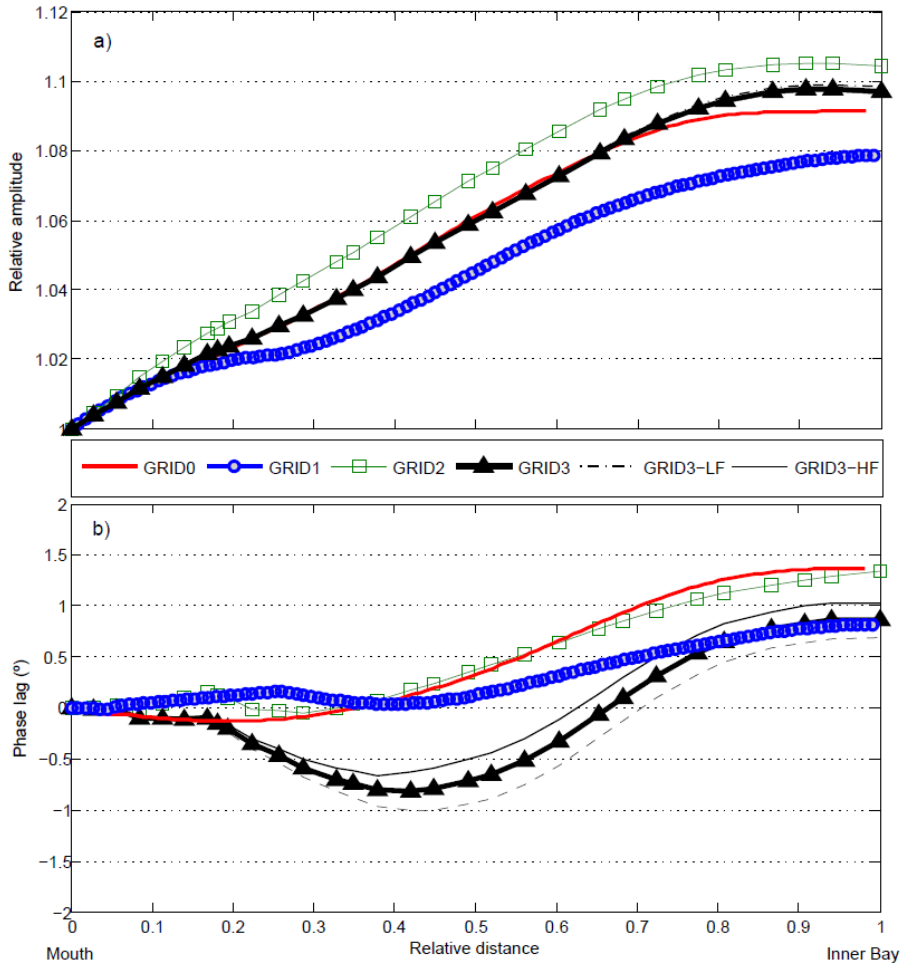

Figure 3.8. Numerical results for tidal propagation and bottom friction tests. a) Relative amplification to the bay mouth (defined on Fig 3.1) of the M_2 tidal signal through the bay (following transect in Fig 3.1a, 1b, 1c and 1d) and bottom friction experiments. Note that GRID3-LF (black dashed line) and GRID3-HF (black line) practically match with the GRID3 (black line with triangles) signal. b) Phase lag in relation to the reference point though the same transect.

Experiments 1 and 3 results are shown in Fig 3.8: tidal propagation (harmonic analysis) for the M_2 harmonic component for the four scenarios (GRID0, GRID1, GRID2 and GRID3) in experiment 1 and the results of the bottom friction experiment (GRID3-HF and GRID3-LF). The along-bay transects are defined in Fig 3.1. The relative amplitudes with respect to the

reference point at the mouth (Fig 3.1) are illustrated in Fig 3.8a. All tests revealed amplification of the tidal signal throughout the bay. Lines for GRID3-HF and GRID3-LF are not visible due to the negligible differences with respect to GRID3. The results show that the highest tidal amplification is in GRID2 (with values close to 1.11), followed by GRID3 (1.098), GRID0 (1.091) and GRID1 (1.079). Table 3.4 summarizes the transect results (differences from head to mouth) for all the harmonics used in the simulations. The same pattern is repeated among all the components, with the highest amplifications occurring in GRID2, followed by GRID3, GRID0 and GRID1. Fig 3.9b shows the phase lag at the mouth. All tests revealed phase variation from the head to the mouth of less than 1.5º. GRID1 and GRID3 exhibited the lowest phase lag (<1º) and the largest differences were found in GRID2 and GRID0 (around 1.5º). Friction tests revealed consistent patterns along the bay with small differences between them. The highest phase lag values were found in the highest friction test (GRID3-HF). Experiments using only one tidal constituent – i.e: O_1 – as boundary conditions, or in conjunction with others – i.e: O_1 and S_1 - do not show appreciable changes in the results.

Table 3.4. Harmonic analysis results for the second numerical experiment. Amplitude values in percentages (relative amplitude on bay head to the mouth, locations on Fig 3.2) and phase lags (in degrees) between same points.

Test / Tide	O_1	K_1	M_2	S_2
Relative Amplitudes (%)				
GRID0	2.9	3.1	9.0	9.8
GRID1	2.5	2.5	7.9	8.3
GRID2	3.4	3.4	10.5	12.0
GRID3	3.4	3.4	9.8	10.7
Phase lag (º)				
GRID0	0.6	0.6	1.3	1.6
GRID1	0.4	0.4	0.8	0.9
GRID2	0.7	0.7	1.3	1.7
GRID3	0.5	0.5	1.0	1.2

4. Discussion

The predominant influence of astronomical tides on sea level for semidiurnal and diurnal frequencies (amplitudes ranging from 5 to 10 cm for neap and spring tides, respectively) is shown in Fig 3.2a. On longer temporal scales than the fortnightly, the residual (thin black line) seems to dominate the sea-level signal. This signal is clearly affected by meteorological forcing such as atmospheric pressure and wind variations. However, Fig 3.2a also shows that the residual dominates the sea-level variations at periods of around 3 to 4-h in some instants (i.e. 27 September 2011).

Analysis of the residual spectrum in Fig 3.2b reveals different bands of interest. Diurnal frequencies (around 24 h), related to typical sea breezes in the spring-summer periods, are recognized (Font, 1990). In this case, diurnal winds from the SW seem to push water against the northern coast, implying a set-up and sea-level rise; when the sea breeze stops, sea level decreases. This behavior has been described in other small Mediterranean lagoons (i.e. Niedda & Greppi 2007).

The clearest spectral peaks (Fig 3.2b and Fig 3.4) are found at around 3 to 4 h. Fig 3.4 also shows noticeable intensities at diurnal and semidiurnal frequencies, but they are related to tidal constituents because the spectral analysis was carried out for total sea level signal, not only for the residual. As shown by Camp (1994) through spectral analysis of mouth currents and by Llebot et al. (2013), by establishing a seiche amplitude of O (10^{-2}) m, we can obtain the fundamental resonance period (Helmholtz mode, or n=0) by applying the quarter-wavelength relationship:

$$T_n = \frac{4L}{(2n+1)\sqrt{gh}}, for\ mode\ n = 0,1,2,.. \quad (5)$$

In Alfacs Bay, where L=16 km (bay length) and the mean depth is between 3 and 4.5 m, the fundamental resonance period ranges from 197 to 160 min (3.28 h to 2.7 h). Spectral analysis reveals three peaks, at 3.7, 3.5 and 3.2 h. These differences are probably related to the bay's irregular shape, which would result in temporal variability in the natural oscillation periods (Pugh 1996). The different amplitude intensities recorded at A1 and A2 (Fig 3.4a and Fig 3.4b) for 0.3 cph follow the description of a typical standing wave, with higher amplitudes close to the head than at the mouth.

Modeling results shown in Fig 3.5 and Fig 3.6 agree with the theoretical development of a standing wave within the bay. The amplification of the 3h wave observed in Fig 3.5b is consistent with the description of the node and antinode position in an open-ended rectangular

basin (Rabinovich, 2009). The highest amplitude values are found at the antinode and lowest values at the node. Fig 3.6 also shows that the node (amplitude variation close to zero) seems to be outside the bay. This agrees with the application of the mouth correction described in Rabinovich (2009), in which the nodal line was located close to but outside the entrance (due to the effects of wave energy radiation through the mouth and into the open sea). The seiche velocities (Fig 3.6c) from the numerical tests were almost 0 cm $\cdot$ s^{-1} at the head (corresponding to maximum amplitudes) and close to 7-8 cm $\cdot$ s^{-1} near the mouth (minimum seiche amplitudes). The highest velocities were located near the headland, consistent with curvature effects (e.g. Geyer 1993) and narrowing of the cross-sectional area between the headland and the coast. Because current maxima were located close to the mouth, they were consistent with theoretical arguments.

Previous studies have measured and detected seiches in water currents of Alfacs Bay. Camp (1994) used data from a current meter moored near Sant Carles de la Ràpita harbor, while Llebot et al. (2013) analyzed data from current meters located close to the center of the bay. Their results indicated the presence of seiching but with noticeable differences in intensity. This is probably associated with the nature of standing waves, which have higher velocities closer to the mouth (as revealed by Camp (1994) with values close to 8 cm $\cdot$ s^{-1}) than at the head (Llebot et al (2013) with values between 1.5 and 2.2 cm $\cdot$ s^{-1}). The results of our numerical tests, which found the highest values near the mouth, are consistent with these previous results. Moreover, Fig 3.6b shows the phase lag from tidal velocities to surface elevation, with values close to 90º, confirming the proposition of a standing wave. The data set presented in this study represents a more complete analysis with respect to the aforementioned studies because resonance was measured simultaneously at two points (versus only one point of previous studies) in terms of both velocity and sea level.

Similar resonance phenomena could be seen at periods around 1 h, as shown in Fig 3.2b, Fig 3.3 and Fig 3.4. In order to explain this phenomenon, lateral seiching seems not feasible because applying Merian's original formula for an enclosed basin: $T = 2L/\sqrt{gh}$ gives 30 minutes or less; which is not corresponding with the 1-h period detected. On the other hand, the first mode of the co-oscillating wave following equation (5, (n=1)) gives values of around 1 hour -similar behavior to that reported by Rabinovich & Levyant (1992), in Rabinovich (2009) -, which should be a reasonable option. Several factors seem to confirm this idea: Fig 3.3 shows that the 1-h sea-level oscillations are mostly detected at A1 (Fig 3.4a) and at the Sant Carles de la Ràpita tide gauge (data from this period are not shown) while not much of interest is detected at A2 and V-2 (Fig 3.3b and Fig 3.3d). Moreover, the currents measured at both A1 and A2 (Fig 3.3e and Fig 3.3f) showed spatial variations: higher velocities (depth-averaged values close

to 60 cm · s^{-1}) in the inner area of the bay and not as high at A1 (45 cm · s^{-1}). This means that, for this long wave, one antinode is located at the head and another inside the bay, near the Sant Carles de la Ràpita harbor (close to A1). As for nodes inside the bay, one is located close to A2. The behavior described in Fig 3.5a and 3.5b for the 1 h period for both modeled and observed data agrees with the co-oscillating theory, being the ratios higher than one in Fig 3.5b and lower in Fig 3.5a. A conceptual idealization of both seiches (3h and 1h) is presented in Fig 3.9 in order to provide a better idea of what is happening inside the bay. The diagram also illustrates the spatial structure of these long waves in relation to the three observation points. For the 1h seiche A2 is located close to the node, having the lowest sea level oscillations. On the other hand, A1 and SC are located at approximately the same distance from the antinode, having higher sea level oscillations but smaller current velocities. For the 3h seiche the A2 is located close to the antinode while SC and A1 are closer to the node. This resonance might be related to wind forcing (Niedda & Greppi 2007; Zong et al. 2008), astronomic tides (Wong, 1990; Bowers & Lennon 1990) and/or atmospheric pressure variability (Rabinovich & Montserrat 1996; Vilibic & Mihanovic 2005). Future research will seek to determine its origin in Alfacs bay.

Interestingly, the 2.5-h peak shown in Fig 3.4 presents similar behavior within the bay than the 1 and 3-h seiche. In this case, SC is located close to the theoretical node as amplitudes for this frequency band (Fig 3.4b) are reduced. Following the scheme presented in Fig 3.9, A2 is further away than A1 from the node, being the A2 around 30% higher (measured and modelled results in Fig 3.5a). The 0.4 cph (or 2.5 h) oscillations may be explained following the behavior of tides in shallow waters (Pugh, 1996). Nonlinear interactions between the two most energetic waves in the bay – the M2 and the 3-h seiche-, yield a distortion with frequencies (sum of M2 and seiche frequencies) around 0.4 cph. This is one of the few places where the interaction of tides and seiches has been documented as being able to produce distorted oscillations.

Tests carried out on GRID3 for the M_2 harmonic revealed a phase lag between the mouth and the head of less than 2º (Fig 3.7). Comparing these results with the theoretical phase lag for a long wave with propagation velocity 6.6m · s^{-1} ($v = \sqrt{g \cdot h}$) but with depth values of around 4.5 m, the phase lag should be close to 20º. Thus, indicating standing wave behavior. Similar phase-lag behavior was presented in Minguito et al. (2012) and Bower & Lennon (1990) for the innermost parts of estuaries in relation to the presence of a standing wave. Moreover, tidal propagation in the realistic domain (Fig 3.7, Fig 3.8, Table 3.4) reveals amplification of the tidal amplitude along the main axis of the bay with similar patterns for all constituents; the highest values were found for semidiurnal tides (10%, head to mouth) and the lowest values were found for diurnal tides (3%).

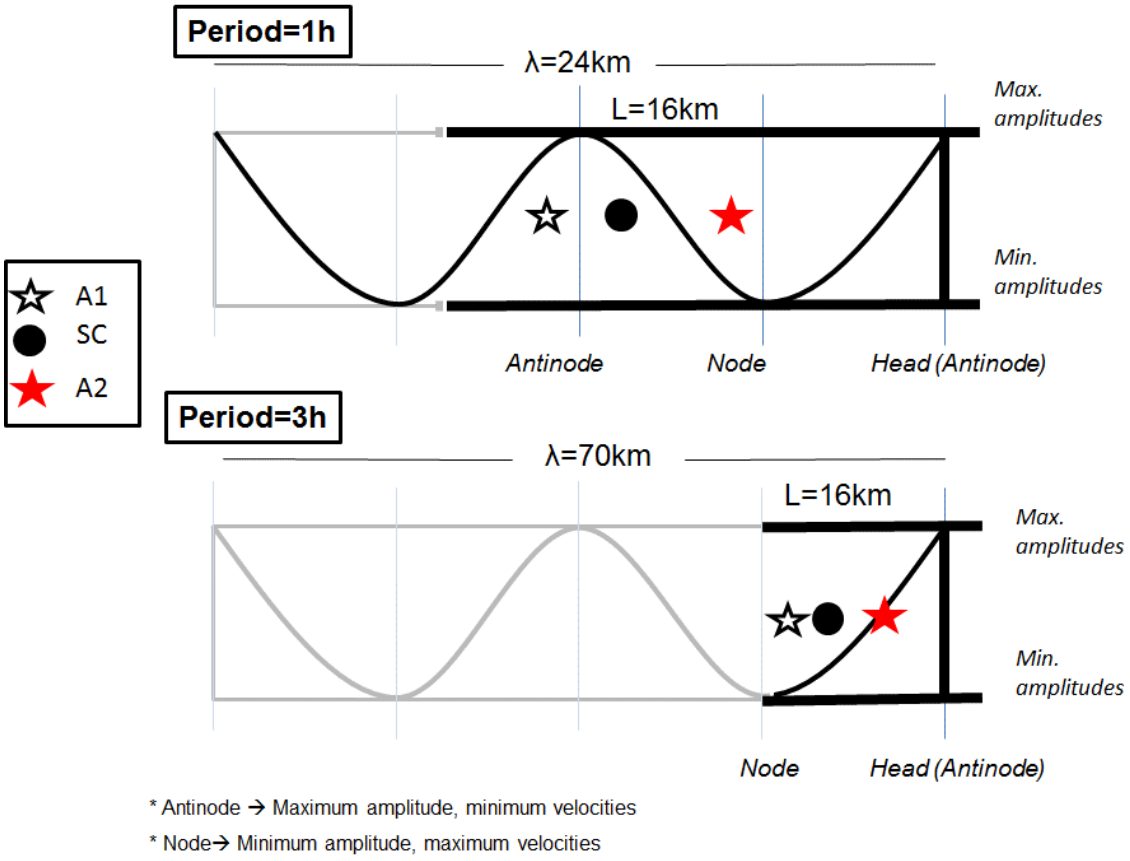

Figure 3.9. Conceptual scheme for 1 and 3h seiches in the Alfacs Bay. For 4.5m depth the wave propagation velocity is 6.6m · s^{-1}, which corresponds to a 23-24km and 70km wavelength for 1 and 3h respectively. Distances from the heads bay for A2, SC and A1 are 7km, 11 and 14km respectively.

Experiment 1 was designed to study geometry effects on water level amplification in this semi-enclosed water body. In particular the effects of resonance, coastline morphology and friction were investigated. The results for idealized schemes GRID0, GRID1 and GRID2 (Fig 3.8a) show tidal amplification, with higher values found over GRID2 than over GRID0 and GRID1. With its rectangular shape and flat bottom GRID0 only takes into account the amplification due to the dimensions of the basin. In turn, GRID1 describes how a basin orientation change would influence the tidal behavior. Results show relative M2 amplification from head to mouth (Fig 3.8a) around 9 and 8% in GRID0 and GRID1 respectively. Amplification differences between these configurations could be related to the axial change of orientation. In addition, the phase lag from head to mouth was close to 1.5º and 0.8º, thereby establishing standing-wave behavior with high water occurring simultaneously everywhere in both cases. When the actual coastline is added (GRID2) and the effects of the actual coastline are taken into account, tidal amplification is around 11% (3% more than in GRID1) and the phase lag is about 1.5º. Finally, the most realistic case (GRID3) includes non-uniform bottom effects in the analysis. Comparing its results with the simplified geometries, the amplification is clearly not affected

by friction, while subtle coastline effects are observed in GRID2. In consequence, the amplification along the bay is mainly due to the dimensions of the bay. Moreover, bottom fictional effects are relatively weaker than geometric effects in causing tidal behavior in the bay. The values measured at V-1 and V-2, both located in channels—V-2 closer to the bay (<100 m landward) and V-1 further away (approximately 500 m landward)—showed that friction becomes more important in the shallowest areas (like drainage channels), diminishing the tidal amplitudes (Fig 3.4).

Modeling tests with various friction values revealed that this area has low sensitivity to friction coefficients, as no noticeable changes in tidal amplitude variation were detected inside the bay. These results are consistent with those of Prandle et al. (2003), who showed that the relative importance of friction in tidal dynamics is established by a ratio of tidal amplitude over depth: if the tidal amplitude is much lower than 1/10 of depth, then it is not sensitive to friction. In Alfacs Bay, the highest tidal range during spring tides is around 0.2 m, which suggests irrelevance of friction in tidal amplitude distributions. The tidal phase lag shows similar patterns as GRID3 but with small differences due to the increase (+0.2º) or decrease (-0.2º) of bottom friction. Moreover, the highest differences in phase lag between numerical tests are observed between two sets of experiments: idealized systems (GRID0, GRID1 and GRID2; without bathymetry) versus GRID3 and frictional tests. In consequence, phase lag differences are related to actual coastal morphology and bathymetry. It could also be instructive to compare these results to macro-tidal conditions on more complex – i.e. channel ramification- and deep estuaries.

Taking into account all findings described above, we conclude that tidal behavior in this short embayment is mainly determined by the shape of the bay: nearly rectangular, with a change of orientation and not influenced by a river mouth at the head. For this reason, the tidal wave is not damped enough to lose its energy, thus allowing a partial reflection at the head. Because of the shortness and the geometry of Alfacs Bay, friction is not an efficient energy damper for the wave in the bay. This contrasts with the findings in longer estuaries such as Chesapeake Bay (Zong et al. 2008), where friction plays an important role in tidal propagation. In Alfacs Bay, the standing wave behavior agrees with the definition proposed by Li & O'Donnell (2005), in which a bay with the ratio $4L/\lambda_{M2} << 0.6$ (where λ_{M2} is the M_2 wavelength, and L is the bay's length) could be considered to be short and, consequently, to have standing-wave behavior (in Alfacs Bay, this relation is around 0.2). Therefore, the short basin geometry is evident in all astronomical tidal harmonics, and its effects decrease with wavelength (longer periods). The increase in amplitude is higher as the node gets closer to the mouth (shortest wavelength). This is clearly observed with the permanent presence of a resonant wave or seiche (Fig 3.2b). This

kind of behavior has been described in longer estuaries and bays with resonance periods close to those of M_2. For instance, Winant (2007) used an analytical model to show similar behavior for a system as long as one quarter of the wavelength of M_2.

Estuary types can also be categorized on the basis of the competition between estuary coastline convergence and frictional effects. Three types of estuaries are determined by the relative magnitude of the two terms (Dyer, 1997). Assuming this classification, Alfacs Bay can be classified as hypersynchronous, which means that geometric effects prevail over bottom friction within the central basin of the bay.

Finally, the presence of seiching modes (1 and 3-h) and their interaction with tides (2.5 h) within the bay, must influence water-column mixing and the circulation pattern. The rich variability in amplitude likely affects the stability of moored vessels and mussel farms. For similar high-resonance semi-enclosed water bodies one needs to be careful with the prescription of open boundary conditions for numerical studies. The inclusion of sea-level measurements within the bay or at its mouth may lead to under or overestimation of sea level because of tidal transformations and resonance phenomena in action at those sites. Future studies should therefore include an analysis of the meteorological forcing mechanisms responsible for the enhancement of seiches, the behavior of the associated horizontal currents, as well as the differences between the two other oscillation modes.

5. Conclusions

Tides in a short, microtidal embayment were analyzed using observations and a numerical model. Data analysis indicated standing waves in Alfacs Bay (NW Mediterranean Sea) with periods of about 3-h and 1-h, which, during some events, could be influenced by forcing and have amplitudes higher than those of astronomical tides. These waves were consistent with a quarter-wavelength resonance. The numerical model demonstrated an 8-fold amplification of the 3h oscillations from the mouth to the head of the bay. This followed a classical description of nodes and antinodes in a standing wave, and was also clearly seen in the associated high current velocities. Moreover, a previously unreported 1-h resonant wave was detected in the bay with velocities > 50 cm $\cdot$ s^{-1} in the inner bay. Also, an oscillation motions around 2.5-h was found related to the interaction of semidiurnal tides and 3-h motions. Analysis of the propagation of astronomical tides within the bay revealed an increase in amplitude ranging from 3% to 10% for diurnal and semidiurnal constituents, respectively. This behavior was studied through numerical experiments and was related to reflection at the head of the bay for all astronomical tides. The orientation change, the coastline morphology, and the frictional effects are relatively weak on tidal behavior, indicating a weak but clear geometric dominance.

6. Acknowledgments

This work was supported by a FPI-UPC pre-doctoral fellowship from European project FIELD_AC (FP7-SPACE- 2009-1-242284 FIELD_AC). The campaigns have been carried out thankfully to MESTRAL project (CTM2011-30489-C02-01). We would like to thank to Joan Puigdefàbregas, Jordi Cateura and Joaquim Sospedra for all the help on campaigns and data analysis, as well as Ebro Irrigation Community ("Comunitat de Regants de la dreta de l'Ebre", www.comunitatregants.org") and XIOM network ("Xarxa d'Instruments Oceanogràfics de Catalunya";www.xiom.cat) for the information and their commitment to the study. AVL acknowledges support from USF project OCE-1332718. The comments from four anonymous reviewers are appreciated.

4

Hydrodynamic response in a microtidal and shallow bay under energetic wind and seiche episodes

A scientist in his laboratory is not a mere technician: he is also a child confronting natural phenomena that impress him as though they were fairy tales.

Marie Curie

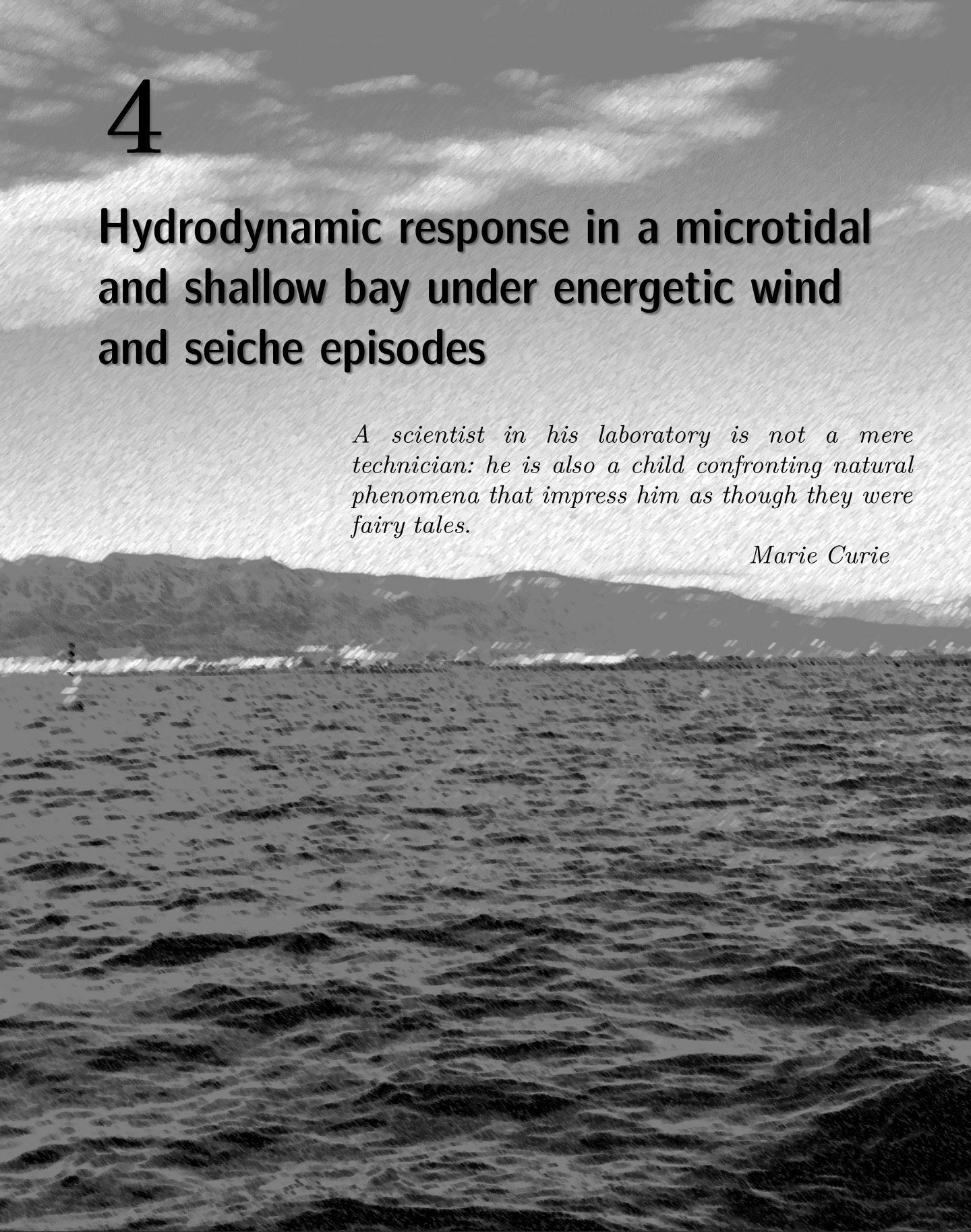

Cerralbo, P., Grifoll, M., Espino, M., 2015. Hydrodynamic response in a microtidal and shallow bay under energetic wind and seiche episodes. J. Mar. Syst. 149, 1–13. doi:10.1016/j.jmarsys.2015.04.003

Abstract

In this contribution we investigate the hydrodynamic response in a micro-tidal and shallow semi-enclosed domain. We chose a set of observations which include currents, hydrography and meteorological data obtained in Alfacs Bay (NW Mediterranean Sea). Short-term response to energetic winds events was found in the hydrography and water velocity observations, sometimes inverting the estuarine circulation or developing one-layered flow. In comparison to previous investigations in Alfacs Bay, we observed that water current variability, and also maximum velocities, were directly related to the development of surface standing waves (i.e. seiches). Mixing mechanisms versus buoyancy sources are studied through potential energy anomaly equation, proving the leading freshwater contribution to stratification, enhanced by heat fluxes in summer. On the other hand, mixing is directly related to winds, mainly in winter and early spring when both buoyancy forces are lower. We also study turbulent bottom mixing by seiches through observations, dimensionless relations and numerical modelling. Seiche induced mixing is suggested as an eventual mechanism that may break the stratification within the Bay under special circumstances.

1. Introduction

On estuaries and semi-enclosed bays, variations in current intensity during energetic events modifies the water circulation pattern, affecting water exchange with the open sea (Valle-Levinson et al. 2001), enhancing mixing process (Whitney and Codiga 2011) deepening or even breaking of the pycnocline (Dyer, 1991), changing biophysical properties (Jordi et al. 2008) and determining water quality issues (Grifoll et al. 2010). Moreover, the stratification grade of the water column can modulate the hydrodynamic response of the water body (Guo and Valle-Levinson 2008). The variety of typology of these coastal areas (Dyer, 1997), as well as the wide range of meteo-oceanographic forcings difficult the generalization and accentuate the importance of detailed analysis in each particular case.

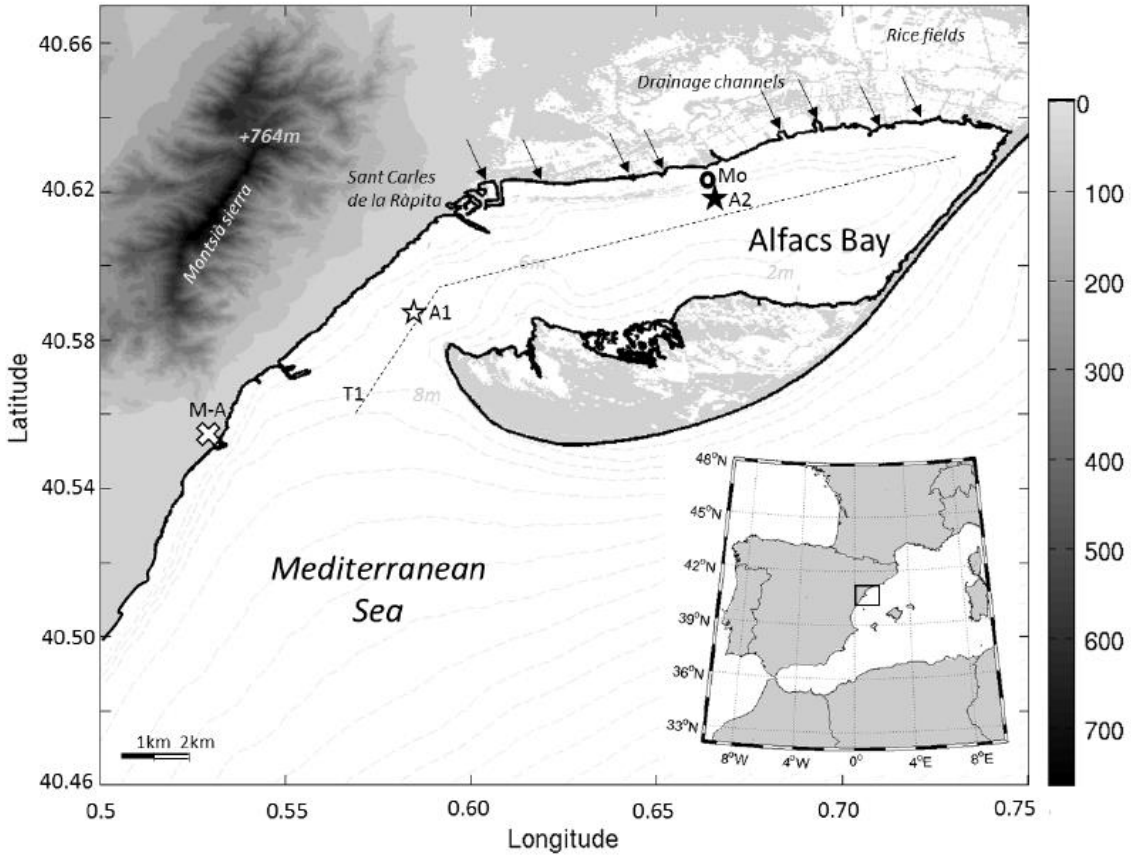

Figure 4.1. Location map of Alfacs Bay in NW Mediterranean Sea. White cross shows meteorological station (Met-A). White and black gilled starts marks A1 (ADCP Mouth) and A2 (ADCP and CTD in the inner Bay) locations respectively. Black circle marks Mo (modelling result) location. Black dotted line indicates transect T1. Bathymetry is represented by 2m isobaths. Colorbar for land topography.

In order to analyse the response of shallow semi-enclosed domains we choose Alfacs Bay, located in the Northwest Mediterranean Sea (Fig 4.1). Hydrodynamics of this bay have been studied intensively throughout the past 30 years (Camp and Delgado 1987; Camp 1994; Solé et al. 2009; Llebot et al. 2011). Both Camp and Delgado (1987) and Camp (1994) analyse the hydrography of the Bay through a set of Conductivity, Temperature and Density (CTD) profilers during different periods, classifying the estuary as salt-wedge -with an almost stable stratification throughout the year- due to freshwater fluxes received from Ebro Delta drainage channels. Previous studies identified the wind (Llebot et al. 2013) as the main forcing mechanism in a relatively short timescale. In chapter 3 we also identified sea-level variations at temporal scales of a few hours (called seiches), while tidal-induced velocities are negligible due to its microtidal regime -i.e. 10 cm during spring tides (Llebot et al. 2013)-. Despite the well-noted water circulation in Alfacs Bays, several questions remain open. For instance, a detailed description of the hydrodynamic response to energetic episodes is still poorly understood due to the short timescale associated to relatively shallow water depths (max. water depth is 6.5m), in which the frictional layers can overlap, thus influencing the mixing capacity under energetic events (Dyer 1991). In this sense, physical processes at these water depths are complex and challenging due to the amount of forcing involved and the non-linearity of the system (Noble et al. 1996). As a consequence, this contribution focuses on describing the eventual hydrodynamic response to the aforementioned forcings. The link between hydrography (density fields) and hydrodynamics is also addressed. To this end, a series of atmospheric, hydrodynamic and hydrographic variables are used. This example can be used to interpret hydrodynamics and mixing in similar domains.

2. Results

2.1 Wind, hydrographic and hydrodynamic description

Wind roses for both field studies (summer 2013 and spring 2014) are shown in Fig 4.2. Summer period (Fig 4.2a) reveals a clear bimodal behavior, without intense winds ($< 5 m \cdot s^{-1}$), and with prevailing directions from south and northwest. These wind patterns respond to the typical sea breeze patterns, with day time winds blowing from the sea alternating with calm night-time winds, typically present along the entire Catalan coast in these periods (spring to summer). In winter and early spring 2014 (Fig 4.2b), north-westerly winds were the most energetic ($> 10 m \cdot s^{-1}$), whilst sea breezes started to appear in late spring. During the both seasons, several energetic north-westerly periods were identified (Table 4.1).

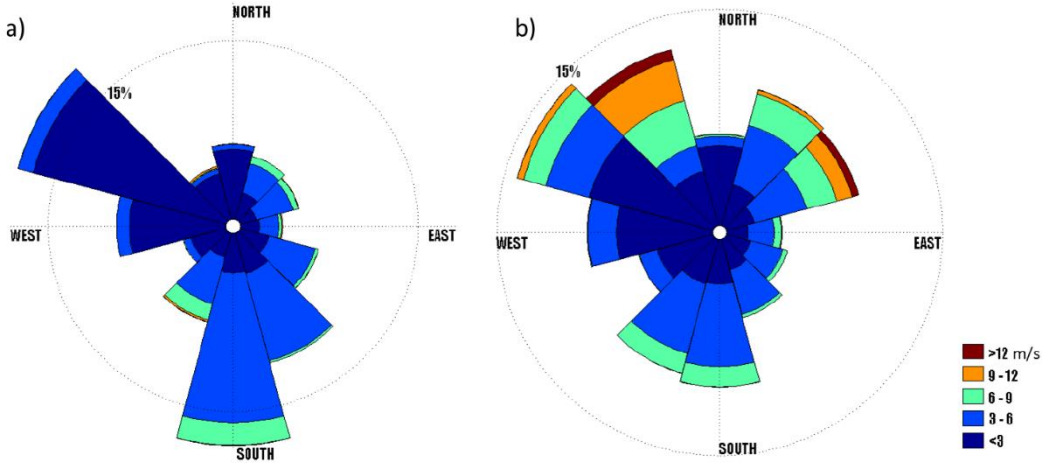

Figure 4.2. Wind Roses for Alcanar station (M-A on Fig 4.1) on both summer 2013 (left panel) and winter 2014 (right panel) campaigns. Wind intensities are grouped by intervals of 3m/s.

Longitudinal CTD transects along the main axis of the Bay (in Fig 4.1 as T1), during warm periods (I-1, I-2 and I-5, details in Table 2.1, chapter 2) for temperature and salinity show similar values (Fig 4.3a and 4.3e). Salinity contributions prevail in vertical density gradients, and their variations match with isopycnals (not shown), showing the saltiest water from outer sea in the deepest mouth layers (almost 38 PSU) and the freshest water on the surface (35-36 PSU). Stratification was lower in the inner bay, with lower salinity values on the water column and no signal of sea water mass on the bed. Within the Bay, freshwater was observed at surface layer extending from northwest to southeast, with lateral salinity differences across

the Bay of around 2-3 PSU and density variations around 3-4 $kg \cdot m^{-3}$. Although freshwater signal was also observed in the mouth, it was more obvious near the drainage channels (Fig 4.1). Temperature observations revealed a clear diurnal cycle (oscillation range ≈ 2ºC). Winter data (I-4) exhibited a well-mixed situation in the whole domain (Fig 4.3c) with almost vertical thermal and salinity isopleths. Temperature remained constant along the Bay with values around 12.5ºC; similar to the value obtained in the open sea (~13ºC). Evident gradients were observed in salinity distribution between the in and out. Within the Bay, salinity was almost constant on both vertical and horizontal sections with values between 35 and 36 PSU, whilst in the outer Bay it was greater than 37 PSU, forming an estuarine front in the mouth.

Table 4.1. Energetic scenarios definition, period, duration and mean depth averaged current speeds (in parenthesis the maximum hourly mean speeds).

Seiches					
Name	Definition	Period (dd/mm/yy)	Duration (h)	Speed ($m \cdot s^{-1}$)	
				A1	A2
S0_1	Fundamental seiche mode (Period=3h)	30/08/13	24	0.16 (0.24)	0.1 (0.17)
S1_1	First seiche mode (n=1) (Period=1h)	3/08/13	12	0.18 (0.26)	0.23 (0.3)
S0_2	-	26/03/14	12	0.16 (0.21)	0.13 (0.17)
S1_2	-	11/04/14	24	-	0.12 (0.19)
Winds					
Name	Definition	Period		Speed ($m \cdot s^{-1}$)	
				A1	A2
NW_1	North-western wind (summer)	8/08/13	4h	0.14 (0.16)	0.08 (0.13)
NW_2	North-western wind (winter)	23/03/14	12h	0.15 (0.18)	0.12 (0.17)

The Brunt-Väisälä frequency, $N^2 = -(g/\rho)(\partial\rho/\partial z)$, at A2 location is shown in Figures 4.3b, 4.3d and 4.3f. Un-stratified conditions ($N^2<10^{-3}$ s^{-2}) were only observable in winter (Fig 4.3d), during the closed channel period. In other profiles, double halocline at 1-2m and 4-5m in the water column (N^2 between 0.01 s^{-2} and 0.02 s^{-2}) was observable in both midsummer and late spring (Fig 4.3b and 4.3f), showing the largest density differences from surface to bottom. In these profiles, both temperature and salinity contribute positively to water column stratification, thus indicating the important role of both freshwater inputs and heat fluxes. The CTD profiles measured agree with previous studies that identify the pycnocline at 3-4m depth (Camp 1994; Llebot et al. 2013). However, our observations show well-mixed water column under particular conditions, as observed in (Camp and Delgado 1987), in contrast to

previous studies which define quasi-permanent stratification throughout the year (Llebot et al. 2011).

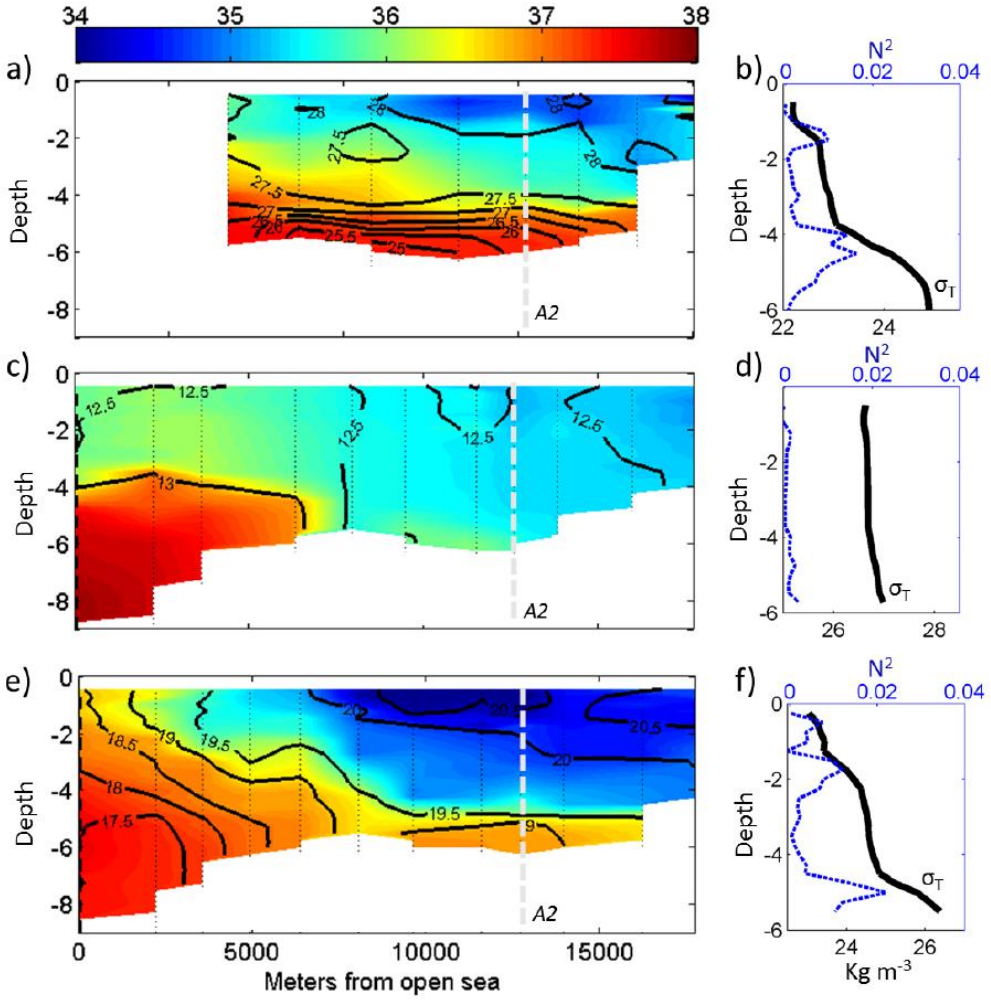

Figure 4.3. Transect T1 (shown in Fig 4.1) for both salinity (color) and temperature (black lines) for July 2013 (a), February 2014 (c) and May 2014 (e). Panels b, d and f for corresponding squared Brunt-Väisälä (N2) in dashed blue line, and σt density in black thick line, to each period on A2 location (black dashed thick line shows A2 location in each transect). Temperature is in ºC and salinity in PSU.

Temperature data from CTs sensors deployed in the Bay (A2 in Fig 4.1) for both summer and spring periods is summarized in Fig 4.4 (images a and b respectively). In summer, surface temperature time series showed a clear diurnal pattern. This pattern occurred until the end of summer. Differences between surface to seabed temperatures were greatest at the beginning of summer (6-7ºC), decreasing until the start of August, when suddenly (few hours) surface temperatures fell by more than 4ºC. From the end of July to early September, these differences were negligible (around 1-2ºC). Finally, during September, two periods of thermal inversion (deeper waters being 0.5-1.5ºC warmer than surface waters) occurred. Correlation

between surface and bottom waters was low, indicating no relation between surface and bottom layers in a short time scales. During winter and spring (Fig 4.4b), well-mixed conditions were more prevalent, with mean temperature gradients between surface and bed being lower than 2ºC. On May 2014, thermal stratification started.

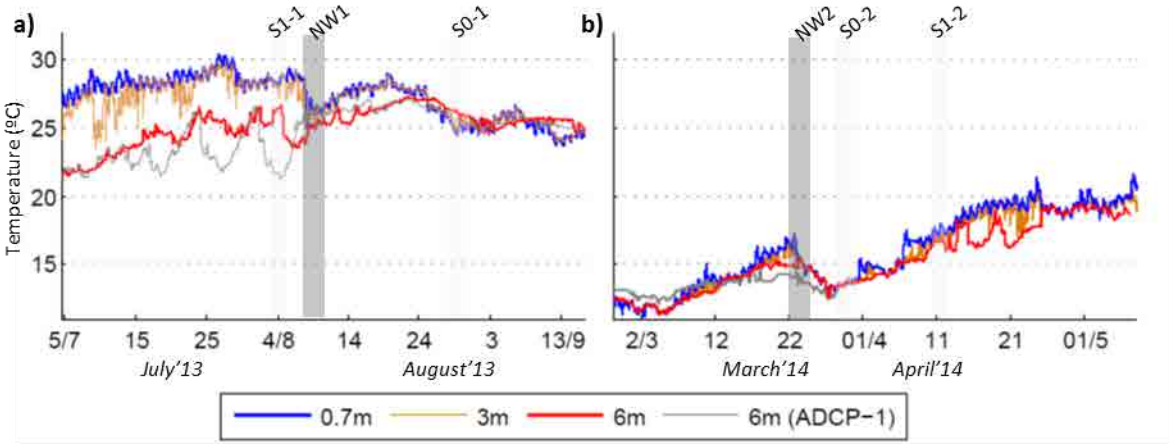

Figure 4.4. Panels a and b shows temperature evolution of CTs sensors in A2 and ADCPs (A1 and A2) on bottom for both summer (a) and spring (b). Energetic events described in Table 1 are marked by gray boxes: darker for wind and light for seiche episodes

On the other hand, two frequencies revealed significant spectral energy around 0.125 and 0.03125 days^{-1} (corresponding to periods of 3h and 1h respectively) in water currents, which prevail over the tidal signal. The effects of these oscillations on water currents were analyzed using wavelet analysis (Fig 4.5b and 4.5d). This analysis was performed using software referenced in Torrence and Compo (1998) and using standard Morlet wavelet function. The results allow us to determine periods in which both fundamental (3h) and first mode seiches (1h) are the most energetic contributors to sea-level and corresponding velocity variations (Fig 4.5).

The axis system was rotated using Principal Component Analysis (PCA) in order to obtain the maximum variability, which approximately follows an alongshore direction. Thus, alongshore direction was rotated 59º -similar to main direction described in Camp (1999)- and 36º for summer and spring campaign on A1, and 21º and 26º (anti-clockwise positive from North) for A2 in the same periods. These directions account for 95% and 96% of the depth-averaged velocity variability in summer (Fig 4.5a and Fig 4.5c A1 and A2 respectively), and 90 and 94% in spring for both A1 and A2 respectively. Data and some statistical values are summarized in Table 4.2. No appreciable rotation was observed in the variability angle

direction for each layer (differences of +/- 2º). The principal eigenvector from Empirical Orthogonal Functions -EOF analysis description in Emery and Thomson, 2001- explained around 74 and 71% (summer) and 74 and 74% (spring), for A1 and A2 respectively, and showed a clear barotropic behavior. On the other hand, baroclinic behavior (defined as an eigenvector crossing 0 line in Winant and Bratkovich, 1981) was determined by the second and third eigenvector. These values are summarized in Table 4.2. Cross-shore EOF for both locations (not shown) shows baroclinic behavior for all the eigenvectors. The results of EOF analysis (Table 4.2) highlight the importance of barotropic seiche in this Bay at short timescales. An analysis of maximum alongshore currents revealed maximum values during summer for both locations (and related to seiches). Maximum cross-shore components were identifiable during spring periods with negative values and related to wind events. On the other hand, astronomic tide represents a second-order forcing due to the microtidal behavior. Maximum depth-averaged tidal currents obtained using TTIDE software (Pawlowicz et al. 2002) were approximately 2-3 $cm \cdot s^{-1}$.

Table 4.2. ADCP basic statistics of Depth-Averaged velocities (10-minutal data). 'Direction' indicates direction of first axis in PCA analysis, and '%' for corresponding percentage of variability explained. U' and V' for corresponding along and crosshore velocities (re-oriented in its corresponding 'Direction'). Last three rows resume first three vertical eigenvectors of EOF analysis on alongshore component (U'). Baroclinic eigenvector (cross-zero) underscored.

		Summer 2013		Winter 2014	
		A1	A2	A1	A2
Direction (º)		59	21	35*	26
% variability		95	96	90	94
U' (ms^{-1})		-.41 / .52	-.53 / .42	-.28 / .29	-.28/.35
V' (ms^{-1})		-.07 / .09	-.08 / .08	-.2 / .1	-.14/09
EOF	1st	74	71	74*	74
	2nd	12	11	15*	12
	3rd	5	4	4*	3

* Only one month of data

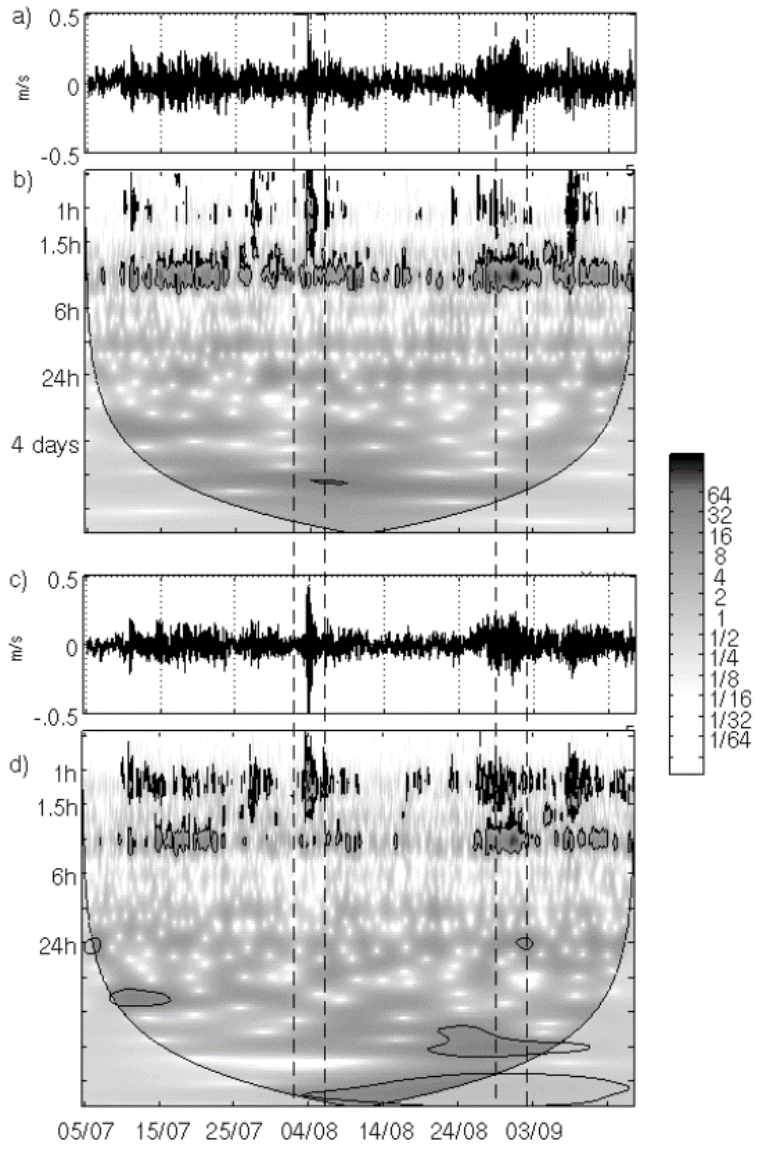

Figure 4.5. Depth averaged velocities and local wavelet power spectrum. Panels a and c shows the depth-averaged velocities (10') for both A1 and A2 respectively in summer campaign. Images b and d shows corresponding local wavelet power spectrum (in units of normalized variance) of depth averaged alongshore velocities in A1 and A2 respectively. Shaded regions indicate the cone of influence where edge effects become important.

2.2 Hydrodynamics during seiche and wind episodes

Different seiche events were defined throughout the summer and spring periods. The events are defined as S*-**, where * could be 0 or 1, and indicates the standing wave mode (0 for fundamental mode, and 1 for the first one), and ** indicates the corresponding number of event. The definition of each event was made according to the observation of corresponding wavelet figures (summer wavelets for A1 and A2 in Fig 4.5). Most clear episodes are summarized in Table 4.1, and also indicated with a dashed box in Fig 4.4 and Fig 4.5. In Fig 4.6a and 4.6b, velocity profile for one-day length and for two periods, S0-1 (in A1) and S1-1 (A2), are shown. One-layered motion of the water column is clearly observable for both cases. The maximum alongshore velocities for S1-1 are almost 50 $cm \cdot s^{-1}$ in A2 and approximately

40 cm · s^{-1} in A1, and in opposite phase. This agrees with the 1st seiche mode described in chapter 3, defining the seiche node closer to A1. For fundamental 3-h seiches (S0-1, in Fig 4.6a) maximum current speeds were around 40 cm · s^{-1} in A1 and 24 cm · s^{-1} in A2.

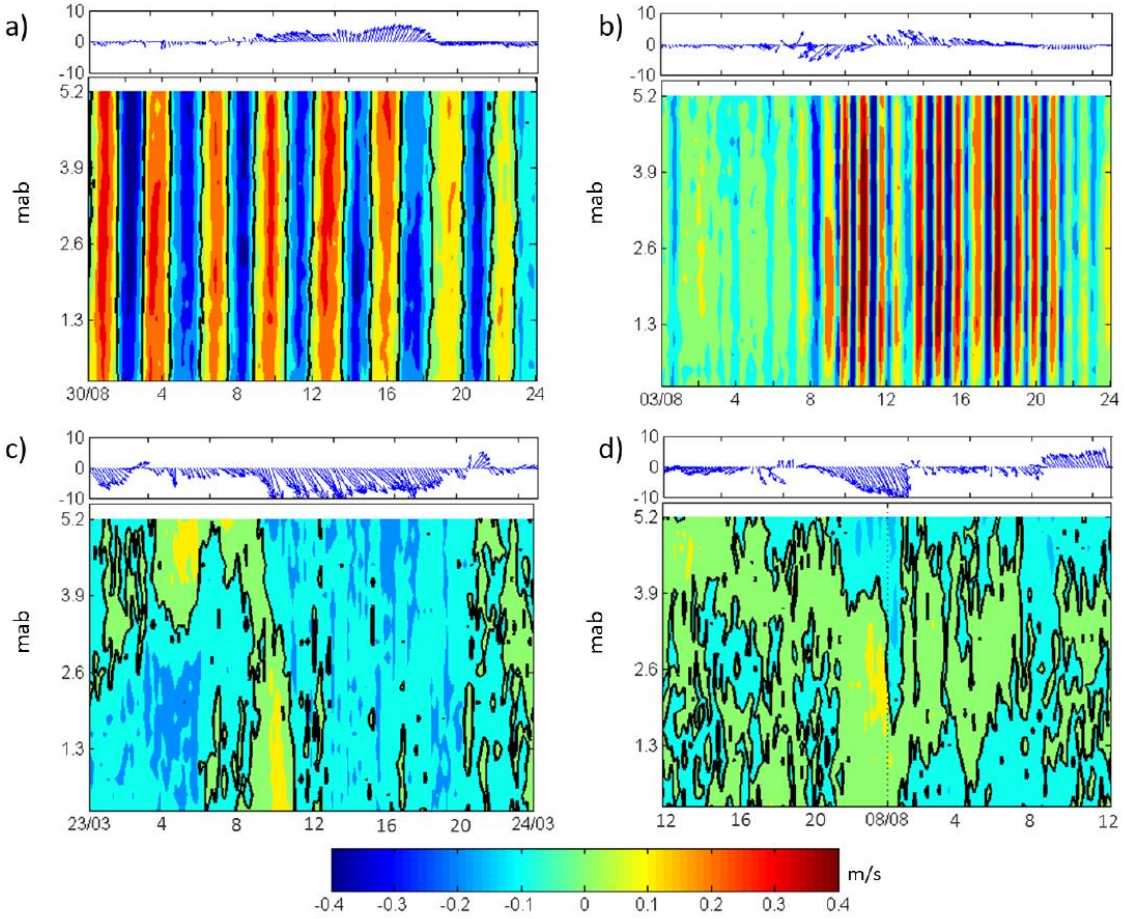

Figure 4.6. Each panel shows on the top the wind measured at M-A, and on the bottom the vertical profiles of current velocities measured at ADCP locations. Velocities contours plotted in depth (mab: meters above bottom) versus time (24h). Different events are showed. a) A1 for 30/8/2013, showing 3h seiche (S0-1). b) Bay ADCP for 3/8/2013, showing 1h seiche (S1-1). Image c) for crosshore velocities during NW events on 23/3/2014 in A1. d) Crosshore velocities for A2 in 8/7/2013 (NW-1). Black lines shows 0 velocity isolines.

This fundamental mode was persistent during summer consistent with wavelet analysis presented in Fig 4.5b. The mean seiche excursion length, defined here as the distance travelled by a body of water between low and high water slack, could be estimated from the RMS current speed times the half tidal period (Waiters et al. 1985). For first mode (S1-*) events was around 650m in A2 and 500m in A1 (in 30 minutes). For fundamental mode, these excursion lengths move between 1400m for A1 and 700m for A2 (in 90 minutes). Finally, effects of these seiches on temperature records are recognizable in summer (S1-1), and in spring (S1-2) in Fig 4.4a and Fig 4.4b. Intensive CTD studies did not coincide with any of the

intense seiching episodes observed, so no relationship between density fields and seiches could be determined using CTD profiles.

On the other hand, two energetic events (intensity > 10 $m \cdot s^{-1}$) of north-westerly (Mistral) winds were selected in order to understand the short-time response of the Bay to the most energetic winds in this area (Table 4.1). On summer, late at night on August 7, 2013 (NW-1) when the sea breeze stopped, an N-NW intensification ($10m \cdot s^{-1}$) was observed in Met-A station (lasting for 3-4h). In A2, the alongshore velocities did not reveal a clear effect due to the N-NW wind; but the effects were observable in cross-shore velocities (Fig 4.6d), showing a two-layer flow with a southward component at the surface layers.

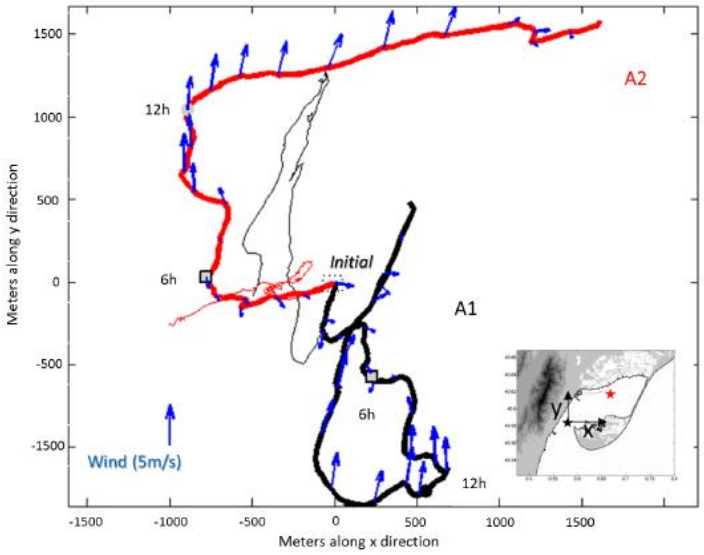

Figure 4.7. Progressive Vector Diagram for surface (thick) and bottom (thin) layers in A1 (black) and A2 (red). Period length about 24h, and corresponding to sea breeze period on 6th July 2013. Hourly wind data measured in Met-A is ploted (blue arrows) in corresponding hour.

On A1, usual estuarine –two layered- circulation on alongshore currents were observed (not shown) with no noticeable effects of wind stress. In spring, N-NW are more frequent and with higher speeds (Fig 4.2). In most episodes, the wind blows for more than 12h at intensities around 10 $m \cdot s^{-1}$ with gusts of approximately 25 $m \cdot s^{-1}$ for NW-2. Effects on water circulation are clearly observable on A1 on March 23 (NW-2). Whereas alongshore currents were dominated by seiching, cross-bay wind effects were clearly observed on the cross-shore component (Fig 4.6c), disappearing the two-layered structure observable on 23rd morning. This structure disappeared as the hours passed (as wind increased in intensity) and circulation became unidirectional, with water temperature mixing observed in Fig 4.4b (NW-2).

In order to analyse the current dependence with sea breeze winds, we plotted the Progressive Vector Diagram (PVD) in Fig 4.7. Surface currents in A2 (thick red line) followed the main breeze direction (on surface) while bottom currents (thin red line) showed lower speeds and opposite direction proving a two-layered structure. During this period the behavior in A1 (black lines in Fig 4.7) was almost the same but more oriented towards the main axis (and winds) of the Bay. Circulation reversing due to sea breeze was observed on several days during the summer period, thus indicating that alongshore wind stress contribution to water advection inside the Bay easily balances the gravitational circulation.

3. Discussion

3.1 Hydrodynamic response

The different energetic events presented in the previous section should be summarized into two types: winds and seiches, both representing different response to energy inputs in the Bay. Wind effects are transmitted to the water column from the surface layers and through the sea level gradient (wind set-up) generated along the main blowing wind axis (Pugh 1996). In idealized test case, with wind blowing along the main axis of the bay, frictional time response could be approximated as: $t_f = H/\left(2u_*\sqrt{C_d}\right)$, where H is the water depth, u_* is the frictional velocity ($u_* = \sqrt{\tau/\rho}$) and C_d is the drag coefficient (supposing 0.002) (Csanady, 1982). For instance, winds of 5-10 $m \cdot s^{-1}$ would imply a frictional equilibrium after 3-1.5 hours considering 6m water depth. This frictional time response is shorter than most of wind events. Moreover, the time response dependence on water depth across the bay –i.e for shoals of 3m depth the corresponding time response moves between 1.6 and 0.8h- promotes a velocity gradient (dv/dx) between central areas and shoals. Typical surface frictional layers (10-50m, Haidvogel and Beckmann, 1999) are higher than the maximum depths in the Bay, reinforcing the importance of the frictional term in the hydrodynamic response. Moreover, the bathymetry and coastline would drive the circulation in their vicinity, enhancing the circulation parallel to them (Csanady 1973). In this sense, observations in Alfacs bay case have shown alternating periods with a moderate (e.g. sea breeze in Fig 4.7) and low correlation (e.g. north-western event in Fig 4.6d) between currents and winds. It is evident that other processes entirely mask the linear response, assuming a linear behavior as an expected direct response of the water current at wind forcing. It means that the hydrodynamic response is conditioned by nonlinear and non-stationary processes due to the intricate bathymetry, the unsteadiness of the wind magnitude and direction and probably the spatial wind heterogeneity in the bay (more details in chapter 5). Aside Alfacs Bay, this behavior is common in highly-stratified and shallow estuaries where the correlation with wind events is complex and nonlinear (Noble et al. 1996, Narváez and Valle-Levinson, 2008).

On the other hand, many studies in Alfacs hydrodynamics and similar domains have focused on wind-induced circulation and its effects on hydrography (Camp, 1994; Mancero-Mosquera et al. 2010; Llebot et al. 2011), but none of the aforementioned contributions have investigated in detail the influence of seiching on measured water velocities, due to the fact that most hydrodynamic studies on bays underestimate high-frequency processes averaging recorded data (hourly or even 3-hourlya averaged). For instance, Llebot et al. (2013), defined

seiche sea level amplitudes at an order of 10^{-2} m in and tidal excursion length around 70m for 3h seiches, thus not considering oscillations with periods lower than 3h. Our analysis confirms the ongoing presence of seiches in both field studies, as observed in sea level in chapter 3. In this case, the simple relaxation of the wind setup could be a source of seiches in the Bay (Boegman 2009). The fundamental seiche mode has been reported using sea-level data from previous studies in Alfacs Bay. These oscillations are important for flux interchange through the mouth of Alfacs Bay (Camp and Delgado 1987) and the potential mixing of water masses in the shallowest areas and effects on the feeding dynamics of sessile filterers (Camp 1994). Examples of seiches and their influence on mixing and re-suspension processes are found in Ostrovsky et al. (1996), indicating that cross-isopycnal mixing occurs at the littoral zone as a consequence of seiche activity, or in Jordi et al. (2008), who relate different sediment re-suspension episodes to seiche currents. During both field campaigns, it has been proved that the most energetic non-stationary processes occur in these seiche periods (Fig 4.5 and Table 4.1). Several examples are found in similar microtidal and semi-enclosed bays (Luettich et al. 2002; Niedda and Greppi 2007). The aforementioned works focused on similar environments but differences were found in the oscillating modes due to area and geometrical effects. It is worth noting that we found response at two oscillating modes (≈1 h and ≈3 h) in contrast with other bays where only the fundamental modes occur, and according to similar examples described in (Rabinovich 2009). The mechanisms of seiching excitation are linked to atmospheric convection cells which cause fluctuation in wind speed and atmospheric pressure (i.e. Rabinovich and Monserrat 1998; de Jong and Battjes 2004). In our observations, no clear relationship was noted between seiches and wind or atmospheric pressure variations. The generation mechanism is out of the focus of our work and deserves an investigation using longer atmospheric and sea-level data time series, as well as complementary numerical outputs.

3.2 Potential Energy Analysis

Balance between positive buoyancy forces, heat fluxes and freshwater inputs to wind stress, seiches and tidal stirring should determine the distribution of T/S along the water column, defining it as stratified or mixed. The usual approach to compare these terms was described through the potential energy anomaly (Simpson, 1990), defined as the difference of potential energy before and after mixing. The equation for potential energy anomaly -also referred to as stratification parameter in Simpson, 1981- which originally only takes into account heat fluxes as buoyancy forces, is summarized as:

$$\frac{d\theta}{dt} = \underbrace{\frac{\propto g\overline{Q_I}}{2C_p}}_{Heat} + \underbrace{\frac{gR\Delta\rho}{2A}}_{Freshwater} - \underbrace{\frac{ek_b\rho_w|\bar{u}|^3}{h}}_{Seiche\ \&\ Tides} - \underbrace{\frac{e_s C_d y_s \rho_a \overline{W}^3}{h}}_{Wind} \quad (1)$$

Where C_p is the specific heat of seawater at constant pressure, Q_I is the net surface heat flux, h is water depth, g is gravity, $\propto$ is the thermal expansion coefficient ($2.08 \cdot 10^{-4}$ ºC at 20ºC), e_s is the wind mixing efficiency, C_d is the surface drag coefficient (0.0012), k_b is the bottom drag coefficient (0.002), ρ_a is air density, y_s is the ratio of the wind-induced surface current to the wind speed (0.02), W is wind speed, R is river input, A is the area of freshwater influence and $\Delta\rho$ referring to density difference between both fresh and salt waters. The wind mixing efficiency (e_s) is assumed to be 0.03 following Atkinson and Blanton (1986) and tidal/seiche efficiency (e) 0.005 from Simpson and Sharples (2012). The overbar (-) indicates daily averages. Several authors have applied potential energy balances oriented to describe mixing and stratification processes at different scales and regions (e.g. de Boer et al. 2008; Simpson and Sharples, 2012, Grifoll et al. 2013). The Q_I is obtained from direct measurements on Alfacs Bay and following the relation between solar heating (Q_s) which accounts for the albedo effects (Al), net longwave radiation (Q_b), sensible (Q_c) and latent heats (Q_e), as:

$$Q_I = Q_s(1 - Al) - Q_c - Q_e - Q_b \quad (2)$$

Net heat flux is defined in equation (2) as the balance between incoming and outgoing heat fluxes. Approximation to them could be assessed using bulk formulas (Simpson & Sharples, 2012). Latent Heat (Q_e, in $W \cdot m^{-2}$) is obtained through:

$$Q_e = 1.5 \cdot 10^{-3} \cdot L_h \cdot W \cdot \rho_a \cdot (qs - qa) \quad (3)$$

Being L_h the latent heat of vaporization for water $\approx 2.5 \cdot 10^{-6}$ $J \cdot Kg^{-1}$, the $1.5 \cdot 10^{-3}$ is the Dalton number, and q_a and q_s the specific air humidity and saturated specific humidity at sea surface temperature respectively.

The Sensible Heat (Q_c, in $W\ m^{-2}$) is defined as:

$$Q_c = 1.45 \cdot 10^{-3} \cdot C_a \cdot W \cdot \rho_a \cdot (Ts - Ta) \quad (4)$$

Where Ca ≈ 1000 $J \cdot Kg^{-1} \cdot K^{-1}$ is the specific heat capacity of air and T_s and T_a the sea surface temperature and air temperature respectively. The Coefficient $1.45 \cdot 10^{-3}$ is the Stanton number.

The term corresponding to longwave radiation (Q_b) needs cloud coverage information (not available) to account for the atmosphere backscatter effects. However, Allen et al. (1998) presented a formula considering the air humidity and the relation between measured and theoretically incoming solar radiation to account for the effects of downward longwave radiation.

Approximation to net longwave radiation (Q_b, $W \cdot m^{-2}$) has been done through:

$$Q_b = \sigma \left(\frac{T_{max}^4 - T_{min}^4}{2} \right) (0.34 - 0.14 \cdot \sqrt{e_a}) \left(1.35 \cdot \frac{Q_s}{Q_{s0}} - 0.35 \right) \cdot 0.0116 \quad (5)$$

Where σ is Stefan-Boltzmann constant, T_{max} and T_{min} are maximum and minimum diurnal temperature (in K), e_a is the actual vapour pressure (KPa), Q_s for the measured shortwave and Q_{s0} for the theoretical shortwave radiation (both in daily radiation, $MJ \cdot m^{-2} \cdot day^{-1}$). Details for this formula on Allen et al. (1998). The 0.0116 has been added here and is used to convert $MJ \cdot m^{-2} \cdot day^{-1}$ to $W \cdot m^{-2}$.

The approximation used to obtain the heat fluxes through the observations still presents some lacks: e.g. SST is defined here from temperature measurements at 1m depth and cloud coverage inferred from shortwave radiation. However, the results were compared with European Center for Medium-Range Weather Forecast (ECMWF, www.ecmwf.int) surface net heat flux variable (3h accumulated data) showing good agreement.

The results for the different observational periods are presented on Table 4.3. Equation (1) considers heat fluxes inputs as buoyancy forces (first term on right hand side) and freshwater inputs through the rice channels (second term). The inclusion of this second term is not simple due to the freshwater area of influence. In this sense, this area itself is a function of the freshwater input and the mixing process, so is part of the solution rather than a fixed input parameter (Simpson et al. 1990). Even more complex approximations were made by

taking into account gravitational circulation due to freshwater inputs, we have considered these inputs as uniformly distributed over the surface, as was proposed for precipitation rate in (Simpson et al. 1990), thus defining precipitation as *R/A*. Freshwater contribution is considered $10 m^3 \cdot s^{-1}$ in both summer and spring conditions. The area in which this flux is believed to be distributed is $40 km^2$. The freshwater buoyancy work is then considered to be almost constant and around $30 \cdot 10^{-6}$ Wm^{-3} (Table 4.3), which is the same order of magnitude as heat work by net heat fluxes in summer and spring. At this point, and taking into account that the T/S characterization of the bay has shown high horizontal variability due to the freshwater influence much more noticeable closer to the channels, the same term has been obtained but considering a smaller area of $10 km^2$ (approximation to area on the northern shore of the bay with width of around 1km), thus leading to 10^{-4} Wm^{-3}, indicating the dominance of this input in the potential equation. These results agree with Solé et al. (2009), who considered the importance of freshwater inputs in stratification. Moreover, both stratification terms act together in summer, whereas in winter-spring heat fluxes can contribute negatively to water stratification. During the closed channels period (January to late March or beginning of April) the freshwater term must be 0. However, several authors have observed stratification (leaded by salinity) even with closed channels, thus indicating the existence of other freshwater sources in the bay (Camp and Delgado 1987). Heat fluxes show similar mean values for both periods. During winter-spring period the daily values moves from $-10 \cdot 10^{-6}$ (February, implying mixing) to $+30 \cdot 10^{-6}$ $W \cdot m^{-3}$ (April). During summer, highest contribution to stratification was on July around $+40 \cdot 10^{-6}$ $W \cdot m^{-3}$, but negative values during September and coinciding with dry and colds winds on cloudy days were observed. On Table 4.3, daily values for heat fluxes during the seiche events are resumed, being always negative and contributing to stratify the water column.

Mixing terms present noticeable differences between one another. Winds in the Bay reveal their importance during both periods. In the summer mean values are one order of magnitude lower than freshwater and heat fluxes. However, maximum daily values during windy events (NW-1) shows values of $20 \cdot 10^{-6}$ $W \cdot m^{-3}$, contributing to mix the water column as shown in Fig 4.4 due to surface cooling and shear. In winter-spring, the work done by winds in mixing is one order of magnitude higher than in summer, coinciding with small or negative heat contribution to stratification (winter) and the closing of drainage channels. This situation encourage a major occurrence of mixing events in Alfacs Bay as we show in the N^2 profiles (Fig 4.3d) and being consistent with other winter observations (Camp and Delgado, 1987). During winter and spring, mistral wind events lasting for more than one day imply maximum values for this term on equation (1) around $2 \cdot 10^{-4}$ Wm^{-3}. This value clearly exceeds the

stratification terms, even considering the freshwater effects on the proximities of drainage channels (defined around 10^{-4} Wm^{-3}).

The water currents associated to the third term in equation 1 could be related to astronomical tide or seiches as: $\bar{u} = \bar{u}_{tides} + \bar{u}_{seiche}$. Tidal stirring ($\bar{u}_{tides}$) is demonstrated to be a negligible term in Alfacs Bay, showing values around 3 and 4 order of magnitude lower than stratifying terms. The seiche stirring term ($\bar{u}_{seiche}$) is associated at measured depth-averaged current speed. The observed velocities may include effects from other hydrodynamic forcing as pressure gradients (in and out the bay) or winds, even during the seiche events are low as we shown in Figure 4.6a and 4.6b. The mean values for both seasonal period's shows values much lower than the stratification terms, indicating the low importance on mixing the water column at this time-length scales (see Table 4.3). Nevertheless, the energetic scenario mean values corresponding to the seiche events shows the maximum mixing contribution of this term during that days.

Table 4.3. Estimation of the size of the terms (daily averages) of the potential energy balance (equation 1) computed for both summer and winter campaigns (x 10^{-6} $W \cdot m^{-3}$). Scenario estimations are done over the event duration defined on table 4.1.

		$\propto gQ_i/2C_p$	$gR\Delta\rho/2A$	$ek_b\rho_w\lvert\hat{u}_{tide}\rvert^3/h$	$ek_b\rho_w\lvert\hat{u}_{seiche}\rvert^3/h$	$e_sC_dy_s\rho_aW^3/h$
				Seasonal estimations		
Summer	Mean (std)	15 (13)	30	0.06 (-)*	0.8 (0.9)	5.6 (3.5)
Winter-Spring	Mean (std)	10 (14)	0**/30	0.06 (-)*	1.5 (0.8)	20 (35)
				Scenario estimations		
S0-1		3	30	-	2.5	8.7
S1-1		31	30	-	26	15
S0-2		4.2	0**/30	-	4.8	64
S1-2		26	0**/30	-	3.7	20

*Values for tidal stirring term correspond to M2 tidal current amplitude observed (3 $cm \cdot s^{-1}$). Same values for winter.

**During open channels period. From January to late March no direct freshwater inputs from rice fields.

These results show how in daily scales the bay is stratified due to both freshwater and heat fluxes terms. The only term which can balance the stratification due to freshwater input is wind. On the other hand, and on shorter time length scales (<day), seiches seems to be able to balance not only the heat fluxes but also the freshwater term. In order to better

understand this possible source of mixing, additional considerations using dimensionless number and numerical simulations are presented in the next section.

3.3 Mixing due to seiche-induced bottom friction

The lack of salinity measurements during the energetic episodes was a handicap to describe the full mixing processes from observations. However, Fig 4.4a shows a sudden change in temperature time-series during S1-1. Sea water temperature converge around 26ºC in the whole water column suggesting a mixing of the surface and bottom water masses. During this event, the bottom temperature differences between A2 and A1 were greater than 6ºC. We dismissed the effects of advection from the outer Bay because open-sea water temperature tends to be colder, as seen in Fig 4.3c. A possible effective mixing due to seiche-induced turbulence seems to occur. Events related to the fundamental oscillating mode (S0-1 and S0-2) do not show noticeable changes in temperature profiles. However, during these events (and also S1-2) the temperature gradients in the water column were smaller than S1-1, being difficult to identify the water mixing from temperature observations.

Usual approximation to estimate mixing due to barotropic oscillation flow is given by the dimensionless Richardson layered (or Bulk Richardson) number:

$$Ri_L = \frac{\Delta\rho g h}{u^2 \rho_o} \tag{6}$$

Where $\Delta\rho$ is density gradients from surface to bottom layers, g represents gravity, h is depth, $\rho_o$is reference density and u represents the characteristic velocity of oscillatory flow. Values lower than 2 in of Ri_L indicate fully-developed mixing, while greater than 20 means turbulence is ineffective in decreasing stratification (Dyer, 1994). The characteristic velocity ranges from the near-bottom layer velocity (Dyer 1991) to the mean velocity at the water column (Noble et al. 1996). Considering the observed mean depth-averaged velocities in A1 and A2 during each scenario (table 4.1), we can estimate the theoretical maximum density differences which the bottom-induced turbulence is able to mix. During S1-1, mean speed on A2 is around 0.2 $m \cdot s^{-1}$, which implies density differences of 1.2 $kg \cdot m^{-3}$ (for Ri_L=2). These density differences are of lower than observed during summer, but higher than winter scenario (Fig 4.3c and d). In this case, seiche-induced bottom mixing is expected to influence water column stratification (S1-1 in Fig 4.4b) without full mixing. During spring (S0-2 and S1-2) seiche-induced circulation is weaker and the mean velocities do not exceed 0.13 $m \cdot s^{-1}$ in A2. For these cases, Ri_L=2 implies density differences of 0.5 $kg \cdot m^{-3}$, similar to the density differences observed on winter, and probably influencing the mixing on water column. Taking

into account that the most common seiche events are related to fundamental mode (S0-1 and S0-2) with a mixing threshold on A2 around 0.5-1 $kg \cdot m^{-3}$, we suggest that turbulence provided by the seiche oscillatory flow seems not enough to decrease stratification in most cases. However, in some special circumstances, i.e. S1-1, noticeable water column mixing below the pycnocline may occur.

In this case, the bottom boundary layer would occupy an important fraction of the water depth, thus redistributing the temperature from middle layers over the water column below pycnocline (as we show in the temperature time-series), and even mix the entire water column. A similar picture was shown by (Dyer 1991) in a tidal estuary with the salinity profile when both internal mixing and bottom boundary layer coincide in the pycnocline. Consequently, the possible mixing of the water column would depend not only on density variations and velocities, as well as on corresponding depths.

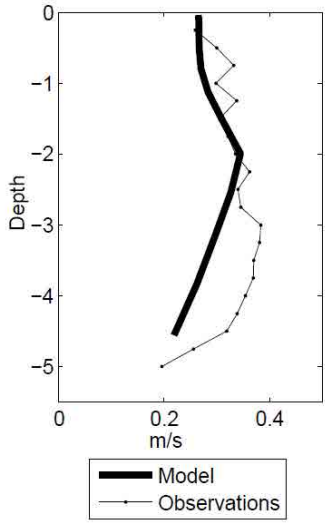

Figure 4.8. Instantaneous alongshore velocity profiles in A2 location for observed and modelled 1-h seiche (S1-1), in black thin and thick lines respectively.

To analyse the relationship between the bathymetry and velocity pattern on the seiche mixing capacity we have implemented a hydrostatic 3-D numerical model. The model used is ROMS (Shchepetkin and McWilliams, 2005), with a grid resolution of 100m and 12 levels on the vertical and considering baroclinic effects (heat fluxes and freshwater as buoyancy sources). Modelling details, configuration domain and validation are shown in chapter 2 (Realistic application). The freshwater inputs are distributed on 8 points along the north coast (Fig 4.1), with a total discharge of ≈10 $m^3 \cdot s^{-1}$. Heat fluxes and winds are imposed from observational data. The turbulence closure scheme for the vertical mixing is Generic Length Scale (GLS), described on Warner et al. (2005) and tuned to behave as MY2.5 (k-kl). Tests with different mixing schemes show low sensitivity on water column stratification during

seiche events. In general, the model reproduces the stratification of the bay, even with lower density gradients between surface and bottom layers. The model agrees with the velocity profiles observed at A2 on S0-1 and S1-1 using a logarithmic profile for the bottom boundary layer and a characteristic bottom roughness height of 0.002 m (Fig 4.8).

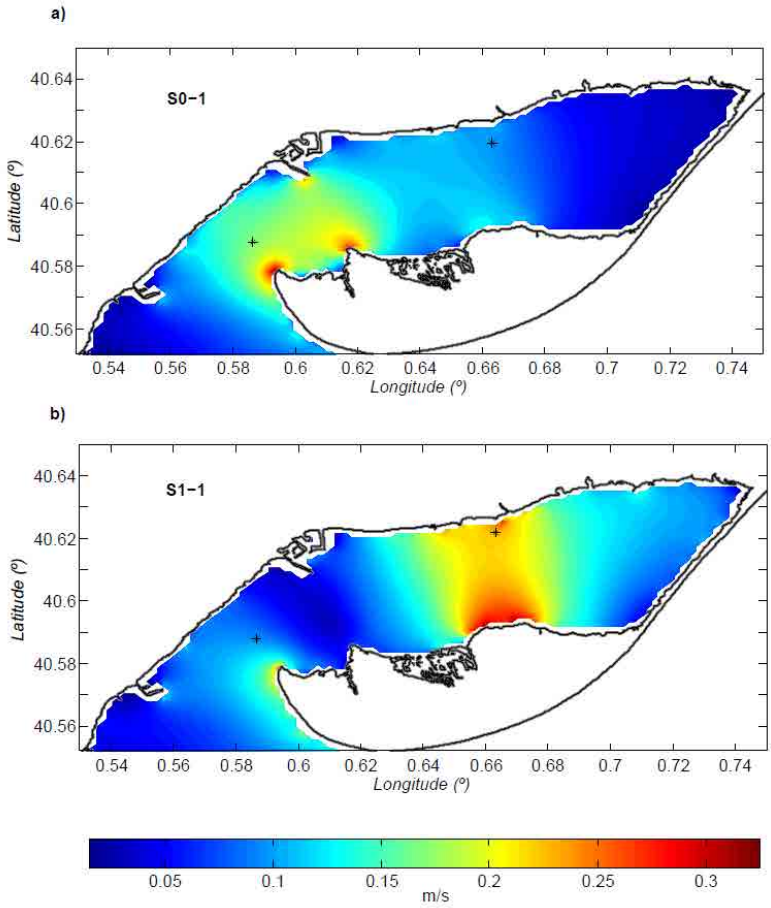

Figure 4.9. Image a) shows numerical results for mean depth averaged computed speeds corresponding to S0-1 scenario. Image b) for scenario S1-1.

Two numerical simulations were used to obtain the mean depth averaged current speeds for scenarios S0-1 and S1-1 (Fig 4.9). For S0-1 (Fig 4.9a) the spatial distribution of current speeds shows how the highest velocities are located around the bay mouth (≈16 $cm \cdot s^{-1}$), with lower velocities on A2 (around 10 $cm \cdot s^{-1}$) and calm waters on the inner area. Comparing these velocities with the required velocities to mix the water column according to equation 3, the 3h-seiche (i.e. S0-1) would be able to mix the water column in the bay mouth and over the shoals (depths around 2m) for typical conditions of stratification. However, full mixing in the water column is not expected in the inner area of the bay. Scenario S1-1 (Fig 4.9b) shows maximum velocities on the A2 vicinity (≈23$cm \cdot s^{-1}$). Equation 6 (with Ri_L=2) leads to potential mixing around 1.2 $kg \cdot m^{-3}$ in the deepest areas (6.5m) and almost 3 $kg \cdot m^{-3}$ for the

shallowest (2m depth) regions. Similar to S0-1 case, S1-1 hydrodynamic conditions seems able to mix the whole water column depending on the density profiles (see Fig 4.3).

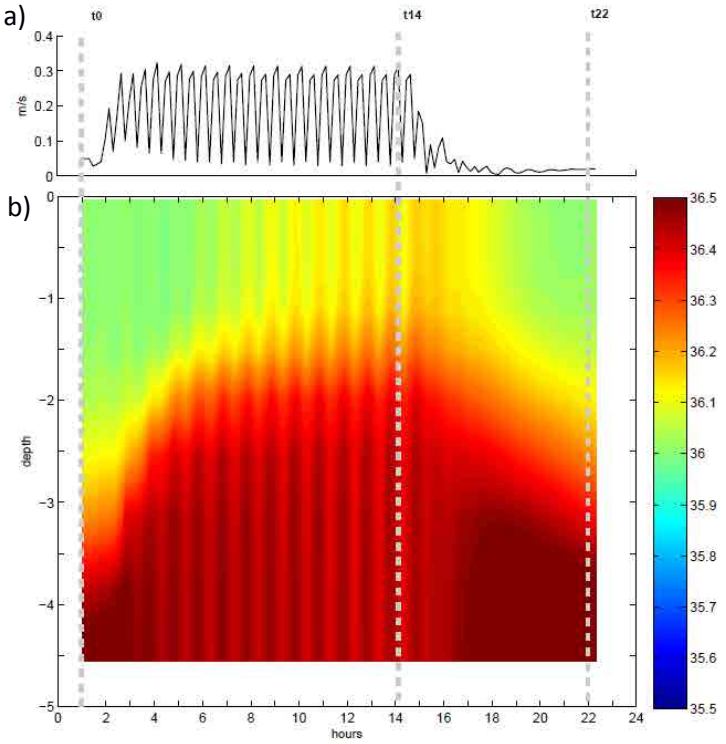

Figure 4.10. Numerical test for S1-1. Top image shows instantaneous depth averaged velocities in A2. Bottom image for the salinity time evolution on A2 over the entire depth. Gray dashed lines shows instants ploted on Fig 4.9.

In order to complement our results, a numerical test case for S1-1 is shown in Fig 4.10 considering stable stratified conditions from heat fluxes and freshwater inputs. The seiche is imposed at the contour after 24 hours of spin up leading an oscillatory flow in A2 with peak velocities of 0.31 $m \cdot s^{-1}$ and averaged for the entire simulation around 0.2 $m \cdot s^{-1}$(see Fig 4.10a). The effects of the oscillatory current speed on salinity distribution in A2 is shown in Fig 4.10b. The bottom frictional layer raises with the seiche evolution and stabilizes close to the surface. The mixing of the water column at this point is not complete, but an effective reduction of density differences between surface and bottom is clearly observed. When seiche stops, the water column recover gradually the initial density profile. The salinity profiles at different instants of the numerical simulation (t0, t14 and t22, where sub index denotes hours since the numerical initialization; see Fig 4.10b) are shown in Fig 4.11 for A2 and Mo location. Mo location represents a shallow point over the shoal (3 m water depth). In both points the density profiles are clearly modified by the seiche currents. In A2 the seiche is not able to mix the entire water column while in Mo the full mixing occurs. The mixing capacity in Mo is larger than 2 $kg \cdot m^{-3}$ from surface to bottom, agreeing with the previous Ri_L analysis and previous hypothesis presented on Camp (1994). The seiche-induced mixing estimated through analytical formulations and numerical modelling agrees with observational data on

Fig 4.4, where A2 temperature contribution to surface-bottom density differences before and after the S1-1 event (Fig 4.4) moves from 1.2 kg · m^{-3} to 0.5 kg · m^{-3} respectively.

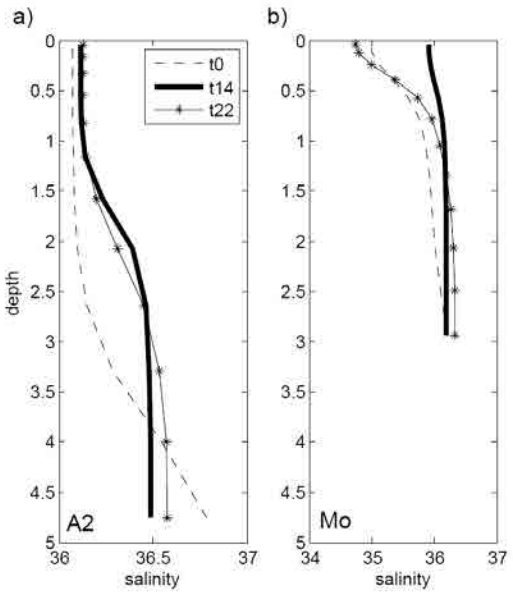

Figure 4.11. Modelled salinity profiles for A2 and Mo (locations on Fig.1) on a and b panels respectively corresponding to instants t=1, t=14 and t=22 (in hours) in Fig 4.10.

These processes would have a decisive influence on the re-suspension and mobilization of sediments and nutrients on the bottom, thus enhancing interchanges of organic and inorganic materials though the pycnocline during particular circumstances. Our results will be useful to relate the seiche dynamics with the role of the nutrients and the biochemical processes observed in the Bay (Loureiro et al., 2009; Llebot et al., 2011). Furthermore, new questions arise from our investigations. For instance, analysis of the meteorological forcing mechanisms responsible for the seiches occurrence as well as their influence over the shoals should be studied in future works through additional observational data. Moreover, the spatial variability in freshwater observed in the transversal CTD transects indicates differences in the velocity threshold to mixing capacity. Additional long-term observations would be desirable to ensure the accuracy of the relation between the seiche-induced mixing and vertical density thresholds. The combined influence of wind and seiche-induced mixing is worthy of future investigations using additional numerical simulations and field measurements.

4. Conclusions

The investigation of the hydrodynamic response in semi-enclosed water bodies under shallow and micro-tidal conditions have revealed a short time response at wind stress and the presence of oscillating mechanisms that may control the flow and mixing processes. Our analysis focussed in Alfacs Bay have revealed for the first time a seiche mechanisms which its associated current variability is at least the same order as energetic wind events. On the other hand, the importance of wind as a mechanism capable of reversing estuarine circulation for short periods is observed under summer conditions. Due to the shallowness (order of few meters), a short time-response (order of few hours) in the water column occurs. Stratification or well-mixed conditions are a balance mainly of freshwater inputs and winds according to the size of the terms of the potential energy equation. Heat fluxes in summer periods also contribute to stratifying the water column, thus indicating that not only freshwater influence determines the stratification on the bay. Seiche-induced mixing has been estimated using observational evidences, dimensionless numbers and numerical modelling, showing its theoretical mixing potential under some circumstances (intensity, stratification and water depth). The results and methodology focused in Alfacs Bay could be translated to similar domains in which tidal influence is not the main driving force and other buoyancy and mixing sources are in a similar order of magnitude.

Acknowledgments

This work was supported by a FPI-UPC pre-doctoral fellowship from the European project FIELD_AC (FP7-SPACE- 2009-1-242284 FIELD_AC). The campaigns were carried out thanks to the MESTRAL project (CTM2011-30489-C02-01). We would like to thank LIM-UPC staff Joan Puigdefàbregas, Jordi Cateura and Joaquim Sospedra for all their help with campaigns and data analysis, as well as the Ebro Irrigation Community ("Comunitat de Regants de la dreta de l'Ebre", www.comunitatregants.org") and the XIOM network ("Xarxa d'Instruments Oceanogràfics de Catalunya"; www.xiom.cat) for the information and their commitment to the study. The authors are also grateful to Arnoldo-Valle Levinson (Department of Civil and Coastal Engineering, University of Florida) for their comments on the manuscript, as well as suggestions and observations received from two anonymous reviewers.

5

Modelling circulation patterns induced by spatial wind variability in small-size microtidal coastal embayment

Science is simply common sense at its best, that is, rigidly accurate in observation, and merciless to fallacy in logic.

Thomas Huxley

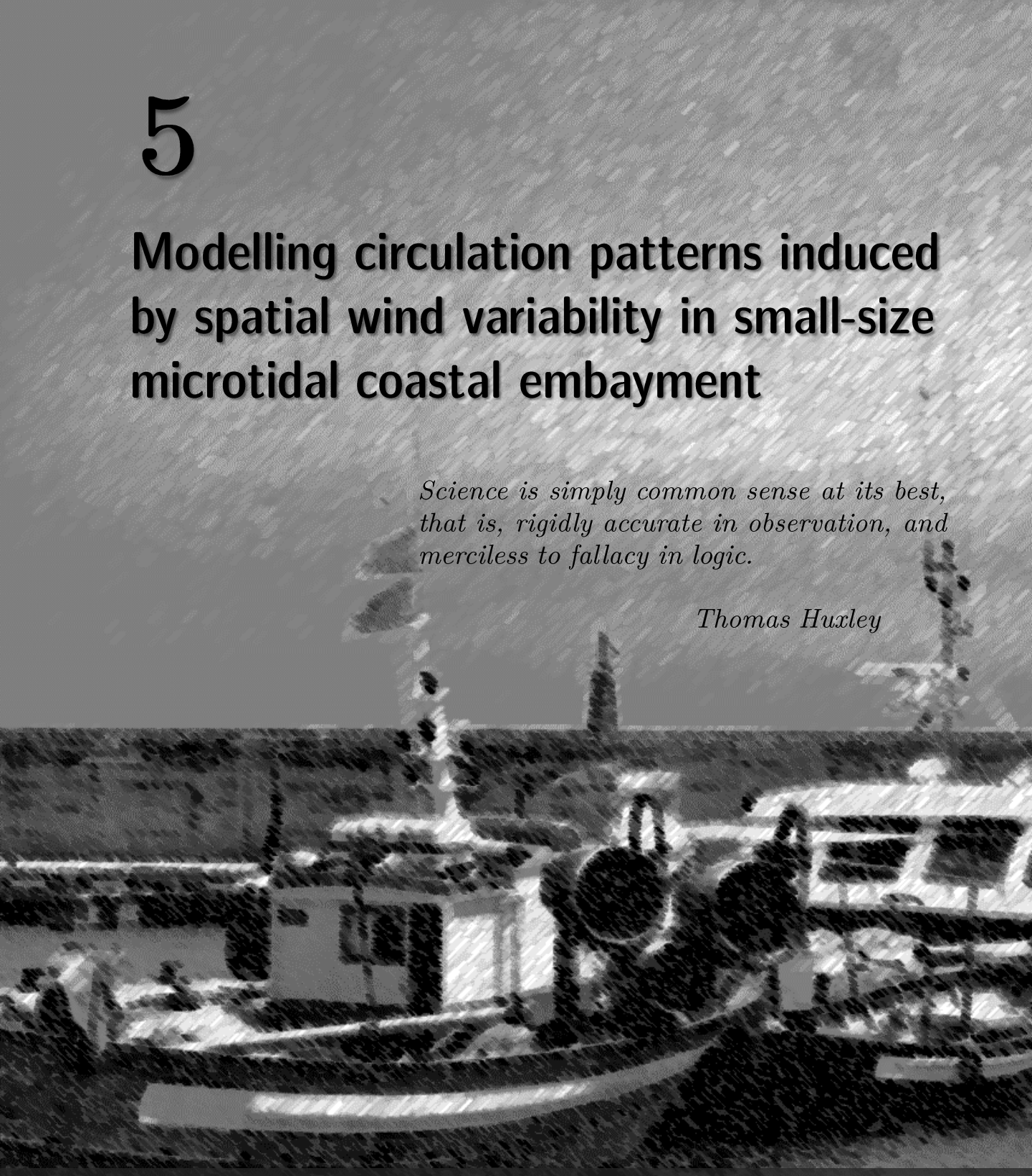

Part of this chapter has been published in:

Cerralbo, P., Grifoll, M., Moré, J., Bravo, M., Afif, A.S., Espino, M., 2015. Wind variability in a coastal area (Alfacs Bay , Ebro River delta). Adv. Sci. Res. 12, 11–21. doi:10.5194/asr-12-11-2015.

And in preparation:

Cerralbo, P., Grifoll, M., Espino, M., (in preparation). Modelling circulation patterns induced by spatial wind variability in small-size microtidal coastal embayment.

Abstract

The importance of wind spatial variability in the water circulation is investigated with a numerical model (ROMS) supported by "in-situ" observations in a small microtidal bay (Alfacs Bay, Ebre Delta). The wind variability observed in meteorological measurements is characterized with atmospheric model (WRF) outputs. From the hydrodynamic simulations of the bay, the water circulation response is affected by the wind variability leading water current structures not observed in homogeneous case. If the wind heterogeneity response is considered, the water exchange in the longitudinal direction increases significantly reducing the water exchange time in around 20% over some areas of the bay. Wind resolutions of the half size of the bay (in our case around 9 km) inhibit wind variability which affect significantly the resultant circulation pattern. The characteristic response at wind variability is also investigated using idealized test cases. These results show how the wind curl contributes to the hydrodynamic response on shallow areas and promote the exchange between the bay and the open sea. Negative wind curl is related to the formation of an anti-cyclonic gyre on the bay mouth. Comparing irregular and bottom flat idealized test cases reveals that the wind variability dominates in front of the bathymetric effects. Our results highlight the importance to consider appropriate wind resolution even in small scales domains to characterize the hydrodynamics (such as bays or harbors), with relevant implications in the water exchange time and the consequent effects on water quality and ecological parameters.

1. Introduction

Tides, winds and freshwater inputs are the main factors determining the hydrodynamics in coastal areas such estuaries and semi-enclosed bays. In microtidal and low freshwater discharge environments the winds should become the main driving mechanisms. Response on bay dynamics to wind forcing has been investigated in detail from different approaches. For instance, Csanady (1973) investigated the current response to a wind in a non-rotating basin, in which the forced response is a surface distortion due to the set-up accompanied by a forced flow pattern due to bathymetry variability. Basically, stable situation shows how in shallower areas than mean water depth the transport is with the wind direction, while it is against the wind direction in deeper areas. Gravitational estuarine circulation is also influenced by winds, intensified with a down-estuary wind, and weakened or even reversed with an estuary up-wind (Valle-Levinson and Blanco, 2004). Besides, interaction between wind and gravitational circulation is able to generate substantial transverse circulation in estuaries with triangular section (Wong 1994), whilst the influence of winds on exchange flows in narrow areas is demonstrated on Narvaez and Valle-Levinson (2008). Recently, application of 3D numerical models has allowed to investigate the physical mechanisms involving wind driven circulation in coastal areas. For instance, asymmetries in the ebb-flood cycle due to wind forcing in surface layers (deCastro et al. 2003), analysis of circulation patterns and water exchange processes (Schoen et al. 2014) and assessment of wind model resolution on circulation and wave model behavior (Signell et al. 2005; Klaic et al. 2011; Schaeffer et al. 2011).

Contributions focused on regional and oceanic scales have demonstrated how wind variability due to topographic constraints would not only influence the local circulation but also affect mesoscale structures (Chavanne et al. 2002; Jiang et al. 2009). Espino et al. (1998) compared the wind curl with mesoscale circulation in NW Mediterranean Sea, and a theoretical approach to wind curl effects on coastal areas such Benguela Current was described by Junker et al. (2015). Zampato et al. (2007) checked out the sensibility of sea level prediction in Adriatic to different atmospheric model resolution, showing how finest models improves the representation of most energetic events. At smaller scales, Rueda et al. (2009) studied the uncertainty of 3D hydrodynamic models associated to the spatially and temporally varying wind fields in a lake, demonstrating how the better results were obtained using the maximum observational available data to interpolate the spatial wind fields (reproducing the maximum spatial wind variability). Besides, Herrera et al. (2005) investigated wind variability on Spain coast, emphasizing the wind channeling effects of Ria de Vigo through comparison of various meteorological stations, and Cerralbo et al. (2012) applied numerical model in same Ria and

observed that atmospheric model (≈4km resolution) was not able to reproduce all the spatial variability, thus leading to remarkable errors on current modelling. However, only few studies on wind spatial variability has been carried out on bays and estuary dynamics, mainly due to the lack of meteorological observations and the coarse resolution of atmospheric models (order of few km). Klaic et al. (2011) compares the hydrodynamic patterns resulting from the application of different atmospheric resolution models on middle-Adriatic, revealing the appearance of new hydrodynamic structures using finest models. An interesting example is found in Podsetchine and Schernewski (1999), based on a lake and showing how wind variability in short spatial scales affects the hydrodynamic response. On the other hand, Grifoll et al. (2012) investigate the influence of the wind variability in harbors where its layout strongly conditioned the preferential directions for the water motion, thus reducing the effects of the wind spatial variability.

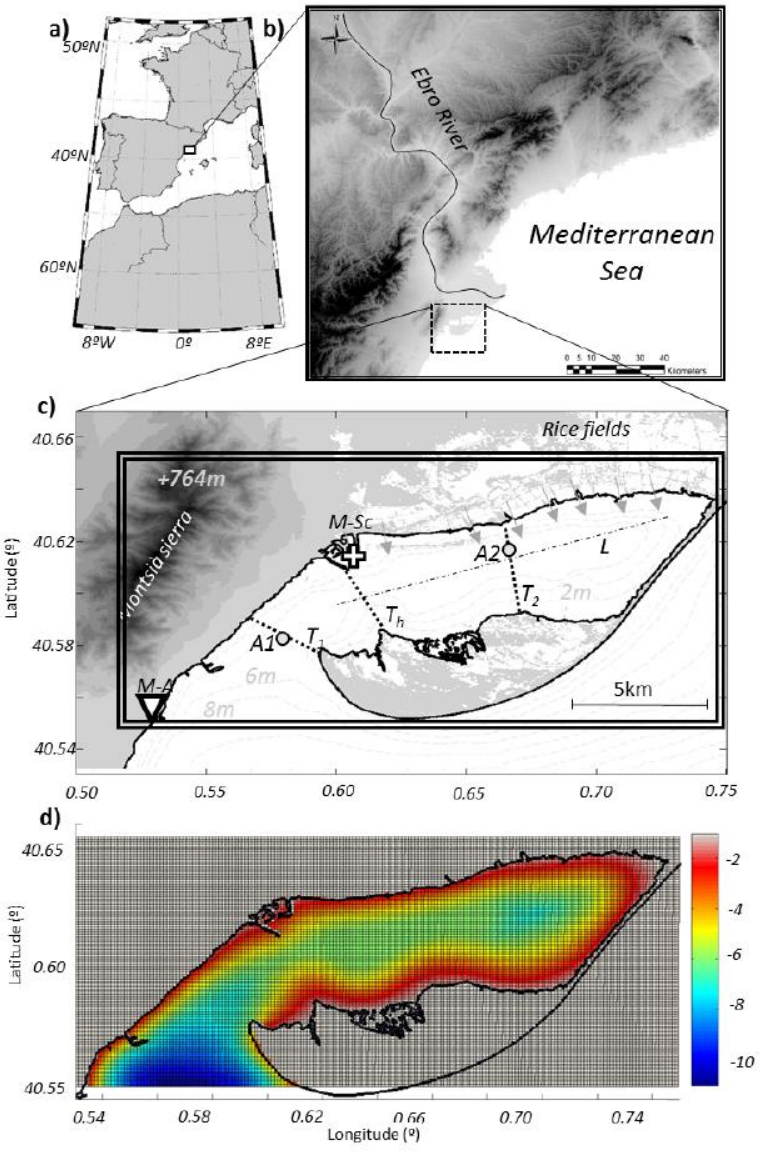

Figure 5.1. Hydrodynamic model domain and observational and modelling stations. b: Alfacs Bay in Ebre River Delta (NW Mediterranean). c: map of Alfacs Bay. Triangle shows the meteorological station: Alcanar (M-A). White cross for Sant Carles de la Ràpita tide gauge. Gray circles shows ADCP locations (A1 and A2). Dashed lines present cross-shore (T_1, T_2 and T_h) and longitudinal (L) section along the bay. Gray arrows on the northern coast shows the freshwater drainage points considered in the simulation. Double line square delimitate the domain for the hydrodynamic numerical model, which is shown in detail in image d (colorbar indicates depth in meters).

The wind variability affects the water exchange between the sheltered waters and the open sea. In this sense, an integrate parameter of water exchange between the bay and the open sea (e.g. water exchange time), is a useful parameter to assess the influence of the spatial wind variability on the hydrodynamics, and determines how the ecological status of a coastal embayment or estuary is affected by human-induced stresses. For example, low water exchange times indicates that there is insufficient time for the dissolved oxygen to be depleted (i.e. Tweed Estuary, U.K) (Wolanski, 2007). On the other hand, long water exchange time in a restricted coastal area will, potentially, allow an increasing buildup of inputs from land and leads to seasonal or even permanent O_2 depletion in bottom layers and consequently ecological problems (Jickells, 1998).

With the purpose of gain knowledge on the effects of wind variability in small semi-enclosed areas on water circulation, Alfacs bay (located on Ebre Delta, Fig 5.1) has been chosen as study site where a set of meteo-oceanographic data were available. The main objectives of this manuscript are to characterize the hydrodynamic response of the bay under spatial wind variability conditions, as well as to investigate their influence on the water exchange between the bay and the open sea estimating the water exchange times. The analysis and discussion of the results is also supported by numerical experiments in idealized domains in order to investigate the physical mechanism responsible of the hydrodynamic response in front of the wind spatial variability. Even the results are particularized by the physical characteristics of the Alfacs Bay, the new insights provided may be exported to similar domains in terms of hydrodynamic response at heterogeneous wind field.

2. Wind Variability

2.1 Observations

The synoptic winds on the Catalan coast are affected by orographic constraints, such as the blocking winds of the Pyrenees that promote tramuntana (N) and mistral (NW) winds over some areas, and the wind channeling due to river valleys (Sánchez-Arcilla et al., 2008). Northerly winds in the region are mainly produced by high pressures over the Azores and lows over the British Isles and Italy; other synoptic situations could also lead to strong winds from the NW in the Ebro Delta (Martín Vide, 2005). Winds in the bay have been characterized as having a northwestern and southwestern predominance, with the strongest ones coming from the NW (channelized by the Ebro River valley; see Fig 5.1b), being also the most common strongest winds on the Catalan coast during autumn and winter (Bolaños et al., 2009). On the other hand, some authors have reported the high spatial heterogeneity of the wind fields inside the bay (Camp, 1994).

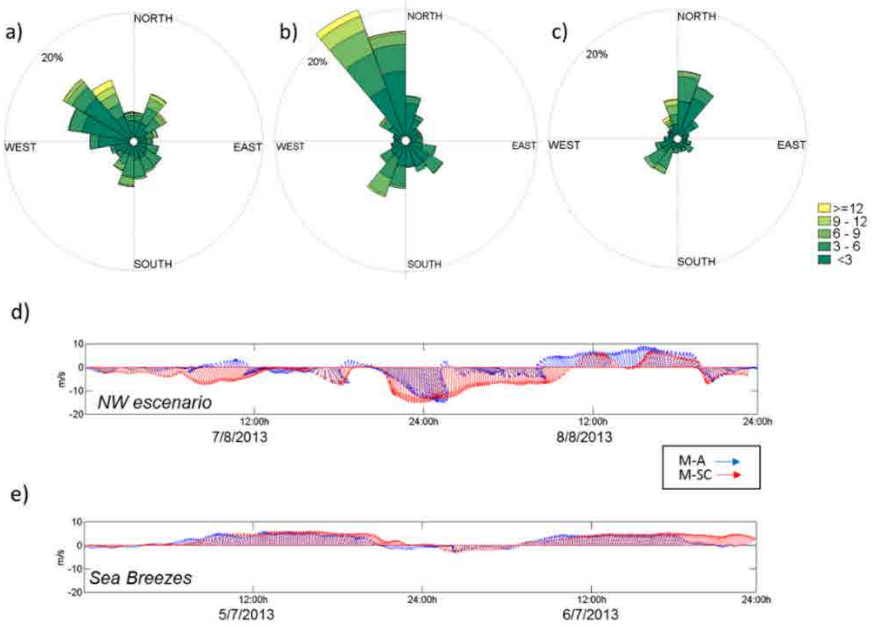

Figure 5.2. Wind roses for M-A (a), M-Met (b) and M-SC (c) during the period 2012–2013. Velocities – colour bar in (c) – are in $m \cdot s^{-1}$. Dotted line indicates frequency of 20%. Wind time series for north-westerlies and sea breeze events in (d) and (e), respectively. For (d) and (e), a Lanczos filter of 2 h has been applied to the 10 min wind data.

Observations from June 2012 to June 2013 at three meteorological stations show noticeable differences (Fig 5.2), confirming the expected variability among them. This period has been chosen for this analysis because it is the only one with data from all three stations. In M-SC

(Fig 5.2c) a bimodal behaviour with the most common winds from the southwest and north–northeast are shown. These winds are in agreement with data acquired at the same station for about 16 years (chapter 1, Fig 1.5), indicating high representation for the period selected. The highest intensities correspond to N–NW winds (>9 $m \cdot s^{-1}$). For M-A (Fig 5.2a) the directions are more scattered, being the most common winds from W-NW to NW. The highest intensity winds still come from the NW–NE, but the purely northern winds are less common. Finally, winds from M-Met (Fig 5.2b) show also a clear bimodal behaviour, with winds from the NW and SW–SE being the most common. However, M-Met is at 2m from the ground and influenced by the human buildings on the south side, which would alter on the wind measurements. Among the three stations most of the differences are clearly seen in land winds due to possible effects of the Serra de Montsià mountain range, showing high heterogeneity in wind fields in short distances.

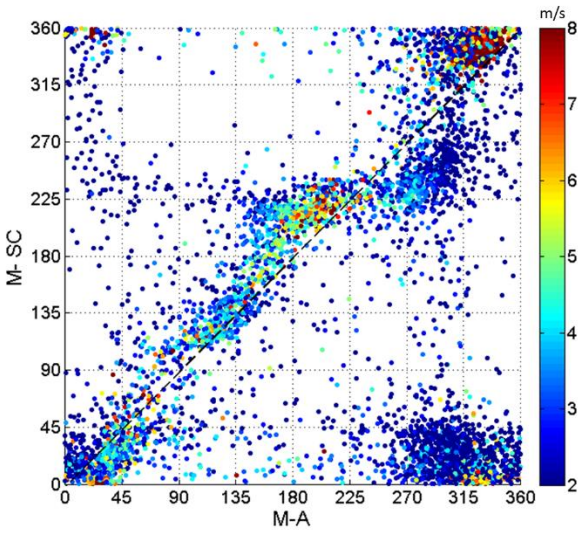

Figure 5.3. Wind direction comparison between M-A and M-SC for 1 year. The coloured data indicate mean wind velocity values (m s−1) from both stations.

To better understand the wind variability, directional scatter plots for stations with data at 10m height (M-A and M-SC) are shown in Fig 5.3a. The corresponding mean velocity for the two stations is also shown in color. This figure shows that winds from the SW–SE in M-A are rotated 20–30º clockwise in M-SC, as well as winds from the NW–N in M-A seem to be rotated a bit clockwise in M-SC (also seen in Fig 5.2). On the other hand, winds from W to NW in M-SC are not observed as in M-A; and M-SC concentrates more on the N–NE winds. All these data illustrate that Serra de Montsià (Fig 5.1) could act as a physical barrier to some type of northerly winds, redirecting them. These effects are probably most clear on mistral winds (NW), which are not completely reproduced by M-SC (Fig 5.2d) but oriented to the north. The winds from the SW–SE correspond mainly to see breezes in spring and summer (Bolaños et al., 2009). The time and spatial evolution of sea breeze differences between stations are also observable (Fig 5.2e). Weak nocturnal offshore winds (NW) rotate

and increase in intensity until the maximum of around $5 m \cdot s^{-1}$ and S–SW direction in M-A is reached. Similar behaviour is observed in M-SC, but the nocturnal winds come from the NE and the rotation is very noticeable, as breezes arise in the afternoon from the SW. In M-Met the behaviour is almost the same as M-A.

All these data reflect that even during sea breezes, the orography and probably the variation of land uses (rice fields in the delta's plain versus brush forest in Serra de Montsià) affect the direction, intensity and durability of winds. Winds from the S–SE (not related to sea breezes) are also probably affected by topography (Fig 5.3), but there are not enough observations to investigate the spatial variability in this case. In general, the wind module reveals good agreement between both stations (not shown). All the observations are based on 1-year-long data, so no climatic conclusion is expected from our analysis. Moreover, the lack of wind data just in front of Serra de Montsià does not allow us to know the exact behaviour of NW (mistral) winds and sea breezes in the mouth of the bay. In that sense, the use of numerical models would allow us to approximate the corresponding theoretical wind patterns

2.2. Numerical Modelling

Numerical wind information were obtained from currently implementations of the Weather Research and Forecasting model -WRF, Skamarock et al., (2008)- applied at two spatial resolution (9km and 3km), and CALMET model at 400m in Alfacs Bay (Fig 5.5), which are oriented to provide public meteorological forecasts by the Meteocat agency. Information, configuration and validation details of the atmospheric models are summarized in chapter 2. Wind snapshots for the three different resolutions are used to understand the spatial structures associated with most common winds in the area (Fig 5.4). For that reason, three events have been chosen, representing a case with higher variability (Fig 5.4a, d and g) to one with an almost homogeneous wind field (Fig 5.4c, f and i). For northwesterly winds (left column panels in Fig 5.4) it is clear that Serra de Montsià exerts a physical barrier on wind fields, thus revealing areas in the inner bay with high wind intensities and areas down the mountain with almost calm winds or with different direction –shadow effect, described in other environments such as the Hawaiian Islands in Chavanne et al. (2002)-. These effects were also observed for winds coming from the north (not shown). Atmospheric pressure at surface on 4 April 2014 shows low pressure over the North Atlantic and a high-pressure area over North Africa. This synoptic situation promotes winds from the north–northwest (triggered by the Ebro River valley) in the study area. The modelled winds corresponding to observations in M-A and M-SC locations are similar, not showing all the direction variability measured in observations (Fig 5.2 and 5.3). On the other hand, the wind patterns in both

WRF3 and CALMET are similar and show spatial wind variability inside the bay, thus indicating that the medium-resolution model is able to reproduce topographic constraints under these circumstances.

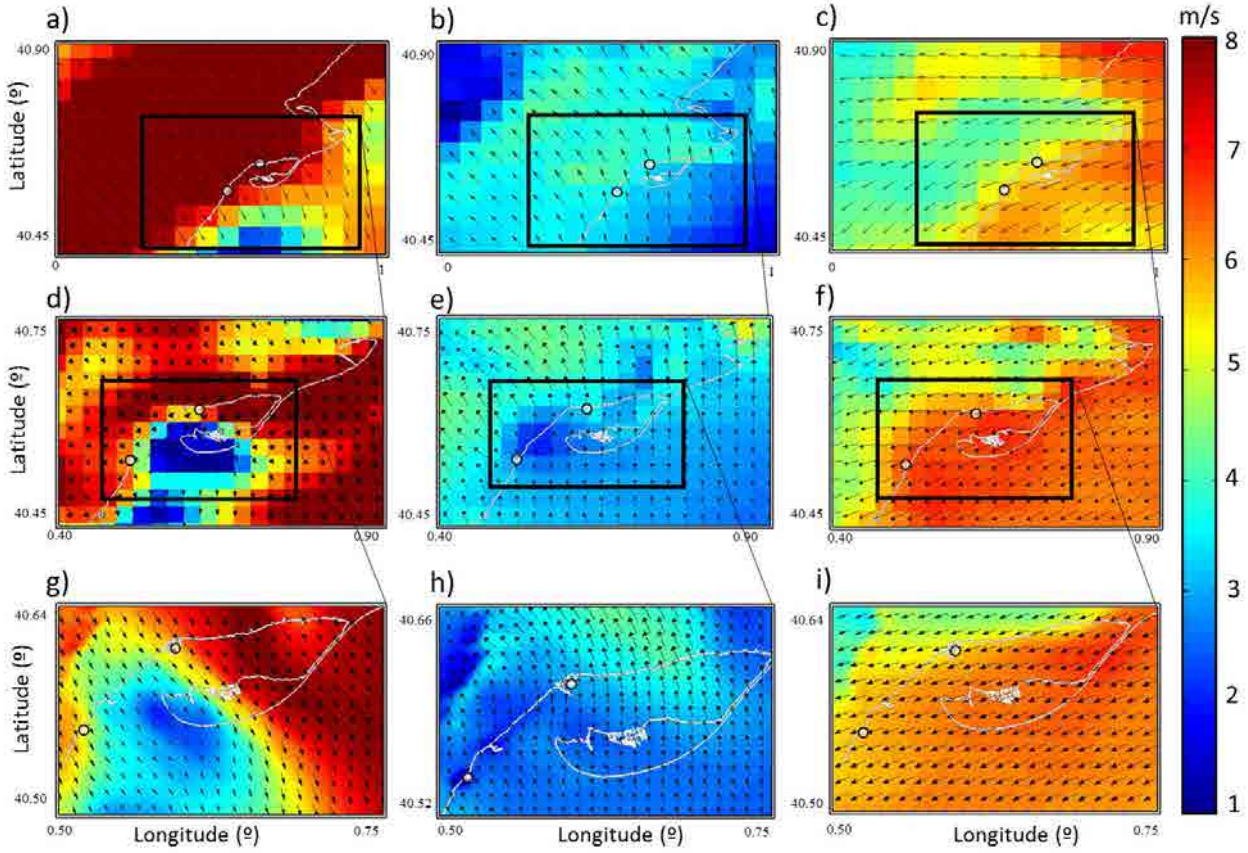

Figure 5.4. The three different models configurations are plotted for three snapshots of typical wind events at Alfacs Bay. (a–c) for WRF9km, (d–f) for WRF3 and (g–i) for CALMET 400 m. Events represent winds from the northwest (left column panels) on 4 April 2014, sea breezes (central panels) on 6 July 2013 and northeasterly winds (right panels) on 12 March 2014. White circles indicate meteorological station locations (M-A and M-SC).

The coarser model (Fig 5.4a) does not reveal such a variability, which is expected for the dimensions of the bay and model resolution, with pixels almost half of the bay size. Both meteorological stations (M-A and M-SC) are located near the maximum transition zone between high and lower intensity winds (Fig 5.4g), corresponding to the areas where modelling errors would be more sensitive to topographic effects. For a typical summer scenario, the intensification of sea breezes (Fig 5.4b, e and h) at midday in inner areas of the bay is clearly represented as well as a clockwise gyre of wind in M-SC related to M-A. The modelled highest intensities in the inner bay are not able to be validated, due to the lack of more observational data in this area. Furthermore, differences from coarser to the finest model configurations are noticeable. Both WRF3 and CALMET show some spatial structures in daily regimes, not solved by WRF9. On the other hand, spatially homogeneous wind fields

have also been observed during several events. In this case, winds from the northeast are shown in Fig 5.4c, f and i. The wind fields reproduced by observations and atmospheric models indicate homogeneous spatial winds, not affected by topography in the Ebro Delta (winds coming along the coast). For these winds, the coarser model does reproduce the wind pattern similar to the finest model.

3. Hydrodynamic Response

3.1 Numerical Experiment Design

The three-dimensional hydrodynamic model used in this study is the Regional Ocean Modelling System (ROMS). General configuration and validation details are summarized in chapter 2. In this chapter, and in order to evaluate the hydrodynamic response at wind variability a set of simulations using different wind fields are presented. Simulation Wr3 used hourly WRF winds at 3km of resolution, simulation Wr3-A considered spatial-averaged wind values at each time-step, and simulation Wr9 used wind fields from 9km WRF implementation with a 3h of temporal resolution. The averaged wind values have been obtained considering strictly the wind data applied on the inner-bay water surface. We focus in the hydrodynamic response of a 6 day period (from 28th February to 6th March 2014, hereafter named PER-NW), during which a set of northwesterly winds (hereafter NW winds) were blowing in the area (maximum velocities of 15-20 $m \cdot s^{-1}$). Fig 5.5 shows 36-hours averaged wind field during 3rd and 4th march. We selected this period because it shows a series of typical northwesterly events recorded during the extensive campaign period, therefore coinciding with data from A1 and A2 current-meters. During PER-NW period, freshwater sources are considered to be equal to 0, corresponding to rice fields' dry conditions. This simulation does not consider baroclinic processes in order to isolate the hydrodynamic response at wind variability.

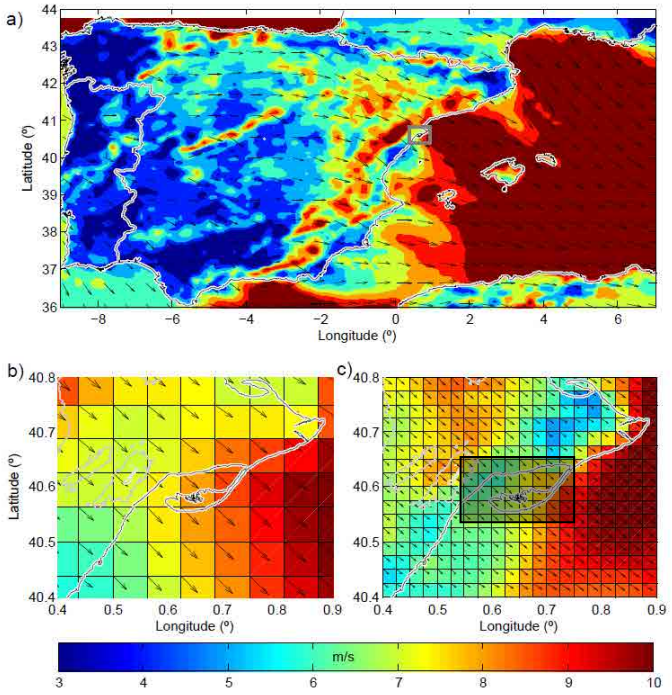

Figure 5.5. Averaged wind speed and directions for a 36 hours north-western event during 3 and 4th march 2013. Image a) shows regional winds over Spain (WRF9). Grey square delimits the Delta Ebre area. Images b) and c) shows WRF9 and WRF3 configurations in Alfacs Bay. In b) and c) Gray lines shows the contour lines for altimetry at 200, 400 and 600m. Coastline is plotted in black.

With the objective of describe the wind spatial variability on the water flows within the bay and open-sea, three cross-sectional sections are defined (T_1, T_h and T_2 in Fig 5.1). T_1 and T_2 coincide with A1 and A2 mooring positions; while T_h represents the narrowest part of the bay mouth. The cross-sectional flows in each transect are analyzed, with positive values indicating direction to the bay's head. Moreover, a longitudinal transect along the main axis of the bay (Fig 5.1, named L) is utilized to observe the differences on cross-sectional flows.

3.2. Results: Hydrodynamic response to wind variability

The hydrodynamic response is investigated in detail during PER-NW period for the three simulations suggested in previous section. In this period, the winds were blowing mostly from the north and north-west lasting for more than 12h with sustained wind speeds higher than 8 $m \cdot s^{-1}$ (Fig 5.6) and maximum wind-gusts of 20 $m \cdot s^{-1}$. Time-averaged modeled winds for 3rd and 4th March showed noticeable spatial variability in the Alfacs Bay (Fig 5.5). These gradients were also appreciated at shorter time-scales. For instance, Fig 5.7e1 shows a snapshot for the wind fields at 10:00h UTC 3rd March (corresponding to simulation Wr3). Maximum velocities are observed on the inner area of the bay, with an almost calm region over the bay mouth. The wind pattern shows a transition zone with maximum wind intensity gradient between T_h and T_2 sections. The averaged wind field (Wr3-A) presented intensities around 6 $m \cdot s^{-1}$ from the NW (see snapshot in Fig 5.7a1).

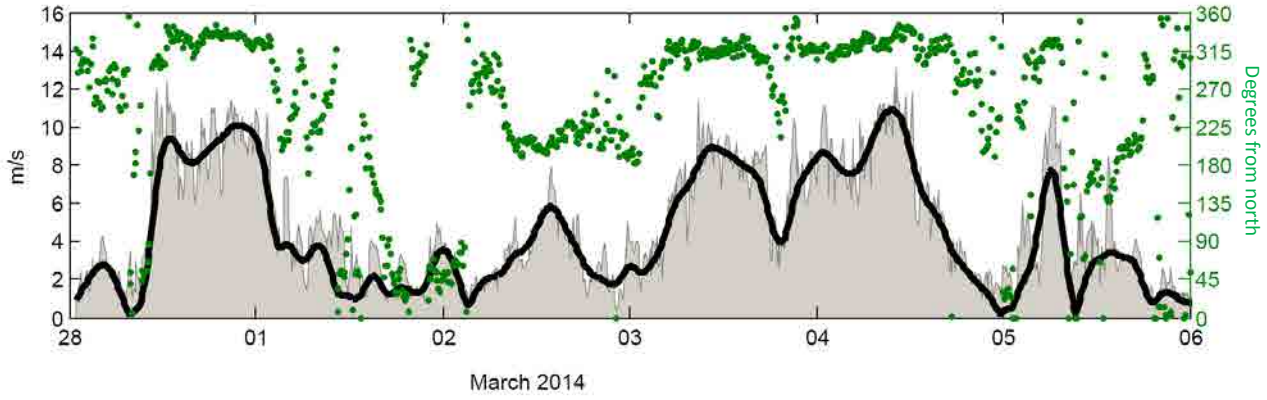

Figure 5.6. Measured wind speeds at between 28th February and 6th March 2014 in M-A. Grey area sows wind speed observations, and black thick line for 6h pass band filtered data. Green dots for true wind direction.

The modelled water circulation for Wr3-A (Fig 5.7a) shows mean surface velocities around 4-5 $cm \cdot s^{-1}$, with surface currents following the wind direction. The maximum intensities are observed on the narrow areas and coinciding with headlands on the southern margin of the Bay. On the east margin, the shoreline and the shallow bathymetry force to align the

currents to the boundaries. Similar current pattern but larger water velocities are modelled for the Wr3 simulation. The most intense currents for Wr3 are obtained in the inner-bay according to higher wind stress. On the bay mouth, surface velocities on Wr3 are lower in comparison to Wr3-A, coinciding with areas with lowest wind stress. Noticeable variations on surface water direction are observed in the bay mouth (between T_1, T_h and offshore). In this area, the water current is intensified in the south side of the mouth and a counter flow towards the inner bay appears in the north side.

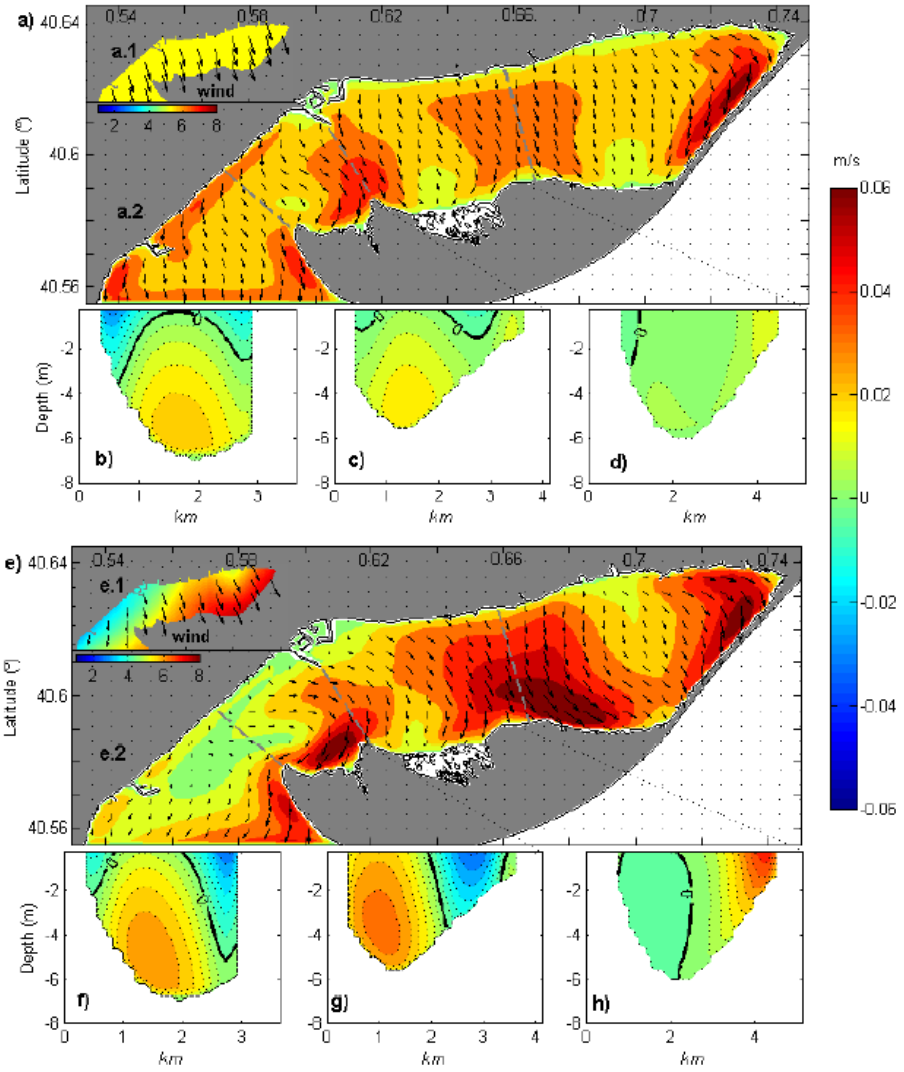

Figure 5.7. Modelling results corresponding to 10:00h UTC 3rd march. Wr3-a experiment in a to d images. Wr3 in e to h. Images on the top left corner of a and e (a.1 and e.1) shows snapshot of wind forcing (m · s-1) in each experiments, while big size images (a.2 and e.2) show surface currents modelled with ROMS. Images b and f for cross-sectional velocities along T_1, c and g for T_h and d and h for T_2. The initial point for each transect (km 0) is located on the northern shoal. In a and e, colors for wind and current speeds (different scales). In cross-sectional plots, colors represent velocities: positive values indicating inward bay velocities, and negative for outward water currents.

The corresponding cross-sectional currents for the three sections considered (i.e T_1, T_2 and T_h) are presented on Fig 5.7b-d, and f-h. Positive means inward flow and negative outward

flow. For transect T_2 in Wr3-A velocities across the section are small and the flow is positive (inwards). For Wr3, larger velocities induced by wind stress over the east margin and southern shore induced a significant increment of inward flow in T_2 (south extreme). Moreover, outward flows occupies half of the section with horizontal shear in the along-shelf direction. Alongshore currents for T_1 section shows similar pattern between Wr3 and Wr3-A simulations with outward flow over margins and inward flow on the deep central channel.

The most relevant differences between numerical tests appears on T_h transect. For Wr3-A water circulation follows the main wind direction on the surface layers, with a divergence flow on the southern headland. On the other hand, for Wr3 this section coincides with the vertex of an anti-cyclonic gyre observed between T_1 and T_h. Alongshore velocities through sections reveal structures completely different between both tests. For Wr3-A, horizontal shear is observed between the margins (outward flow) and the central area, but also vertical shear on the margins, with ingoing flows at the bottom (Fig 5.7c). On the other hand, Wr3 reveals a clear two horizontal layered structure (no vertical shear), with inflows on the northern region and outflow on the south (Fig 5.7g). The intensities of these flows are much higher than Wr3-A.

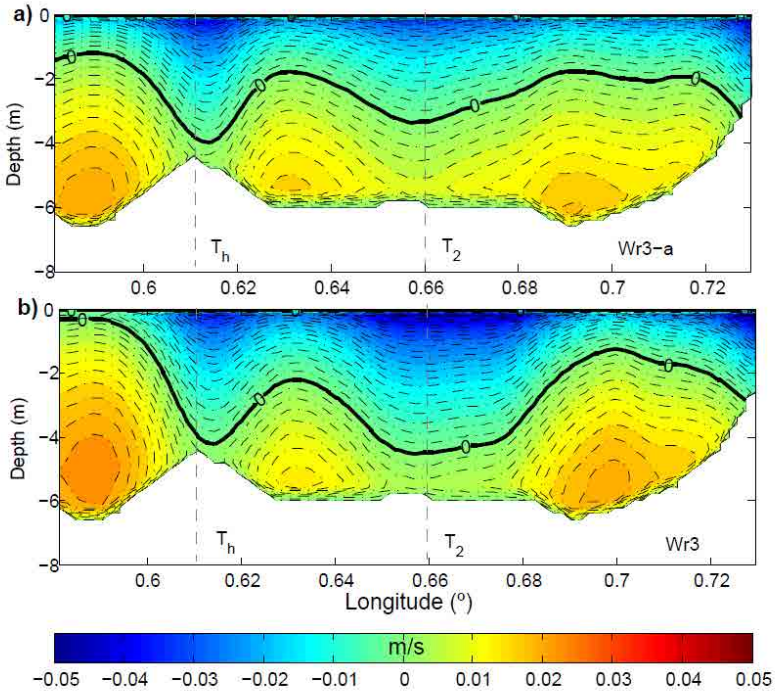

Figure 5.8. Cross-sectional velocities along L section (Fig 5.1) for both Wr3-a (a) and Wr3 (b) numerical tests. Positive values for velocities northward, and negative values for velocities southward. The location for sections T_1 and T_h are marked with dashed lines.

To explore the vertical structure of the flow along the bay and with the same wind direction (almost cross-shore), the velocities across the transect L (Fig 5.1) are shown in Fig 5.8,

corresponding at the same instant than Fig 5.7. Both numerical simulations shows two-layered vertical structure, with surface currents flowing down-wind (negative values), and a northwestward return flow (upwind, positive) on the deeper layers. The bottom circulation shows two regions of maximum velocities: one region between T_h and T_2 and other between T_2 and the eastern boundary of the Bay. These regions are also observable in Fig 5.7a; showing lower surface velocities linked with the return flow observed in the bottom circulation. Differences between Wr3 and Wr3-A relies in the water intensity of upwind and downwind flows. In particular, larger intensities are appreciated for the Wr3 simulation in comparison to Wr3-A around T_2.

The temporal evolution of net exchange flow over each cross-shore transect is obtained for the entire PER-NW in both Wr3 and Wr3-A simulations. The inflow differences between simulations (Wr3 minus Wr3-A) are plotted in Fig 5.9b, c, and d. Mean, standard deviation and the total flow differences through each section are summarized in Table 5.1.

Table 5.1. Statistics from flow differences in each transect (Wr3 - Wr3-A) from 28 February to 5th march 2014.

Section	Standard Deviation	Mean ($m^3 \cdot s^{-1}$)	Total (m^3)
T_1	16.34	-2	- $9.68 \cdot 10^5$
T_2	17.73	+12	+ $65.02 \cdot 10^5$
T_h	19.17	+13.6	+ $68.96 \cdot 10^5$

Differences on T_2 and T_h sections are evident with an increase of net flow (positive) for Wr3 simulation in comparison of Wr3-A case. In opposite, T_1 section does not present significant differences for both simulations. Standard deviations reveals similar values for the three sections. These differences could also be defined in relative terms (percentages of variation). In this case, the Wr3 case versus Wr3-A represents increase of 14 and 22% of mean flows through sections T_2 and T_h respectively, and a decrease of around 3% in T_1. Dashed box in Fig 5.9 corresponds to the snapshot plotted in both Fig 5.7 and Fig 5.8. For both T_h and T_2 this event is related with a period of significant maximum (positive) differences. During this snapshot the flow differences between simulations for T_1, T_2 and T_h were 41, 44 and 88 $m^3 \cdot s^{-1}$ respectively computed from the cross-sectional flow shown in Fig 5.7. The previous numerical results indicates a strong influence of the wind in the vertical structure of the flow.

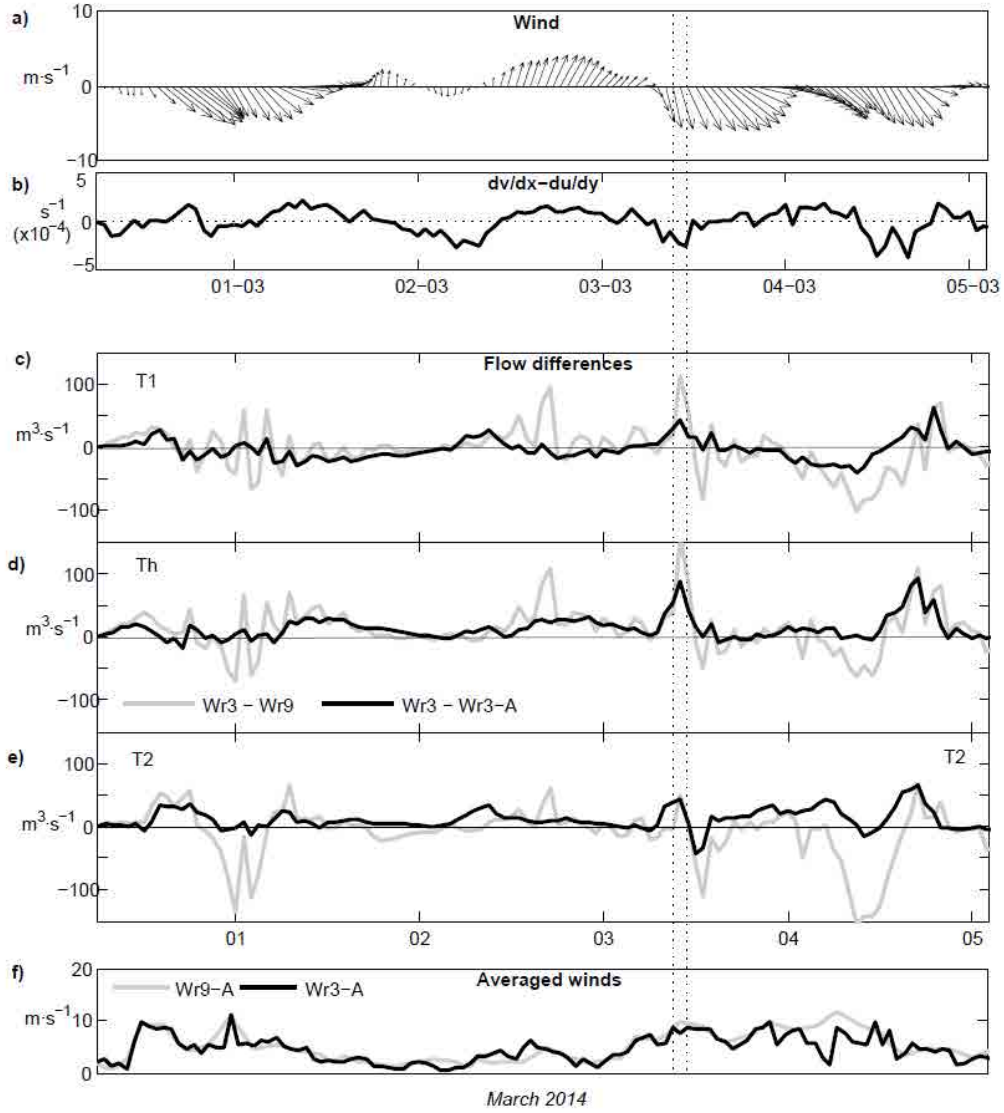

Figure 5.9. Modelling results along the three transects, wind speed and wind curl. a) Spatial averaged winds for Wr3 (=Wr3-A) between 28 February and 6 March 2014. The wind has been filtered using low pass band filter (Lanczos) of 2h. b) Averaged vorticity for Wr3 over the domain marked with black shaded area in Fig 5.5c. Images c, d and e) black thick line shows the flow difference through each section (corresponding panel) between Wr3 and Wr3-a numerical tests (Wr3 minus Wr3-a). The flows are for the corresponding hourly snapshot. Grey line shows the difference from Wr3 to Wr9 tests (Wr3 minus Wr9). Image f shows the spatial averaged wind speeds for both Wr3 and Wr9 in black thick and dashed line respectively.

A hydrodynamic time parameter applied at the defined volumes is used to analyze and compare the flows due to wind variability and their relative effects in the water exchange in Alfacs Bay. There are many definitions to describe the hydrodynamic time parameters for a given domain, being the simplest one the ratio between total volume (V) and the water flow (Q) entering or leaving it (Jouon et al, 2005). The methodology is based on the displacement concept which give us the time required to displace all the water in a volume once,

considering that all water particles have the same transit time through the control volume. It means that using this approximation space and time variability of the hydrodynamics within the control volume are not considered. This is summarized in $\theta = V/Q$ (being θ as water exchange time) as proposed by Jouon et al. 2005. Following the bay division presented on Fig 5.1 by T_1, T_2 and T_h we used the cross-sectional flows and corresponding water volume enclosed at their eastside or inner-bay side (naming each volume as V_{T1}, V_{T2} and V_{Th}). Results for the entire period from 28th February to 6th March (PER-NW) are presented in Table 5.2. With non-variable winds (Wr3-A) the highest flow appears in T_2 (biggest section, with 16.4 $*10^3$ m^2, and around $15*10^3$ m^2 in T_1), twice the observed in T_1 and T_h. In that sense, and considering the volume of water enclosed by each section, the θ shows similar values for both T_1 and T_h and minimum ones for T_2. Then, and taking into account the wind-variability, the averaged flows and corresponding θ are modified in T_2 and T_h (reducing them about 14% and 20% respectively), and remain without noticeable changes at T_1. On the other hand, hourly snapshot observed during 3rd march at 10:00h (Fig 5.7) reveals noticeable variations in all the sections, showing associated water exchange times reductions of 20%, 47% and 40% for T_1, T_h and T_2 between Wr3 and Wr3-A.

Table 5.2. Statistics from flows on sections T_1, T_2 and T_h from 28 February to 6th march 2014 (represented by mean values). The water exchange times (θ) are computed considering the area they have on the east side (Fig 5.1).

T	Volume (x10^8) m^3		Q_{mean}	θ (days)
T_1 (V_1+V_2+V_h)	2.44	Wr3	53.16	53
		Wr3-A	55.07	51.3
T_2 (V_2)	1.06	Wr3	99.47	12.3
		Wr3-A	85.9	14.3
T_h (V_h+V_2)	1.99	Wr3	58.8	39.2
		Wr3-A	45.9	50.2

4. Discussion

Due to the lack of additional meteorological and hydrodynamic observations within the bay to complete the analysis of the wind variability response, the results of the already validated modelling system (atmospheric and hydrodynamic) provided interesting insights. Previous works in Alfacs Bay (Camp 1994; Llebot et al. 2013) have observed well mixed conditions in winter under energetic winds. In addition, observations only one week before the PER-NW showed complete water column mixing in the bay (chapter 2 and 4, Fig 2.4 and Fig 4.3c). In consequence, with the purpose to isolate the hydrodynamic wind response, the stratification and the astronomical tides have not been considered in our simulations.

Numerical simulations using spatially wind variations (Wr3) versus homogeneous case (Wr3-A) reveal noticeable differences on hydrodynamic structures. One of the most noteworthy hydrodynamic feature observed is an anti-cyclonic gyre close to the bay mouth. This structure is clearly observable in Fig 5.7 and Fig 5.8b and is related with an increase of the flow between T_h and T_2. The water fluxes through the sections (summarized in Table 5.1 and Fig 5.9) show how the wind variability not only determines the hydrodynamic response, but also affects the water fluxes through the bay. Similar structure on the bay mouth is found 24h later (not shown). Sectional flow differences between numerical simulations showed two clear different hydrodynamic responses: T_h and T_2 with noticeable differences between tests, and T_1 revealing lower sensitivity to the wind variability. Therefore, the wind variability in inner areas (T_h and T_2) implies noticeable reduction of water exchange times. However, these differences among spatially variable (Wr3) and non-variable (Wr3-a) winds in T_h and T_2 respond to a different physical mechanisms. Over T_2 the differences are due to an increase of wind speed between Wr3-A to Wr3 affecting the circulation pattern (quadratic effects through wind stress). Otherwise, over T_h (and T_1) the wind is much lower in the Wr3 than Wr3-A, and in this case the mechanism that lead the flow increment is related to the anti-cyclonic structure appearance. Idealized tests with the objective to describe and understand this process and evaluate the relative contribution of bathymetry and coastline are discussed below.

In order to understand the mechanism which leads the hydrodynamic pattern observed in Fig 5.7 and Fig 5.8, a set of idealized numerical tests were implemented. The wind variability tests were designed to reproduce the observed wind pattern in Alfacs Bay (see section 2.1) in idealized shape domain in order to minimize the effects of lateral roughness and non-linearity induced by irregular bathymetry and coastline. The geometry is reduced to a rectangular shape (oriented east-west) opened at the south-western side with an oriented north-south

channel keeping away the open boundary (Fig 5.10). Reference test is forced by 5m · s^{-1} north-west wind (Fig 5.10a). The rest of the tests are defined by a zone with constant winds of 2 m · s^{-1} and then wind speed is increased linearly towards the east side. Wind patterns along x-axis are represented above each image in Fig 5.10. Two experiments, with the region of varying wind occupying 2/3 or 1/3 are designed (Fig 5.10, c-d and e-f respectively). Another test with extreme variations is presented in Fig 5.10g-h; in this case the region of constant wind is defined to 0 m · s^{-1}. The spatial integrated wind intensity is the same for all cases and equivalent to 5 m · s^{-1} over each grid in homogeneous test (Fig 5.10a). Same geometry and numerical mesh are used with two different bathymetries: flat bottom with 4m water depth and bathymetry with shoals of 2m depth in the lateral margins and a central channel of 6m (see Fig 5.10b). The model implementation is the same that the realistic case presented in chapter 2, being the water density homogeneous in the whole domain. The numerical solution is analyzed after 24 hours of simulation, when the stationary conditions are reached. For flat bottom with homogeneous wind fields (Fig 5.10a), the surface currents move in the same direction of the wind (+3º clockwise from winds). For the channel bottom case, surface currents are modified in comparison to bottom flat case (Fig 5.10b). Over the shoals the currents flows with the wind direction but rotated 30º anticlockwise, while on deeper areas (central channel) the surface currents rotate 45º degrees clockwise. Cases c and d are similar to wind described on Fig 5.5 and Fig 5.7; although with larger wind gradients. The eastern corner shows highest water intensity with similar direction to wind forcing, whilst over the region with lower wind speeds high variability on water surface currents appears. Similar structure (gyre) described on Fig 5.7 appears on the transition wind area. When the wind gradient is applied more to the east (Fig 5.10e and f) a clear anti-cyclonic gyre is also observed but located in the innermost area of the bay. The last case (with no wind on the western side) maximizes the effects of the anti-cyclonic gyre. The southwestwards currents induced by wind pull water from the areas with no-wind. Then anti-cyclonic gyre is established covering the entire width of the bay. This gyre is observed in all the experiments with wind variability (and with both types of bathymetries). The results from idealized tests indicate that the water circulation on the left (western) side of wind gradient is characterized by a gyre. The responsible mechanism is the wind curl, establishing an eastward surface current on the northern region of the bay with calm winds, and westward flows on the southern regions. Although the bathymetry has been idealized through a central channel, the numerical results show how the wind variability dominates over the bathymetric effects under these circumstances. Therefore, in our idealized case the bathymetric effect is a second order factor.

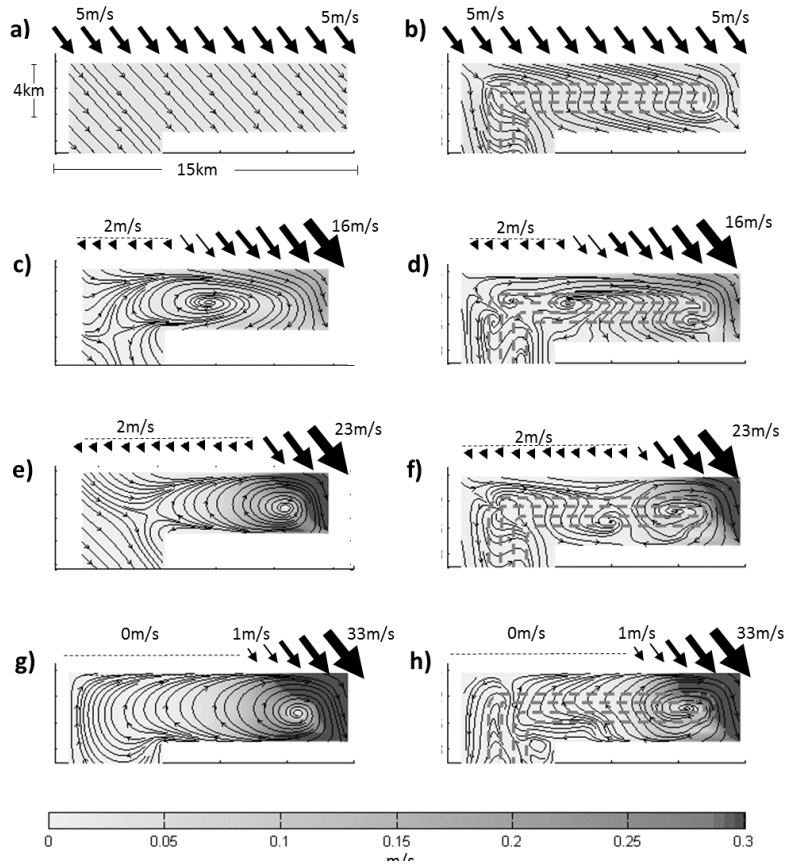

Figure 5.10 Surface streamlines for idealized schemes. Each panel shows the velocity module contours (grey scale) and streamlines for each of the idealized wind tests after 24hours of simulation. The winds along x-axis utilized in each test are shown at the top of each panel. Left images for flat bathymetry (4m depth) and right images for channelized bathymetry. Isobaths 4m and 6m are plotted in dashed grey lines in image b, d, f and h.

At larger spatial scales than Alfacs Bay, several authors have observed how the vorticities of wind fields are related with the generation of mesoscales gyres (eddies) on more regional scales as Mediterranean Sea (Espino, 1997; Schaeffer et al., 2011) or in Hawaii Islands (Chavanne et al., 2002). However, the gyres and vortices modelled in Alfacs Bay related to wind variability are not usually described in small coastal areas (characteristic length of ten km). The spatial mean wind curl ($\frac{\sum_{i=1}^{n}\left(du/dy - dv/dx\right)}{n}$, with n for each data pixel) from Wr3 (domain in Fig 5.7) is shown in Fig 5.9e for PER-NW period. The highest negative values coincide with northwesterly wind events, and respond to the wind variability shown in Fig 5.5 and Fig 5.7. Results indicate that negative vorticity close to T_h is causing the appearance of the anti-cyclonic gyre observed on Fig 5.7 and described in idealized tests (Fig 5.10). At this point, in non-stratified systems the key parameter is the depth (and the response time), which would indicate how much of the water column would respond directly to the wind field. In Alfacs Bay, during most energetic winds, the entire water column would respond to wind stress, thus, revealing the importance of accurate description of spatial wind variability.

The averaged flow and time scales on Alfacs Bay are investigated in order to analyze the influence of wind spatial variability over the entire PER-NW period. Camp (1994) used

salinity balance based approximation to obtain the water exchange time as V/Q, but considering the estuarine circulation as the flow through the section. From salinity values (top and bottom layers) he defined the equivalent estuarine flow (Officer, 1996). In his case, a flow of $150 m^3 \cdot s^{-1}$ and $40 m^3 \cdot s^{-1}$ through similar section of T^h during open and closed channels seasons respectively (corresponding water exchange times of 14 and 50 days) were obtained. Even these flows are approximations, and respond to a completely different physical forcing (gravitational circulation) from what we have used, they gave us an idea of temporal (θ) and intensity scales (flows) in the Bay. Comparing these values with the numerical results during PER-NW it is clear how during closed channels season (winter) the role of the wind variability on the bay exchange flows must be considered. As an example, Wr3 and Wr3-A simulations shows flows of 59 and 46 $m^3 \cdot s^{-1}$ respectively, being similar than winter equivalent estuarine flow (Camp, 1994).

For the PER-NW period we have applied WRF model at 9km of resolution (Wr-9) to assess the results using medium range products of meteorological forecasts. The flow differences between Wr3 and Wr9 are summarized in Fig 5.9, panel c, d and e (grey line). In general, their differences are similar to the ones observed between Wr3 and Wr3-A. The correlation between flow differences from Wr3 to Wr3-A or Wr9 moves from 0.56 to 0.67 in T_l and T_h respectively, indicating that the numerical resolution used in Wr9 equals to Wr3-A and does not reproduce the spatial variability under some circumstances. The spatially averaged velocities for both Wr3 and Wr9 are shown in Fig 5.9f, revealing how the differences between them are minimum most of the time, even under some circumstances (i.e. 1st and 4th March) in which the Wr9 wind is more intense. These differences imply a flow increase through the sections. Moreover, it has been demonstrated how these high resolution models are able to solve spatial structures (not reproduced by coarser models) that implies noticeable variations on hydrodynamic structures, as observed in Klaić et al. (2011) and Zampato et al. (2007). On the other hand, Wr9 has temporal resolution of 3h. Considering the small depths and the high sensitivity to wind forcing observed in the results, we can expect that models with larger time resolution would imply loss of relevant information. Future research lines of investigations will include studies on temporal variability impacts on hydrodynamic response.

For stratified conditions in the water column, the stratification enable wind stress to result in larger velocities in the surface layer diminishing the vertical momentum transfer. However, observational studies and sensitivity test shows how the stratification is altered by the energetic NW wind events (Llebot et al. 2013). Therefore, even the limited depth of the Alfacs Bay and the reported stratification due to freshwater and heat fluxes, we believe that the response pattern to wind variability would not vary significantly under most energetic

winds described in this contribution. However, spatial variability in weaker winds under stratified conditions would promote more complex circulation. The response under weaker winds will benefit for extended and simultaneous stratification and velocity observations.

Several contributions in similar domains as Alfacs Bay (i.e. shallow and microtidal environments) have investigated the hydrodynamic response using homogeneous winds. For instance, Cucco and Umgiesser (2006) in Venice lagoon (Italy), Ferrarin et al. (2010) in Marano and Grado (Italy), Alekseenko et al (2013) in Berre lagoon, (Shoutern France) and Schoen et al., (2014) in an estuarine lake in South Africa. Also the hydrodynamics of commercial harbors have been investigated based on wind measurements in one point (Mestres et al., 2007; Grifoll et al., 2011). Finally, (Llebot et al. 2013) investigated the Alfacs bay using homogenous winds. Using spatial variable winds likely does not change the circulation pattern obtained in some of the mentioned contributions; however its influence may be relevant in particular cases. Although not all these locations may present similar wind variability as we observed in Alfacs Bay, we suggest that proper sensitivity studies may conclude with significant differences and emerge variability in water exchanges between the semi-enclosed water body and open sea. The influence of the shape and dimensions variability of the coastal embayment influences the relative importance of wind variability effects, so further combined numerical and observational studies are desirable to describe the hydrodynamics in coastal areas.

The effects of wind variability over the water exchange time influence the grade of the water flushing, which, in turn control relevant issues of the ecological behavior of the bay. For instance, in Alfacs Bay, the water flushing influences the ecological behavior of the system determining the development of Harmful Algal Blooms (HABS) (Loureiro et al. 2009), the mollusks farms productions (Galimany et al. 2011) and fisheries, as well as importing/exporting species from the open sea inside the bay (as observed in Delgado 1989). Further investigations linking the variability of the water exchange and the ecological evolution will benefit the sustainable management of the bay.

5. Conclusions

Hydrodynamic response in coastal areas is demonstrated to be very sensitive to wind variability. A semi-enclosed bay in Mediterranean Sea is chosen as application site. The wind in the bay is affected by regional and local surrounding orography. Due to the lack of high spatial resolution observational data, atmospheric model is used to explain the main wind patterns and study the surface current response. A barotropic application of the numerical model, due to well mixed conditions on the bay during most extreme winter events, is used in a set of twin experiments, using field winds from WRF3 model and comparing it with spatially homogeneous wind fields. Results show the development of anti-cyclonic structures near the bay mouth, which are related to the variation of net flows through the inner bay. A set of idealized numerical tests confirms the dependency of these hydrodynamic structures to the wind curl (vorticity). The relative effects of bathymetry are also considered, not revealing noticeable influence on currents compared with wind variability under those circumstances. The variability in hydrodynamic patterns linked to the wind heterogeneity implies noticeable variation on associated water exchange times (20%) over some areas of the bay, this probably affecting the O_2 distribution and other ecological key parameters of the bay. Comparison with coarser atmospheric model (9km) demonstrates the information lost using incorrect temporal and spatial resolutions. Our results demonstrate how the spatial variability of cross-winds could notably modify the circulation patterns. These results are applicable to similar coastal areas as harbors, bays and estuaries affected by local or regional wind variability, and confirm the importance of wind spatial variability in such small domains.

Acknowledgments

We want to thank to Joan Puigdefàbregas, Jordi Cateura and Joaquim Sospedra from Laboratori d'Enginyeria Marítima for all their help with campaigns and data analysis, and the XIOM network (www.xiom.cat) for the information provided. We are also indebted with staff from Servei Meteorlogic de Catalunya (Meteocat): Abdelmalik Sairouní Afif, Manel Bravo and Jordi Moré, who shared with us all the atmospheric modelling data. This work was supported by a FPI-UPC pre-doctoral fellowship from the European project FIELD_AC (FP7-SPACE- 2009-1-242284 FIELD_AC). The campaigns were carried out thanks to the MESTRAL (CTM2011-30489-C02-01) and ICoast projects (Echo/SUB/2013/661009). We also want to thank to Secretaria d'Universitats i Recerca del Dpt. d'Economia i Coneixement de la Generalitat de Catalunya (Ref 2014SGR1253).

6

Low frequency circulation in a microtidal semi-enclosed Bay

Time passes irrevocably.

Virgil

The only reason for time is so that everything doesn't happen at once.

Albert Einstein

Abstract

In this contribution we examine the role of different forcings on the long-term circulation in a microtidal bay at the NW Mediterranean Sea (Alfacs Bay). Low frequency observations from summer 2013 and winter 2014 reveal two-layered water circulation. Qualitatively speaking, there is a strong positive relation between surface currents and winds along the main axis of the bay during summer period, while negative correlation is observed on bottom layers. During winter, wind and surface currents on the alongshore axis are not well correlated, whilst the cross-shore response is correlated with most energetic winds, and in the bay mouth have shown a nearly depth-independent water motion due to the high wind intensities. The analysis of the vertical variability (EOF decomposition) confirms that the hydrodynamic response in the water column with winds suggest two different forcing mechanisms: surface layers affected by winds and bottom currents highly correlated (negatively) with winds through the pressure gradient term (wind set-up). At longer time-length scales, averaged circulation reveals estuarine circulation in the bay mouth, being more evident during summer period. On the inner bay, and close to the drainage channels, no clear averaged circulation is observed, and the fluctuations prevail. Using observations it is demonstrated how the density structure inside the bay could be responsible of this behavior. The observed patterns are supported by modelling results which allows to estimate the spatial distribution of the averaged circulation. Re-circulation areas on the inner bay suggests the importance of further studies in order to understand the spatial variability on residence time at the low-frequency time-scales.

1. Introduction

The dynamics and physical processes in estuary environments may be investigated from different time scales. A common way is using the tidal periods as a cut-off frequency considering the variability above these periods. In most of the regions, the main tidal currents are semidiurnal (Browne and Fischer, 1988) or diurnal (van Maren and Hoekstra, 2004). Below these time-scales, processes due to winds (Noble, 1996), co-oscillating waves (Uncles et al., 2014), ocean waves (Mulligan et al., 2008), rain (Grifoll et al., 2011), or intense freshwater inputs (Valle-Levinson, 2011) are the main factors controlling the hydrodynamic response. On the other side -above periods of 24h- the processes are categorized as a subtidal or low-frequency, including wind locally or remote dependent circulation (Janzen and Wong, 1998), atmospheric pressure influence (Salas-Monreal and Valle-Levinson, 2008) and residual circulation (Narváez and Valle-Levinson, 2008). For example, synoptic events have time-scales of few days (2 to 5) related to the passage time for depressions, and influences the circulation on that scales (Dyer, 1997).

On daily time-scales, the processes are usually less energetic than at high frequency scales, but their importance are crucial in determining aspects such the residence times of the area under study. For instance, strong gravitational circulation implies higher interchange between the estuary and the open sea, thus diminishing the residence time and affecting different ecological and biological aspects (e.g Marcelo et al., 2008; Hagy et al., 2000).

As stated in previous chapters, the main source of flow variability in Alfacs Bay are dominated by winds and seiches at periods shorter than days. Llebot et al. (2013) also shows how the wind influences not only the hydrodynamic response but also the hydrographic structures on short-time scales (few hours). However, the low-frequency circulation, and its related forcing mechanisms, have not been investigated before in Alfacs Bay. Therefore, the objective of this chapter is to describe the basic hydrodynamic response at low-frequency in a micro-tidal area such as Alfacs Bay. In this sense, the purpose is to describe the mechanisms that force the residual circulation evaluating the seasonal differences and the spatial description and variability using numerical tools.

The chapter is organized as follows: results for filtered currents and wind observations is presented in section 2; in section 3 the main factors controlling the hydrodynamic response at low frequency and averaged scales are described. In this section, the numerical model results are also presented. In order to analyze the dynamics at low frequencies, both currents and wind observations are filtered using a 30h low-pass band filter (Lanczos filter) (Emery and Thomson, 2004).

2. Results

2.1 Winds

Spectral analysis (Fig 6.1) for a long time-series of wind data observations (1996-2013) in M-SC (location in Fig 2.2) reveals noticeable energy content at 24h period and at 12h. Both periodicities corresponds to the sea breezes with strong asymmetry between daily (inshore winds) and nightly (weaker offshore winds) influences. Lower frequencies does not reveal any significant periodicity, but contains a large amount of energy. This low-frequency energy is usually associated with the synoptic passage of low-pressure systems, which in the Catalan Sea corresponds to 3–12 days (Font, 1990).

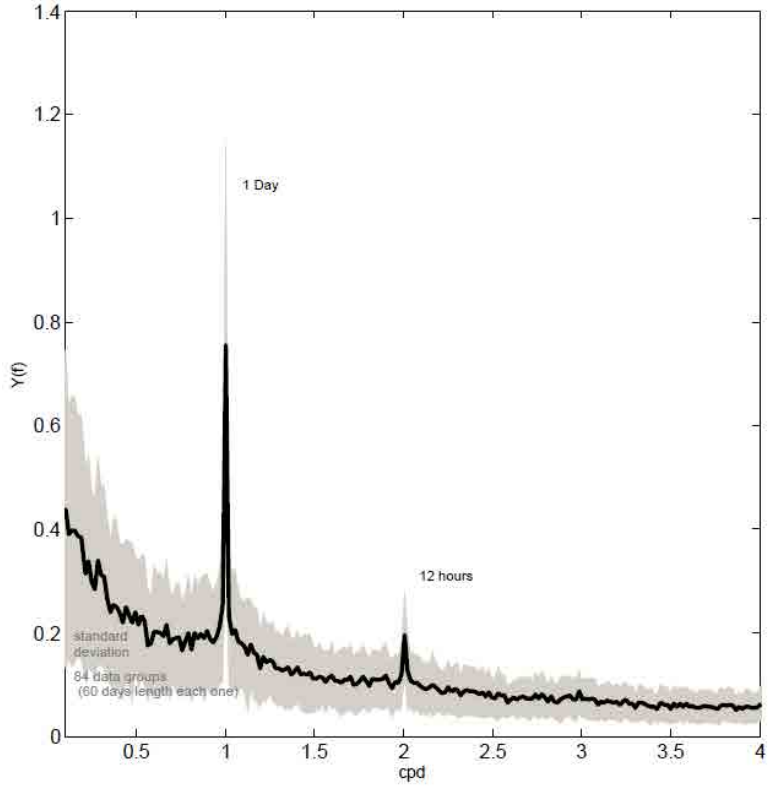

Figure 6.1. Energy spectra for wind observations in M-SC since 1996 to 2013. In order to obtain statistical significance, the data has been analyzed with a temporal window of about 60 days (total amount of 86 data sets used to obtain the mean and standard deviation).

Two periods, with simultaneous observations of currents and winds, have been chosen with the objective to describe the low-frequency dynamics on Alfacs Bay. Both periods, as well as the observation locations and main characteristics are described in chapter 2. During summer, unfiltered data in M-A shows mean wind speed of 3.1 $m \cdot s^{-1}$, with standard deviations of 1.7

$m \cdot s^{-1}$ and maximum hourly winds of 13.4 $m \cdot s^{-1}$. The sea breeze pattern (diurnal cycle) is clearly observable during the entire summer (Fig 6.2a) in unfiltered data, with exception of two periods of seaward winds. These events occurred during 8th and 25th of August and lasts approximately for a few hours. During winter, mean wind speeds rise to 4.2 $m \cdot s^{-1}$, standard deviation to 3 $m \cdot s^{-1}$ and maximum hourly values to 14.2 $m \cdot s^{-1}$. On the other hand, the 30h filtered wind data during summer shows maximum values around 6 $m \cdot s^{-1}$, while it increases to around 12 $m \cdot s^{-1}$ during winter. Moreover, during March 2014, more than four events with winds more intense than 10 $m \cdot s^{-1}$ are observed (Fig 6.2c).

2.2. Water Current

The filtered depth-averaged water current speeds in A1 and A2 (locations in chapter 2, Fig 2.1) are plotted in Fig 6.2b and 6.2d for summer and winter seasons respectively, showing higher velocities in A1. Standard deviations also reveals higher values in A1 than in A2 (2.2 and 1.6 against 1.8 and 1.2 for summer and winter respectively). As a first approximation and in order to compare qualitatively the wind and current intensity, the filtered wind speeds are plotted multiplied by a factor of 0.03. This value corresponds with the theoretical surface layer velocity (u_w) due to the wind speed (W) following the quadratic stress law $u_w = \sqrt{(\rho_a/\rho_w)} \cdot W$ (Large and Pond, 1981; deCastro et al., 2003) where ρ_a and ρ_w are the air and water densities respectively. From 7th to 20th July the depth averaged water speed response (in both A1 and A2) follows the main pattern described by winds, but for the rest of summer period, the graphical comparison in Fig 6.2b does not reveal a clear response pattern between wind and depth-averaged currents. Correlations coefficients between depth-averaged current speeds and winds are close to 0, while during winter their values increases to 0.2 and 0.4 in A1 and A2 respectively. During summer, maximum currents speeds are observed at 4th August, as well as end of August and beginning of September (and with remarkable differences between A1 and A2). In both cases, water currents have been related to co-oscillating waves instead of winds or other hydrodynamic forcing at higher frequency band (more details in chapters 3 and 4). In this case, because the filter is applied on the water speed, the high frequency signal is not completely filtered and some energy remains in low frequency band.

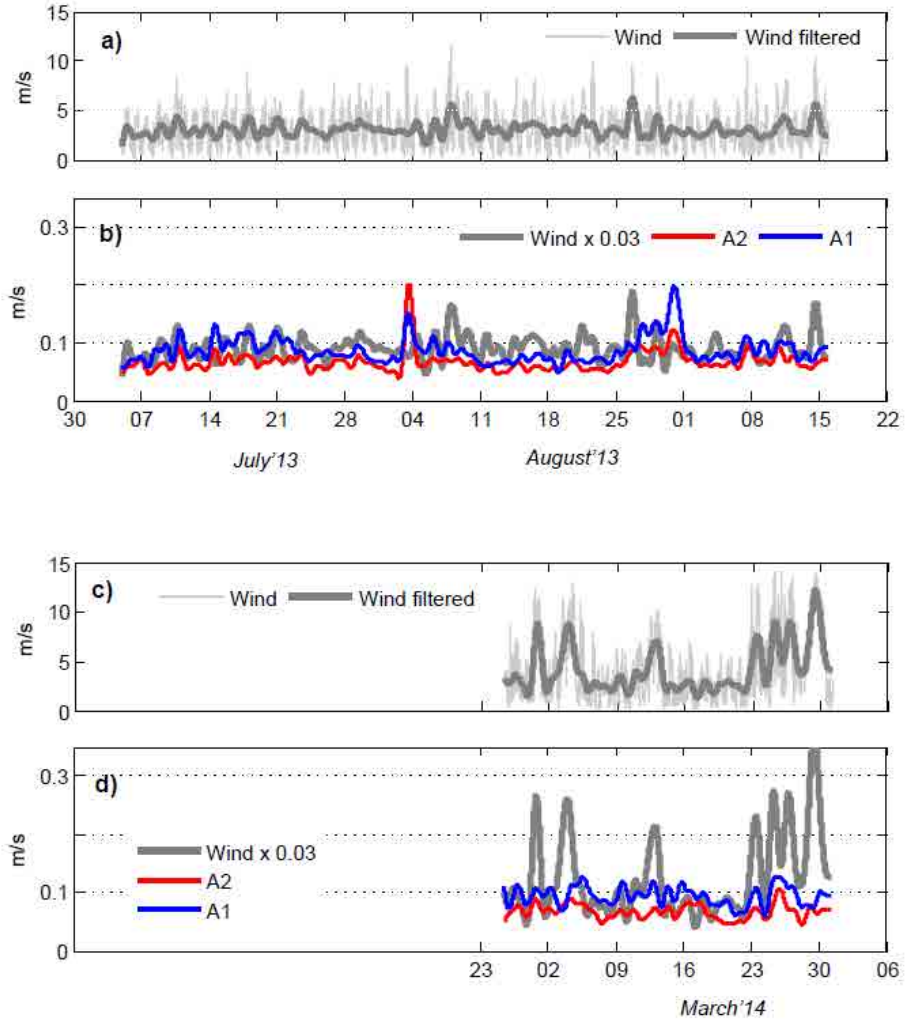

Figure 6.2. Filtered wind and depth averaged currents. In a and c: thin gray for wind speed measured in Met-A during summer'13 and thick gray line for 30h low pass band filtered wind during same period. B and d: gray line for wind speeds multiplied by 0.03, and red and blue lines for depth averaged water current speed on A2 and A1 respectively. All units in $m \cdot s^{-1}$.

Current Rose plots for the filtered currents on surface and bottom layers (1m averaged) are shown in Fig 6.3 and Fig 6.4**.** During summer, two different patterns are observed at A1 and A2. In A1 directions towards the open-sea predominates on surface layers, and inversely in the bottom layers. In A2, the ingoing flows predominates on surface layers. Events with highest current speeds on summer correspond to NW and NE winds (8^{th} and 25^{th} august respectively). During winter, the filtered data is more scattered in A1, showing two predominant directions on surface layers (NE and S-SE). In A2 the surface layers are similar to the observed during summer, although a bit less dispersed from the main axis. Maximum surface velocities in A1 coincides with periods with NW winds (2-5 and 25^{th} March), while

maximum velocities in A2 were observed during 15-17th March (also showing high velocities in A1). This period does not coincide with any intense wind or seiche event.

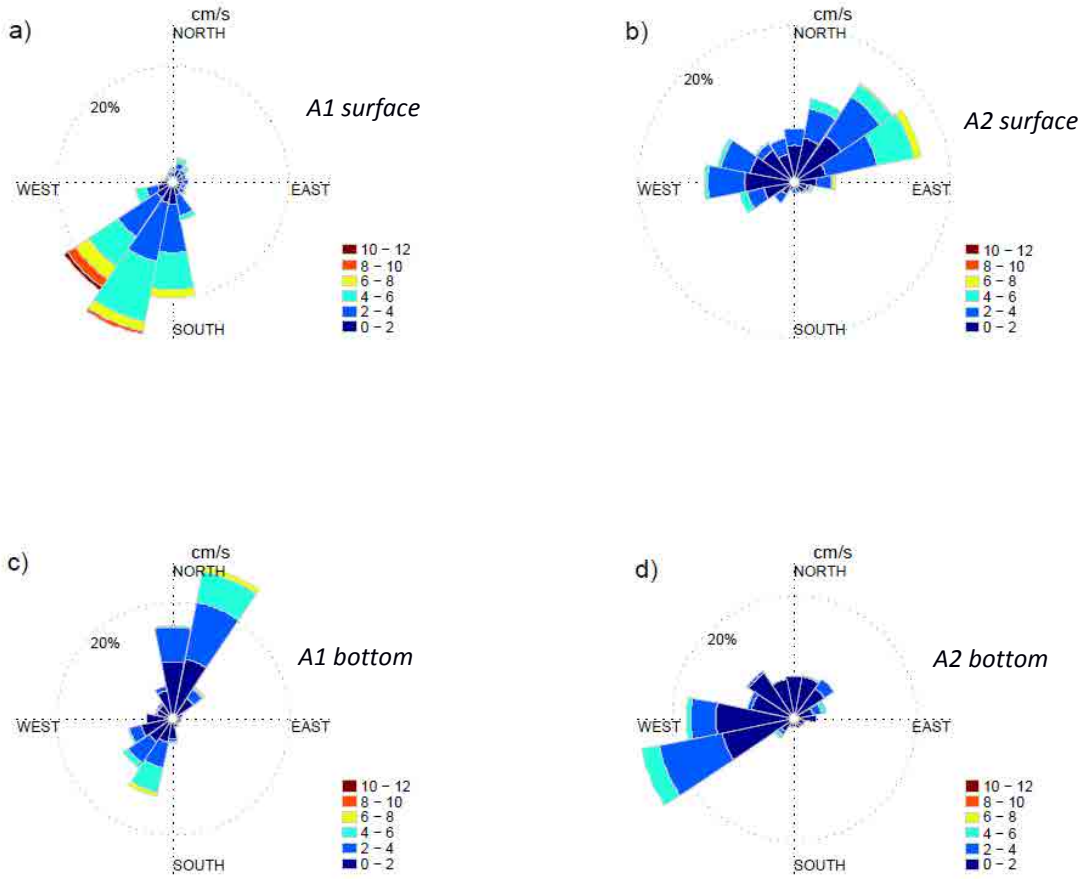

Figure 6.3. Current roses for 1m surface and bottom filtered currents in A1 and A2 during summer'13. Both surface and bottom velocities are grouped in a 1m layer width. Colored data shows the corresponding current speed, grouped with 2 $m \cdot s^{-1}$ interval and with 16 directions.

Correlation between surface and bottom layers in both A1 and A2 during both periods is shown in Table 6.1. In both locations and during all periods, correlation between bottom and surface layers are negative, thus indicating the presence of two differentiate layers. Per contra, during winter, the correlation between surface and bottom layers is 0 at A1 for northward component.

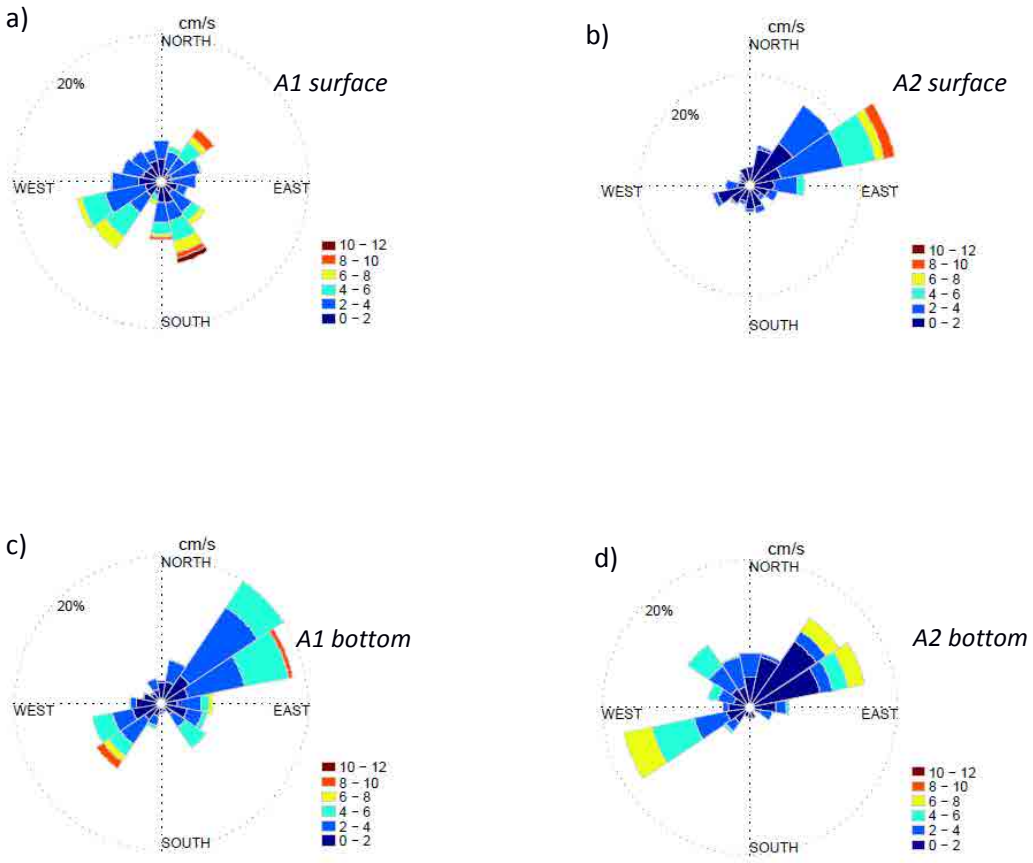

Figure 6.4. Current roses for 1m surface and bottom filtered currents in A1 and A2 during winter'14. Both surface and bottom velocities are grouped in a 1m layer width. Colored data shows the corresponding current speed, grouped with 2 $m \cdot s^{-1}$ interval and with 16 directions.

2.3 Rotated water currents

Low frequency currents observations show how the maximum variability of the water currents in A1 and A2 are associated mostly to one axis aligned with the coastline (following the central axis of the bay) (Fig 6.3 and 6.4). This axis has been obtained adjusting a line (linear regression) between both components and obtaining the angle with east-west axis. For this analysis the data of all the vertical layers have been considered without vertical averaging. Therefore, the explained variability shown in Fig 6.5 (a and c) expresses the variance of each axis respect the total variance. These results are consistent with previous contributions which used unfiltered water current data in Alfacs Bay (e.g. Camp, 1994) and chapter 4 (using depth averaged velocities), although some differences are observed due to the use of vertically averaged data or the complete vertical data set. Velocities corresponding to the rotated axis are defined as u'_{a_b} and v'_{a_b}, being "a" for A1 or A2 observations, and "b" s or w indicating summer or winter period. The u' axis corresponds to the along-bay

(alongshore) circulation, and v' axis for the cross-bay (cross-shore) circulation. Alongshore positive values indicates velocities towards the head of the bay. New axis for the filtered data are rotated 20º anticlockwise in A2 for both seasons because summer and winter observations reveals similar values (19º to 21º). Otherwise, in A1, during summer the new axis is obtained at 43º anticlockwise. However, winter observations does not reveal a major axis of variability because there are two clear dominant components (Fig 6.4a). For this reason, the rotation in A1 observations during winter is carried out considering the same axis than in summer. In order to compare winds and currents, in all the forthcoming results the wind is rotated according to the corresponding location.

Table 6.1. Correlation coefficients between 1m surface and 1m near bottom averaged currents in both A1 and A2 locations during summer 2013 and winter 2014. Eastward and northward (no rotated) components are analyzed.

	Summer		Winter	
	A1	A2	A1	A2
R (Eastward)	-0.40	-0.39	-0.49	-0.32
R (Northward)	-0.72	-0.21	-0.09	-0.24

The variability explained by the new axis at each of the vertical layers is shown in Fig 6.5. Alongshore currents accounts for more than 75% of the total variability in A2 for both seasons and during summer in A1. During winter, the surface layers revealed higher variability in A1 explained by the cross-shore component as was shown in the current rose (Fig 6.4a).

The rotated currents and wind correlations are plotted in Fig 6.5b and d (considering all the water layers depth). The correlation of surface alongshore layer with the alongshore wind component shows only a modest correlation in summer (R=0.4). During winter, surface currents and winds revealed low correlation (i.e $\approx$ 0.2), and in all cases this correlation decreases quickly with depth, changing the sign to negative values with the maximum correlation at bottom layers (e.g. maximum R=-0.7 during winter in A2). In that sense, linear correlation give us an idea of the general behavior measuring the strength and the direction of a linear relationship between the winds and currents. However, no information about the hydrodynamic response under specific events could be derived from these values.

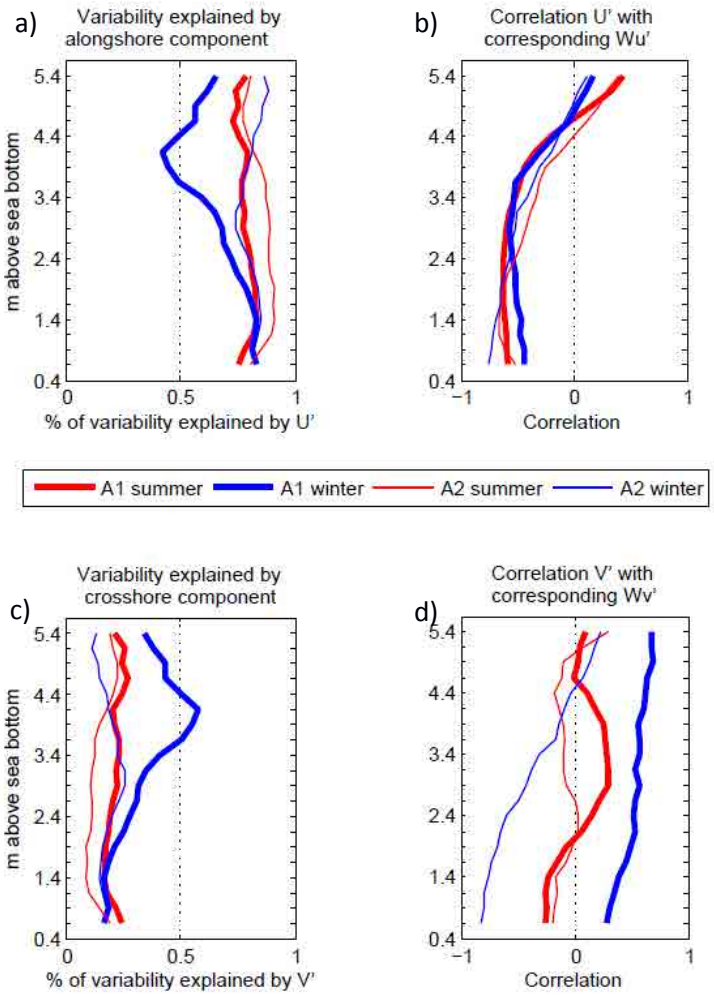

Figure 6.5. Left images for the percentage of variability explained by along (a) and cross-shore (c) components in A1 (thick line) and A2 (thin line) during summer (red) and winter (blue) periods. Same in Panels b) and d) but showing the correlation coefficient of each water current layer with wind.

For that reason, considering the limitations of linear correlation coefficients, alongshore and cross-shore currents (both surface and bottom layers) are graphically compared with corresponding wind component (rotated to the same axis than currents) in Fig 6.6 and 6.7 for summer and winter periods respectively. During summer, results shows maximum wind variability in alongshore axis. Two energetic events are observed at 8th and 25th August. On currents, the maximum variability is observed on alongshore direction with higher speeds on surface layers. The u'_{A1_S} shows 59% of the total speeds higher than 3 cm $\cdot$ s^{-1}, while for u'_{A2_S} only 23% of the total current speeds exceeds this threshold. On cross-shore, only 16% and 3% of the observations shows values higher than 3 cm $\cdot$ s^{-1}. Bottom layers in A2 does not exceeds

3 cm · s^{-1}, and only 14% for A1 alongshore bottom velocities does. Qualitatively, alongshore in both A1 and A2 shows a clear two-layered structure. In general, in A1 the surface layers show negative values, reproducing the oscillations observed by winds, whilst the A2 surface currents oscillates between positive and negative values following the main oscillations of the winds. Thus, relevant surface response to the wind forcing on alongshore currents during summer is qualitatively observed.

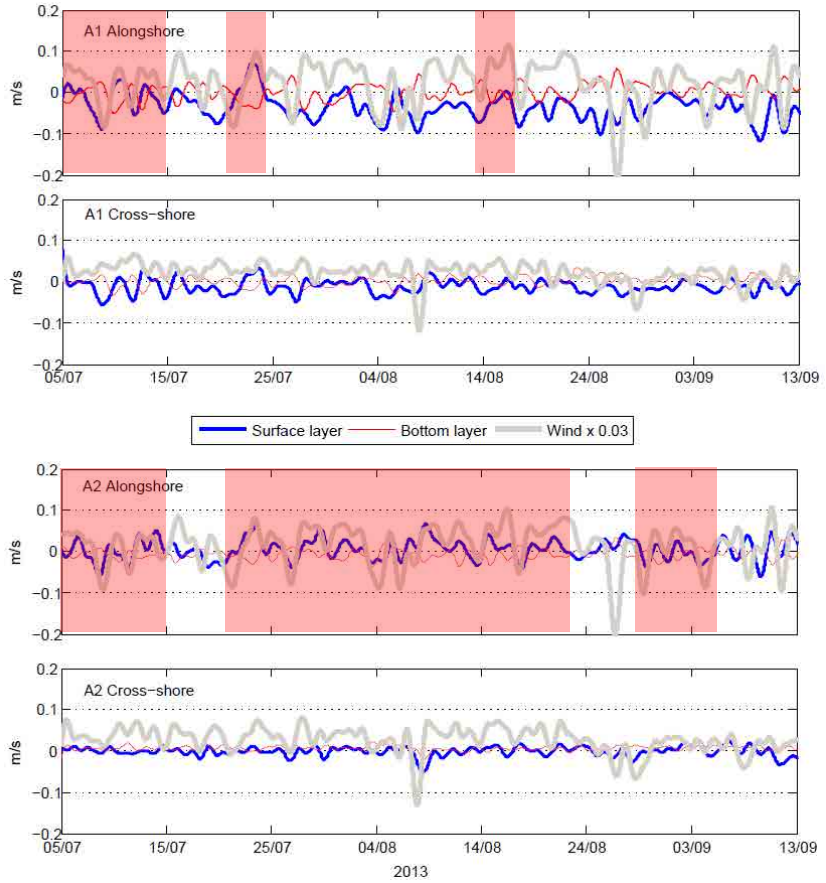

Figure 6.6. Summer A1 (a and b) and A2 (c and d) filtered time series of Wind (x 0.03) and surface (blue) and bottom currents (red). Both wind and currents are plotted following the rotated axis: 21º and 42º anticlockwise for A2 and A1 respectively. Red shadowed areas indicates instants with qualitatively relevant correlation between alongshore surface currents and corresponding winds.

During winter season, two northerly wind events are observed on 3-5th March and between 23rd and 28th of the same month. Also two events of E-NE winds occurred at 13th and 30th march. In general, both surface and bottom currents shows highest velocities on alongshore components.

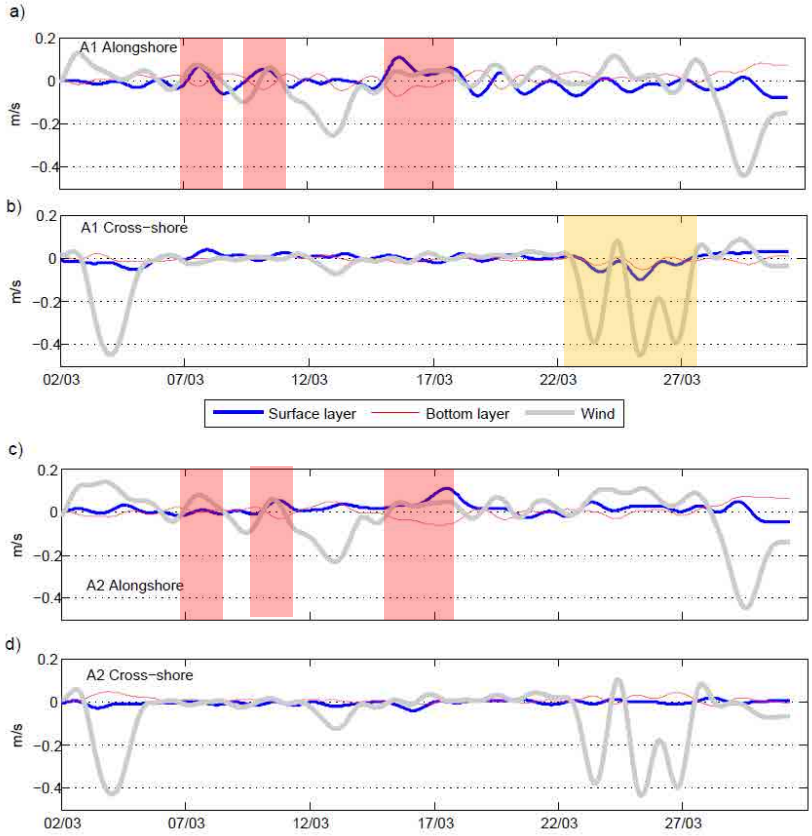

Figure 6.7. Winter A1 (a and b) and A2 (c and d) time series of Wind (x 0.03) and surface (blue) and bottom currents (red). Both wind and currents are plotted following the rotated axis: 21º and 42º anticlockwise for A2 and A1 respectively. Red shadowed areas indicates instants with qualitatively relevant correlation between alongshore surface currents and corresponding winds. Shadow orange areas for cross-shore relevant correlations.

At the beginning of March, two events of SW winds shows direct surface response on alongshore velocities. Between 15-17th march, light winds from SW (aligned with main axis of the bay) are positively correlated with surface currents. The most energetic events (northern winds) does not reveal a clear water response patterns at low frequencies on alongshore velocities. Only between 23-27th march both the surface and bottom layers shows a direct response on cross-shore components to the wind (yellow shadowed in Fig 6.7b). Using a threshold of 3 cm $\cdot$ s^{-1} (as considered for summer observations) the A2 exceeds this velocities 20% and 23% of the time at surface and bottom respectively. In the other hand, in A1 44% and 28% of the time surface layers exceeds 3 cm $\cdot$ s^{-1}. Moreover, 22% of cross-shore surface velocity also shows higher values. This speed threshold is similar to the observed standard deviation.

Comparison between currents at A1 and A2 only reveals correlation higher than 0.40 between alongshore components on surface layers (0.47 and 0.46 in summer and winter respectively).

Maximum correlation are observed in winter at bottom layers in alongshore component (0.60).

Considering the observed variability between surface and bottom layers, a useful tool to investigate the vertical structure of the water column and a possible correlation with different forcing is the Empirical Orthogonal Functions (hereafter, EOF) (Emery and Thomson 2004). Alongshore EOF analysis shows similar structures in all the cases. First component explains from 60% (u' A1 summer) to 72% (u' A1 winter) of the alongshore water column variability. These firsts modes reveals a clear two layer structure and are almost equal in all the cases (i.e. Fig 6.8a for u' EOF at A1). Second mode explains around 20-30% and also shows a two layered structure. The other modes are responsible for less than 6% of the variability. In general, the analysis of cross-shore components does not reveal a clear first mode (1st and second shows similar values around 30 and 40%), and also shows a two layered structure. However, there is an exception in $v'_{\text{-A1-w}}$ behavior, which reveals a barotropic response on the 1st mode accounting for 71% of the total variability (Fig 6.8b). During summer, the correlations between time evolution of the first mode for alongshore currents and winds is 0.64 and 0.57 for A1 and A2 respectively. During winter, correlations moves from 0.41 (A1) to 0.64 (A2). Correlation of first mode with currents shows maximum values at bottom layers.

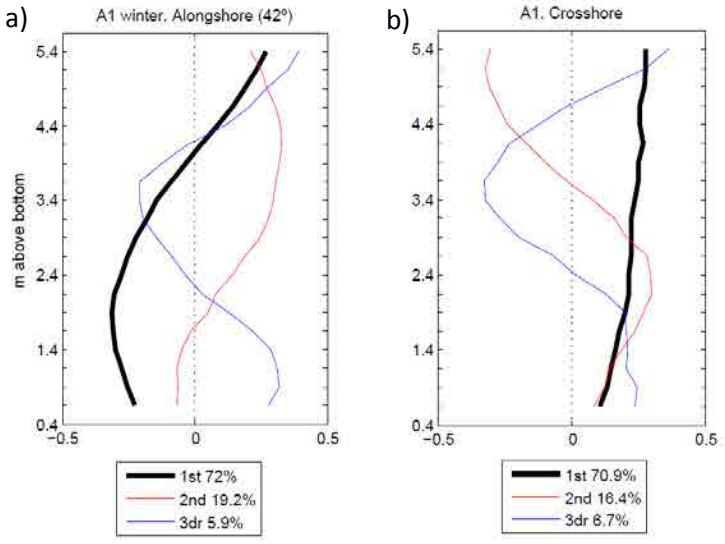

Figure 6.8. EOF analysis for low-frequency filtered data (Lanczos low pass band filter of 30h) during winter for A1 and both components, u' (left) and v' (right). Black lines shows first eigenvector, red and blue for second and third respectively. Legend shows the corresponding percentage of the explained variability for each mode of variability.

2.4 Averaged circulation

Since gravitational circulation typically occurs over long time scales, it is instructive to examine the averaged current at the moorings (Wong and Valle-Levinson, 2002). Averaged circulation for both A1 and A2 have been obtained time-averaging the observations corresponding to filtered u and v velocities for both entire observational periods (summer and winter). Results are summarized in Fig 6.9. A typical estuarine circulation is observed in A1 during both periods, with outflow at the surface and inflow at depth (Hansen and Rattray, 1965; Pritchard, 1952). During summer water currents reveals velocities around 4-5 $cm \cdot s^{-1}$ on surface layers and pointing to the SWº and 2 $cm \cdot s^{-1}$ to the NE at 2-3 meters above bed. During winter, currents are almost to the same direction but lower than $1cm \cdot s^{-1}$. At A2 the situation is completely different. During summer, surface velocities are very small (close to 0), but indicating direction E-NE while on the lower layers the flow is directed towards the W and around 1 $cm \cdot s^{-1}$. During winter a nearly depth-independent flow is observed at A2, flowing towards E-NEº. The corresponding standard deviations for each averaged current is shown in grey. In general, the variability is higher than the mean values, and only during summer in A1, surface currents shows mean values higher than the standard deviation.

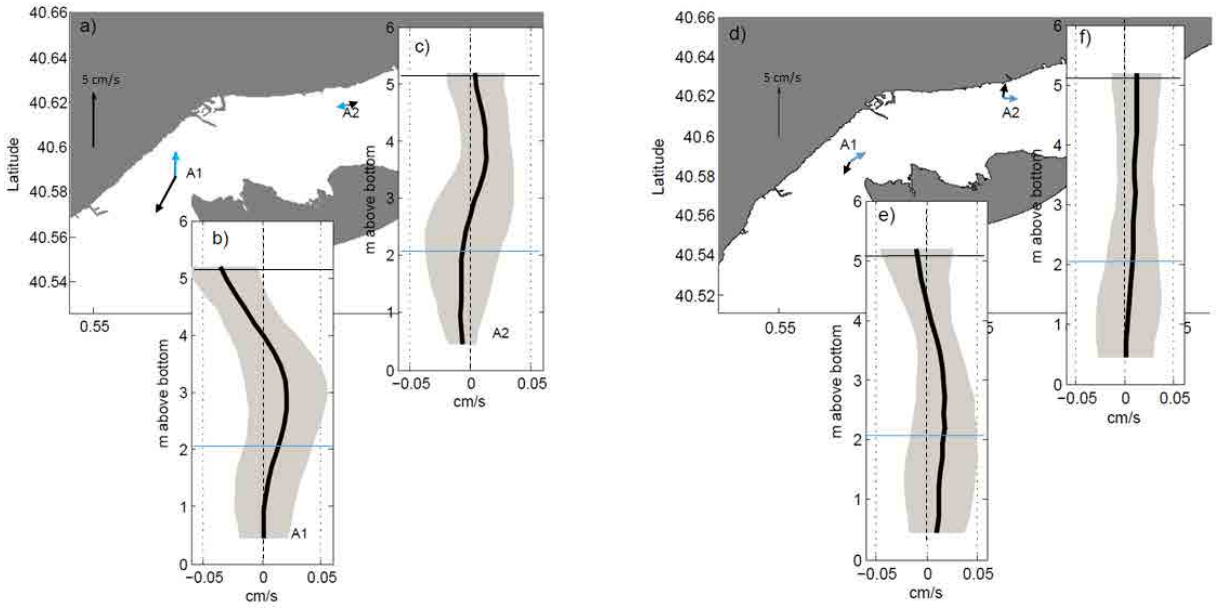

Figure 6.9. Residual circulation in A1 and A2 during summer (a) and winter (d) season at surface and bottom layers (black and blue respectively). The respective alongshore velocities along the water column are plotted in b and e for A1 and c and f for A2. The corresponding range (μ±σ) at each layer is shown in grey. The black and blue lines shows the surface and bottom layer used to plot averaged velocities in a and d images.

3. Discussion

Filtered data revealed a clear 2-layers structure, with 60 to 80% of the time showing opposite directions between surface and bottom layers. Previous investigations (chapters 3 and 4) concluded that unfiltered data shows one layer structure ≈70 % of the time, mostly related to seiches. In consequence, the removal of high-frequency oscillations implies the predominance of 2-layer vertical structure. Moreover, some additional data analysis using low pass band filter of 6h and 12h (not shown) revealed similar percentages than observed with 30h filters. This low frequency characterization is in agreement with previous studies from Llebot et al. (2013) who observed predominance of two layer structure on averaged circulation. Alfacs bay has been defined as a salt wedge estuary almost all the year (Camp and Delgado, 1987), with a noticeable influence of freshwater fluxes (Llebot et al., 2011; Solé et al., 2009) and heat fluxes during spring and summer (chapter 4). The surface heating and freshwater inputs stratifies the bay, promoting two layered structure on the water column, and influencing on the circulation patterns.

In A2, the main axis of the bay coincides with the axis of major variability in currents during both seasons and is almost equal at all depths: percentage of variability explained by the first axis is higher than 80% for the entire water column. However, A1 shows larger variability on cross-shore component during winter (mostly on surface layers), which is related to the wind influence. In fact, A1 is located 1.5 km from the coast, while A2 is closer (600m). As observed by Noble (1996) nearer the shoreline, strongly sheared boundary layer currents are predicted to flow parallel to the coast. Thus a clear transference from cross-shore winds in both locations to the alongshore currents is evident, being higher in A2. A similar example of strong influence of layout on water circulation is described in Grifoll et al. (2012).

The EOF analysis of unfiltered data presented on chapter 4 revealed a clear barotropic first mode on the alongshore component for all locations and periods, which was related to the seiches (for both fundamental and first seiche modes). Contrarily, low frequency EOF analysis shows an evident baroclinic behavior of the water column response in both places, with the first mode explaining percentages of variability around 60-70% in all the cases. These results are similar with Llebot et al. (2010), even in that case they suggest that the first baroclinic mode (obtained using weekly time-scale analysis) was related exclusively to the estuarine circulation instead to wind forcing. In our case, the time variability of the first mode positively correlates with wind in all periods and locations, linking the main water column variability mode to winds. In that sense, the analysis of time-evolution of each mode is useful in order to determine possible relations between physical forcing and the variability

described by the EOFs (Salas-Monreal and Valle-Levinson, 2008; Schaeffer et al., 2011), even it is well known that the results of EOF analysis may have non-physical meaning (Huang et al. 1998; https://climatedataguide.ucar.edu). So, although it is tempting to compare the EOF results with physical parameters, it must be done with some caution. Furthermore, barotropic behavior is only observed in cross-shore component at A1 during winter. In this case, water response coincides with most energetic N-NW winds direction, which would induce a depth-independent current response in that direction (equal in all water column).

Qualitative comparison between filtered winds and surface currents indicates noticeable correlation in alongshore component in both places during summer. Nevertheless, during winter, the effects of winds in alongshore surface currents are lower, and only remarkable hydrodynamic response is observed in the cross-shore component of A1 during the most intense northwester wind. The most striking aspect using linear correlation statistics is that the low frequency response shows the highest correlations between winds and bottom currents. Different reasons could be responsible of this hydrodynamic response. On one hand, stratification of the bay modifies the response to wind forcing on water column. Surface layers are directly affected by wind, while bottom layers would respond to the pressure gradient established along the bay due to the wind set-up, as observed in a shallow stratified system by Noble (1996). So, even the origin is the same (i.e. wind forcing), the current-driven mechanism is different. Surface currents observations are restricted to the 1m layer below free-surface (more details on chapter 2). Therefore, the oscillations on the pycnocline (close to the surface) may induce high variability in the water response related to surface winds and the depth of surface mixed layer. Contrarily, bottom layers are further from the effects of pycnocline oscillation, thus implying a more stable and consistent hydrodynamic response. Besides, the distance of the observational points to the coast suggest strong layout influence (higher in A2), which in turn implies some energy transferring from cross-shore winds to alongshore surface currents. Another option is related to the effects of remote forcing. Winds can induce low-frequency variability in estuaries through a combination of remote and local effects. For the remote effect, winds on the continental shelf adjacent to an estuary can produce sea level fluctuations at the estuary mouth (Wong and Valle-Levinson, 2002). For instance, variations on the coastal sea level due to the effects of winds (and atmospheric pressure variations) will induce incoming and outgoing flows to the bay. To this end, we compared the alongshore velocities to the sea level variations and the results shows correlations of 0.6 at bottom layers, and lower on the surface (-.23 to -.43) during winter season. On contrary, no correlation is found during summer period. These results insinuate the possible influence of shelf dynamics in the bay low frequency response, as observed in other environments (Gačić et al., 2004; Murphy and Valle-Levinson, 2008; Valle-Levinson et

al., 2001). However, more observations on the shelf and numerical experiments covering the Ebro delta region would be necessary to confirm these hypothesis.

One of the observed most energetic response at this time-scales during winter season does not correlate with wind or sea level variation. Between 14th and 17th March 2014 the strongest alongshore filtered currents were observed in both A1 and A2. Bottom layers were flowing towards the open sea and surface layers flow into the bay (Fig 6.10c and d). Winds during that days were weak (<2-3 $m \cdot s^{-1}$) and from SW-W, promoting ingoing surface velocities (following the main axis of Alfacs Bay). No seiches were observed, and sea level variations does not reveal any remarkable oscillation. Nevertheless, Ebro River Delta discharge values measured at Tortosa station shows one peak of freshwater discharge between 5th and 12th of March, with average values higher than 1000 $m^3 \cdot s^{-1}$ during the entire period (Fig 6.10b). Several authors have described that the river plume tends to flow southwestward due to its interaction with the mesoscale currents over the Ebro shelf (Font et al., 1990; Salat, 1995) and northerly winds (Mestres et al., 2003). Moreover, satellite observations (Fernández-Nóvoa et al., 2015) during north winds events have revealed how the plume flows southwards and attached to the coast. Considering that from 11th to 13th night, a NE winds were blowing, with mean intensities of around 5 $m \cdot s^{-1}$, the displacement of the river plume is expected to be close to the coast and to the south. When wind stops, a density gradient in front of the Alfacs bay (freshest water than inside the bay) would imply the development of an inverse estuarine circulation: bottom saltier waters from the inner bay would flow to the open sea, inducing a counter flow on the surface layers, with freshest water from the River plume flowing into the bay. This pattern is consistent with the current observations, starting the bottom currents in A1 around 24h before than in A2. Moreover, salinity observations in A2 (although effects of biofouling would have influenced on the absolute values) shows the diminishing of salinity at 2m at the same instant that waters from the bay mouth arrived. However, more data would be necessary to confirm the eventual river plume influence on Alfacs hydrodynamics and future studies must consider this topic.

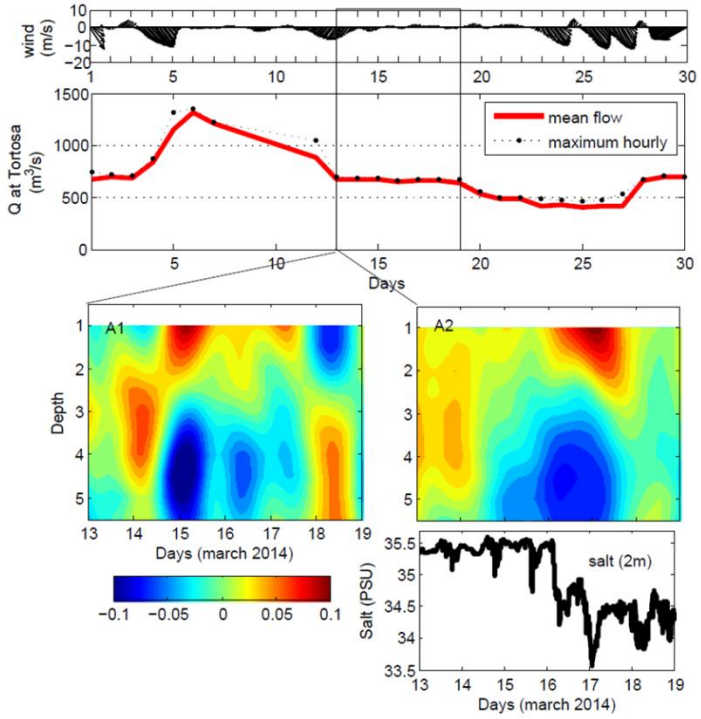

Figure 6.10. a) winds measured at M-A from 1 to 30 march 2014. b) Mean river flow measured at Tortosa station (source: *Confederacion Hidrografica del Ebro*). Images c) and d) shows the subtidal alongshore velocities observed at A1 and A2 between 13 and 19th March. Positive flows (yellow to red) indicating direction towards the Bay's Head, and negative to the open sea. Image e) shows salinity measured at 2m depth in A2 during same period (original data, no filtered).

From the longest time-scale point of view, the average circulation shows remarkable differences in long-term water response at A1 and A2 (Fig 6.9). The theoretical gravitational circulation due to freshwater influences on the bay would be represented by surface velocities to the West at A2 and South-West at A1. Only observations in A1 coincides with the expected estuarine circulation. Moreover, considering some basic statistics like standard deviation (Fig 6.9), only in A1 and during summer (and especially at surface), the averaged currents are higher than the standard deviation, thus indicating the predominance of an averaged pattern at this frequency band. Depth-averaged density fields observed during 7th May 2014 (I-5 campaign) are shown in Fig 6.11. Two density distribution patterns are observable: 1) in the along-shore direction, from saltier water in the open sea to freshest in the inner bay (1027 to 1022 $kg \cdot m^{-3}$); and 2) a cross-shore gradient on the inner bay, with freshest water on the northern margin. Moreover, the freshest water on the north is concentrated around A2, close to the main drainage channels. Considering that this density field is representative for density fields during open channel season -similar to observed during summer 2012 and summer 2013, as well as different scenarios described in Camp (1994) and Llebot et al. (2013)-, it seems reasonable to conclude that averaged circulation in A1 is explained by the density distributions and differences between in and out the bay (considering all freshwater sources on the inner bay), as well as the narrow of the bay, which would increase the velocities on the proximities.

Contrarily, A2 is located in the middle of the bay and close to drainage channels. In that sense, dividing the bay in two areas from a cross-sectional axis at A2, freshwater inputs are distributed on both sides, diminishing (even cancelling) the possible gravitational circulation along the main axis on A2. Then, the average circulation on the along shore direction in this point would be more influenced by other factors such winds.

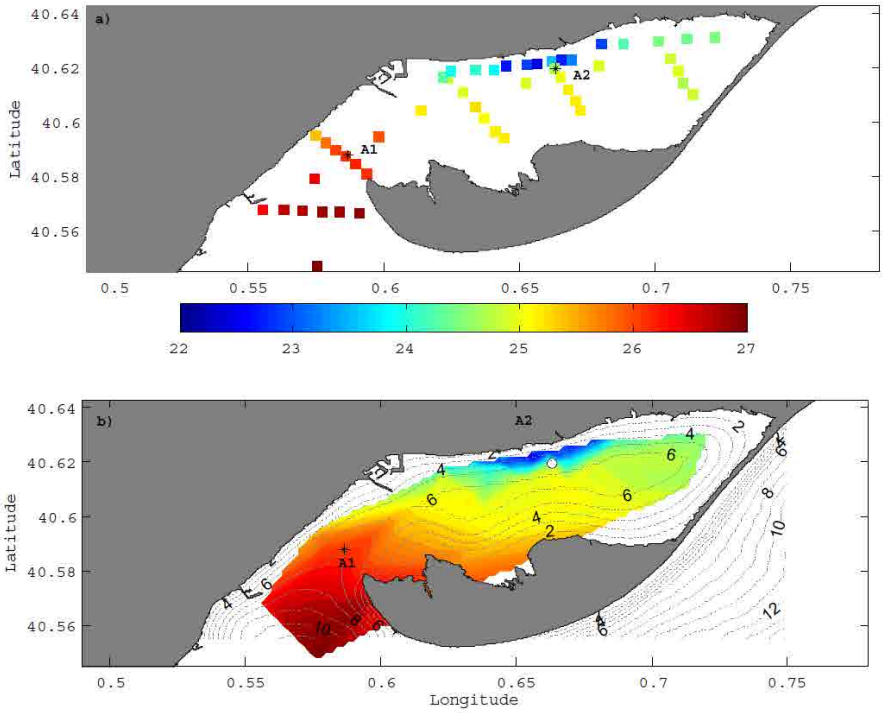

Figure 6.11. Top image shows the depth-averaged water densities from the CTD observations during field campaign at 7th May 2014. Black crosses shows A1 and A2 locations. Image b shows interpolated depth-averaged density field from CTDs, with contours each 0.02 kg · m^{-3}. Isobaths at 1m intervals are plotted in dashed grey lines.

In order to explore the spatial variability of the averaged circulation, results from numerical model are presented on Fig 6.12. The model configuration and validation is described in detail in chapter 2. Modelled averaged salinity and temperature fields (Fig 6.12 images a to d) revealed similar structures described by observations. For example, model surface 2D salinity fields are very similar with the density structures observed in May 2014 (Fig 6.11b and Fig 6.12a). Moreover, modeled salinity during close channels season (Fig 6.12a) revealed similar structure than observed and described in chapter 2 and 4 (Figures 2.4 and 4.3), and previously described by Camp (1994), with density gradients along the bay and well mixed water column (not shown). Averaged surface currents (Fig 6.12e) shows the maximum velocities located close to the bay mouth. On the other hand, modelled velocities in A2 are much weaker than in A1, agreeing with observational data, although the directions does not

perfectly match as well as the vertical velocity distribution. As stated before, this location (A2) is more sensitive to the freshwater inputs, which would determine the density driven circulation.

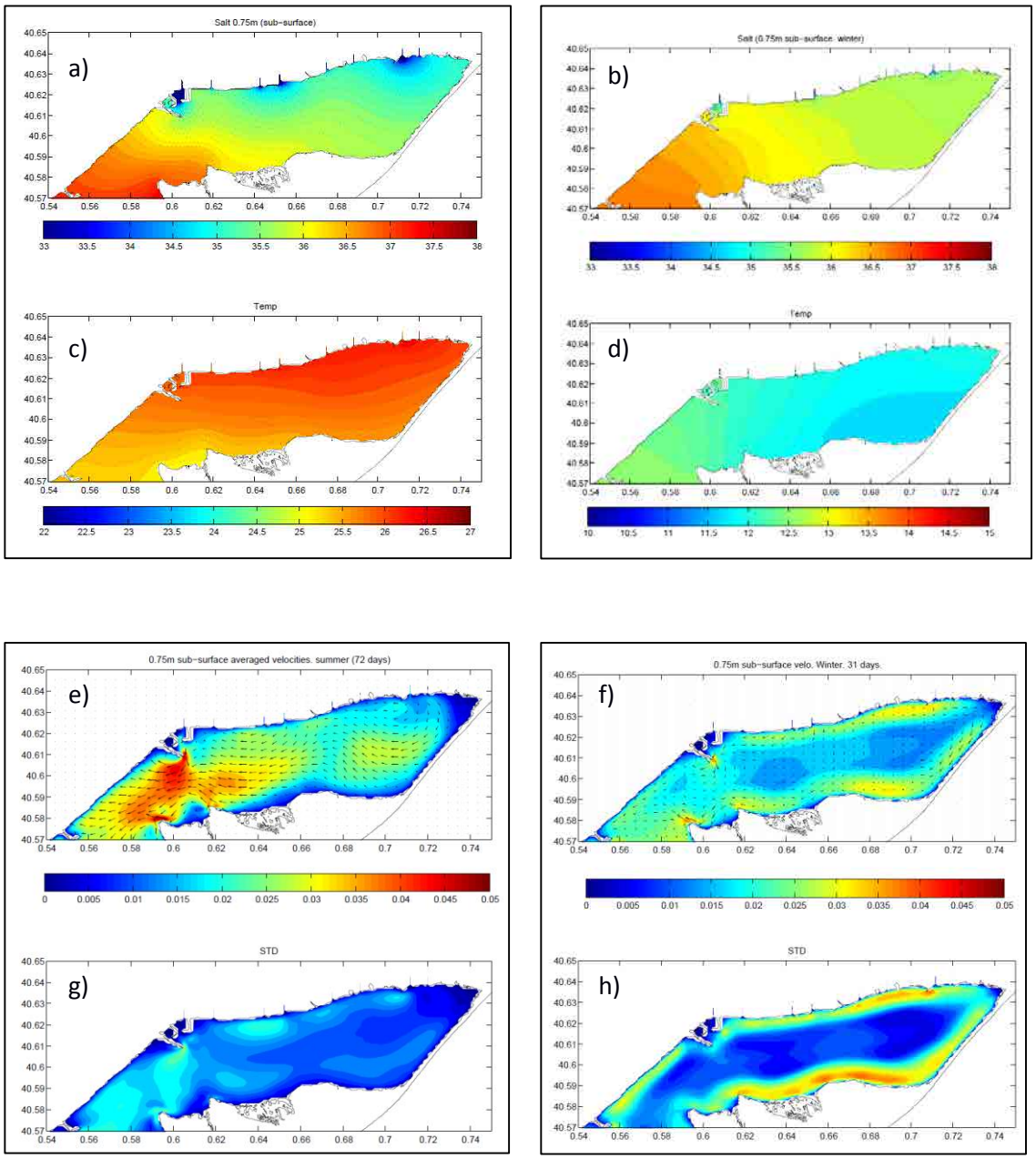

Figure 6.12. Left images for summer simulation (July-September 2013) results, and right images for winter simulation. Images a and b for averaged salinity at 0.75m below surface, c and d same but for water temperature. Images e and f shows averaged daily currents at 0.75m below surface during summer and winter simulations. The corresponding standard deviation is shown in images g and h.

Numerical results show how the average circulation on surface layers has two different behaviors inside the bay. Inner area (from A2 to the bay's head) reveals a surface flow following the isobaths with an anti-cyclonic gyre. On the other hand, from A2 to the open sea, the main surface currents are directed to the outer bay, similar to the classical estuarine

circulation Results for winter simulation (Fig 6.12f) reveals lower velocities all along the bay, and maximum averaged velocities are found over the margins (on the shallower areas). Moreover, two different structures are visible: being the most clear an anticyclonic gyre on the inner bay (close to the head), which clearly separates the average circulation from the region close to the bay mouth.

These patterns suggests an independent behavior for the two bay volumes, which would imply differences on residences time along the bay in low frequency scales. Further studies should consider the effects of these density induced circulation on the water flows through the bay (as shown in similar emplacements like Venice Lagoon by Cucco and Umgiesser (2006). The prevalence of the mean flow or the fluctuations are investigated comparing the mean (μ) and the standard deviation (σ). This is shown in Fig 6.12g and 6.12h. During summer, σ are small and mainly located on the bay mouth and over the northern margins (close to A2). During winter, σ is much higher but concentrated on the margins (shallower areas). A graphical comparison between μ and corresponding σ is shown in Fig 6.13 through signal-to-noise ratio ($SNR = \mu / \sigma$). Summer results revealed how during that period the average behavior of the bay seems to predominate at this time scales (low frequency, with cut-off time of 30h) over the variability. This dominance is clearer on the bay mouth, and probably directly correlated with the gravitational circulation. During winter, the predominance of an averaged circulation is not as much evident like it was during summer, and the variability predominates over the mean behavior on the shallower areas.

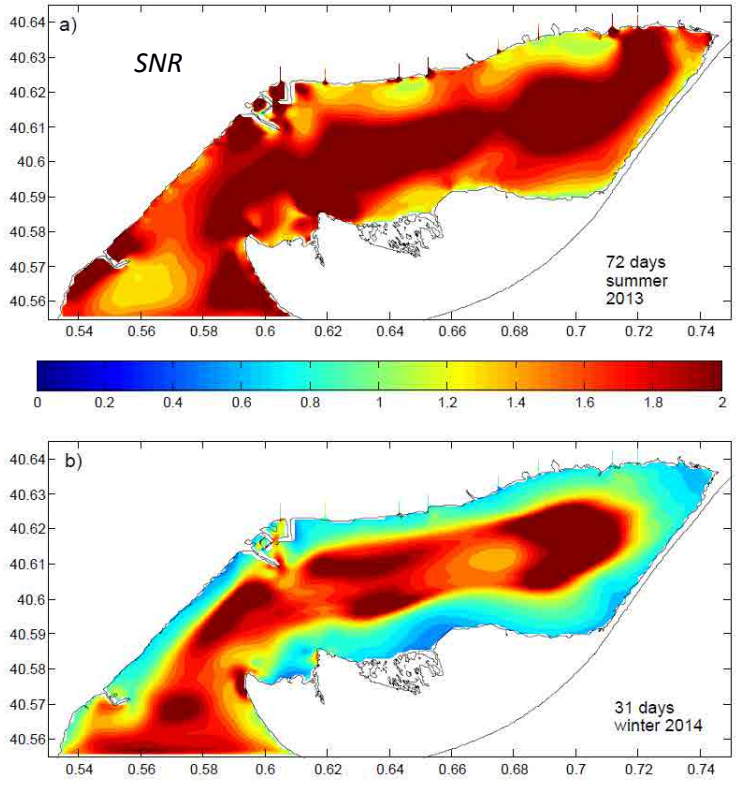

Figure 6.13. SNR Modelling results for averaged surface currents (0.75m below surface) and standard deviation. Values higher than 1 indicates average currents higher than standard deviation. Image a) for summer period, and b) for winter period.

4. Conclusions

The analysis of the water column variability comparing surface and bottom currents as well as the variability modes (EOF analysis) revealed a clear 2-layer response. Qualitatively speaking, there is a strong positive relation between surface currents and winds along the main axis of the bay during summer period, while negative correlation is observed on bottom layers. During winter, the most noticeable dependence on hydrodynamic response to winds is observed on cross-shore component in the bay mouth, showing one-layer flow. Moreover, during winter a noticeable correlation coefficients are found between alongshore winds and bottom alongshore currents (negative values), indicating that the near-bottom currents bay response at wind set-up.

At much longer time-scales, averaged circulation reveals estuarine circulation in the bay mouth, being only noticeable during summer period. On the inner bay (A2), and close to the drainage channels, no clear averaged circulation is observed, and the variability from wind influence is more evident. Using observations it is demonstrated how the density structure within the bay could be responsible for this behavior. Modelling results supports observational analysis allowing an assessment of the spatial distribution of the averaged circulation. Re-circulation areas on the inner bay suggests the importance of further studies in order to understand the spatial variability on residence time at the described time-scales.

Finally, both wind and gravitational induced circulation are evident at low frequency band. Although the prevalence of estuarine circulation during summer, episodic on-shore winds alters this pattern (i.e. reversals in the estuarine circulation due to sea breezes). Discern the importance of each of these factors implies additional measurements and numerical efforts.

7

General Discussion and Final Conclusions

Science never solves a problem without creating ten more.

George Bernard Shaw

A person who never made a mistake never tried anything new.

Albert Einstein

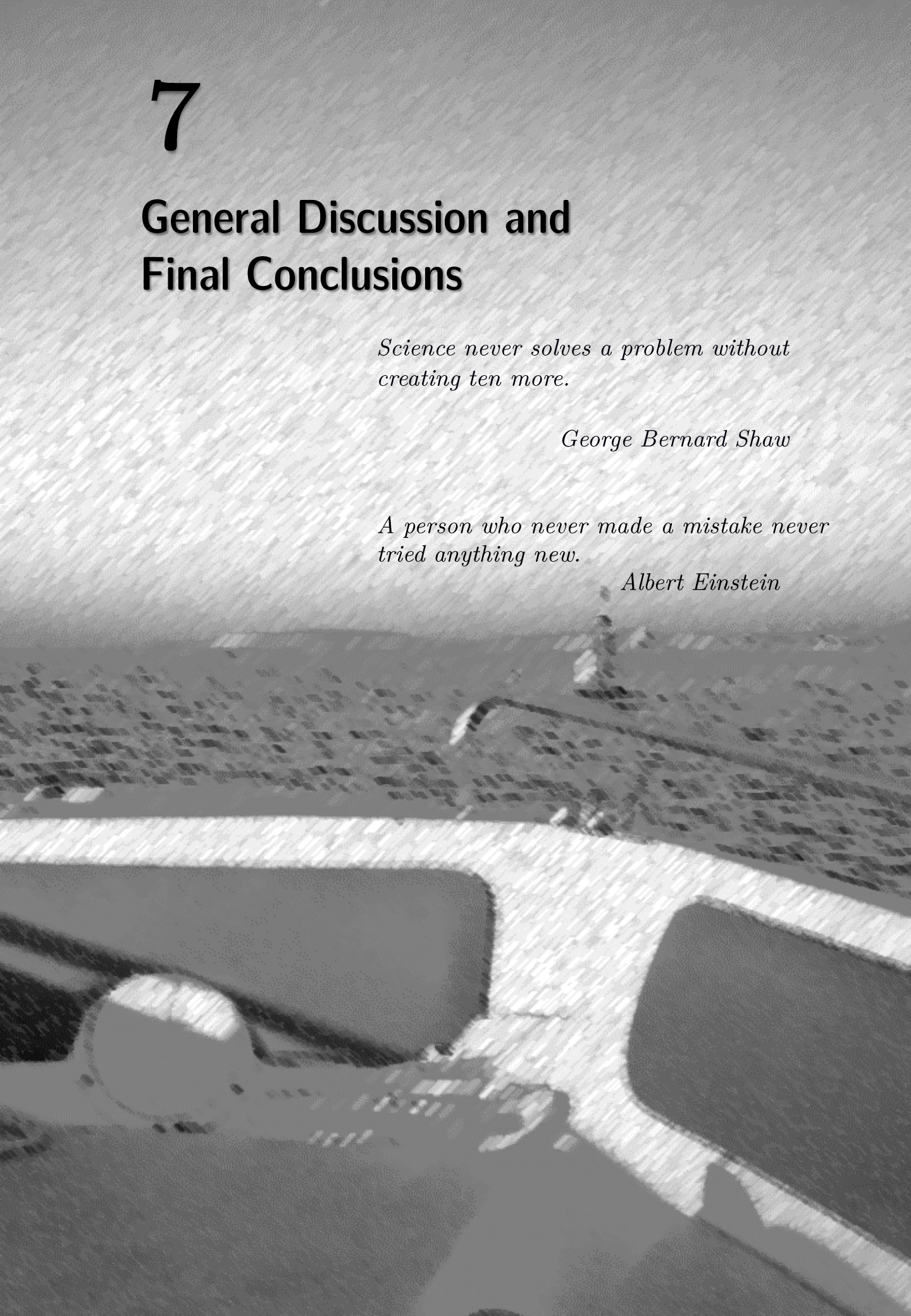

1. General Discussion

The main objective of this thesis is to gain knowledge on the hydrodynamic behaviour of a microtidal and shallow (≈4m) bay in the Mediterranean Sea: Alfacs Bay. Although several previous studies have identified some the main characteristics of the hydrodynamic behaviour, few of them still not been described by previous contributions. In consequence, the chapters included in the thesis pointed out different aspects still not solved. The results discussed all along the document are exportable to future studies and researches on similar estuarine environments, although considering the particularities of each of them.

Firstly, in chapter 3 the main tidal components in Alfacs Bay are described using a 15-year harmonic analysis of sea level in Sant Carles de la Rapita harbor, showing amplitudes ranging from 5 to 10 cm for neap and spring tides. Residual sea level is clearly affected by atmospheric and wind variations at similar and longer scales than the fortnightly. Moreover, it is demonstrated how the residual dominates the sea level variations at periods lower than 3-4h. These oscillations are related to the quarter wave-length relationship, and defined as seiches. Previous authors had observed them through sea level or current measurements (Camp, 1994; DePedro, 2007; Llebot, 2010; Llebot, 2013), but none of them have characterized the spatial characteristics of these seiches in Alfacs Bay and their role on the bay hydrodynamics. This has been possible to achieve due to the deployment of more than three simultaneous sea level measurement systems and current-meters, as well as the utilization of modelling tools. Thereafter, the influence of the seiches on water currents and mixing is described in chapter 4. Moreover, the sample frequency of the measurement systems -10 minutes- enable the description of a similar resonance but at periods of around 1h. This oscillation has been defined as 1st mode of Alfacs Bay co-oscillation, and it is related to the highest currents observed inside the Bay (depth averaged values close to 60 cm $\cdot$ s^{-1}). The resonance phenomena might be related to wind forcing, astronomic tides and atmospheric pressure variability. Therefore, future research must seek to determine its origin in Alfacs Bay and fill this gap. On the other hand, a set of numerical tests in Alfacs Bay have revealed that the main factor controlling the tidal propagation is the shape of the bay: nearly rectangular, with a change of orientation and not influenced by a river mouth at the head. The tidal wave is not damped enough to lose its energy, allowing partial reflection at the head. Therefore, Alfacs Bay could be considered to have standing wave behaviour. This is clearly observed with the permanent presence of a resonant wave. In consequence, bottom frictional effects on tidal propagation in Alfacs Bay is suggested to be irrelevant.

The effects of seiches on the water currents response is assessed on chapter 4. Wavelet analysis results has revealed the permanent presence of these oscillations in Alfacs Bay, as well as the periods in which they show the highest sea level variations and corresponding current intensities. The 1-h seiches are also identified through this analysis, showing also its persistence, and how during some periods become the most energetic periodicity in the bay. The study of the vertical column variability through the Empirical Orthogonal functions (EOF) revealed the one-layer motion of the seiches. Moreover, this analysis have shown how this oscillations are responsible of more than 70% of the alongshore variability. Additionally, the importance of the standing waves on water fluxes through the bay mouth is determined by seiche-excursion lengths of around 1.5 km for the fundamental mode (in 1.5h) and 0.5 km for the first mode (in 30min). For the fundamental mode, and considering the spatial distribution of currents seems clear how the seiche could be an important mechanism influencing the water renewal times at the bay mouth. Specific research through numerical model tools is suggested to gain knowledge in water renewal and its influence on ecological parameters of the bay. On the other hand, the role of these seiches on water column mixing is also studied in chapter 4 through dimensional approximation (Richardson number), equation of potential energy and numerical modelling. The results indicates the second order role of seiche mechanism in the mixing processes at long time scales, when the influence of freshwater and heat fluxes easily exceeds the turbulence induced by seiches. However, under special circumstances: when maximum seiche currents occurs and in the regions over the margins (2-3m water depth), it is demonstrated how the seiches could be an effective mixing factor. Moreover, on deeper areas (4-5m) and coinciding with maximum speed seiche location -the nodes, which coincides with areas with minimum sea level amplitudes- the interaction of seiche induced mixing (bottom friction) and wind stress could influence the water column stratification. As far as I know no previous studies in Alfacs Bay or similar domains have revealed the role of this standing waves on the water column mixing. Moreover, the high current speeds observed during these events must imply re-suspension of the sediments, nutrients and plankton from the bed. Taking into account the importance of water quality issues related to the apparition of HABS (Harmful Algal Blooms) and anoxia situations inside the bay, further studies on this field should be addressed.

The linkage between winds and currents are studied in chapters 4, 5 and 6. The role of the winds on the Alfacs Bay hydrodynamics probably is one of the most studied aspects by previous thesis and scientific reports (e.g. Camp and Delgado, 1987; Camp, 1994; De Pedro, 2007; Llebot et al., 2013). In that sense, all of them have investigated the hydrographic response of the bay (i.e. density field patterns) to different wind events. For instance, both Llebot (2010, 2013) and Camp (1994) emphasize the role of strong NW winds (Mestral), mixing the water column and changing the density pattern: stablishing horizontal instead of vertical gradients, and defining

the original bay state recovery few hours after the end of the wind event. In the chapter 4 it is demonstrated the role of winds in the water column mixing using the equation of potential energy and observations of water temperature inside the bay. This analysis confirms the freshwater influence as the main stratifying agent in the bay (as described by Sole et al. 2009), but also reveals the contribution of heat fluxes during spring and summer. During summer mean wind work is one order of magnitude lower than freshwater and heat fluxes. However, maximum daily values during windy events could contribute to mix the water column due to surface cooling and vertical shear. During winter-spring, the work done by winds in water column mixing is one order of magnitude higher than in summer, coinciding with small or negative heat contribution to stratification (winter) and the closing of drainage channels. This situation encourages a major occurrence of mixing events in Alfacs Bay, consistent with other winter observations (Camp and Delgado, 1987). During winter and spring, northerly wind events lasting for more than one day imply maximum values for this term on the potential equation much higher than the stratification terms, even considering the maximum freshwater effects, located on the proximities of the drainage channels.

The hydrodynamic response (currents) to wind forcing was stablished to be inexistent by DePedro, 2007 (correlation between winds and currents <0.2). His measurements consisted in a current meter at 4.5m in the bay entrance and meteorological data from Amposta. Only under special circumstances (NE event) he observed clear influence of wind effects on water circulation, with a reinforcing of the estuarine circulation. On the other hand, Llebot (2010, 2013) identified the sea breezes (i.e. winds from S-SW) as an eventual mechanism for flow reversals on the estuarine circulation; in contrast winds from NE reinforced the estuarine circulation. Observations described in chapter 4 shows how the sea breeze influences the current response on both mouth and inner bay (reversing the typical estuarine circulation). Moreover, the influence of NW events on the currents reveals a one-layer response, probably influencing the column stratification.

One of the research lines identified by Camp (1994) was the possible existence of spatial wind variability inside the bay. In that sense, the chapter 5 describes the observed wind variability in different meteorological stations, indicating some differences in northern and sea breezes winds. The limitation of more observational points encouraged the usage of meteorological models (model outputs provided by MeteoCat). These models -with different kind of spatial resolution- revealed the influence of local and regional orography over the most energetic winds in the area (predominantly from NW). A typical spatial pattern indicates noticeable wind speed gradients from the bay head to the mouth (NE- SW). Furthermore, the analysis of these wind modeled results shows the requirement of enough spatial resolution for a proper modelling of

the bay. Then, the effects of these wind variability in the Alfacs Bay hydrodynamics is evaluated. Numerical simulations using spatially wind gradients versus homogeneous winds reveals noticeable differences on hydrodynamic structures. One of the most noteworthy hydrodynamic feature observed is an anti-cyclonic gyre close to the bay mouth. In order to understand the mechanism which leads to that patterns a set of idealized numerical tests were implemented in idealized shape domain -to minimize the effects of lateral roughness and non-linearity induced by irregular bathymetry and coastline-. The results indicate that the water circulation on the left side of wind gradient is characterized by a gyre. The responsible mechanism is the wind curl, establishing an eastward surface current on the northern region of the bay with calm winds, and westward flows on the southern regions. No remarkable bathymetric effects are observed. Simulation of 6 days-long period during winter (with predominance of NW winds) shows the importance of considering or not the wind variability on water exchange times, with variations under these circumstances around 20%. These results demonstrates how at small length scales (order of few km) the spatial wind variability could be an important factor to consider. In this sense, the effects of wind variability over the water exchange time influence the grade of the water flushing, which undoubtedly, in turn controls relevant issues of the ecological behavior the bay. For instance, in Alfacs Bay, the water flushing influences the ecological behavior of the system determining the development of Harmful Algal Blooms, the mollusks farms productions and fisheries. Further investigations linking the variability of the water exchange and the ecological evolution will benefit the sustainable management of the bay. The wind variability characterization has been done considering few observational points, and future studies must try to contrast our results using more observational points. Recently, new opportunities are emerging from citizen science, in which a correct design of a participative campaign involving people of the region and new technologies would allow a better wind spatial variability description. On the other hand, several numerical experiments with the atmospheric models could be used to better understand the sensitivity of the wind in the Alfacs Bay to the local and regional topography (i.e. removing the topography in different tests).

While the hydrodynamic behavior of the bay revealed a predominant one-layer structure strongly determined by seiches masking the wind effects, the analysis of low frequency response performed in chapter 6 exposes the predominance of two layer water column structure at this time scale. Besides, the influence of winds on water circulation become relevant on alongshore currents during summer conditions. Surface layers directly move with winds, while bottom layers flows on contrary direction mostly driven by the barotropic pressure gradient stablished by the corresponding wind set-up. The almost permanent summer stratification enhances these response. During winter, the main hydrodynamic response is observed on cross-shore currents

but in this case with barotropic (one layer) motion, clearly affected by the most energetic winds coming from NW-NE. In that period, the direct response to winds at alongshore surface currents is minimum. At lowest time-band frequency (averaged circulation), both summer and winter periods reveal noticeable seasonal differences. During summer the effects of gravitational circulation dominates the average currents, while in winter the low (or null) freshwater inputs and much intense wind events does not allow to define a clear average circulation (higher variability).

Confirming the famous quote of George Bernard Shaw: "*Science never solves a problem without creating ten more*", a few more questions or possible future works have appeared from this thesis (some of them have already been described in previous paragraphs). For example, an update of the bathymetric data (more contemporary) is necessary. Like explained for wind variability, the citizen science could be a useful option: for example, obtaining the data recorded from the echo sounders of the different boats (tourism and fisheries) that usually navigates in the bay. Because the freshwater inputs in the bay are the main factor controlling the stratification and influencing the gravitational circulation, a correct freshwater input information would determine the numerical model results (not only salinity fields, but also stratification and then the hydrodynamic response). In this sense, the lack of the correct characterization of freshwater inputs during closed channels season does not allow the proper understanding and modelling of hydrodynamic and hydrographic structures during that period. Furthermore, the modelling results revealed a noticeable variability on the cross-sectional structure of the water currents along the bay mouth (also observed in temperature and salinity variability from CTD profiles). Current measurements on the bay mouth trying to characterize this variability could imply a significant new information. Another interesting point is to investigate the possible influence of Ebro shelf water circulation on the inner bay and the bay effects on the water shelf circulation (i.e. density variations on the shelf waters). The possible breakage of Trabucador barrier and the effects on water density structure and currents could be also studied using numerical tools presented in this thesis.

2. Final Conclusions

According to the objectives of this thesis, the conclusions are:

1. *To investigate the tidal propagation within the bay and the 3h periodicity (seiches).*

   1.1. Residual sea level is dominated by high frequency variations at periods lower than 3-4h. These are related to fundamental and first mode of resonance.

   1.2. Astronomic tides are controlled by the shape of the bay. Frictional effects are negligible. The tidal wave is not damped enough to lose its energy, thus allowing partial reflection at the head.

2. *To investigate the hydrodynamic/ hydrographic response to the most energetic events (high frequency processes)*

   a. *Response to winds*

      2a.1. Direct water current response under some circumstances is found, specially under sea breeze conditions. However, due to seiche effects and the importance of frictional terms, this direct response is not observed all the time.

      2a.2. The influence of winds on water column stratification is demonstrated through the potential equation, revealing higher contribution during winter-spring season.

   b. *Response to seiches*

      2b.1. Currents related to seiches dominates high frequency processes in some areas of the bay and especially during extreme seiche events.

      2b.2. Influence on water column mixing under some circumstances (shallow areas coinciding with maximum velocity regions) is demonstrated.

3. *To characterize the wind spatial variability and its influence on the hydrodynamic patterns.*

   3.1. Wind spatial variability in the bay is demonstrated to be relevant.

   3.2. The effects on water circulation are studied through numerical model revealing noticeable sensitivity. Most noteworthy hydrodynamic pattern is the formation of an anti-cyclonic gyre on the bay mouth related to the wind vorticity. This structure implies variation on water flows and water renewal times.

4. *To define the hydrodynamic response at low-frequency time-scales*:

   4.1. Two layer water column response influenced by both stratification and winds is observed at low frequency time-scale.

   4.2. Alongshore surface currents response to winds during summer, while no direct response is observed in winter.

   4.3 Winter is characterized by cross-shore intense winds and the major response is observed on the entire water column in the bay mouth (one-layer response).

   4.4. At both seasons, alongshore near bottom currents are directly influenced by wind through barotropic pressure gradient, moving on the contrary direction.

   4.3. Average currents shows typical estuarine pattern on the bay mouth, while in the inner bay, the influence of widespread freshwater input, wind influence and proximity of observation point to the coastline does not allow to observe the expected circulation.

3. Final thoughts

As a last point, I want to express a few personal opinions and considerations that have emerged from this thesis.

It can be certainly asserted that Alfacs Bay is one of the most studied coastal areas in the region. This is mainly due to the relative small dimensions, shallow depths, influence of freshwater inputs, economical uses and the proximity of an investigation center (IRTA). However, during all the meetings with scientific and technical staff from various universities and institutions (IRTA, CSIC, UB and UPC) I have been witness to the (in general) small cooperation and lack of scientific and observational data discussion and sharing (mainly due to the lack of time of the main investigators). In that sense, I think that a special kind of committee must be formed to group all the universities and research groups with interests in Alfacs Bay that would facilitate the performance of future investigations (as an example, http://www.chesapeake.org/), enhancing the interchange of knowledge from different areas of interest, and avoiding the repetition of similar researches. I strongly believe that Alfacs Bay is a perfect place to develop this kind of scientific project.

Moreover, the apparition in the recent times of the citizen science concept (http://www.citizensciencealliance.org/, http://scistarter.com/) opens a wide variety of possibilities in the scientific research, involving the local communities of the area. In that sense, I hope that the illusion and leadership of Dr. Jaume Piera (ICM) and his group would turn into future research projects.

Finally, I want to emphasize that with this thesis there are nowadays, as far as I know, two different hydrodynamic models applied, calibrated and validated with observational data in Alfacs Bay (the other one was presented by Llebot, 2010 and Llebot et al. 2013). Despite its shortcomings, the set-up of this kind of models requires a large amount of time and money in order to obtain the corresponding observational data to validate the main results and time to understand the main dynamics of the bay. For this reason, I hope that future studies could take profit of these works and lead their research on improving some of the aspects that still not completely well solved such as: the modeled water column stratification or coupling the hydrodynamic model with biogeochemical, sediment and oil spill models.

Bibliography

Agterberg, R., Wieringa, J. 1989. Mesoscale terrain roughness mapping of the Netherlands. In: Royal Netherlands Meteorological Institute (Ed.), Technical Report TR-115.

Alekseenko, E., Roux, B., Sukhinov, a., Kotarba, R., and Fougere, D. 2013. Nonlinear hydrodynamics in a Mediterranean lagoon. Nonlinear Processes in Geophysics, 20(2), 189–198. doi:10.5194/npg-20-189-2013

Allen, R., L.S. Pereira, D. Raes, and M. Smith. 1998. Crop evapotranspiration: Guidelines for computing crop requirements. Irrigation and Drainage Paper No. 56, FAO. doi:10.1016/j.eja.2010.12.001.

Alvarado-Aguilar, D., Jiménez, J. a., Nicholls, R.J., 2012. Flood hazard and damage assessment in the Ebro Delta (NW Mediterranean) to relative sea level rise. Nat. Hazards 62, 1301–1321. doi:10.1007/s11069-012-0149-x

Artigas, M.L., Llebot, C., Ross, O.N., Neszi, N.Z., Rodellas, V., Garcia-Orellana, J., Masqué, P., Piera, J., Estrada, M., Berdalet, E., 2014. Understanding the spatio-temporal variability of phytoplankton biomass distribution in a microtidal Mediterranean estuary. Deep Sea Res. Part II Top. Stud. Oceanogr. 101, 180–192. doi:10.1016/j.dsr2.2014.01.006

Atkinson, L. P., and J. O. Blanton. 1986. Processes that affect stratification in the shelf 504 waters, in Baroclinic Processes on Continental Shelves, Coastal Estuarine Sci., vol. 3, edited by C. 505 N. K. Mooers, pp. 117–130, AGU, Washington, D. C., doi:10.1029/CO003p0117

Batalla, R.J., Gómez, C.M., Kondolf, G.M., 2004. Reservoir-induced hydrological changes in the Ebro River basin (NE Spain). J. Hydrol. 290, 117–136. doi:10.1016/j.jhydrol.2003.12.002

Benito, X., Trobajo, R., Ibáñez, C., 2015. Benthic diatoms in a Mediterranean delta: ecological indicators and a conductivity transfer function for paleoenvironmental studies. J. Paleolimnol. doi:10.1007/s10933-015-9845-3

Berdalet, E., Artigas, M.L., Llebot, C., Ross, O.N., Hoyer, A.B., Neszi, Z., Piera, J., Rueda, F., Estrada, M., 2014. Phytoplankton variability modulation by the hydrodynamic regime in Alfacs Bay (NW Mediterranean). A combined experimental and modelling study, in: 15th ICHA. pp. 2007–2010.

Biasio, F. De, Miglietta, M. M., Zecchetto, S., and della Valle, A. 2014. Numerical models sea surface wind compared to scatterometer observations for a single Bora event in the Adriatic Sea. Advances in Science and Research. 41–48. 2014. doi:10.5194/asr-11-41-2014

Bignami, F., R. Sciarra, S. Carniel, and R. Santoleri. 2007. Variability of Adriatic Sea coastal turbid waters from SeaWiFS imagery, Journal of Geophysical Research. 112, C03S10, doi:10.1029/2006JC003518

Boegman L. 2009. Currents in Stratified Water Bodies 2: Internal Waves. In: Gene E. Likens, (Editor) Encyclopedia of Inland Waters. Volume 1, pp. 539-558 Oxford: Elsevier.

Bolaños, R., G. Jorda, J. Cateura, J. Lopez, J. Puigdefabregas, J. Gomez, and M. Espino. 2009. The XIOM: 20 years of a regional coastal observatory in the Spanish Catalan coast. Journal of Marine Systems 77. Elsevier B.V.: 237–260. doi:10.1016/j.jmarsys.2007.12.018.

Boldrin, A., S. Carniel, M. Giani, M. Marini, F. Bernardi Aubry, A. Campanelli, F. Grilli, and A. Russo. Effects of bora wind on physical and biogeochemical properties of stratified waters in the northern Adriatic, Journal of Geophysical Research. 2009, 114, C08S92, doi:10.1029/2008JC004837

Bowers, D., and Lennon, G. 1990. Tidal Progression in a Near-Resonant System - A Case study from South Australia. Estuarine, Coastal and Shelf Science, 17-34. DOI: 10.1016/0272-7714(90)90074-2.

Brecht, B., and Frank, H. 2014. High resolution modelling of wind fields for optimization of empirical storm flood predictions. Advances in Science and Research 11: 1–6, 2014. doi:10.5194/asr-11-1-2014.

Browne, D.R., C.W. Fisher. 1988. Tide and tidal currents in the Chesapeake Bay. NOAA Technical Report NOS OMA 3, Rockville, MD, 84 pp. plus appendices

Cameron, W.M., Pritchard, D.W. 1963. Estuaries. In: Hill MN (ed) The sea, vol 2. Wiley Interscience, New York., pp 306–324

Camp, J. 1994. Aproximaciones a la dinamica estuarica de una bahia micromareal Mediterranea. Thesis. Universitat de Barcelona.

Camp, J., Delgado, M. 1987. Hidrografia de las bahías del delta del Ebro. Investig. Pesq. 51, 351–369.

Canicio, A., Ibañez, C. 1996. Evaluation of water fluxes and sediment supply, in: Impact of Climatic Change on Northwestern Mediterranean Deltas: p. ?

Canicio, A., Ibañez, C., 1999. The Holocene Evolution of the Ebre Delta Catalonia , Spain. Acta Geogr. Sin. 54.

Carter, G., and Merrifield, M. 2007. Open boundary conditions for regional tidal simulations. Ocean modelling, 18, 194-209. DOI: 10.1016/j.ocemod.2007.04.003

Cerralbo, P., Grifoll, M., Espino, M., López, J., 2012. Predictability of currents on a mesotidal estuary (Ria de Vigo, NW Iberia). Ocean Dyn. 63, 131–141. doi:10.1007/s10236-012-0586-9

Cerralbo, P., Grifoll, M., Valle-Levinson, A., Espino, M., 2014. Tidal transformation and resonance in a short, microtidal Mediterranean estuary (Alfacs Bay in Ebre delta). Estuar. Coast. Shelf Sci. 145, 57–68. doi:10.1016/j.ecss.2014.04.020

Cerralbo, P., Grifoll, M., Moré, J., Bravo, M., Afif, A.S., Espino, M., 2015. Wind variability in a coastal area (Alfacs Bay , Ebro River delta). Adv. Sci. Res. 12, 11–21. doi:10.5194/asr-12-11-2015

Cerralbo, P., Grifoll, M., Espino, M., 2015. Hydrodynamic response in a microtidal and shallow bay under energetic wind and seiche episodes. J. Mar. Syst. 149, 1–13. doi:10.1016/j.jmarsys.2015.04.003

Chavanne, C., Flament, P., Lumpkin, R., Dousset, B., and Bentamy, A. 2002. Scatterometer observations of wind variations induced by oceanic islands: Implications for wind-driven ocean circulation. Canadian Journal of Remote Sensing 28: 466–474. doi:10.5589/m02-047.

Costa, P., Gómez, B., Venâncio, A., Pérez, E., Pérez-Muñuzuri, V. 2012. Using the Regional Ocean Modelling System (ROMS) to improve the sea surface temperature predictions of the MERCATOR Ocean System. Sci. Mar. 76, 165–175. doi:10.3989/scimar.03614.19E

Council of Europe. 2005. Protection of European Deltas. Report Doc: 10542. Parliamentary assembly of the council of Europe. Documents and working papers. Strasbourg.

Csanady, G.T. 1973. Wind induced barotropic Motions in long lakes. Journal of Physical Oceanography 3: 429–438.

Csanady, G.T. 1982. Circulation in the Coastal Ocean. Reidel Publising Company. ISBN: 90-277-1400-2

Cucco, A., Umgiesser, G., 2006. Modeling the Venice Lagoon residence time. Ecol. Modell. 193, 34–51. doi:10.1016/j.ecolmodel.2005.07.043

Curcó, A., 2006. Aiguamolls litorals: el delta de l'ebre. L'Atzavara 55–72.

De Boer, G. J., J.D. Pietrzak, and J.C. Winterwerp. 2008. Using the potential energy anomaly equation to investigate tidal straining and advection of stratification in a region of freshwater influence. Ocean Modelling 22: 1–11. doi:10.1016/j.ocemod.2007.12.003.

De Jong, M.P.C., and J.A. Battjes. 2004. Seiche characteristics of Rotterdam Harbour. Coastal Engineering 51: 373–386. doi:10.1016/j.coastaleng.2004.04.002.

De Pedro, X., 2007. Situacions d'anòxia en zones estuàriques sense forçament mareal: una aproximació als balanços producció/consum oxigen. Thesis. Universitat de Barcelona.

deCastro, M, M Gómez-Gesteira, R Prego, and R Neves. 2003. Wind influence on water exchange between the ria of Ferrol (NW Spain) and the shelf. Estuarine, Coastal and Shelf Science 56: 1055–1064. doi:10.1016/S0272-7714(02)00302-5.

Delgado, M. 1989. Abundance and Distribution of Microphytobentjhos in the Bays of Ebro Delta (Spain). Estuar. Coast. Shelf Sci. 29, 183–194. doi:10.1016/0272-7714(89)90007-3

Delgado, M., Estrada, M., Camp, J., Fernandez, J. V., Santmarti, M., Lleti, C., 1990. Development of a toxic Alexandrium minutum (Dinophyceae) bloom in the harbour of Sant Carles de la Rapita (Ebro Delta, northwestern Mediterranean). Sci. Mar. 54, 1–7.

Delgado, M. 1998. Report of the monitoring of toxic phytoplankton in Catalonia, No. 1. CSIC and DARP, Barcelona

Dyer, K.R. 1991. Circulation and mixing in stratified estuaries. Marine Chemistry 32: 111–120. doi:10.1016/0304-4203(91)90031-Q.

Dyer, K.R. 1994. Estuarine sediment transport and deposition. In: Pye, K. (Ed.), Sediment Transport and Depositional Processes. Blackwell Scientific Publications, Oxford, pp. 193e218.

Dyer, K.R. 1997. Estuaries: A Physical Introduction (2nd edition). Chichester: John Wiley and Sons. ISBN 0-471-9741-4.

Elliott, M., McLusky, D.S. 2002. The need for definitions in understanding estuaries. Estuar. Coast. Shelf Sci. 55, 815–827. doi:10.1006/ecss.2002.1031

Emery, W. J., and R. E. Thomson, 2004: Data Analysis Methods in Physical Oceanography. 2nd ed. Elsevier, 638 pp

Espino, M., A.S Arcilla, and M A Garcıa. 1998. Wind-induced mesoscale circulation off the Ebro delta , NW Mediterranean : a numerical study. Journal of Marine Systems 16: 235–251.

Fernández-Nóvoa, D., Mendes, R., deCastro, M., Dias, J.M., Sánchez-Arcilla, a., Gómez-Gesteira, M., 2015. Analysis of the influence of river discharge and wind on the Ebro turbid plume using MODIS-Aqua and MODIS-Terra data. J. Mar. Syst. 142, 40–46. doi:10.1016/j.jmarsys.2014.09.009

Ferrarin, C., Umgiesser, G., Bajo, M., Bellafiore, D., De Pascalis, F., Ghezzo, M., Scroccaro, I. 2010. Hydraulic zonation of the lagoons of Marano and Grado, Italy. A modelling approach. Estuarine, Coastal and Shelf Science, 87(4), 561–572. doi:10.1016/j.ecss.2010.02.012

Ferrer, L., Fontán, a., Mader, J., Chust, G., González, M., Valencia, V., Uriarte, A., Collins, M.B., 2009. Low-salinity plumes in the oceanic region of the Basque Country. Cont. Shelf Res. 29, 970–984. doi:10.1016/j.csr.2008.12.014

Fischer, H.B., List, E.J., Koh, R.C.Y., Imberger, J., Brooks, N.H., 1979. Mixing in Inland and Coastal Waters. Academic Press Inc., New York, NY, 483 pp

Font, J., 1990. A comparison of seasonal winds with currents on the continental slope of the Catalan Sea (northwestern Mediterranean). J. Geophys. Res. 95, 1537. doi:10.1029/JC095iC02p01537

Font, J., Salat, J., Julià, A. 1990. Marine circulation along the Ebro continental margin. Mar. Geol. 95, 165–177. doi:10.1016/0025-3227(90)90114-Y

Friedrichs, C. T. 2010. Barotropic tides in channelized estuaries. In A. Valle-Levinson, Contemporary Issues in Estuarine physics (p. 327). Cambridge: Cambridge University press. ISBN: 9780521899673

Friedrichs, C. T., and D. G. Aubrey .1994. Tidal propagation in strongly convergent channels, J. Geophys. Res., 99(C2), 3321–3336. DOI: 10.1029/93JC03219

Gačić, M., Mancero Mosquera, I., Kovačević, V., Mazzoldi, A., Cardin, V., Arena, F., Gelsi, G., 2004. Temporal variations of water flow between the Venetian lagoon and the open sea. J. Mar. Syst. 51, 33–47. doi:10.1016/j.jmarsys.2004.05.025

Galimany, E., Ramón, M., Ibarrola, I., 2011. Feeding behavior of the mussel Mytilus galloprovincialis (L.) in a Mediterranean estuary: A field study. Aquaculture 314, 236–243. doi:10.1016/j.aquaculture.2011.01.035

Ganju, N.K., Hayn, M., Chen, S.-N., Howarth, R.W., Dickhudt, P.J., Aretxabaleta, A.L., Marino, R., 2012. Tidal and Groundwater Fluxes to a Shallow, Microtidal Estuary: Constraining Inputs through Field Observations and Hydrodynamic Modeling. Estuaries and Coasts 35, 1285–1298. doi:10.1007/s12237-012-9515-x

Garcés, E., Delgado, M., Masó, M., Camp, J., 1999. In situ growth rate and distribution of the ichthyotoxic dinoflagellate Gyrodinium corsicum Paulmier in an estuarine embayment (Alfacs Bay, NW Mediterranean Sea). J. Plankton Res. 21, 1977–1991.

Garrett, C., 1972. Tidal resonance in the Bay of Fundy and Gulf of Maine. Nature 238, 441–443. DOI: 10.1038/238441a0

Geyer, W. R. 1993. Three-dimensional tidal flow around headlands, J. Geophys. Res., 98(C1), 955–966. DOI: 10.1029/92JC02270

Geyer, W.R., 1997. Influence of Wind on Dynamics and Flushing of Shallow Estuaries. Estuar. Coast. Shelf Sci. 44, 713–722. doi:10.1006/ecss.1996.0140

Cheng, P., Valle-Levinson, A., Winant, C.D., Ponte, A.L.S., de Velasco, G.G., Winters, K.B., 2010. Upwelling-enhanced seasonal stratification in a semiarid bay. Cont. Shelf Res. 30, 1241–1249. doi:10.1016/j.csr.2010.03.015

Gracia, V., García, M., Grifoll, M. and Sánchez Arcilla, A. 2013. Breaching of a barrier under extreme events. The role of morphodynamic simulations, Journal of Coastal Research 951–956. doi:10.2112/SI65-161.1.

Grifoll, M., Jordà, G., Borja, A., Espino, M., 2010. A new risk assessment method for water quality degradation in harbour domains, using hydrodynamic models. Mar. Pollut. Bull. 60, 69–78. doi:10.1016/j.marpolbul.2009.08.030

Grifoll, M., Del Campo, A., Espino, M., Mader, J., González, M., Borja, Á., 2011. Water renewal and risk assessment of water pollution in semi-enclosed domains: Application to Bilbao Harbour (Bay of Biscay). J. Mar. Syst. doi:10.1016/j.jmarsys.2011.07.010

Grifoll, M., Jordà, G., Espino, M., Romo, J., García-Sotillo, M., 2011. A management system for accidental water pollution risk in a harbour: The Barcelona case study. J. Mar. Syst. 88, 60–73. doi:10.1016/j.jmarsys.2011.02.014

Grifoll, M., Jordà, G., Sotillo, M.G., Ferrer, L., Espino, M., Sánchez-Arcilla, A., Álvarez-Fanjul, E., 2012. Water circulation forecasting in Spanish harbours. Sci. Mar. 76, 45–61. doi:10.3989/scimar.03606.18B

Grifoll, M., Aretxabaleta, A.L., Pelegrí, J.L., Espino, M., Warner, J.C., Sánchez-Arcilla, A., 2013. Seasonal circulation over the Catalan inner-shelf (northwest Mediterranean Sea). J. Geophys. Res. Ocean. 118, 5844–5857. doi:10.1002/jgrc.20403

Guillén, J., and Díaz, J. 1990. Elementos morfológicos en la zona litoral: ejemplos en el delta del Ebro. Scientia Marina, 54, 359-373.

Guillén, J., and Palanques, A. 1997. A historical perspective of the morphological evolution in the lower Ebro river. Environ. Geol. 30, 174–180. doi:10.1007/s002540050144

Guo, X., and Valle-Levinson, A. 2007. Tidal effects on estuarine circulation and outflow plume in the Chesapeake Bay. Continental Shelf Research, 27(1), 20–42. DOI: 10.1016/j.csr.2006.08.009

Guo, X., and A. Valle-Levinson. 2008. Wind effects on the lateral structure of density-driven circulation in Chesapeake Bay. Continental Shelf Research 28: 2450–2471. doi:10.1016/j.csr.2008.06.008.

Hagy, J.D., Sanford, L.P., Boynton, W.R., 2000. Estimation of Net Physical Transport and Hydraulic Residence Times for a Coastal Plain Estuary Using Box Models. Estuaries 23, 328–340.

Haidvogel, DB, and A. Beckmann. 1999. Numerical ocean circulation modeling. 1st ed. London: Imperial College Press. ISBN: 978-1-86094-114-6 (hardcover).

Halpern, B.S., et al. 2009. A Global Map of Human Impact on Marine Ecosystems. Science (80-.). 948, 948–952. doi:10.1126/science.1149345

Hansen, D., Rattray, M., 1965. Gravitational Circulation in Straits and Estuaries. Dep. Oceanogr.

Herrera, J.L., Piedracoba, S., Varela, R.A. and Rosón, G. 2005. Spatial analysis of the wind field on the western coast of Galicia (NW Spain) from in situ measurements. Continental Shelf Research 25: 1728–1748. doi:10.1016/j.csr.2005.06.001.

Holt, J.T., Allen, J.I., Proctor, R., Gilbert, F., 2005. Error quantification of a high-resolution coupled hydrodynamic–ecosystem coastal–ocean model: Part 1 model overview and assessment of the hydrodynamics. J. Mar. Syst. 57, 167–188. doi:10.1016/j.jmarsys.2005.04.008

Hong, S.-Y., Noh, Y., and Dudhia, J. 2006. A new vertical diffusion package with an explicit treatment of entrainment processes, Mon. Weather Rev., 134, 2318–2341, doi:10.1175/MWR3199.1, 2006.

Huang, N.E., Shen, Z., Long, S.R., Wu, M.C., Shih, H.H., Zheng, Q., Yen, N.-C., Tung, C.C., Liu, H.H., 1998. The empirical mode decomposition and the Hilbert spectrum for nonlinear and non-stationary time series analysis. Proc. R. Soc. A Math. Phys. Eng. Sci. 454, 903–995. doi:10.1098/rspa.1998.0193

Ibañez, C., Canicio, A., Day, J.W., Curco, A. 1997. Morphologic Development, Relative Sea Level Rise and Sustainable Management of Water and Sediment in the Ebro Delta, Spain. J. Coast. Conserv. 3, 191–202.

Ibáñez, C., Prat, N. and Canicio, A. 1996. Changes in the hidrology and sediment transport produced by large dams on the lower Ebro river and its estuary. Regulated Rivers 12(1):51-62.

Ibáñez, C., Sharpe, P.J., Day, J.W., Day, J.N., Prat, N. 2010. Vertical accretion and relative sea level rise in the Ebro Delta wetlands (Catalonia, Spain). Wetlands 30, 979–988. doi:10.1007/s13157-010-0092-0

Janzen, C., Wong, K., 1998. On the Low-Frequency Transport Processes in Shallow Coastal Lagoon. Estuaries 21, 754–766.

Jiang, H., Farrar, J.T., Beardsley, R.C., Chen, R. and Chen, C. 2009. Zonal surface wind jets across the Red Sea due to mountain gap forcing along both sides of the Red Sea. Geophysical Research Letters 36: L19605. doi:10.1029/2009GL040008.

Jickells, T.D., 1998. Nutrient biogeochemistry of the coastal zone. Science 281, 217– 222

Jiménez, J. a., Sánchez-Arcilla, A., Valdemoro, H.I., Gracia, V., Nieto, F., 1997. Processes reshaping the Ebro delta. Mar. Geol. 144, 59–79. doi:10.1016/S0025-3227(97)00076-5

Jordi, A., G. Basterretxea, B. Casas, S. Anglès, and E. Garcés. 2008. Seiche-forced resuspension events in a Mediterranean harbour. Continental Shelf Research 28: 505–515. doi:10.1016/j.csr.2007.10.009.

Jouon, A., Douillet, P., Ouillon, S., Fraunié, P., 2006. Calculations of hydrodynamic time parameters in a semi-opened coastal zone using a 3D hydrodynamic model. Cont. Shelf Res. 26, 1395–1415. doi:10.1016/j.csr.2005.11.014

Junker, Tim, Martin Schmidt, and Volker Mohrholz. 2015. The relation of wind stress curl and meridional transport in the Benguela upwelling system. Journal of Marine Systems 143. Elsevier B.V.: 1–6. doi:10.1016/j.jmarsys.2014.10.006.

Ketchum, B. H. 1952. Circulation in Estuaries. Coastal Engineering Proceedings, 1(3), 6.

Klaić, Z. B., Z. Pasarić, G. Beg Paklar, and P. Oddo. 2011. Coastal sea responses to atmospheric forcings at two different resolutions. Ocean Science 7: 521–532. doi:10.5194/os-7-521-2011.

Large, W. G. and S. Pond. 1981. Open-ocean momentum flux measurements in moderate to strong winds. J. Phys. Oceanogr., 11, 324–336

Lee, J., Valle-Levinson, A., 2012. Influence of bathymetry on hydrography and circulation at the region between an estuary mouth and the adjacent continental shelf. Cont. Shelf Res. 41, 77–91. doi:10.1016/j.csr.2012.04.006

Li, Chunyan and James O'Donnell. 2005. The effect of channel length on the residual circulation in tidally dominated channels. J. Phys. Oceanogr., 35, 1826–1840. DOI: 10.1175/JPO2804.1

Llebot, C., 2010. Interactions between physical forcing, water circulation and phytoplankton dynamics in a microtidal estuary. Universidad de las Palmas de Gran Canaria.

Llebot, C., Solé, J., Delgado, M., Fernández-Tejedor, M., Camp, J., Estrada, M., 2011. Hydrographical forcing and phytoplankton variability in two semi-enclosed estuarine bays. J. Mar. Syst. 86, 69–86. doi:10.1016/j.jmarsys.2011.01.004

Llebot, C., Rueda, F.J., Solé, J., Artigas, M.L., Estrada, M., 2013. Hydrodynamic states in a wind-driven microtidal estuary (Alfacs Bay). J. Sea Res. doi:10.1016/j.seares.2013.05.010

Lopez, M., Gisbert, E., 2009. Evaluation of a by-catch reduction device for glass eel fishing traps. Fish. Manag. Ecol. 16, 438–447. doi:10.1111/j.1365-2400.2009.00692.x

Loureiro, S., Garcés, E., Fernández-Tejedor, M., Vaqué, D., and J. Camp. 2009. Pseudo-nitzschia spp. (Bacillariophyceae) and dissolved organic matter (DOM) dynamics in the Ebro Delta (Alfacs Bay, NW Mediterranean Sea). Estuarine, Coastal and Shelf Science 83: 539–549. doi:10.1016/j.ecss.2009.04.029.

Luettich, R. a., Carr, S.D., Reynolds-Fleming, J. V., Fulcher, C.W., McNinch, J.E., 2002. Semi-diurnal seiching in a shallow, micro-tidal lagoonal estuary. Cont. Shelf Res. 22, 1669–1681. doi:10.1016/S0278-4343(02)00031-6

Maldonado A. 1972. El Delta del Ebro: Estudio sedimentologico y estratigrafico. Ph.D. Thesis, Boletin de Estratigrafia, University of Barcelona. pp.486.

Mancero-Mosquera, I., M. Gačić, and a. Mazzoldi. 2010. The effect of wind on the residual current velocities in the inlets of Venice lagoon. Continental Shelf Research 30: 915–923. doi:10.1016/j.csr.2010.02.011.

Marcelo Acha, E., Mianzan, H., Guerrero, R., Carreto, J., Giberto, D., Montoya, N., Carignan, M., 2008. An overview of physical and ecological processes in the Rio de la Plata Estuary. Cont. Shelf Res. 28, 1579–1588. doi:10.1016/j.csr.2007.01.031

Martín Vide, J. 2005. Los mapas del tiempo. Volumen 1 de Colección Geoambiente XXI. Davinci Continental, 219pp. ISBN: 8493373265.

Mass, C. F. and Ovens, D. 2011. Fixing WRF's high speed wind bias: a new subgrid scale drag parameterization and the role of detailed verification, in: 24th Conference on Weather and Forecasting and 20th Conference on Numerical Weather Prediction, Preprints, 91st American Meteorological Society Annual Meeting, 23–27 January 2011, Seattle, WA, 2011.

Mestres, M., Sierra, J. P. A. U., and Sánchez-arcilla, A. 2007. Baroclinic and wind-induced circulation in Tarragona harbour (northeastern Spain). Scientia Marina, 71(June), 223–238.

Mestres, M., Sierra, J.P. a U., Sánchez-arcilla, A., González, J., Río, D.E.L., Wolf, T., Rodríguez, A., 2003. Modelling of the Ebro River plume . Validation with field observations *. Delta 67, 379–391. doi:10.3989/scimar.2003.67n4379

Miglietta, M. M., Thunis, P., Pederzoli, A., Georgieva, E., Bessag- net, B., Terrenoire, E., and Colette, A. 2012. Evaluation of WRFmodel performances in different European regions with the DELTA- FAIRMODE evaluation tool, Int. J. Environ. Pollut., 50, 83–97.

Millero, F. J. and Poisson, A. 1981. International one-atmosphere equation of state of seawater, Deep-Sea Res., 28, 625–629, 1981.

Millot, C., 1999. Circulation in the Western Mediterranean Sea. J. Mar. Syst. 20, 423–442. doi:10.1016/S0924-7963(98)00078-5

Minguito, M.D., Baquerizo, A., Ortega-Sánchez, M., Navarro, G., and M.A. Losada. 2012. Tide transformation in the Guadalquivir estuary (SW Spain) and process-based zonation. J. Geophys. Res., Vol. 117, No. C3, C03019, 14pp. DOI: 10.1029/2011JC007344

Mirfenderesk, H., and Tomlinson, R. 2009. An investigation of the change in tidal signal in an estuary as a result of Sea Level Rise and Development at short Medium Time Scale. 10th International Coastal Symposium (pp. 641-645). JCR.

Monismith, S. 1986. An experimental study of the upwelling response of stratified reservoirs to surface shear stress. J. Fluid. Mech., 171, 407–439.Murphy, P.L., Valle-Levinson, A., 2008. Tidal and residual circulation in the St. Andrew Bay system, Florida. Cont. Shelf Res. 28, 2678–2688. doi:10.1016/j.csr.2008.09.003

Monserrat, S., Ibbetson, A., and Thorpe, A. J. 1991. Atmospheric gravity waves and the 'rissaga' phenomenon, Q. J. Roy. Meteorol. Soc. 117, 553–570. DOI: 10.1002/qj.49711749907

Mulligan, R.P., Hay, A.E., Bowen, A.J., 2008. Wave-driven circulation in a coastal bay during the landfall of a hurricane. J. Geophys. Res. 113, C05026. doi:10.1029/2007JC004500

Narváez, D. A., and Valle-Levinson, A. 2008. Transverse structure of wind-driven flow at the entrance to an estuary: Nansemond River. Journal of Geophysical Research: Oceans, 113(9), 1–9. doi:10.1029/2008JC004770

Niedda, M., and M. Greppi. 2007. Tidal, seiche and wind dynamics in a small lagoon in the Mediterranean Sea. Estuarine, Coastal and Shelf Science 74: 21–30. doi:10.1016/j.ecss.2007.03.022.

Noble, M.A., Schroeder, W.W., Wiseman, W.J., Ryan, H.F., Gelfenbaum, G., 1996. Subtidal circulation patterns in a shallow, highly stratified estuary Mobile Bay, Alabama. J. Geophys. Res. 101.

Officer, C.B., 1976. Physical Oceanography of Estuaries (and Associated Coastal Waters). Wiley, New York, 465 pp

Oke, T.R. 1987. Boundary Layer Climates, 2nd. edn, Routledge, London. 1987.

Ostrovsky, I., Yacobi, Y. Z., Walline, P., and Kalikhman, I. 1996. Seiche-induced mixing: Its impact on lake productivity. Limnology and Oceanography, 41(2), 323–332. doi:10.4319/lo.1996.41.2.0323

Palacín, C., Gili, J.-M., Martín, D., 1992. Evidence for Coincidence of Meiofauna Spatial Heterogeneity with Eutrophication Processes in a Shallow-Water Mediterranean bay. Estuar. Coast. Shelf Sci. 35, 1–16. doi:10.1016/S0272-7714(05)80053-8

Palacin, C., Martin, D., Gili, J.M., 1991. Features of spatial distribution of benthic fauna in a Mediterranean shallow-water bay. Mar. Biol. 110, 315–321. doi:10.1007/BF01313718

Pawlowicz, R., Beardsley, B., and S. Lentz. 2002. Classical tidal harmonic analysis including error estimates in MATLAB using T_TIDE. Computers and Geosciences 28: 929–937. doi:10.1016/S0098-3004(02)00013-4.

Perez, M., Duarte, C., Romero, J., Sand-Jensen, K., Alcoverro, T., 1994. Growth plasticity in Cymodocea nodosa stands: the importance of nutrient supply. Aquat. Bot. 47, 249–264.

Podsetchine, V., and Gerald S.. 1999. The influence of spatial wind inhomogeneity on flow patterns in a small lake. Water Resources Research 33: 3348–3356.

Prandle, D. 2003. Relationships between tidal dynamics and bathymetry in strongly convergent estuaries. J. Phys. Oceanogr., 33, 2738–2750. DOI: 10.1175/1520-0485(2003)033<2738:RBTDAB>2.0.CO;2

Prat, N., and C. Ibañez. 1995. Effects of water transfers projected in the Spanish National Hydrological Plan on the ecology of the lower River Ebro (N.E. Spain) and its delta. Original Research Article Water Science and Technology, Volume 31, Issue 8, Pages 79-86

Pritchard, D. W. 1952. Estuarine Hydrography. Advances in Geophysics, Volume 1. Edited by H. E. Landsberg, Geophysics Research Directorate, Air Force Cambridge Research Center. Published by Academic Press, Inc., New York, USA, 1952, p.243

Pritchard, D. W., 1952: Salinity distribution and circulation in the Chesapeake Bay estuarine system. J. Mar. Res., 11 (2), 106–123

Pugh, D.T., 1996. Tides, Surges and Mean Sea-Level. John Willey and Sons, Chichester. ISBN: 047191505 (hardback)

Quijano-Scheggia, S., Garcés, E., Flo, E., Fernandez-Tejedor, M., Diogene, J. and Camp, J. 2008. Bloom dynamics of the genus Pseudo-nitzschia (Bacillariophyceae) in two coastal bays (NW Mediterranean Sea). Scientia Marina 72: 577–590.

Rabinovich, A.B, and S. Monserrat. 1998. Generation of Meteorological Tsunamis (Large Amplitude Seiches) Near the Balearic and Kuril Islands. Natural Hazards: 27–55. Doi: 10.1023/A:1008096627047

Rabinovich, A.B. 2009. Seiches and Harbor Oscillations. In Handbook of Coastal and Ocean Engineering, ed. Y.C.Kim, 193–236. Singapore: World Scientific.

Rabinovich, A.B., Monserrat, S., 1996. Meteorological tsunamis near the Balearic and Kuril Islands: Descriptive and statistical analysis, Natural Hazards, 13, (1), 55-90. DOI: 10.1007/BF00156506

Ramón, M., Cano, J., Peña, J.B., Campos, M.J., 2005. Current status and perspectives of mollusc (bivalves and gastropods) culture in the Spanish Mediterranean. Boletín Inst. Español Oceanogr. 21, 361–373.

Ranasinghe, R., and Pattiaratchi, C. 2000. Tidal inlet velocity asymmetry in diurnal regimes. Continental Shelf Research, 20, 2347-2366. DOI: 10.1016/S0278-4343(99)00064-3

Rockwell Geyer, W., Trowbridge, J.H., Bowen, M., 2000. The Dynamics of a Partially Mixed Estuary*. Am. Meteorol. Soc. 2035–2048.

Rueda, F., J. Vidal, and G. Schladow. 2009. Modeling the effect of size reduction on the stratification of a large wind-driven lake using an uncertainty-based approach. Water Resources Research 45: 1–15. doi:10.1029/2008WR006988.

Sainz-Elipe, S., Latorre, J.M., Escosa, R., Masià, M., Fuentes, M.V., Mas-Coma, S., Bargues, M.D., 2010. Malaria resurgence risk in southern Europe: climate assessment in an historically endemic area of rice fields at the Mediterranean shore of Spain. Malar. J. 9, 221. doi:10.1186/1475-2875-9-221

Salas-Monreal, D., Valle-Levinson, A., 2008. Sea-Level Slopes and Volume Fluxes Produced by Atmospheric Forcing in Estuaries: Chesapeake Bay Case Study. J. Coast. Res. 2, 208–217. doi:10.2112/06-0632.1

Salat, J., 1995. The interaction between the catalan and balearic currents in the southern catalan sea. Oceanol. Acta 18, 227–234.

Salat, J., Tintoré, J., Font, J., Wang, D.-P., Vieira, M., 1992. Near-Inertial Motion on the Shelf-Slope Front off Northeast Spain. J. Geophys. Res. 97, 7277–7281.

Sánchez-Arcilla, A., González-Marco, D., Bolaños, R., 2008. System Sciences A review of wave climate and prediction along the Spanish Mediterranean coast. Nat. Hazards Earth Syst. Sci. 8, 1217–1228.

Schaeffer, A., Garreau, P., Molcard, A., Fraunié, P., Seity, Y., 2011. Influence of high-resolution wind forcing on hydrodynamic modeling of the Gulf of Lions. Ocean Dyn. 61, 1823–1844. doi:10.1007/s10236-011-0442-3

Schoen, J., D. Stretch, and K. Tirok. 2014. Wind-Driven circulation patterns in a shallow estuarine lake: St Lucia, South Africa. Estuarine, Coastal and Shelf Science. doi:10.1016/j.ecss.2014.05.007.

Scire, J. S., Robe, F. R., Fernau, M. E., and Yamartino, J. 1999. A User's Guide for the CALMET Meteorological Model (Version 5.0), Earth Tech, Concord, MA.

Serra, P., G. More, and X. Pons. 2007. Monitoring winter flooding of rice fields on the coastal wetland of Ebre delta with multitemporal remote sensing images. 2007 IEEE International Geoscience and Remote Sensing Symposium. Ieee: 2495–2498. doi:10.1109/IGARSS.2007.4423350.

Shchepetkin, A. F., and McWilliams, J. C. 2005. The regional oceanic modeling system (ROMS): a split-explicit, free-surface, topography-following-coordinate oceanic model. Ocean Model, 9(4), 347–404. doi:10.1016/j.ocemod.2004.08.002

Signell, R.P., Carniel, S., Cavaleri, L., Chiggiato, J., Doyle, J.D., Pullen, J., and Sclavo, M. 2005. Assessment of wind quality for oceanographic modelling in semi-enclosed basins. Journal of Marine Systems 53: 217–233. doi:10.1016/j.jmarsys.2004.03.006.

Simpson, J.H, J. Brown, J. Matthews, and G. Allen. 1990. Tidal straining, density currents, and Stirring in the Control of Estuarine Stratification. Estuaries 13: 125–132. Doi: 10.2307/1351581

Simpson, J.H., and Bowers, D. 1981. Models of stratification and frontal movement in shelf seas. Deep Sea Res, 28(7), 727–738. doi: 10.1016/0198-0149(81)90132-1.

Simpson, JH and Sharples, J. 2012. Introduction to the Physical and Biological Oceanography of Shelf Seas. Cambridge University Press, Cambridge, p. 424. ISBN 978-0-521-70148-8

Skamarock, W. C., Klemp, J. B., Dudhia, J., Gill, D. O., Barker, D. M., Duda, M., Huang, X.-Y., Wang, W., and Powers, J. G. 2008. A description of the advanced research WRF version 3, NCAR Tech. Note NCAR/TN-475+STR, Nat. Cent. for Atmos. Res., Boulder, Colorado.

Slootweg, R., Rajvanshi, A., Mathur V.B. and A.K.Frontmatter. 2009. Biodiversity in Environmental Assessment: Enhancing Ecosystem Services for Human Well-Being. Cambridge University Press 978-0-521-88841-7 -

Solé, J., Turiel, A., Estrada, M., Llebot, C., Blasco, D., Camp, J., Delgado, M., Fernández-Tejedor, M., Diogène, J., 2009. Climatic forcing on hydrography of a Mediterranean bay (Alfacs Bay). Cont. Shelf Res. 29, 1786–1800. doi:10.1016/j.csr.2009.04.012

Song, Y., Haidvogel, D., 1994. A semi-implicit ocean circulation model using a generalized topography-following coordinate system. Journal of Computational Physics 115, 228–244

Speer, P., Aubrey, D., and Friedrichs, T. 1991. Nonlinear hydrodynamics of shallow tidal inlet/bay systems. In B. Parker, Tidal Hydrodynamics (pp. 321-339). New York.

Taylor, K.E., 2001. Summarizing multiple aspects of model performance in a single diagram. J. Geophys. Res. 106, 7183–7192.

Tewari, M., F. Chen, W. Wang, J. Dudhia, M. A. LeMone, K. Mitchell, M. Ek, G. Gayno, J. Wegiel, and R. H. Cuenca. 2004. Implementation and verification of the unified NOAH land surface model in the WRF model. 20th conference on weather analysis and forecasting/16th conference on numerical weather prediction, pp. 11–15.

Thompson, G., R. M. Rasmussen, and K. Manning. 2004. Explicit forecasts of winter precipitation using an improved bulk microphysics scheme. Part I: Description and sensitivity analysis. Mon. Wea. Rev., 132, 519–542.

Tonani, M, N Pinardi, C Fratianni, J Pistoia, S Dobricic, S Pensieri, M De Alfonso, and K Nittis. 2009. Mediterranean Forecasting System : forecast and analysis assessment through skill scores. Ocean Science: 649–660.

Torrence, C., and G.P Compo. 1998. A Practical Guide to Wavelet Analysis. Bulletin of the American Meteorological Society 79: 61–78.

Uncles, R.J., Stephens, J.A., Harris, C., 2014. Estuarine, Coastal and Shelf Science. Estuar. Coast. Mar. Sci. 150, 242–251.

Valle-Levinson, A., J.A. Delgado, and L.P. Atkinson. 2001. Reversing Water Exchange Patterns at the Entrance to a Semiarid Coastal Lagoon. Estuarine, Coastal and Shelf Science 53: 825–838. doi:10.1006/ecss.2000.0813

Valle-Levinson, A., Blanco, L., 2004. Observations of wind influence on exchange flows in a strait of the Chilean Inland Sea. J. Mar. Res. 62, 721–741.

Valle-Levinson, A., 2010. Contemporary Issues in Estuarine Physics.

Valle-Levinson, A., Mariño-Tapia, I., Enriquez, C., Waterhouse, A.F., 2011. Tidal variability of salinity and velocity fields related to intense point-source submarine groundwater discharges into the coastal ocean. Limnol. Oceanogr. 56, 1213–1224. doi:10.4319/lo.2011.56.4.1213

Van Maren, D., and Hoekstra, P., 2004. Seasonal variation of hydrodynamics and sediment dynamics in a shallow subtropical estuary: the Ba Lat River, Vietnam. Estuar. Coast. Shelf Sci. 60, 529–540. doi:10.1016/j.ecss.2004.02.011

Venäläinen, A., Sahlgren, V., Podsechin, V., and Huttula, T. 2003. Small-scale variability of the wind field over a typical Scandinavian lake. Boreal Environmental Research 8: 71–81.

Vila, M., Camp, J., Garcés, E., Masó, M., Delgado, M., 2001. High resolution spatio-temporal detection of potentially harmful dinoflagellates in confined waters of the NW Mediterranean. J. Plankton Res. 23, 497–514.

Vilibic, I., and Mihanovic, H. 2005. Resonance in Ploce Harbor (Adriatic Sea). Acta Adriat., 46(2): 125-136.

Waiters, R.A, Cheng, R.T., and T.J Conomos .1985. Time scales of circulation and mixing processes of San Francisco Bay waters. Hydrobiologia, 129(1): 13-36. Doi: 10.1007/BF00048685

Warner, J. C., Sherwood, C. R., Arango, H. G., and Signell, R. P. 2005. Performance of four turbulence closure models implemented using a generic length scale method. Ocean Modelling, 8(1-2), 81–113. doi:10.1016/j.ocemod.2003.12.003

Warner, J. C., Sherwood, C. R., Signell, R. P., Harris, C. K., and Arango, H. G. 2008. Development of a three-dimensional, regional, coupled wave, current, and sediment-transport model. Computers and Geosciences, 34(10), 1284–1306. DOI: 10.1016/j.cageo.2008.02.012

Warner, J.C., 2005. Numerical modeling of an estuary: A comprehensive skill assessment. J. Geophys. Res. 110, 1–13. doi:10.1029/2004JC002691

Waterhouse, A. F., Valle-Levinson, A., and Winant, C. D. 2011. Tides in a System of Connected Estuaries. Journal of Physical Oceanography, 41(5), 946–959. DOI: 10.1175/2010JPO4504.1

Whitney, M.M., Codiga, D.L., 2011. Response of a Large Stratified Estuary to Wind Events: Observations, Simulations, and Theory for Long Island Sound. J. Phys. Oceanogr. 41, 1308–1327. doi:10.1175/2011JPO4552.1

Wilmott CJ. 1981. On the validation of models. Phys Geogr 2:184–194

Winant, C. D. 2007. Three-Dimensional Tidal Flow in an Elongated, Rotating Basin. Journal of Physical Oceanography, 18. DOI: 10.1175/JPO3122.1

Winant, C.D. and A.W. Bratkovich, 1981: Temperature and currents on the southern California shelf: a description of the variability. J Phys Oceanogr, 11, 71–86. doi: 10.1175/1520-614 0485(1981)011.

Wolanski, E. 2007. Estuarine Ecohydrology. Elsevier. 157pp. ISBN: 978-0-444-53066-0

Wong, K.-C. 1990. Sea level variability in Long Island Sound. Estuaries 13 (4), 362–372. DOI: 10.2307/1351781

Wong, K.-C. 1994. On the nature of transverse variability in a coastal plain estuary, J. Geophys. Res., 99 (C7), 14209–14222, doi:10.1029/94JC00861.

Wong, K.-C., Valle-Levinson, A., 2002. On the relative importance of the remote and local wind effects on the subtidal exchange at the entrance to the Chesapeake Bay. J. Mar. Res. 60, 477–498. doi:10.1357/002224002762231188

Woo, S., and Yoon, B. 2011. The Classification of Estuary and Tidal Propagation characteristics in the Gyeong-Gi Bay, South Korea. ICS2011 (pp. 1624-1628). Poland: Journal of Coastal Research.

Zampato, L., G. Umgiesser, and S. Zecchetto. 2007. Sea level forecasting in Venice through high resolution meteorological fields. Estuarine, Coastal and Shelf Science 75: 223–235. doi:10.1016/j.ecss.2007.02.024.

Zhong, L., Li, M., Foreman, M.G.G., 2008. Resonance and sea level variability in Chesapeake Bay. Cont. Shelf Res. 28, 2565–2573. doi:10.1016/j.csr.2008.07.007